HOT ISOSTATIC PRESSING OF HIGH TEMPERATURE MATERIALS

by

ALESSANDRO SERGI

A thesis submitted to the University of Birmingham for the degree of

DOCTOR OF PHILOSOPHY

School of Metallurgy and Materials

College of Engineering and Physical Sciences

University of Birmingham

August 2022

Abstract

Near Netshape Powder Metallurgy Hot Isostatic Pressing (NNS PM HIP) is an advanced manufacturing process capable of manufacturing a variety of materials with superior mechanical properties, improved buy-to-fly ratio and complex geometrical design. NNS PM HIP could represent an advantageous alternative to conventional manufacturing routes for the manufacture of high-value components across multiple industrial sectors. However, despite the evident advantages of NNS PM HIP technology and the recent research interest in the topic, there is a current lack of knowledge associated with the processability of some materials, which limits the potential benefits of this manufacturing technology. Thus, the main scope of this thesis is to investigate some key challenges, report the main findings and demonstrate the possibility of manufacturing different classes of high temperature materials through NNS PM HIP. This will be achieved by assessing the HIP behaviour for a wide variety of high temperature materials including IN625, IN625-based metal matrix composites (MMCs), Nb and C-103 Nb alloy. The first study concerns the HIP behaviour of Ni-base superalloys using IN625 as case study. To this end, four different IN625 powders obtained using four different atomisation routes including argon, nitrogen, plasma and water atomisation (AGA, NGA, PA and WA) were characterised through scanning electron microscopy (SEM), energy dispersive X-ray (EDS) and X-ray photoelectron spectroscopy (XPS) techniques. The differences in as-HIPed microstructure and mechanical properties were assessed for the four powders via SEM, EDS, tensile and Charpy impact tests. The results indicate a direct correlation between powder quality, presence of PPBs and mechanical properties, highlighting the importance of powder characteristics on PPBs formation for Ni-base superalloys.

The knowledge acquired in the first study was exploited to develop a high temperature wear resistant material through NNS PM HIP as part of the second study. To enhance the wear properties of IN625, two different reinforcements respectively SiC and TiB_2 with various reinforcement fractions ranging from 5vol% to 25vol% were used. The microstructural characterisation of the HIPed material performed using SEM and EDS techniques highlighted the presence of a fully dense microstructure with a continuous network of ceramic reinforcements at PPBs. The wear test performed on IN625-MMCs demonstrated a progressive improvement in tribological properties with the increase of the reinforcement volume fraction for both IN625-SiC and IN625-TiB_2. Finally, IN625-10v%SiC was down-selected for room temperature and high temperature tensile tests. The results indicate a drastic reduction in elongation, which is a direct consequence of the presence of ceramic reinforcement at PPBs.

As part of the third study, the HIP behaviour of refractory metals with pure Nb as case study was investigated. In this study, three Nb powders with varied particle size ranges (fine, mid-range and coarse) and C-103 Nb alloy powder were investigated to understand the differences in particle size distribution (PSD), morphology and oxygen content present in the alloy chemistry. The as-HIPed microstructures of pure Nb and C-103 were near to fully dense with the absence of PPBs. Additionally, it was observed that oxygen content plays a crucial role in the microhardness and mechanical properties of pure Nb. On the other hand, as-HIPed C-103 powder showed superior tensile properties if compared to the minimum specifications for wrought C-103. Finally, in the fourth study, the potentials of HIP diffusion bonding (DB) were exploited to demonstrate the possibility of manufacturing high temperature oxidation resistant coatings for pure Nb using Pt and the feasibility of joining Nb-Ti6Al4V.

To appraise the industrial viability of the NNS PM HIP process route and materials studied in this thesis, three different prototypes were manufactured. In particular, the manufacturing steps involved in the production of IN625 Y-shaped pipe, IN625-10v%SiC mechanical seals and Nb combustion chamber were presented and discussed.

Acknowledgements

I would like to express my gratitude to the School of Metallurgy and Materials of the University of Birmingham and TWI Ltd through the National Structural Integrity Research Centre (NSIRC) for providing me access to indispensable research facilities. Additionally, I would like to thank the Engineering & Physical Sciences Research Council (EPSRC) through the Centre of Doctoral Training in Innovative Metal Processing (IMPaCT) for the financial support provided.

Extraordinary thanks go to my supervisors Prof. Moataz Attallah and Dr. Raja Khan for agreeing to be my supervisors, for their scientific expertise and for supporting me throughout my PhD. Their guidance and support provided during the last four years were invaluable and allowed me to learn and achieve a considerable personal growth. I express my gratitude to my secondary academic supervisor Dr. Khamis Essa for his support and help provided throughout my PhD.

A big thank goes to all the technical staff at the University of Birmingham and TWI Ltd for helping me in the experimental characterisation and for providing me with indispensable technical knowledge.

I would like to acknowledge the European Space Agency (ESA) for supporting part of my research through the project “Powder Metallurgy Based Materials for High Wear Resistance, High Hardness and High Temperature”. I also would like to acknowledge European Union for supporting part of my research through the H2020 project titled “Sustainable and flexible powder metallurgy processes optimization by a holistic reduction of raw material resources and energy consumption (SUPREME)”. Moreover, I would like to thank Nammo Westcott Ltd and Johnson Matthey for providing me with some material and industrial expertise.

Furthermore, I would like to express my gratitude to Henry Royce Institute that allowed me to perform X-ray photoelectron spectroscopy (XPS) analysis on IN625 powders through the Imperial College London.

My deepest thank goes to my family and friends. I would like to thank my father Francesco and my brother Domenico who has supported me throughout my PhD and gave me essential suggestions that helped me to improve the quality of my work. A big thank goes to Omar, Nicoletta and the little Zahra who played an important role in cheering me up during difficult times. I also would like to express my gratitude to my friends from Italy for their huge support and for being close to me despite the distance.

Most importantly, I would like to finish my acknowledgment by thanking my partner Maria Grazia for believing in me once more and for supporting me in everything I do.

Table of Contents

List of Figures

List of Tables

Abbreviations

AGA	Argon Gas Atomisation
BSE	Backscattered Electron
CIP	Cold Isostatic Pressing
CMM	Coordinate-measuring Machine
CoF	Coefficient of Friction
CSL	Coincidence Site Lattice
CTE	Coefficient of Thermal Expansion
CVD	Chemical Vapor Deposition
DB	Diffusion Bonding
DLC	Diamond Like Carbon
DSC	Differential Scanning Calorimetry
EBM	Electron Beam Melting
EBSD	Electron Backscatter Diffraction
EBW	Electron Beam Welding
EDM	Electrical discharge machining
EDX-EDS	Energy Dispersive X-ray
EL%	Elongation
FGM	Functionally Graded Material
GA	Gas Atomisation
HAZ	Heat Affected Zone
HDH	Hydride Dehydrate
HT	Heat Treatment

ICP OES	Inductively Coupled Plasma Optical Emission Spectroscopy
IPF	Inverse Pole Figure
LBW	Laser Beam Welding
LH_2	Liquid Hydrogen
LOX	Liquid Oxygen
L-PBF	Laser Powder Bed Fusion
MMCs	Metal Matrix Composites
NGA	Nitrogen Gas Atomisation
NNS PM HIP	Near Net-shape Powder Metallurgy Hot Isostatic Pressing
ODS	Oxide-dispersion-strengthened
PA	Plasma Atomisation
PPBs	Prior Particle Boundaries
PREP	Plasma Rotating Electrode Process
PSD	Particle Size Distribution
PVD	Physical Vapor Deposition
RT	Room Temperature
SEM	Scanning Electron Microscope
SHT	Solution Heat Treatment
SPS	Spark Plasma Sintering
TIP	Thermal Induced Porosity
UTS	Ultimate Tensile Strength
VIM	Vacuum Induction Melting
WA	Water Atomisation

XPS	X-ray Photoelectron Spectroscopy
YS	Yield Strength

This thesis was submitted using the alternative thesis format. A list of the experimental chapters, the status and Co-authors contributions is reported below.

Thesis Chapter	Publication Title	Status	Authors and contributions
Chapter 5	*The Role of Powder Atomisation Route on the Microstructure and Mechanical Properties of Hot Isostatically Pressed Inconel 625*	*Published in Materials Science and Engineering A*	***Alessandro Sergi:*** *concept, experimental methodology, writing original draft, response to reviewers.* ***Raja Khan:*** *concept, experimental guidance, review of the manuscript and supervision.* ***Moataz Attallah:*** *concept, experimental guidance, review of the manuscript and supervision.*
Chapter 6	*Development of Ni-base Metal Matrix Composites by Powder Metallurgy Hot Isostatic Pressing for Space Applications*	*Published in Advanced Powder Technology*	***Alessandro Sergi:*** *concept, experimental methodology, writing original draft, response to reviewers.* ***Raja Khan:*** *concept, experimental guidance, review of the manuscript and supervision.* ***Sandeep Irukuvarghula:*** *experimental support, evaluation of results.* ***Martina Meisnar:*** *industrial steer, review of the manuscript.*

			Advenit Makaya: *industrial steer.* ***Moataz Attallah:*** *concept, experimental guidance, review of the manuscript and supervision.*
Chapter 7	*Powder HIP of pure Nb and C-103 alloy: the influence of powder characteristics on mechanical properties*	*Published in International Journal of Refractory Metals and Hard Materials*	***Alessandro Sergi:*** *concept, experimental methodology, writing original draft, response to reviewers.* ***Raja Khan:*** *concept, experimental guidance, review of the manuscript and supervision.* ***Kostantinos Georgilas:*** *experimental support, evaluation of results.* ***Martina Meisnar:*** *industrial steer, review of the manuscript.* ***Advenit Makaya:*** *industrial steer.* ***Moataz Attallah:*** *concept, experimental guidance, review of the manuscript and supervision.*
Chapter 8	*HIP Diffusion Bonding of Nb and Nb-alloys for*	*Not submitted yet.*	***Alessandro Sergi:*** *concept, experimental*

	Space Applications		*methodology, writing original draft.* ***Raja Khan:*** *concept, experimental guidance, review of the manuscript and supervision.* ***Malallah Al Lawati:*** *experimental support.* ***Francesco Careri:*** *experimental support.* ***Hugh Hamilton:*** *industrial steer, experimental support.* ***Martina Meisnar:*** *industrial steer, review of the manuscript.* ***Advenit Makaya:*** *industrial steer.* ***Moataz Attallah:*** *concept, experimental guidance, review of the manuscript and supervision.*

Chapter 1. Introduction

1.1 Motivation & Background

A broad range of manufacturing methods can be adopted for manufacturing high temperature engineering components. In particular, manufacturing of these parts can rely on the traditional methods such as casting and forging and on more recently developed PM-based manufacturing processes including near net-shape powder metallurgy hot isostatic pressing (NNS PM HIP), spark plasma sintering (SPS), additive manufacturing (AM) and metal injection moulding (MIM). The performances of high-value engineering components manufactured through conventional processes are often limited by the presence of defects including porosity, elemental segregation and anisotropic microstructure. Furthermore, traditional manufacturing routes do not offer the required flexibility to manufacture complex shapes and/or to generate novel materials for specific demanding applications. Thus, due to a progressive increase in operating conditions requirements, design complexity and due to the need of reducing material waste, the use of PM advanced manufacturing processes can represent a valid alternative to manufacture high temperature engineering components across a variety of sectors including but not limited to aerospace & space, nuclear, marine, oil & gas, etc. Among the abovementioned PM advanced manufacturing processes, NNS PM HIP can represent a valid alternative to current traditional manufacturing techniques, due to its combination of excellent mechanical properties, reduced material waste and enhanced design flexibility. To translate the use of NNS PM HIP to end-users, additional research is required in the field of high-temperature materials to understand their properties and limitations for the manufacture of high-value engineering parts. Thus, this PhD study will focus the attention on the NNS PM HIP of a variety of high temperature materials including Ni-base superalloys, Ni-base metal matrix composites (MMCs) and refractory metals. In particular, one of the

major issues related to PM HIP of Ni-base superalloys is linked with the formation of prior particle boundaries (PPBs), reducing the as-HIPed performances and consequently limiting their processability through NNS PM HIP. Thus, in the first study, the importance of powder characteristics on the HIP behaviour of Ni-based superalloys will be highlighted to understand their impact on the prior particle boundaries (PPBs) formation and consequently on mechanical properties. Even though Ni-base superalloys are characterised by excellent high temperature strength and corrosion resistance, their wear resistance is not adequate for certain demanding applications. Additionally, despite the possible advantages of using NNS PM HIP to manufacture Ni-based MMCs there is limited literature available investigating this class of materials. Thus, the knowledge acquired in the first study will be exploited to develop a high temperature wear resistant material through NNS PM HIP as part of the second study. During the third study, the HIP behaviour of refractory metals with pure Nb as a case study will be investigated. In fact, for applications exceeding the maximum operating temperature of Ni-base superalloys, the use of refractory metals can represent an interesting scenario. Among all the refractory metals, pure Nb was specifically selected due to its combination of relatively low density if compared to other refractory metals and the high oxygen solid solubility with the possibility of tailoring the mechanical properties by adjusting the oxygen levels. Moreover, one of the major problems associated with refractory metals is represented by their inadequate high temperature oxidation resistance. Thus, in the fourth study, the use of HIP DB was investigated for the generation of high temperature Pt coating on pure Nb. Additionally, HIP DB was also exploited to assess the possibility of solid-state joining Nb-Ti6Al4V for space applications.

To demonstrate the industrial viability of this advanced manufacturing process, this thesis will explore the use of NNS PM HIP focusing on three different applications by

manufacturing three near net-shape demonstrator parts, normally utilised in submarine and space sectors. This would allow enhancing the knowledge in the HIP behaviour of these classes of materials, demonstrating the possibility of manufacturing near net-shape complex parts and assessing their potentials for high-temperature applications.

1.2 Hot Isostatic Pressing & Diffusion Bonding

1.2.1 Introduction

Hot Isostatic Pressing (HIP) is an advanced manufacturing process used to manufacture high-value components in different fields including aerospace, nuclear, marine, automotive, medical, defence, etc. [1].

HIP technology was firstly employed in 1955 for diffusion bonding (DB) applications [2]. HIP process consists of the simultaneous application of high temperature and pressure capable of consolidating a wide range of materials to full or near to full density. HIP is currently used to densify pre-sintered components, densify castings, powder consolidation (PM HIP), and in recent years, it has been used as post-treatment for additively manufactured components.

What makes HIP unique is the simultaneous application of high temperatures and isostatic pressures. These pressures are applied by an inert gas (usually argon). During HIP process, each individual gas atom acts as an individual forge on the component, guaranteeing uniform densification even for parts with extremely complex shapes and small features [1]. The main advantage of HIP compared to conventionally manufacturing routes are:

- Increasing design flexibility. It is possible to tailor the mechanical properties of the material by changing the process parameters such as temperature, pressure and holding time.
- Improving mechanical properties. HIP generates an isotropic, fine-grained structure with excellent levels of strength, fracture toughness and fatigue properties [1].
- Reduction of the buy-to-fly ratio. NNS PM HIP process is capable of reducing the machining operation and consequently the material waste, reducing the lead times for the production of complex geometries.
- Ability to produce components with graded functionality or multi-material components.
- Possibility to join dissimilar materials through HIP DB.

During HIP densification process, pores are closed by the combined action of pressure and temperature. The driving force for pores closure is the reduction of surface area, consequently accompanied by the reduction of their surface energy. In particular, densification is achieved by three different mechanisms; respectively yield collapse, creep and diffusion. These three mechanisms are governed by three main process parameters i.e. temperature, pressure and dwell time. Other variables, which can greatly affect the HIP response, are the heating and cooling rates and the canister material (in the case of NNS PM HIP).

One of the main advantages of HIP is the generation of an isotropic fine-grained microstructure resulting in excellent mechanical properties and reduced scattered band in properties, comparable to the forged material. The main effects of post-HIP treatment on castings and additively manufactured components are to reduce the porosity and improve the

fatigue life by pore and defect closure. This is demonstrated by different studies available in literature [3], [4], [5].

1.2.2 HIP system

A simple schematic representation of the HIP system is reported in Figure **1.1**. The HIP system is characterised by a steel pressure vessel, sealed on the top by a top closure. An insulator acting as a thermal barrier between the heated part and the HIP water cooling system surrounds the furnace. In order to achieve high pressures, an inert gas such as argon, nitrogen, or helium is pumped into the HIP chamber via a gas inlet situated on top closure by using a compressor. After the HIP cycle, a great part of the gas is recycled and used for the next HIP run. One of the most important components of a HIP system are the heating elements. Depending on the application, different heating elements can be found [6]:

- Fe-Cr-Al alloy (Kanthal) heating elements for temperatures up to 1200°C
- Molybdenum heating elements, that can be used up to 1450°C
- Graphite heating elements for temperatures of 2000°C or above

The water cooling system is responsible for controlling the temperature of the insulator and the pressure vessel. In the cooling system, water is recirculating, thus drastically reducing water waste [6]. The size of the HIP chamber depends on the system; the diameter of the chamber can vary from 100mm up to 2050mm allowing to HIP at the same time a considerable amount of parts, reducing the overall running costs. Pressures inside the chamber can reach 300MPa, while the maximum allowable temperature is 2200°C [6]. The temperature of the workload, as well as the heating elements, are controlled by the presence of thermocouples.

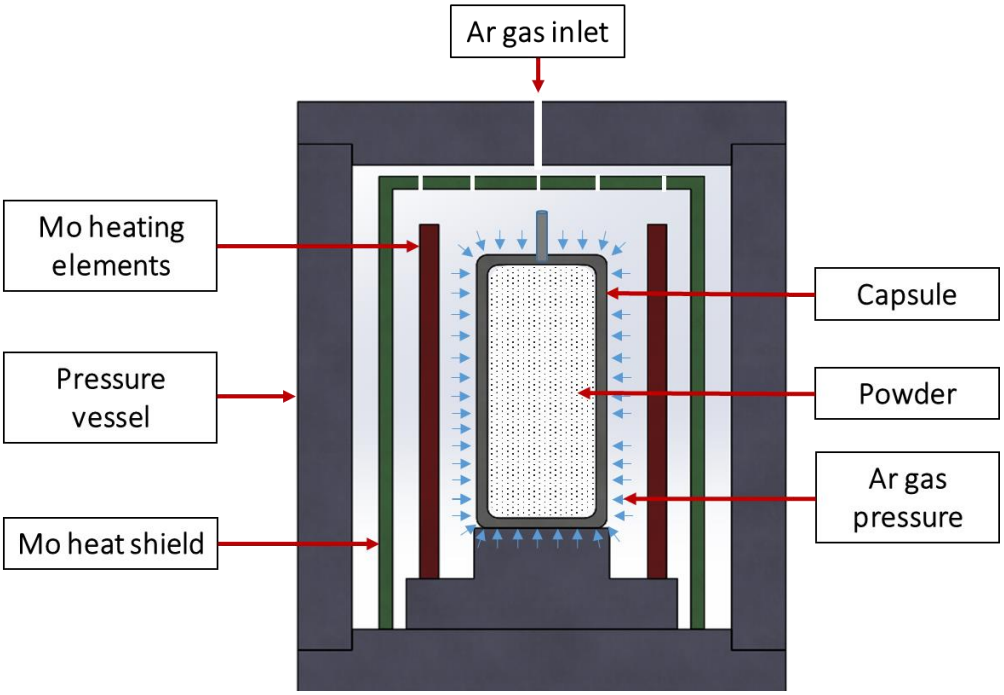

Figure 1.1 Schematic of the HIP system.

1.2.3 NNS PM HIP

Near netshape powder metallurgy hot isostatic pressing (NNS PM HIP) represents one of the predominant applications of HIP technology. The main advantage of this technique is the production of parts with a reduced buy-to-fly ratio if compared to conventional casting and forging, while maintaining excellent mechanical properties. Another important advantage of NNS PM HIP is the generation of a fully dense microstructure with the absence of segregation, allowing more flexibility in producing alloys, which cannot be produced by other manufacturing techniques due to elemental segregation. In NNS PM HIP a capsule, commonly called a canister, is filled with powders. After the filling procedure, the canister is outgassed, sealed and then HIPed by applying temperatures between 0.5 and 0.7 T_m and pressures between 100 and 200MPa. After the HIP stage, the canister is removed by machining or by acid attack (pickling). A schematic of the NNS HIP process can be seen in Figure **1.2**.

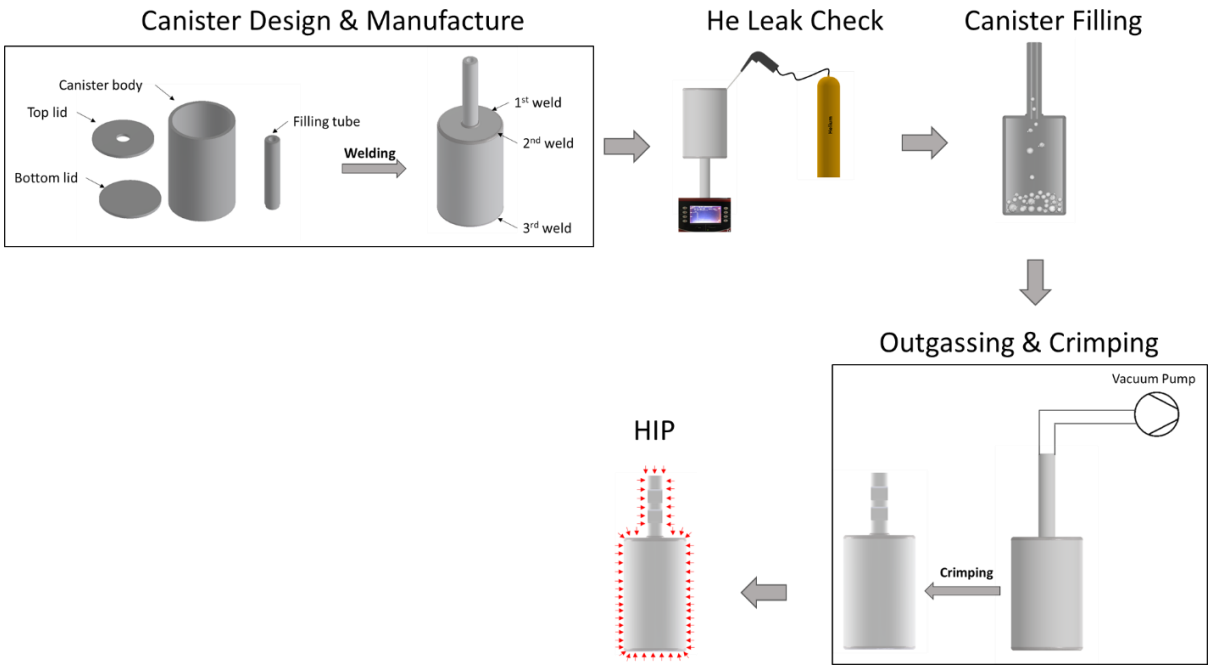

Figure 1.2 Schematic of NNS PM HIP Process.

Canister material: Canister material requires an accurate selection, taking into account the following properties:

- Mechanical properties (Yield Strength, Young Modulus, Elongation to Failure)
- Thermal Properties (Thermal Conductivity, Melting Point, Coefficient of Thermal Expansion)
- Deformability at HIP conditions
- Reactivity and metallurgical compatibility with the HIPed material
- Machinability
- Weldability
- Formability and Availability in various forms and shapes
- Cost

A ductile material is required during HIP in order to avoid failure on the surface of the canister due to the severe deformations experienced as part of the consolidation process. Furthermore, machinability is fundamental if a particular shape has to be manufactured. Since the body of the canister is always joined with the lids through welds, weldability is another parameter influencing the canister's selection.

One of the advantages of the net-shape HIP is represented by the limited amount of machining required if compared to the conventional manufacturing techniques. The amount of secondary machining processes is directly linked with the depth of the diffusion layer due to the interaction of the canister with PM HIPed material. For instance, a glass canister does not interact with the HIPed materials, while a titanium or aluminium canister increases the interaction regions due to the higher reactivity and diffusivity rates.

Canister welding: welding has to be performed to high standards in order to achieve a defect-free weld. After welding, it is mandatory to check the integrity of the welds by using a leak check or other systems capable of detecting small defects including open porosity or cracks. In fact, if a small defect is present in the weld, the gas will penetrate inside the canister leading to a lack of densification or complete failure of the canister.

Canister filling: powder filling is tipically performed in an inert atmosphere due to two main reasons. Firstly, due to the powder's high surface to volume ratio, in fact powders are extremely reactive, thus reducing the oxygen levels would drastically reduce the risks of reaction, especially for reactive powders such as Zr, Ti, Nb etc. The second reason is to avoid any contamination with the external environment, filling the powders in a controlled environment will reduce the risks of contamination, which would cause severe consequences in the HIPed microstructure, such as the generation of PPBs. The filling procedure is accompanied by the vibrating stages, which are essential to guarantee a correct fill of the

powder into the canister to its packing density, especially for big canisters or for complex canister geometries. An incomplete canister fill would compromise the final geometry of the net-shape component, and in some cases, it can lead to excessive plastic strains of the canister during the HIP cycle, resulting in canister failure.

Canister de-gassing: the presence of internal gases in the canister would compromise the densification process. In fact, if an excess of gas is present inside the canister it will expand in the HIP chamber due to the high temperatures opposing the densification action of the pressure.

HIP Cycle and Process Parameters: the driving force for densification in NNS PM HIP as well as in powder sintering is the reduction of the free energy associated with the transition from extremely high levels of free energy due to high levels of surface to volume ratio in the powders, to lower free energy levels in the solid part [7]. In order to achieve full densification and optimal microstructure and mechanical properties, the process parameters such as temperature, pressure and dwell time need to be selected correctly.

The HIP temperatures usually range between 0.5-0.7T_m. When choosing the HIP temperature is important to understand the interaction between the metallic canister and the material to be HIPed. In fact, the interaction with the canister could lead to the formation of low-temperature eutectics, which could result in a failure of the HIP run.

The pressure is usually in the range of 100-200MPa. The important role of the pressure is to generate a yield collapse at the early stages of the densification, which contributes to a great part of the densification mechanism. Similarly to temperature, the required pressure is dependent on the material to be HIPed. Pressure should be sufficient to generate a yield

collapse during the HIP cycle. Pressure is crucial as well for accelerating other densification mechanisms such as creep and diffusion [8].

A certain dwell time is necessary to allow some time-dependent mechanisms such as creep and diffusion to take place. Typical dwell times for hot isostatic pressing can range from 2-4h [9], [10], [11]. Dwell time should be optimised to guarantee a full densification and avoid excessive grain growth.

Temperature and pressures in a conventional HIP cycle are ramped-up and down simultaneously, with relatively low heating and cooling rates (between 5-10°C/min), but higher cooling rates (up to 1000°C/min) can be adopted in modern HIP vessels.

1.2.3.1 Advantages and Limitations of NNS PM HIP

NNS PM HIP has several advantages if compared to conventional manufactured techniques. The advantages include:

- **Reduction of the buy-to-fly ratio**: if compared to conventional manufacturing processes such as forging, a great reduction of material waste and machining can be achieved through NNS PM HIP. Reduction of machining required is important in materials which are difficult to be machined.
- **Increasing design flexibility:** It is possible to tailor the mechanical properties of the material by changing the process parameters such as temperature, pressure and holding time. Additionally, it is possible to generate novel classes of materials including metal matrix composites (MMCs) or in-situ alloys.
- **Improving mechanical properties**: NNS PM HIP generates a fine-grained microstructure, with a good level of strength and ductility. Additionally, the absence

of elemental segregation contributes in attaining a homogeneous microstructure if compared to castings or other melting and solidification based processes.

- **Isotropic properties of the final product:** NNS PM HIP guarantees a homogenous and isotropic microstructure, reducing the scatter band in the properties of the material.
- **Reduction in machining operations:** NNS PM HIP results in near to net-shape components, with a consequent reduction in machining operations required.
- **Possibility to generate a functionally graded structure:** NNS PM HIP offers the possibility of generating a graded structure useful to improve the wear properties of oxidation and corrosion properties of the manufactured part.

However, NNS PM HIP process is associated with some disadvantages. They are related both to the process itself and more specifically to the microstructure of the as-HIPed parts. The main issues related to the HIP process are:

- **Equipment cost and availability:** HIP furnaces are extremely expensive and there is a limited number of them around the country and the world.
- **Running costs:** the running costs for a HIP cycle are high if considering the amount of inert gas used and the electric power required to run it. This is the reason why HIP is considered so far just for high-value components.
- **Production rate:** the production rate depends on the size of the HIP chamber. Although the biggest HIP chamber has a diameter approaching 2m, conventional-sized chambers do not guarantee a high production rate.
- **NNS PM HIP preparation:** NNS PM HIP procedure involves different steps, including welding, filling, outgassing, hot crimping and HIP densification. Each of

these steps has to be completed with attention in order to avoid a canister failure or undesired results.

- **Create a leak-proof capsule:** this represents one of the major issues in NNS PM HIP in particular if the presence of a complex capsule geometry. Due to the high temperature and pressures exerted during the HIP cycle, the smallest defect can compromise the entire HIP cycle, leading to a failure in the densification mechanism.

The disadvantages related to the as-HIPed microstructure strongly depend on the material to be HIPed and on other factors such as powder quality and atomisation route. The main microstructure disadvantages include:

- **Generation of prior particle boundaries (PPBs):** this represents the most common and challenging issue associated with HIP of some specific classes of materials. The generation of PPBs is rather a complex mechanism and will be treated separately. It is widely reported in the literature that PPBs are responsible for degrading the mechanical properties of as-HIPed parts, reducing the elongation to fracture, fracture toughness and fatigue life [12], [13].
- **Thermal induced porosity (TIP):** TIPs arise from gas entrapped within the powders produced by gas atomisation. This entrapped gas, after the post-HIP heat treatments, can give rise to some “gas bubbles”, which will generate some porosity in the material [14], thus an adequate HT temperature must be adopted in order to decrease the TIPs. These pores can act as crack initiation sites lowering the fatigue life of the HIPed component.
- **Ceramic inclusions:** similarly to TIP, this issue is linked with the atomisation process. During gas atomisation, the melt flows through a ceramic tundish. It is reported in literature that some ceramic inclusions may arise from the interaction of

the melt with the ceramic tundish. The presence of ceramic inclusions may act as a crack initiation site and reduce the ductility of the material. However, this issue can be readily eliminated by the adoption of an improved gas atomisation process or by using a different atomisation technique such as plasma atomisation (PA) or plasma rotating electrode process (PREP).

1.3 HIP Diffusion Bonding

Diffusion bonding (DB) is a solid-state joining technique capable of joining similar and dissimilar materials through the application of high temperatures (0.5-0.7 T_m) and high pressures [15]. Similarly to PM HIP, DB evolves at the beginning by yield collapse of the surface asperities and the bonding mechanism continues through temperature and time-dependent mechanisms such as power-law creep and diffusion [16].

DB has several advantages if compared to conventional joining technologies such as welding or brazing. The advantages include:

- Generation of joints with similar microstructure to the bulk materials. In particular, DB guarantees the formation of a strong joint without the presence of heat affected zone (HAZ), which represents a detrimental characteristic of the fusion welding techniques.
- Possibility of joining dissimilar materials. A wide range of materials can be successfully joined using DB, including ceramics.
- Possibility of joining multiple layers. DB allows to generate functionally graded materials (FGM), with the possibility of altering the properties from the surface to the bulk of the component.

- Possibility of joining reactive metals with reduced chance of contamination including reactive materials such as Zr, Ti and refractory metals.

However, there are some disadvantages associated with DB including:

- Equipment and running costs. DB involves the presence of high temperature and pressure, thus dedicated furnaces capable of generating high bonding pressures is required.
- Low surface roughness requirements. The process of DB requires clean and extremely smooth surfaces in order to maximise the contact surfaces.
- Standard procedures for DB not yet developed for all alloys. The process parameters such as temperature, pressure and holding time are not yet optimised for the DB of different materials and alloys.

Diffusion bonding can be performed between base-metals or by using intermediate layers between the two materials to be joined. No intermediate layers are required if the materials to be joined are metallurgically compatible. On the other hand, diffusion bonding using an intermediate layer has the advantage of using lower pressure and lower temperatures, since the intermediate layer has enhanced diffusivity in the base metals. Additionally, the use of an intermediate layer with high oxygen solubility can guarantee a better joint quality [17]. For DB between two different base-metals with or without an intermediate layer, the difference in coefficient of thermal expansion is an important parameter to consider. In fact, if there is a considerable difference in the coefficients of thermal expansion (CTE), it can potentially lead to an excess in thermal stresses, which can determine a failure of the joint. A possible solution to this problem is to use intermediate layers with an intermediate CTE between the two materials, thus reducing the thermal stresses [18].

1.4 Research Aims and Objectives

Manufacture of high temperature parts through NNS PM HIP can be regarded as an attractive alternative to the conventional manufacturing routes. Despite the advances in PM HIP during the past decade, HIP behaviour of some materials such as Ni-based superalloys, MMCs and refractory metals is still not fully understood. In particular, the influence of powder quality and powder atomisation route on the microstructure and mechanical properties of Ni-based superalloys is not clear. There are limited studies on the influence of reinforcement type and volume fraction on metal matrix composites (MMCs) wear and mechanical properties. Additionally, a considerable literature gap in the PM HIP response of refractory metals was observed, both in terms of HIP process parameters and of final as-HIPed properties. Thus, in this study, three different areas of investigation were considered to assess the PM HIP response and gain a comprehensive understanding on the PM HIP behaviour of three different classes of materials. The first study focused on the HIP response of Ni-based superalloys to assess the influence of powder atomisation techniques on the microstructure (PPBs formation) and mechanical properties, using IN625 as a case study. The second research topic focused MMCs to characterise the effect of ceramic reinforcements addition on the wear properties of the materials using IN625-based MMCs as case study. The third part of this work was dedicated to the influence of interstitials on the mechanical properties of refractory metals using pure Nb as case study material.

The overall aim of this study can be summarised as follow:

"To understand the PM HIP response of three different classes of high temperature materials, with particular focus on the influence of powder characteristics on the as-HIPed microstructure and mechanical properties. Furthermore, to demonstrate the net-shape

capabilities of NNS PM HIP process by manufacturing three different near net-shape demonstrators"

The overall objectives of the study are:

- Understand the influence of powder quality and powder atomisation route on the microstructure and mechanical properties of Ni-base superalloys (Chapter 5).
- Assess the influence of ceramic reinforcement material and volume fraction on the microstructure and wear properties of as-HIPed MMCs (Chapter 6).
- Evaluate the influence of powder characteristics on the mechanical properties of pure Nb, with particular focus on the role of oxygen in the strength of the material (Chapter 7)
- Understand the possibility of generating a high temperature resistant coating for refractory metals through HIP DB (Chapter 7).
- Assess the feasibility of manufacturing near net-shape high value components through NNS PM HIP (Chapter 5, Chapter 6, and Chapter 7).

1.5 References

[1] H.V. Atkinson, S.Davies, Fundamental aspects of hot isostatic pressing : An overview, Metall. Mater. Trans. A. 31 (2000) 2981–3000.

[2] N.L. Loh, K.Y. Sia, An overview of hot isostatic pressing, J. Mater. Process. Tech. 30 (1992) 45–65. https://doi.org/10.1016/0924-0136(92)90038-T.

[3] W. Schneller, M. Leitner, S. Springer, F. Grün, M. Taschauer, Effect of hip treatment on microstructure and fatigue strength of selectively laser melted AlSi10Mg, J. Manuf. Mater. Process. 3 (2019). https://doi.org/10.3390/jmmp3010016.

[4] J.T. Staley, M. Tiryakioğlu, J. Campbell, The effect of hot isostatic pressing (HIP) on the fatigue life of A206-T71 aluminum castings, Mater. Sci. Eng. A. 465 (2007) 136–145. https://doi.org/10.1016/j.msea.2007.02.009.

[5] P. Li, D.H. Warner, J.W. Pegues, M.D. Roach, N. Shamsaei, N. Phan, Investigation of the mechanisms by which hot isostatic pressing improves the fatigue performance of powder bed fused Ti-6Al-4V, Int. J. Fatigue. 120 (2019) 342–352. https://doi.org/10.1016/j.ijfatigue.2018.10.015.

[6] P. Antona, C. Mapelli, Hot Isostatic Pressing (HIP): the State of the Art & Improvement on Two Steels, Metall. Sci. Tecnol. (2013) 3–7. http://www.gruppofrattura.it/ors/index.php/MST/article/view/1076.

[7] J.K. Mackenzie, R. Shuttleworth, A Phenomenological Theory of Sintering, Proc. Phys. Soc. Sect. B. 62 (n.d.) 833–852.

[8] R.M. German, Sintering With External Pressure, in: Sinter. from Empir. Obs. to Sci. Princ., 2014: pp. 305–354.

[9] Y. Li, H. Qi, H. Hou, L. Lei, Effects of Hot Isostatic Pressing on Microstructure and Mechanical Properties of Hastelloy X Samples Produced by Selective Laser Melting, 102 (2017) 31–40. https://doi.org/10.2991/icmmse-17.2017.6.

[10] L. Xu, R. Guo, C. Bai, J. Lei, R. Yang, Effect of Hot Isostatic Pressing Conditions and Cooling Rate on Microstructure and Properties of Ti-6Al-4V Alloy from Atomized Powder, J. Mater. Sci. Technol. 30 (2014) 1289–1295. https://doi.org/10.1016/j.jmst.2014.04.011.

[11] H.R. Dugdale, J.B. Borradaile, H.R. Dugdale, J.B. Borradaile, Development of hot isostatically pressed nickel based alloys for nuclear applications Development of hot isostatically pressed nickel based alloys for nuclear applications, 5899 (2016). https://doi.org/10.1179/1743290113Y.0000000076.

[12] Q. Bai, J. Lin, G. Tian, J. Zou, D. Ta, Review and Analysis of Powder Prior Boundary (PPB) Formation in Powder Metallurgy Processes for Nickel-based Super Alloys, Powder Metall. Min. 4 (2015) 1–6. https://doi.org/10.4172/2168-9806.1000127.

[13] Y.L. Kuo, K. Kakehi, Effect of the prior particle boundary on the microstructure and mechanical properties of hot-isostatic-pressed IN718 Alloy, Mater. Trans. 58 (2017) 1042–1048. https://doi.org/10.2320/matertrans.M2017045.

[14] C. Qiu, NET-SHAPE HOT ISOSTATIC PRESSING OF A NICKEL-BASED POWDER SUPERALLOY, University of Birmingham, 2010.

[15] H.S. Lee, Diffusion bonding of metal alloys in aerospace and other applications, in: Weld. Join. Aerosp. Mater., 2012: pp. 320–344.

[16] M.A. Ashworth, M.H. Jacobs, S. Davies, Basic mechanisms and interface reactions in HIP diffusion bonding, (2000) 351–358.

[17] B.R. Garrett, G.F. Blank, A.J. Ranadive, Broad Applications of Diffusion Bonding, Washington, 1966.

[18] O.M. Akselsen, Review Diffusion Bonding of Ceramics, J. Mater. Sci. 27 (1992) 569–579. https://doi.org/10.1007/bf02403862.

Chapter 2. Literature Review IN625 and IN625-MMCs

2.1 Introduction

This literature review chapter will provide a review of the fundamental metallurgical aspects of Ni-base superalloys and Ni-base MMCs focusing respectively on the role of each individual element and the effect of reinforcements on the microstructure and mechanical properties of these two classes of materials. The chapter will then focus on reviewing the advantages and limitations of NNS PM HIP material for these two materials.

The objective of this literature review chapter is to understand the current gaps and limitations regarding the HIP behaviour of these materials. This will allow to gain comprehensive knowledge of the current challenges and obtain valuable information that will be used as a baseline for the experimental investigations.

To this end, the literature review on Ni-base superalloys will be focusing on the PPBs formation mechanisms, which represents one of the biggest challenges in PM HIP of these materials. The review will then focus on the proposed strategies to reduce PPBs formation. Since PPBs are strongly related to powder characteristics and quality, a detailed review of various powder atomisation techniques and their impact on powder's chemical and physical properties is proposed.

The second part of the chapter will focus on Ni-base MMCs. The review will target to understand the feasibility of manufacturing Ni-base MMCs through NNS PM HIP and how the addition of ceramic reinforcement affects the final properties of the material. Additionally, the literature review on Ni-base MMCs would aim to understand the most compatible and promising ceramic reinforcement for IN625 matrix.

2.2 Metallurgy of Ni-base Superalloys

Ni-base superalloys represent a wide class of high-temperature alloys having Ni as base material. Ni-base superalloys can be further categorised into three main categories i.e. solid solution, precipitation and oxide dispersion strengthened [1], [2]. Ni-base superalloys in all the cases are characterised by a complex metallurgy with the presence of a γ solid solution phase and the presence of many other elements, responsible for the precipitation of different phases, including γ′, γ″, carbides, oxides and some other detrimental phases such as δ and Laves phase [3]. A list of some of the most common alloys categorised into solid solution, precipitation and oxide dispersion strengthened alloys can be seen in Table 2.1 [1], [2], [4]. A detailed description of the different phases present in Ni-base superalloys will be presented in the next sessions.

Table 2.1 List of commercial Ni-base superalloys.

Solid solution strengthened alloys

Alloy	Composition wt.%										
	Ni	Cr	Co	Mo	W	Nb	Ti	Al	Fe	C	Other
IN625	61.0	21.5	-	9.0	-	3.6	0.2	0.2	2.5	0.05	-
Haynes 214	76.5	16.0	-	-	-	-	-	4.5	3.0	0.13	-
Nimonic 75	75.0	19.5	-	-	-	-	0.4	0.15	2.5	0.12	<0.25 Cu
Hastelloy X	49.0	22.0	<1.5	9.0	0.6	-	-	2.0	15.8	0.15	-

Precipitation hardened alloys

Alloy	Composition wt.%										
	Ni	Cr	Co	Mo	W	Nb	Ti	Al	Fe	C	Other
IN718	52.5	19.0	-	3.0	-	5.1	0.9	0.5	18.5	<0.08	<0.15 Cu
Astroloy	56.5	15.0	15.0	5.25	-	-	3.5	4.4	<0.3	0.06	0.03 B, 0.06 Zr

Waspaloy	57.0	19.5	13.5	4.3	-	-	3.0	1.4	<2.0	0.07	0.006 B, 0.09 Zr
Rene 41	55.0	19.0	11.0	10.0	-	-	3.1	1.5	<0.3	0.09	0.01 B

Oxide dispersion strengthened alloys

Alloy	**Composition wt.%**										
	Ni	**Cr**	**Y_2O_3**	**Mo**	**W**	**Ta**	**Ti**	**Al**	**Fe**	**C**	**Other**
MA754	78.0	20.0	0.6	-	-	-	0.5	0.3	1.0	0.05	-
MA 6000	68.0	15.0	1.1	2	4	2	2.5	4.5	0.72	0.05	0.15 Zr, 0.01 B
PM 3030	67.8	17.0	1.1	2	3.5	2	-	6.6	-	-	-

2.2.1 The γ Phase

The γ matrix in Ni-base superalloys has an austenitic FCC structure. The crystal structure of γ phase is shown in Figure **2.1**. The γ phase is characterised by good mechanical properties, resistance to high temperature due to the low diffusivity of the alloying elements and the possibility of wide solubility in Ni of different alloying elements [5]. In addition, Ni conserves its FCC structure up to the melting point, making Ni-base superalloys stable up to considerable high temperatures.

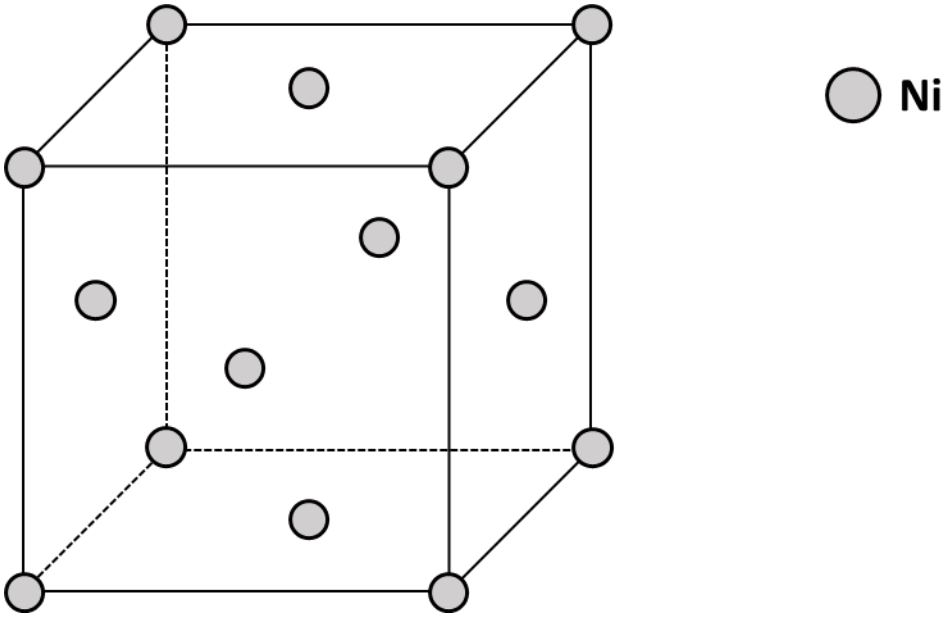

Figure 2.1 FCC structure of γ Ni-phase.

In Ni-base superalloys, the γ phase is strengthened by the solid solution of different elements such as Co, Cr, Fe, Mo, W, Ta and Re. Their role is to increase the strength of the γ matrix by opposing dislocation movement. These elements have similar atomic radii, electron configurations and this is the main reason why they are in solid solution [3], [6]. Jena *et al.* found that the capacity of elements to be present in solid solution is influenced by the deviation of atomic diameter % from that of Ni, through the formula $d_{Ni}[100(d_i-d_{Ni})/d_{Ni}]$, where d_{Ni} represents the atomic radius of the Ni atom, while d_i is the atomic diameter of the alloying element [7]. By plotting the deviation of the atomic diameter against the atomic number, it is possible to draw a diagram to understand which elements are most prone to be in solid solution. Figure **2.2** shows that elements such as Mo, Cr, Fe, V, Co and W are highly favourable to be in solid solution. In particular, in IN625 the main solid solution strengthening elements are Cr, Mo and Fe. Each element has a different role in the metallurgy of IN625 and will be discussed separately.

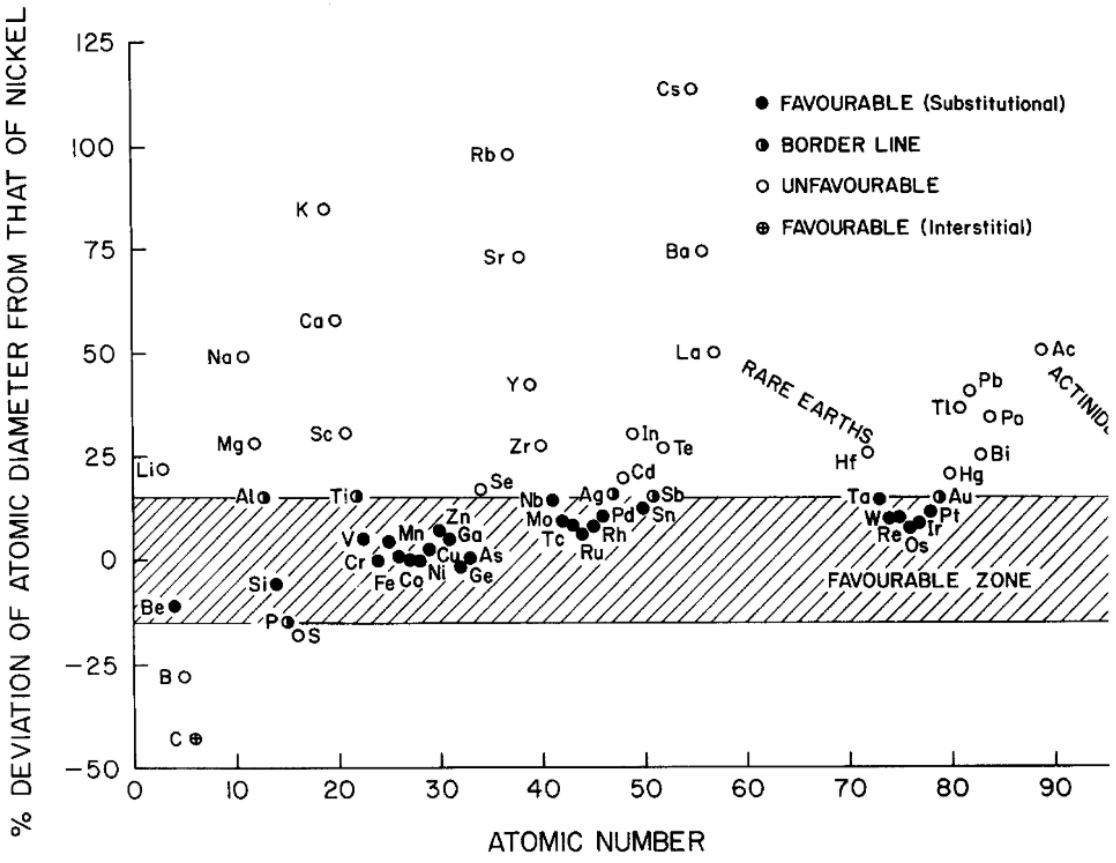

Figure 2.2 Favourable zone for substitutional solid solution in Ni [7].

Chromium

Chromium (Cr) is a key element in Ni-base superalloys metallurgy. Cr has a BCC structure and similar atomic radius if compared to Ni. This will influence both the solid solubility and the strengthening contribution of the element to the γ phase. The maximum solid solubility of Cr in Ni is 47% at the eutectic temperature [3]. The contribution to specific solid solution strengthening for Cr is not elevated due to its similar atomic size to Ni, but a high concentration of Cr can have a noticeable contribution to the γ matrix strength [8], [7]. The main role of Cr in the metallurgy of superalloys is to improve the high-temperature oxidation and corrosion resistance of the material by creating a passive oxide layer (Cr_2O_3) on the surface of the material. However, the presence of the oxide layer is not always considered

beneficial. In fact, the high levels of Cr in IN625, cause the formation of an oxide laver during the powder atomisation process. This oxide laver is responsible for the formation of PPBs with a consequent reduction in ductility, fracture toughness and fatigue life for the material. Cr is also a strong carbide former, and it can precipitate as $Cr_{23}C_6$ carbides during low-temperature heat treatment, which precipitates preferentially at grain boundaries [1], [2]. Cr contributes to the formation of Laves phase together with Fe, Mo, Nb and Si.

Molybdenum

Molybdenum (Mo) is a refractory metal and has a BCC crystal structure. The addition of Mo confers to the alloy some corrosion resistance, similarly to Cr [9]. The main effect of Mo in the metallurgy of Ni-base superalloys is its effect on the solid solution strengthening. In fact, it has a much higher impact if compared to Cr and Fe, thanks to its greater difference in atomic size if compared to Ni (-9%). Mo has a wide solid solubility in Ni (34wt.% at 1000°C), however, the Mo solubility in the matrix is decreased by the addition of other elements such as Cr and Fe [3]. Mo has a beneficial effect on the creep strength of the alloy. Giamei *et al.* reported an improvement in creep life by increasing the Mo levels from 12.8 to 14.3wt% thanks to the low diffusivity of Mo in Ni [3], [10]. MacKay *et al.* found that the optimum creep resistance for a nickel-base alloy was achieved using a concentration of 14wt.% of Mo [11]. Mo can as well precipitate as M_6C type carbide and can substitute Nb to form (Nb, Mo)C carbides. The limitation of Mo in Ni-base superalloys, despite its benefits, can be found in its high density 10.28g/cm^3, higher if compared to the density of 8.90g/cm^3 for Ni.

Iron

Iron (Fe) has a BCC structure at room temperature, transforming into an FCC structure around 900°C. Fe has full solubility in Ni at 1000°C [3], it has the lowest contribution to strength among all the substitutional solid solution elements due to its negligible difference in atomic size with Ni (Table **2.2**) [8]. Similarly to Cr, since Fe has a low specific contribution to strength, its effect on strength becomes effective just if present in high concentrations. One of the main roles of Fe is to induce the precipitation of γ'' in the matrix, in fact, Fe is considered to be a γ'' stabilizer by lowering the solid solubility of the precipitating elements [7], [12], [13]. Fe together with Cr contributes to the formation of the detrimental Laves phase [9], [14].

Table 2.2 Solid solution strengthening coefficients in the γ matrix [8].

	Coefficient	
Element	β_i^{γ} (MPa/at.%$^{1/2}$)	$\beta_i^{\gamma'}$ (MPa/at.%)
Cr	337	11
Co	39.4	
Mo	1015	41.88
W	977	40
Nb	1183	56
Al	225	–
Ti	775	18.3
Ta	1191	78.33
Fe	153	20.78
Hf	1401	159
V	408	
Zr	2359	163.7

2.2.2 γ'' and δ Phases in Ni-based Superalloys

Niobium (Nb) has certainly the most complex role and is one of the most important elements in the metallurgy of Ni-base superalloys. One of the key factors influencing the role of Nb in

superalloys is its low solid solubility in the γ matrix of 2.5wt.%, which can decrease with increasing content of Cr and Mo concentrations [15]. In fact, Nb has the lowest solid solubility in nickel and nickel-chromium alloys if compared to other refractory elements such as Mo, W and Ta, this is attributed to the high atomic mismatch with Ni, about 15%, which is the highest among all the refractory metals [16]. In the Ni-base superalloys with a relatively high concentration of Nb the main strengthening mechanism comes from the precipitation of γ".

γ" (Ni_3Nb) is a metastable DO_{22}-ordered body-centered tetragonal strengthening phase (Figure **2.3**). Since γ" has similar lattice parameters to the γ matrix, it precipitates as coherent very fine disc-shaped particles, and the strengthening effect is caused by the large mismatch strains formed upon the precipitation of γ" [2], [17], [3]. The unit cell of the Do_{22} structure can be observed in Figure **2.3**. The corners of the unit cell are occupied by the Nb atoms (black circles), while the shaded circles represent the Ni atoms [18].

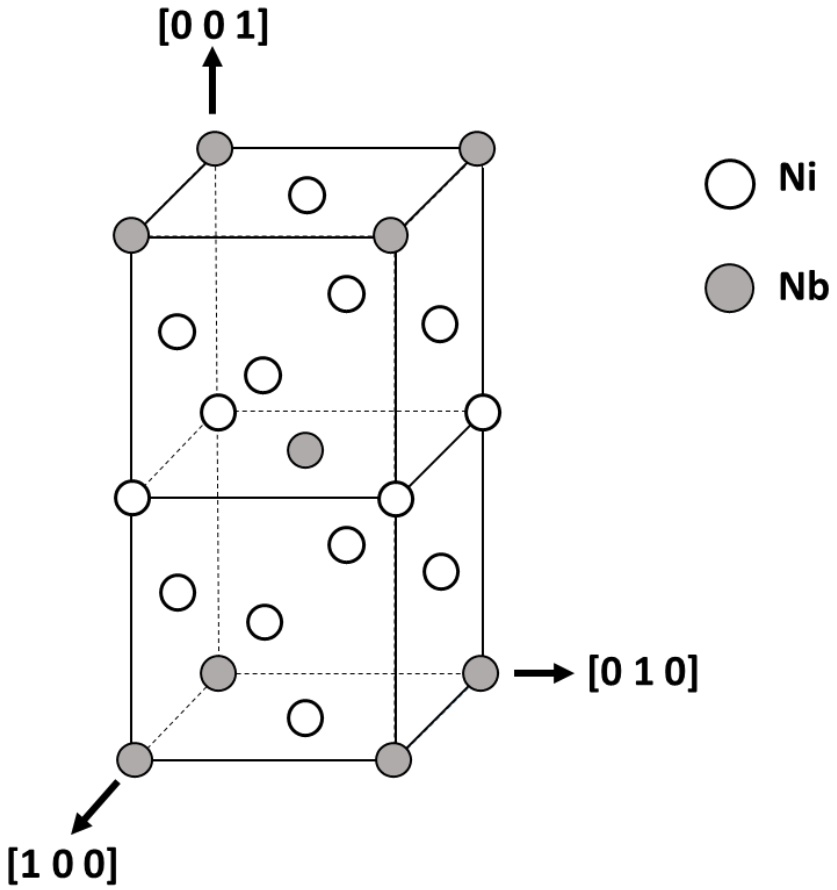

Figure 2.3 Schematic representation of γ" crystallographic structure.

γ" strengthening phase is normally stable up to 650°C, above this temperature, it starts to transform into the more stable δ phase with a consequent loss in strength [19]. Meaning that γ" phase provides precipitation strengthening up to 650°C, which limits the high-temperature applications of γ" nickel-base superalloys if compared to γ' alloys [20].

δ is a stable phase with the same chemical composition of γ" (Ni_3Nb), but with a Cu_3Ti-ordered orthorhombic structure (Figure **2.4**), it can precipitate as a fine needle, plate or globular shape [21]. The δ phase is incoherent with the γ matrix, and thus it does not confer strength to the alloy, and it was reported to be detrimental to creep ductility and fracture toughness [22]. It starts forming at the expense of γ" when the material is exposed to a temperature higher than 650°C and up to 980°C. However, if the material is exposed to

temperatures higher than 800°C, the δ phase will directly precipitate from the γ matrix [23]. In the work of Sundararaman *et al.*, a small volume fraction of the δ phase was observed in IN625 when exposing the material to a temperature above 750°C. However, δ started to precipitate after long ageing at that temperature. It was also found that increasing the temperature to 800°C would promote a much higher level of δ precipitation both at the grain boundaries and within grains [23]. It was furthermore observed that the presence of γ'' was very weak after the heat treatment at 800°C. The solvus temperature for δ phase is around 1000°C it was demonstrated that if the material is exposed to a solution treatment of 1025°C on the final microstructure of IN625 and IN718 was free from δ phase [23].

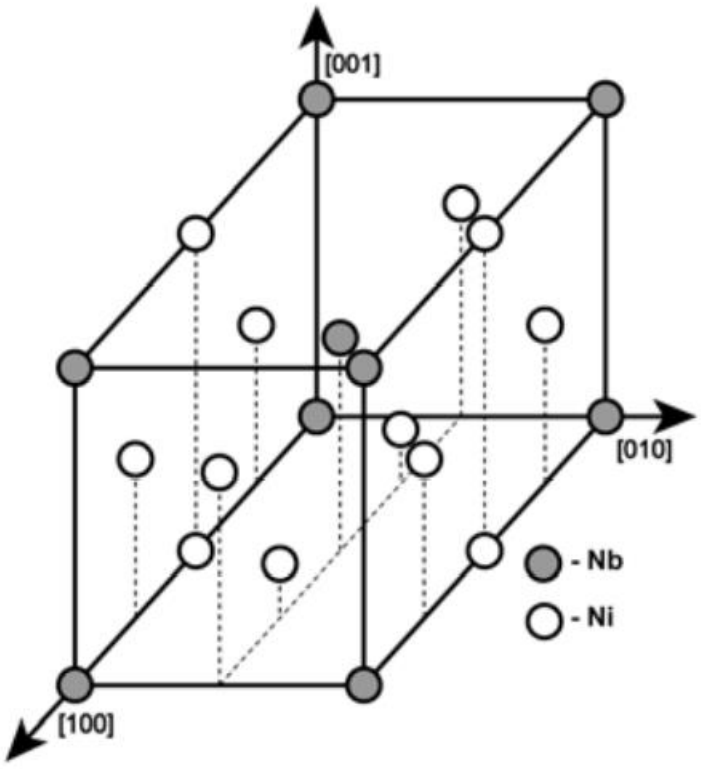

Figure 2.4 Unit cell representation of the δ phase.

The precipitation range for γ" was identified in the range between 550-900°C in IN718. It can precipitate in the range between 550-660°C using a long time ageing, while in the range 700-900°C, γ" precipitates using a short time ageing. However, in the high-temperature ageing, γ" transforms to δ phase as discussed above [24].

One of the main characteristics of γ" is its sluggish reaction which makes the γ"-strengthened alloys more suitable for welding and 3D printing, preventing crack formation if compared to γ'-strengthened superalloys [25].

Since γ" is rich in Nb, its precipitation and volume fraction is influenced by the presence of other Nb-rich phases. In fact, it was observed that in regions where there is a strong presence of NbC, the local composition of the alloy was poor in Nb, meaning that the precipitation of γ" will be unlikely to happen, leading to uneven precipitation of γ" [26]. Thus, it is crucial to reduce the levels of C in the alloy in order to increase the precipitation of γ".

2.2.3 γ' in Ni-based Superalloys

The γ' phase Ni_3(Al, Ti) has a $L1_2$ FCC crystal structure with the presence of Al or Ti atoms at the corners of the cube as reported in Figure **2.5**a [2], [3]. γ' phase initially precipitates as spherical-shaped particles, however as the heat treatment progresses it will transform into cuboidal precipitates Figure **2.5**b [27]. The γ' phase is the principal strengthening phase of several Ni-base superalloys [6], due to its increase in strength up to approximately 800°C and enhanced creep resistance [3].

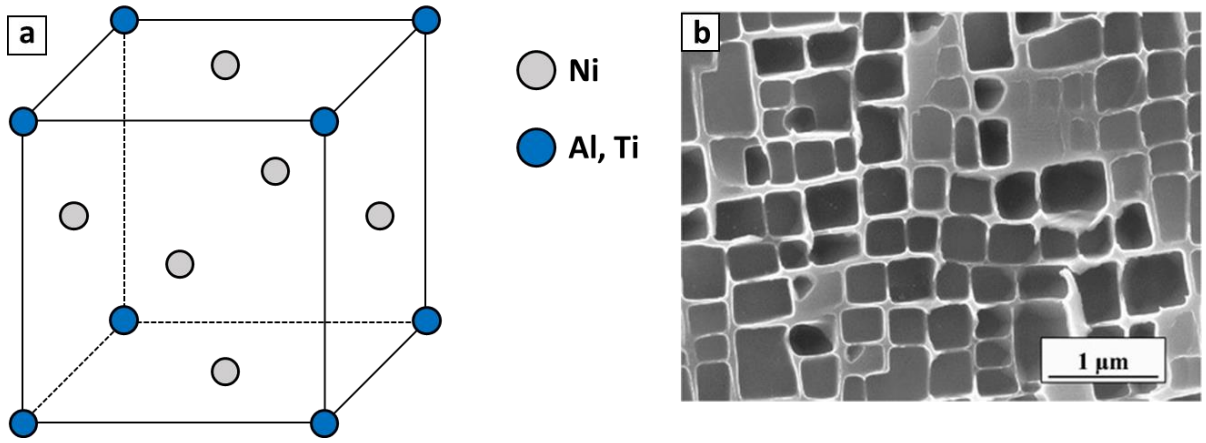

Figure 2.5 Schematic representation of γ' crystallographic structure (a); microstructure of CMSX-4 Ni-base superalloy highlighting the presence of cuboidal γ' precipitates [27].

2.2.4 Laves Phase in Ni-base Superalloys

Laves is a very complex phase, in fact, it can have different compositions depending on the elements present in the alloy, their compositions and thermal history. Table **2.3** summarises different compositions for Laves phase in IN625 using different processing histories [9]. Laves can be dissolved into the matrix using a solution heat treatment at a temperature between 1170-1180°C [28]. Sohrabi *et al.*, reported that dissolution of Laves phase can happen at lower temperatures exposing the material to a homogenisation heat treatment for a long time [29]. The presence of a relatively high fraction of Laves contributes to the weakening of the γ-matrix by depleting it from the solid solution elements such as Nb, Cr, Fe [14], [20]. Furthermore, Laves is associated with a loss of ductility and above all, with a sharp reduction in fracture toughness [14]. The thermal processing of the alloys represents another important aspect of Laves formation. In particular, the cooling rates have an important impact on the formation of secondary phases such as carbides or Laves phases in IN625. The study carried out by Tinoco *et al.* showed that the solute segregation in IN625 is strongly dependent on the cooling rates. Low cooling rates promote segregation while

increasing the cooling rate has a positive effect on reducing the segregation of the solute elements i.e. Nb, Cr, Mo and Fe [30].

Table 2.3 Composition of Laves phase from different Alloy625 materials [9].

Element	Banded Plate Stock	Base Plate Heat Treated 48h at 1600°F	6 Inch GTA Weldment	GTA Welds [31]	Three Weld Processes [32]
Ni	38	41	48	45.6 - 48.2	20.3 - 40.5
Cr	17	20	22	13.6 - 15.6	12.4 - 18.3
Mo	23	21	12	17.6 - 19.8	13.6 - 18.6
Nb	19	6	11	16.8 - 19.2	12.2- 27.5
Fe	3	5	3	0.9 - 1.4	6.9 - 12.9
Si	6	6	4	0 - 2.2	6.1 - 9.7

2.2.5 Carbides, Nitrides and Oxides in Ni-base Superalloys

Carbides

The role of carbides in nickel-based superalloys is extremely difficult to understand. The influence of carbides on the mechanical properties is highly dependent on their type, size, location and distribution [19]. Three main carbide types can precipitate in Ni-base superalloys, including MC, M_6C and $M_{23}C_6$. Carbides in Ni-base superalloys form by the interaction of some solute elements such as Nb, Ti, Cr, Hf and Mo with carbon to form (Nb, Mo)C, TiC, HfC and $Cr_{23}C_6$ [9],[1]. The presence of carbides in Ni-base superalloys provides some indirect grain boundary strengthening via grain pinning and enhances creep properties [2]. However, it is known that the presence of carbides reduces the fracture toughness of the material and continuous precipitation at grain boundaries transform the fracture mode from

transgranular to intergranular, reducing the ductility of the material [26], [33]. Carbide formation is dependent on the heat treatment/service temperature. MC carbides are the first carbides forming upon solidification, they have FCC structure and can appear in coarse or globular forms, the latter is linked with good ductility, while the presence of coarse carbides adversely affects the mechanical properties [25]. The preferred order of formation for MC carbides in Ni-base superalloys is HfC, TaC, NbC, TiC [19]. In nickel-based superalloys, the most common form of carbide present is MC type carbide, thus NbC carbide for IN625, with the possibility of Mo to substitute Nb, forming (Nb, Mo)C [1]. MC carbides are found evenly distributed within the grains but can also be found at grain boundaries [1], [25]. MC carbides are stable at higher temperatures (>1038°C). However, they can decompose to form M_6C and $M_{23}C_6$ carbides at lower temperatures [33]. M_6C carbides have an FCC structure, they are rich in Mo, with the possibility of the presence of Ni, Cr and Nb in solution [1], while $M_{23}C_6$ carbides also have a FCC structure where M is rich in Cr with the possibility for Ni and Fe to substitute [19].

Carbides have an important role in the stability of the γ phase, they can deplete solute elements such as Nb, Ti, Mo or Cr from the matrix [19], [26]. They also have an important role in the precipitation of the strengthening phases. In fact, Sundararaman *et al.* observed γ" precipitation-free zones at grain boundary in the proximity of NbC presence [26].

Carbide precipitation size, location and type are strongly dependent on the chemistry of the alloy. A high concentration of Nb favourites the precipitation of NbC carbides [9]. Silicon is believed to have an effect of retarding the precipitation of carbides in alloys with low carbon contents. Furthermore, it was noted that M_6C in IN625 has 5% of Si, meaning that Si could potentially promote the nucleation of M_6C in IN625 [34]. Depending on the elemental composition of the alloy, different types of carbides can precipitate. Figure **2.6** shows the

Ellingham diagrams for the second and third transition metal carbides [35]. Albeit the carbide with the lowest Gibbs free energy of formation is Nb_2C, however, in Ni-base superalloys, it was observed that NbC is more favourable to form [36].

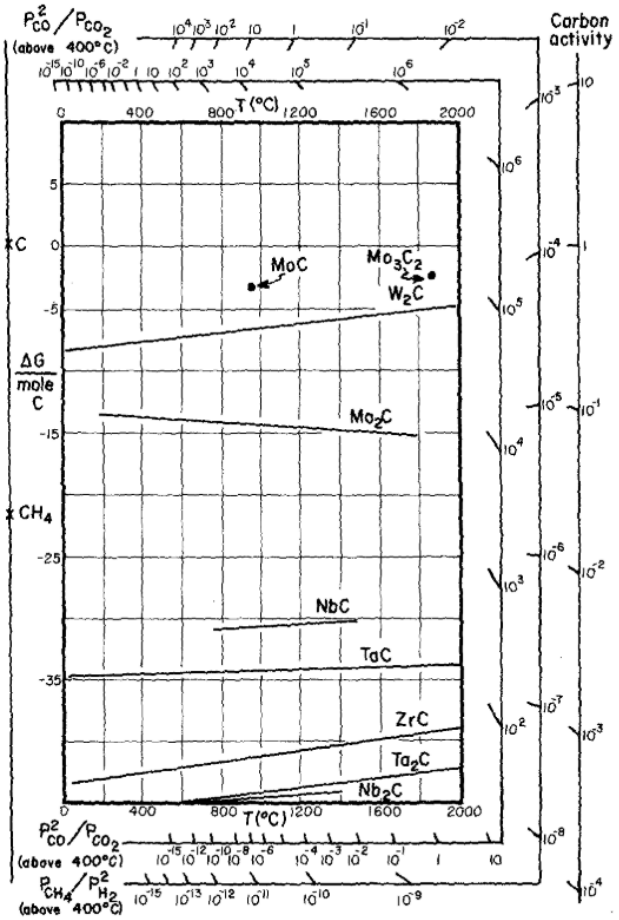

Figure 2.6 Ellingham diagrams for the second and third transition metal carbides [35].

The role of carbides is often liked with the manufacturing process. For example, carbides adversely influence the elongation and fracture toughness of PM HIPed parts due to the precipitation of a continuous network of MC-type carbides precipitation at PPBs [37]. These carbides are often very stable, thus, it is very difficult to dissolve into the γ matrix [9]. R.H.U. Khan *et al.* used differential scanning calorimetry (DSC) technique to understand the solution temperature of different phases in IN718 after PM HIP. They found that the dissolution

temperature of NbC in the matrix is 1280°C, which is close to the solidus of IN718 [28]. Due to the limiting role of carbides on the mechanical properties of PM HIPed parts, alloys with lower carbon levels are often chosen to reduce the detrimental effect of the formation of a continuous network at PPBs [33].

Nitrides

Different types of nitrides can be present in nickel-based superalloys. The most common are TiN, HfN and NbN due to the high affinity of Nb, Ti and Hf to N [38]. Due to the limited solubility of nitrogen in the γ matrix [39], nitrides readily precipitate during solidification and act as precipitation sites for MC carbides [19]. In fact, nitrides play a crucial role in carbides precipitation, and in order to reduce the primary carbide precipitation in superalloys, reduced levels of nitrogen are required [40]. Similar to carbides, nitrides have very high dissolution temperatures, and it is not possible to dissolve them at temperatures below the melting point [1].

Carbonitrides can be found in alloys with relatively high levels of N. In fact, nitrogen can replace some of the carbon atoms in MC-type carbides, by forming M(C, N) carbonitrides where M can be Nb, Mo or W [1], [3].

Oxides

Oxides play an important role in the metallurgy of Ni-base superalloys. In particular, for IN625 the presence of Cr_2O_3 is important for its oxidation and corrosion resistance by forming a protective oxide layer. However, oxides in Ni-base superalloys are also used as strengthening media, to form the so-called oxide-dispersion-strengthened (ODS) superalloys. In this case, Al_2O_3 and Y_2O_3 are normally used to act as strengtheners [19]. Oxides are believed to act as precipitation sites for MC carbides, this phenomenon has a great impact on

the microstructural and mechanical properties in PM HIP and will be discussed in detail in later sections [41].

2.2.6 Metallurgy of IN625

IN625 is a solid solution strengthened nickel-based superalloy, mainly strengthened by the addition of Cr, Mo and Fe [9], [42] (Table **2.4**). It is intensively used in marine, aerospace and nuclear sectors due to its high-temperature strength and corrosion resistance. Although it was originally designed as a solid solution strengthened material, it was observed the precipitation of the ordered body-centered tetragonal γ'' (Ni_3Nb) if the material is exposed for long time at a temperature in the range 600-760°C [9]. Furthermore, IN625 is characterised by the precipitation of MC, M_6C and $M_{23}C_6$ carbides. Other detrimental phases can also be observed in the alloy. Those phases are δ (Ni_3Nb) which has an orthorhombic structure [43] and Laves phase which has a hexagonal closed-packed A_2B structure, where A is represented by Ni, Cr, Fe and B by Nb, Si, Ti and Mo [9]. Other elements are present in IN625 such as Al, Ti and Si, which are added for refining purposes [9]. If in enough quantity, Al and Ti (>0.5wt%) can lead to the precipitation of the ordered fcc γ' ($Ni_3(Ti,Al)$) [43].

Table 2.4 Chemical composition IN625 [9].

Ni	Cr	Fe	Mo	Nb	C	Mn	Si	Al	Ti
58.0 min	20.0 - 23.0	5.0 max	8.0-10.0	3.15 - 4.15	0.10 max	0.50 max	0.50 max	0.40 max	0.40 max

As reported in Table **2.4** the main alloying elements are Cr and Mo. The addition of Cr and Mo confer to the alloy an excellent oxidation and corrosion resistance [9]. The addition of Cr and Mo provides some solid solution strengthening to the alloy [8]. Another important effect of Cr and Mo is to decrease the solid solubility of the reactive elements such as Nb, Ti and Al

in the γ matrix, encouraging the precipitation hardening of the material [15]. In particular, Cr provides also high-temperature oxidation resistance by creating a protective oxide layer on the outer surface of the material [1]. Furthermore, Cr plays an active role in the formation of Laves phases. In addition, Cr contributes to the formation of $Cr_{23}C_6$ during lower temperature heat treatment [1].

Fe is mainly added to the alloy for improving the solid solution strengthening. It has been found however that Fe and Co accelerate the precipitation of γ" phase [13]. Fe is directly linked with the formation of Laves phase, in fact it has been found that higher levels of Fe promote the formation of Laves phase during solidification [9], [14].

Nb in IN625 can precipitate different phases such as the coherent metastable γ" phase and the incoherent stable δ phase. As discussed above, Nb is one of the strongest carbide formers as demonstrated in Figure **2.6**. It was noted that Nb does not have much influence on the strength of IN625 alloy for levels of Nb lower than 2wt%. If the concentration of Nb is increased to 3wt.%, there is an increase in strength after ageing, this because the solid solubility limit of Nb in IN625 is 2.5wt.% [15] (Figure **2.7**).

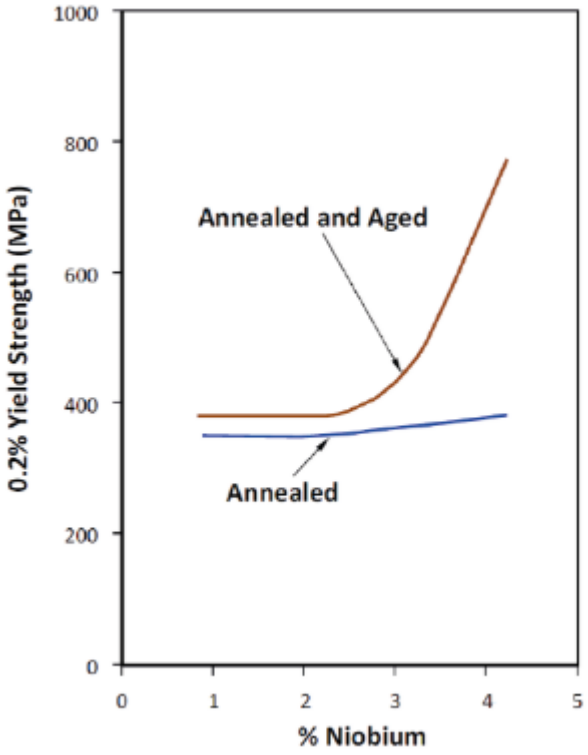

Figure 2.7 The effect of Nb on the 0.2% Yield Strength of Alloy625 [15] (original graph edited by Rupert Wickens).

Some other elements, such as Al and Ti are also present in the alloy. The maximum solid solubility of Al in the alloy is 0.5%. Al and Ti are kept low in order to reduce the age hardenability of the alloy. However, a low presence of these elements (around 0.2%) has proven to be beneficial for creep properties. An additional reason for maintaining the Al and Ti low is because low levels of these elements enhance the weldability of the alloy [15]. Ti also influences the precipitation of γ" during ageing at 650°C, in fact, higher concentrations of Ti promotes γ" precipitation, while Al has little or no effect on the precipitation of γ" (Figure **2.8)** [9].

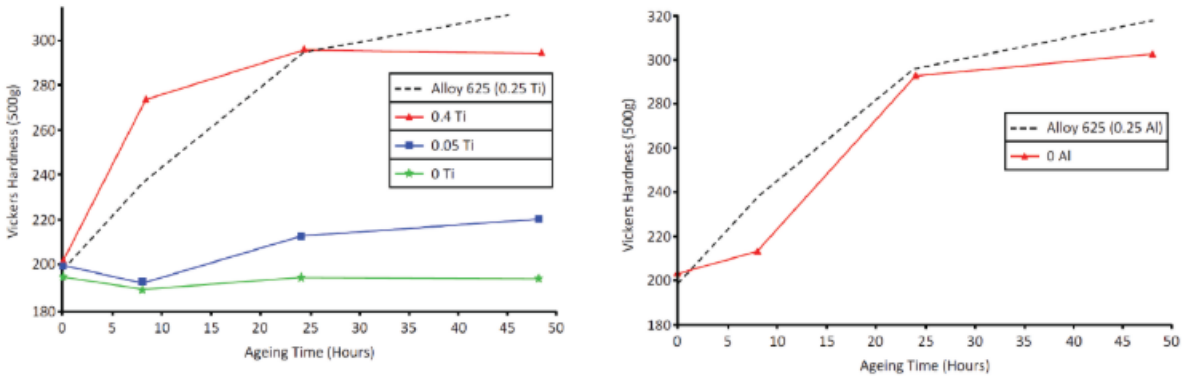

Figure 2.8 Effect of Ti and Al addition on the ageing hardenability of IN625 at 650°C [9] (original graph edited by Rupert Wickens).

The influence of minor elements such as Si and C on the solidification behaviour of the IN625 was investigated by Cieslak et.al. [42]. The high levels of C promote the formation of NbC at the expense of Laves phase, while the presence of high levels of Si promotes the formation of Laves phase and M_6C type carbides [9], [14], [44].

A summary of the influence of each element on the properties and phase precipitation, based on the information available in the literature is given in Table **2.5** [9], [15], [45].

Table 2.5 Influence of different elements on the phase formation and properties for IN625 alloy.

	Phase Formation			Properties			
Elements ↑	γ′/γ″	δ and Laves	Carbides	Strength	Ductility	Corrosion Resistance	Creep Resistance
Cr	-	↑	↑	↑	↓	↑	-
Mo	-	↑	↑	↑	↓	↑	-
Fe	-	↑	-	↑	-	-	-
Nb	↑	↑	↑	↑	↓	-	↑
Al	↑	-	-	-	-	-	↑
Ti	↑	-	↑	-	-	-	↑
C	-	-	↑	↑	↓	-	↑
Si	-	↑	-	-	↓	-	-
N	-	-	↑	-	↓	↑	-
O	-	↑	↑	↑	↓	-	-

2.3 HIP consolidation mechanisms

As described above, the densification during HIP evolves via three different mechanisms, respectively plastic collapse, creep and diffusion. Plastic collapse represents the most significant densification mechanism in PM HIP, accounting for an increase in relative density up to 90% or above, depending on the material and the initial powder packing density [46]. The main parameter influencing the yield collapse is the applied pressure. For this reason, is crucial that the gas pressure in the HIP chamber is high enough to guarantee the plastic yield of the material. Values for the gas pressure conventionally used range from 100-200MPa, depending on the characteristics of the material to be HIPed. Temperature plays as well an important role in the plastic collapse densification mechanism by lowering the yield strength and thus allowing an increase in plastic deformations.

At higher temperatures above $0.6T_m$, and with the application of the pressure, the consolidation process evolves via creep. Once the pressure and temperature reach a constant value during the dwell period, the contribution of plastic collapse ceases to influence the densification. However, particle plastic deformation is still happening due to the effect of creep deformation. In fact, creep is defined as the plastic deformation of a body under a constant load at high temperatures [47]. When creep takes place, the material deforms under loads that would not lead to plastic collapse. This can be attributed to dislocation and diffusion creep, respectively. Dislocation creep is strongly dependent on the applied stress, thus is remarkable in HIP because of the large stresses involved in the process. The process of dislocation creep is linked with the diffusion of atoms, which facilitates the dislocation climbing and consequently induces plastic deformation [47]. The law governing the dislocation creep is represented by *Eq. 2.1* [47]:

$$\dot{\varepsilon}_{ss} = A\sigma^{n} e^{-Q/RT} \qquad \textit{Eq. 2.1}$$

The dependence of the stress in *Eq. 2.1* is directly related to the climbing force component $\tau \tan\theta$ (Figure **2.9**).

Where:

$\dot{\varepsilon}_{ss}$= strain rate [s^{-1}]

A = pre-exponential constant

σ = differential stress [MPa]

Q = activation energy [$kJ \cdot mol^{-1} \cdot K^{-1}$]

R = universal gas constant 8.315 [$kJ \cdot mol^{-1}$]

T = temperature [K]

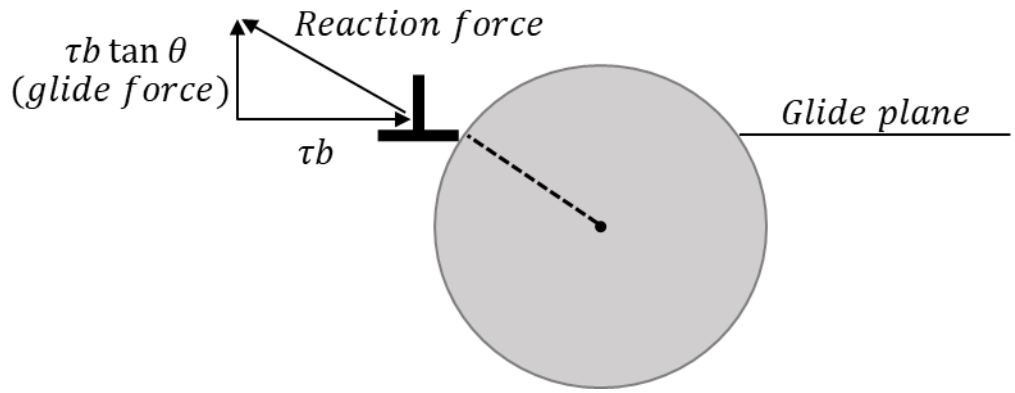

Figure 2.9 Schematic representing dislocation gliding [47].

The other creep mechanism is the diffusion one, which is also triggered by stress levels. In fact, when a grain is subjected to a stress level, it accelerates the diffusion of grain boundary atoms from the direction parallel to the applied stress to a direction perpendicular to it inducing a grain elongation and consequently deformations (Figure **2.10**). Diffusion creep depends on the applied stress, diffusion coefficient, temperature and grain size and can be represented by *Eq. 2.2* [47]:

$$\dot{\varepsilon}_{ss} = C\frac{D\sigma}{d^2} = \frac{C'\sigma e^{-Q/RT}}{d^2} \qquad \textit{Eq. 2.2}$$

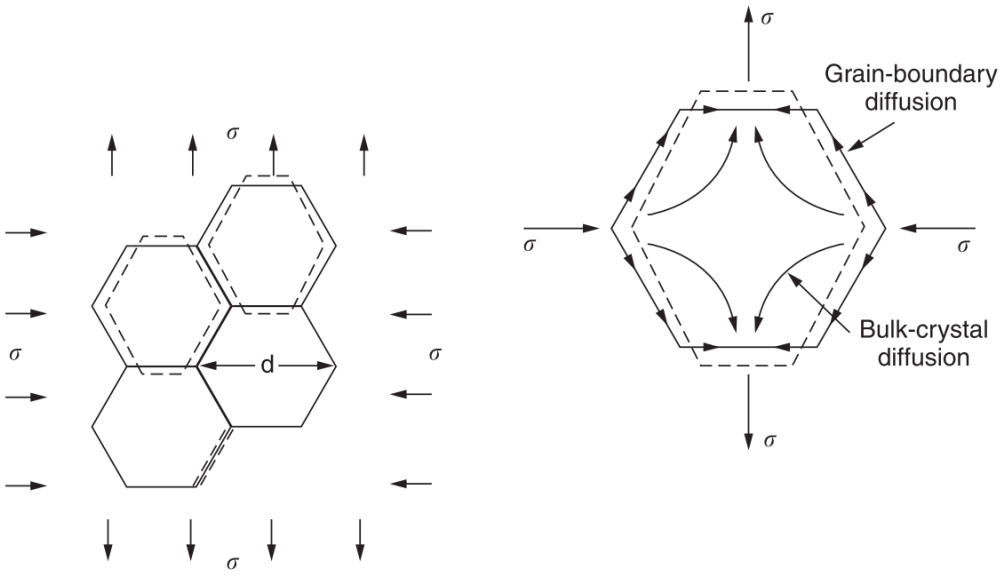

Figure 2.10 Schematic representation of diffusion creep [47].

2.4 NNS PM HIP of Ni-based Superalloys

As described above, Ni-base superalloys are characterised by a complex microstructure due to the presence of many elements and the formation of different phases. Thus, the effect of utilising a non-conventional manufacturing process such as PM HIP on the microstructure

and the properties of Ni-base superalloys should be carefully assessed. In the research domain, many studies investigated the as-HIP response of Ni-base superalloys. It is reported that PM HIP is capable of producing components with similar mechanical properties if compared to the conventional manufacturing process such as casting-forging. In particular, the work of G. Rao *et al.*, demonstrated that the HIPed mechanical properties for IN718 alloy are comparable to wrought IN718 [48]. Dugdale *et al.*, showed as well that as-HIPed mechanical properties for IN625 are similar or superior to wrought IN625 [49].

Thus, NNS PM HIP can represent a valid manufacturing process for the manufacture of Ni-base superalloys components owing a lower material wastage and reducing the amount of machining, which could be particularly challenging for Ni-base superalloys [3].

However, one of the limiting factors in the application of the NNS PM HIP technique to Ni-base superalloys is the presence of PPBs. In the following sections, a detailed review of PPBs in Ni-base superalloys will be presented.

2.5 PPBs in nickel-based superalloys

2.5.1 Understanding of PPBs formation

One of the major concerns regarding HIP of nickel-based superalloys is represented by the presence of precipitates at prior particle boundaries (PPBs). These precipitates can be oxides, carbides or oxycarbides. The presence of precipitates at the PPBs influences the densification of the material, tensile properties, fatigue life and fracture toughness. It has been demonstrated in different works that PPBs reduce the inter-particle bonding, thus dramatically reducing the elongation to failure and fracture toughness [50–52].

In order to mitigate this preferential precipitation process, it is crucial to understand how these precipitates are generated and how HIP parameters influence the precipitation mechanisms. It is reported in the literature that the generation of PPBs has its origin during the atomisation process, where a thin oxide layer is formed [53]. This statement is clearly supported by different works, where the presence of a thin oxide layer at the surface of the powder of different alloys is detected via X-ray photoelectron spectroscopy (XPS) [54], [55], [56], [57]. In particular, the work of Z. Gao *et al.* highlights the presence of high concentrations of O and C on the surface of FGH96 Ni-base superalloy. O and C detected on the surface of the powder, coexist with some reactive elements such as Al, Ti, Zr and Cr, forming carbides and oxides during the atomisation process. The presence of O and C is drastically reduced at 50nm from the surface [54] (Figure **2.11**).

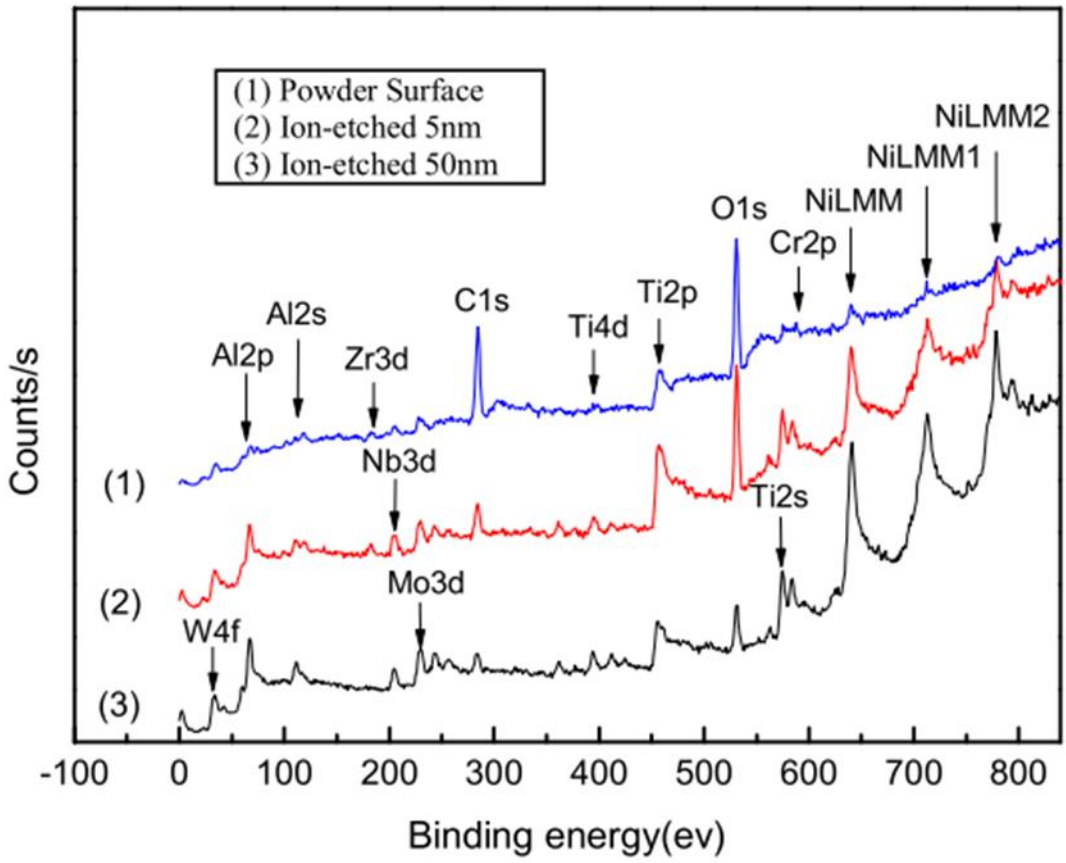

Figure 2.11 XPS analysis on the surface of AGA FGH96 superalloy at the surface of the powder, 5nm and 50nm [54].

The generation of carbides at PPBs is explained by Gessinger [25]. He is stating that if the alloy does not have enough carbide formers, free carbon will diffuse to the free surface of the powder generating carbides. However, there are different theories and hypotheses regarding the precipitation of carbides at the PPBs. One of the strongest hypotheses found in literature is that oxides generated during the atomisation process act as precipitation sites for carbides during the early stages of the HIPing process [48], [58], [59].

However, Crompton showed the existence of some ZrO_2 acting as nucleation site for MC carbides, but also many other carbides were not coexisting with the oxides, suggesting a random rather than a preferential nucleation site for carbides [59].

2.5.2 How to reduce PPBs formation

Different studies have focused on the reduction or elimination of precipitates at PPBs. There are different approaches used in literature. The most commonly used approach is represented by post HIP heat treatment. Trying to dissolve carbides and oxides through heat treatment is revealed to be challenging. That is because these carbides and oxides are stable up to very high temperatures. For example, in the case of IN625, NbC is the main carbide present, and its solution temperature is 1270°C in IN718 [48], which is very close to IN625 solidus (1252-1304°C) [60]. The approach of using HIP temperature above solidus was used by Chang *et al.*, in their work, PPBs were eliminated by using a HIP temperature of 1275°C on IN718 [52]. However, this contributed to abnormal grain growth (Figure **2.12**).

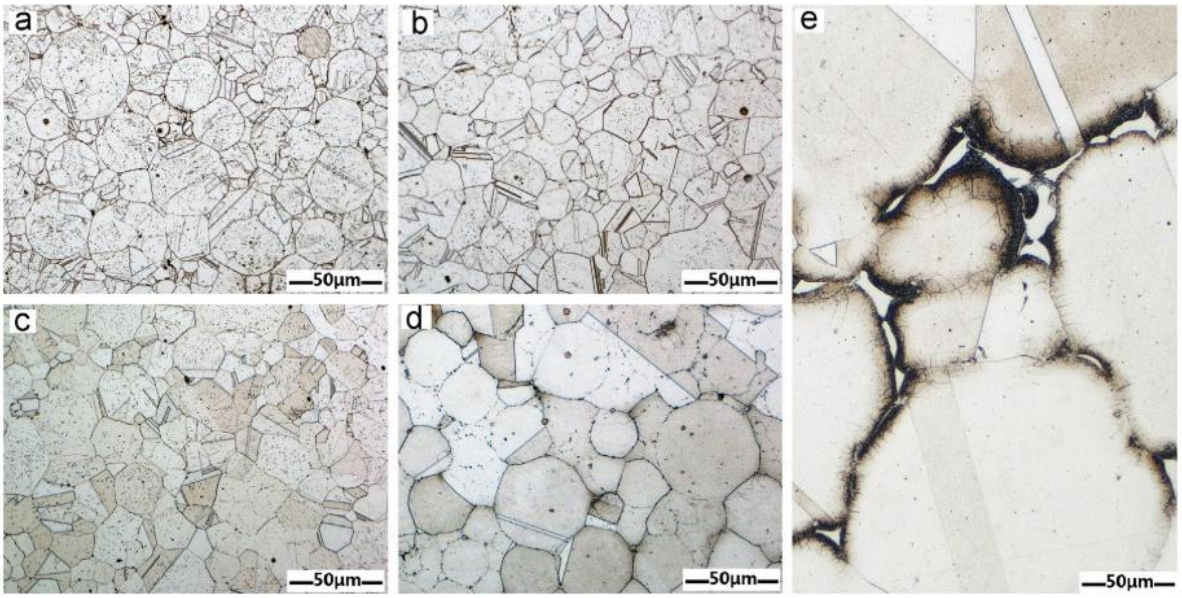

Figure 2.12 Optical micrographs on IN718 HIPed at a) 1140°C, b) 1180°C, c) 1210°C, d) 1260°C and e)1275°C [8].

A similar approach was previously used by Macdonald *et al.* by HIP CM247 above γ' solvus temperature. The use of coarse powders, together with the super-solvus HIP temperature was responsible for reducing PPBs and consequently increasing the elongation to fracture of the as-HIPed material [51].

Another suggested approach is to include in the alloy some strong carbide formers such as Hf and Zr (Table 2.6) [25]. By doing so, carbon will not diffuse on the surface of the powder, and it will rather create some carbides inside the powder. Bigger powders should be used when possible in order to reduce the surface to volume ratio and, thus the oxygen contamination [53]. Another reason for using bigger particles stands in the fact that it is easier to make the grains grow past the PPBs during HIP or post HIP heat treatment [51]. Another successful strategy to reduce the precipitation at PPBs is to improve the powder quality. It is known that reducing the oxygen level helps to mitigate the PPBs, and as well is reported that reducing the carbon content can reduce the formation of carbides and thus its precipitation at PPBs [61].

Table 2.6 Standard free energy formation of carbides [25].

Carbide	Energy of formation at 1700 K (kcal mol-1)
Mo_2C	-14.7
Cr23C6	-20
NbC	-32.2
TiC	-39.1
ZrC	-44.2
HfC	-50.9

2.5.3 HIP of IN625

Based on the abovementioned description of PPBs, it is expected to find their presence in IN625 as a result of PM HIP of IN625. The existence of PPBs in IN625 should be predominantly linked with the presence of Cr, Nb and Mo, but as well with other elements present in a much lower fraction such as Ti, Al and Si. To have an understanding of the formation of PPBs in IN625, the formation of carbides and oxides should be investigated. In

the case of IN625, there are different strong carbide formers. In order to understand which type of carbides can be formed, it is useful to check the free energy formation of the carbides [25].

Since IN625 is rich in Cr, Nb and Mo it is expected to form NbC, Mo_2C and $Cr_{23}C_6$ carbides. However, since Cr has a strong affinity to oxygen it will be most favorable for Cr to form the Cr_2O_3 rather than $Cr_{23}C_6$. Not just Cr_2O_3, but also other oxides can form on the surface of IN625. The study from S. Feng *et al.*, analysed the Gibbs free energy of formation for different oxides during the atomisation process for FGH96 superalloy [62]. According to their study, Al has the greatest affinity to oxygen, followed respectively by Ti, Nb, Cr, Mo. Thus, due to the low presence of Al and Ti in IN625, we would expect the presence of Nb, Cr and Mo carbides and Cr, Nb and Mo rich oxides.

Different studies have been published on the HIP response of IN625. Many papers focused their attention on HIP as post-processing heat treatment after L-PBF process to homogenise the microstructure, obtain isotropic microstructure, increase densification and reduce the interdendritic segregation [63], [64]. On the other hand, not many works have been published on the PM HIP behaviour of IN625 powders. Dugdale *et al.* HIPed IN625 powders using a temperature of 1160°C, pressure of 103MPa with 4h holding time. The HIPed samples were then subjected to a heat treatment at 900°C for 1h per inch of material [65]. Berglund *et al.* used a similar HIP temperature of 1150°C, pressure of 100MPa for 3h [66]. Finally, a lower HIP temperature of 1100°C with a pressure of 110MPa for 3h was used by Wang *et al.* [67]. To understand the influence of powder characteristics on the HIP response, the powder's chemical composition of the three studies was compared. For all of them, the main elements are within the requirements. However, for Wang *et al.* the levels of O and N are far above the requirements for IN625. In the work of Dugdale *et al.*, there is a slightly

higher level of oxygen if compared with the requirements, while the chemical analyses reported by Berglund are in line with the requirements (Table 2.7).

The presence of high levels of O and N in the works of Wang *et al.* are responsible for the formation of oxynitridrides at the PPBs. A similar microstructure, characterised by the presence of oxides, carbides and nitrides was observed by Berglund *et al.*, despite the low levels of interstitials. In fact, it was observed that most of the O is concentrated on the surface of the powders, promoting the formation of PPBs as reported in the previous paragraphs.

Table 2.7 Comparison of IN625 chemical composition for AMS requirements and the work of Dugdale, Berglund and Wang. *Chemical composition is referred to the as-HIPed material.

Elements	C	O	N	Cr	Fe	Cu	Mn	Mo	Ni	P	S	Si	Nb	Al	Ti	Co
Required [68]	<0.10	<0.02	<0.02	20.0-23.0	≤5.0	<0.50	<0.50	8.0-10.0	Bal ≥58	<0.015	<0.015	<0.50	3.15-4.15	0.1-0.4	0.1-0.4	≤1.0
Dugdale et al.*	0.026	0.027	0.009	22.27	1.82	0.005	0.001	9.63	62.21	0.008	0.001	0.085	3.77	/	/	0.09
Berglund et al.*	0.007	0.009	0.007	21.14	1	/	/	8.99	Bal.	0.003	0.002	0.02	3.55	0.21	0.22	/
Wang et al.	0.01	0.08	0.12	21.5	0.96	/	0.47	8.8	Bal.	/	/	0.41	3.71	0.02	0.03	/

The room temperature tensile properties reflect how important are the levels of interstitials on the HIP response of IN625. This is confirmed by the high levels of YS experienced by Wang *et al.*, which can be directly related to the strong precipitation of oxides and nitrides, while the levels of elongation are below the requirements because of the strong formation of PPBs and consequently the presence of an inter-particle fracture mode. The level of YS, UTS and elongation for Dugdale and Berglund are above the requirements for wrought IN625 [69] (Figure 2.13).

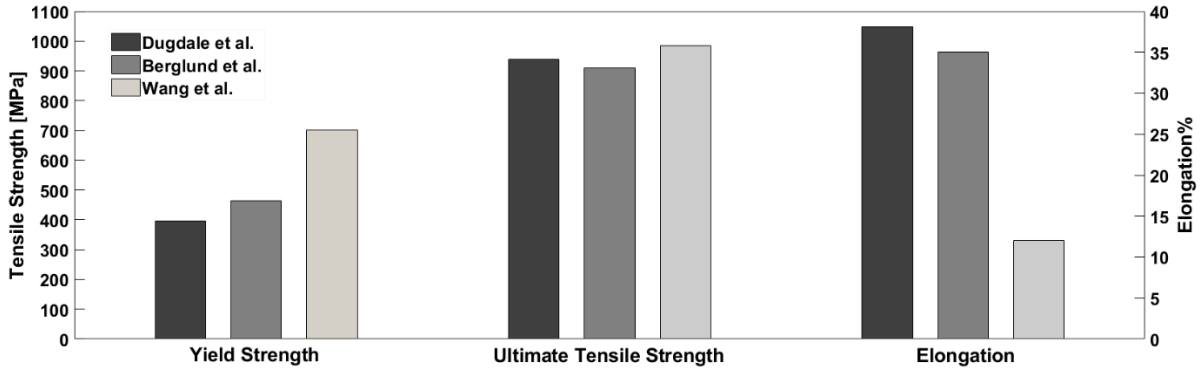

Figure 2.13 Comparison of room temperature tensile properties for as-HIPed IN625 for the work of Dugdale et al., Berglund *et al*, and Wang *et al*.

The comparison of three different works carried out on PM HIP of IN625 has outlined the variability in performances caused by the difference in chemical composition, in particular by the difference in the interstitials levels at the powder's surface, which can readily react with Cr, Nb, Mo, Al and Ti to form a continuous network of oxides, carbides and nitrides at PPBs. However, limiting the level of interstitials can lead to excellent mechanical properties, well above the minimum specification for wrought IN625, as reported by the works of Dugdale *et al.* and Berglund *et al.* [65], [66].

2.6 Powder Atomisation

As highlighted in the previous section of this literature review chapter, the presence of PPBs and consequently the mechanical properties of as-HIPed Ni-base superalloys are strongly affected by the powder quality. Thus, an investigation of different atomisation routes is proposed below to understand the main fundamental differences across different atomisation techniques.

In powder metallurgy, atomisation is defined as a process capable of breaking the molten metal into small droplets. Normally the size of atomised powders can vary from the

nanoscale, up to 1mm [70]. The powder characteristics are governed by the atomisation type used and by the process parameter adopted. Depending on the application, different powder characteristics are required with different specifications. The most widely used atomisation techniques include gas atomisation (GA), water atomisation (WA), plasma atomisation (PA) and centrifugal atomisation. Other techniques to produce powders are plasma rotating electrode process (PREP), hydride dehydrate process (HDH) and mechanical comminution (Figure **2.14**) [71].

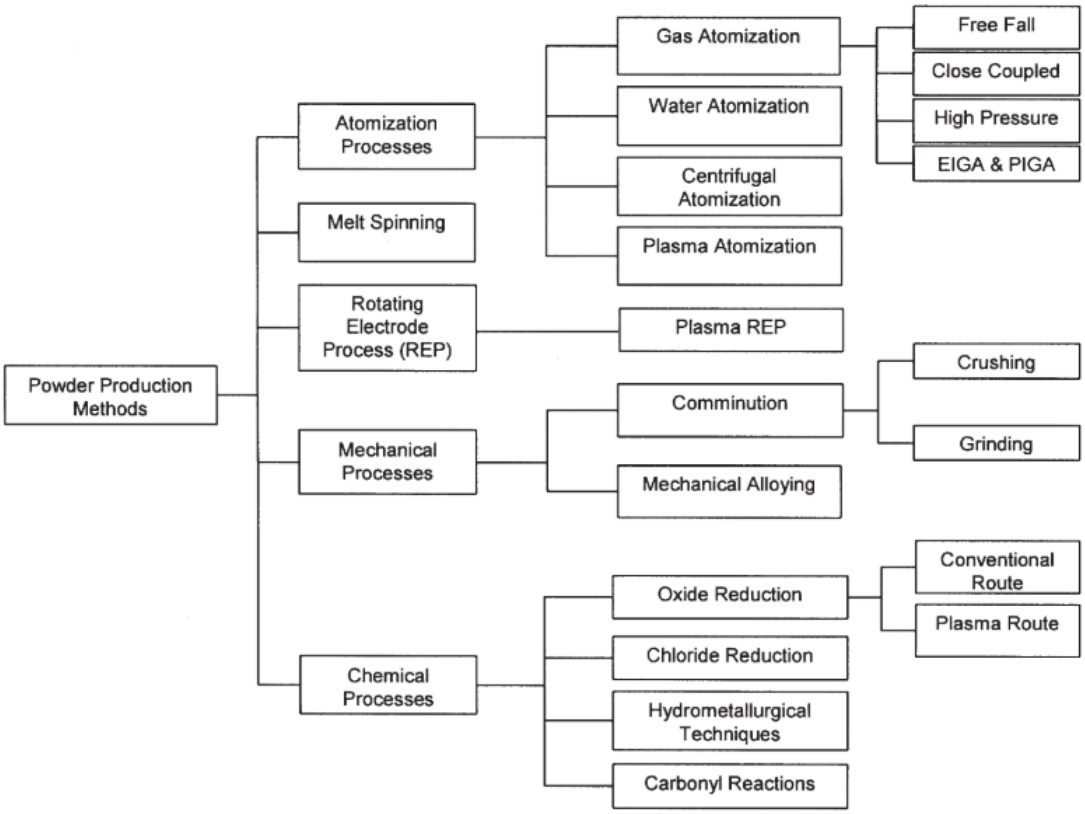

Figure 2.14 Powder processing methods [71].

In powder atomisation technique, the material to start with is in most cases an alloyed ingot. The ingots are normally melted using vacuum induction melting (VIM), to keep as low as possible the interstitial elements such as oxygen and nitrogen, which are detrimental in PM applications [25]. The molten metal then flows into a tundish nozzle, the flowing liquid is

then infringed by a high velocity and high-pressure media (gas or water) or plasma jet [71]. This will be responsible for breaking the melt into small droplets, which will tend to spheroidise to minimise their surface energy and then solidify.

Among all the atomisation methods available, this chapter will focus its attention on GA, WA and PA. The main advantage of atomisation is related to its high cooling rate. In fact, atomised powders are characterised by low levels of elemental segregation and low levels of phase segregation if compared to castings [25]. However, there are some disadvantages associated with some of the atomisation techniques. The main disadvantage is the presence of some non-metallic inclusions such as Al_2O_3, Cr_3O_3 or SiO_2 coming from the interaction of the melt with the ceramic crucible. These inclusions are particularly detrimental to fatigue life. Other defects in powder are the generation of internal porosity, typical for argon gas atomised (AGA) powders, and the generation of satellites forming by the collision of smaller not entirely solidified particles with bigger solidified particles, which can adversely influence the flowability and the consolidation behaviour during PM HIP [72]. The microstructure of atomised powders is highly influenced by the extremely high cooling rates (10^4-10^6 K/s) typical from the atomisation process, due to the high surface to volume ratio of the fragmented droplets. Another important phenomenon of powder atomisation and more in general rapid solidification is the high undercooling effect, which is dependent on the process parameters [73]. The cooling rate is highly dependent on the process parameters and the particle size, with smaller particles exhibiting higher cooling rates in light of their higher surface to volume ratio [74]. Rapid solidification has some advantages such as the improvement of solid solubility, reduction in phase segregation and fine grain structure [75], [76]. The properties and microstructure of the atomised powders are strongly dependent on the physical characteristics of the melt, such as melting temperature, alloy composition,

surface tension, viscosity and thermal conductivity. The atomised powder properties are also influenced by the atomisation process parameters such as atomising media, gas pressure and melt/gas flow ratio [76]. The atomised microstructure is highly influenced by the process parameters, in fact, the main factor dictating the powder microstructure is the cooling rate. Higher cooling rates lead to the formation of a dendritic microstructure, while lower cooling rates tend to form a cellular structure [77]. During the atomisation of reactive materials or materials with reactive elements in the alloy chemistry, a thin oxide film is formed during the solidification process [78], [79]. This is supported by XPS analysis performed on stainless steel powders and nickel base superalloys have confirmed the presence of a thin oxide layer enriched with Al_2O_3 and Cr_2O_3 [56], [54].

2.6.1 Water Atomisation (WA)

Water atomisation is one of the most used methods for producing metal powders. The main advantages of WA are the higher production rate and the low costs if compared to the other atomisation techniques [80]. WA is mainly used for iron, steel, copper, nickel-based alloys and zinc powders [81], [82]. During WA, the melted alloy is transferred to a crucible, which regulates the flow rate. When the melted alloy reaches the atomisation chamber it is invested by a water jet, which breaks the melt stream into small droplets, finally, those droplets solidify during the free fall as represented in Figure **2.15**.

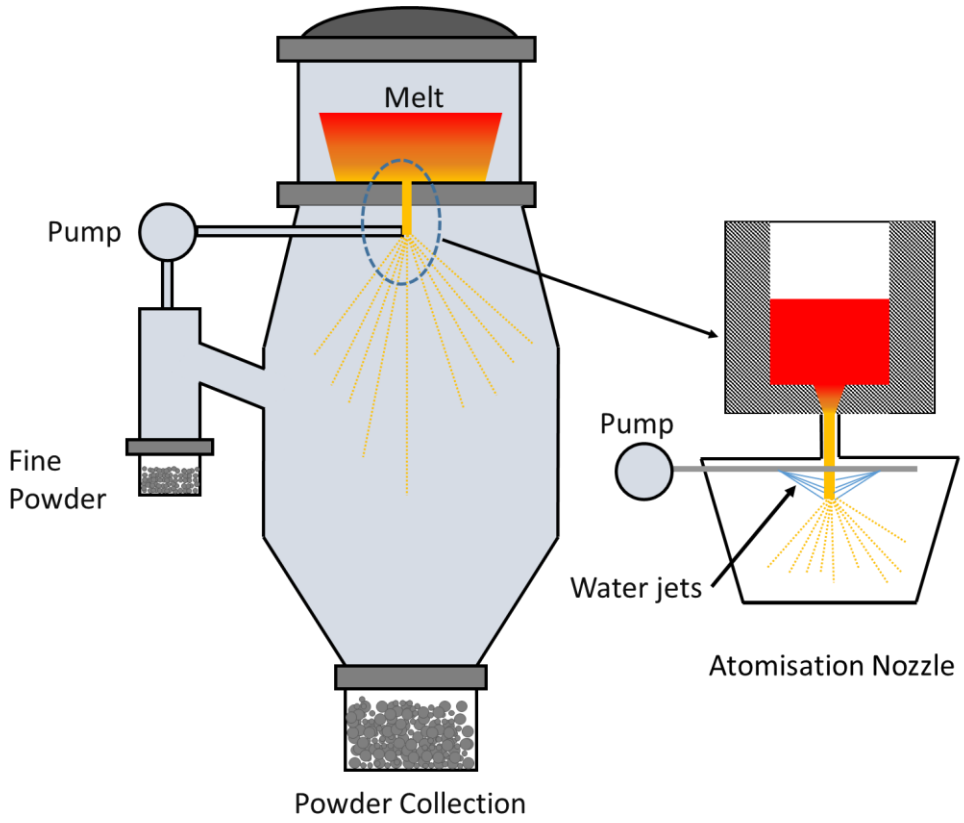

Figure 2.15 Schematic representing the WA process.

The atomisation parameters depend on the desired particle size. One of the most important process parameters in WA is the water pressure. For example, to achieve a D_{50} of 30-50 µm a water pressure of 5-20 MPa is required, while the pressure has to be raised to 50-150 MPa to achieve a D_{50} of 1-20µm [82].

Among all the atomisation processes, WA has the highest cooling rate if compared with gas and plasma atomisation [82], [83]. The WA process produces, in most cases, powders with an irregular shape. Two main aspects influence the irregular shape; the first one is related to the high cooling rate of the process. When a droplet is cooling, it changes its shape to a spherical one, which guarantees the minimum of Gibbs free energy for the system. The time to achieve this configuration is called spheroidisation time. However, since WA involves very high cooling rates, the freezing time is shorter than the spheroidisation time for most of the

materials, this will produce an irregular shape. The other phenomenon involved is the generation of an oxide layer on the surface of the powder. The oxides present on the surface will increase the surface tension of the droplet, opposing to a change in shape, and consequently opposing to spheroidisation [82], [83]. Just some materials can be readily atomised using water without the formation of oxides. To form an oxide, the Gibbs free energy of the oxide has to be lower if compared to the energy of water formation [84]. As is possible to see from Figure **2.16**, water has a lower Gibbs free energy if compared to copper and nickel oxide, thus water atomisation will probably be suitable for the production of Cu and Ni powders [85]. While, for example, the Gibbs free energy for chromium oxide formation is much lower if compared to the one of water, this means that to reduce the energy of the system, oxygen will it find more convenient to be linked with Cr forming Cr_2O_3. This is the reason why in nickel-based superalloys, which are rich in Cr, Al and Ti a considerable formation of oxides on the powder's surface if processed by WA is expected.

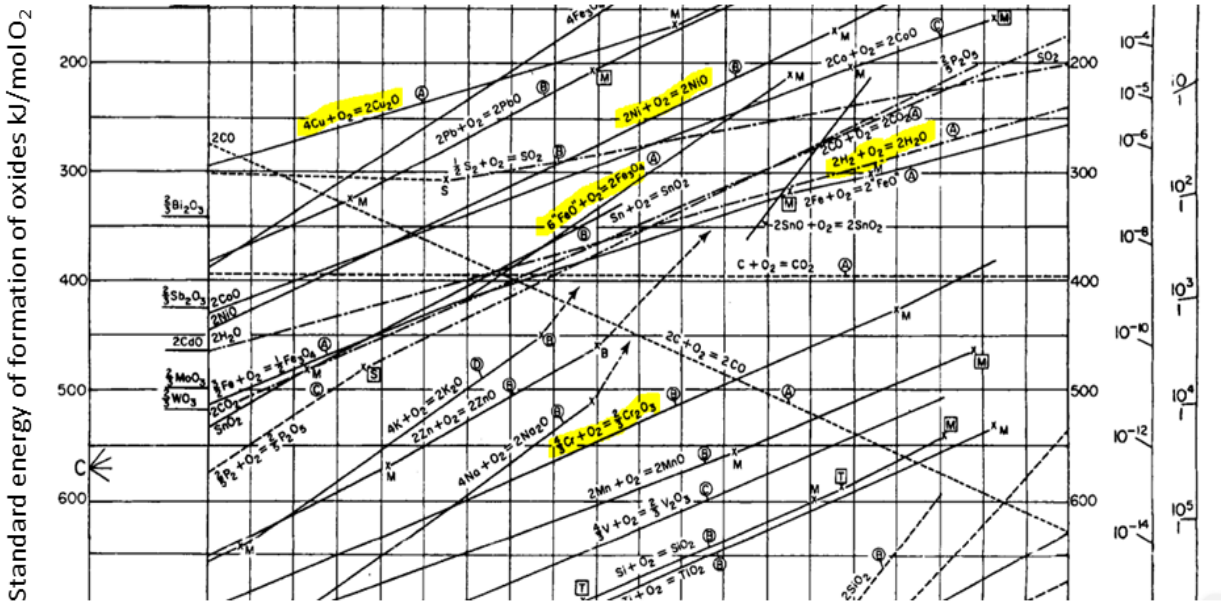

Figure 2.16 Ellingham Diagrams showing the Gibbs free energy vs temperature [5].

2.6.2 Gas Atomisation (GA)

Gas atomisation is the most popular atomisation method for the production of metal powders. In gas atomisation, the ingot is melted using vacuum induction melting (VIM) [86]. Gas atomisation follows the same principle as WA, with the difference that the media is a high pressure gas stream. The action of the high-pressure atomisation gas, disintegrates the molten metal forming small droplets which solidify during the free fall in the cooling tower and then the solidified powders are collected from a collection chamber. The most widely used gases are inert gases like argon or helium, but also other gases like nitrogen and air can be used. In this study, the attention will be focused on just argon and nitrogen. A schematic of the GA apparatus can be seen in Figure **2.17**. Typical levels of oxygen for inert GA powders are 40 to 200ppm [25].

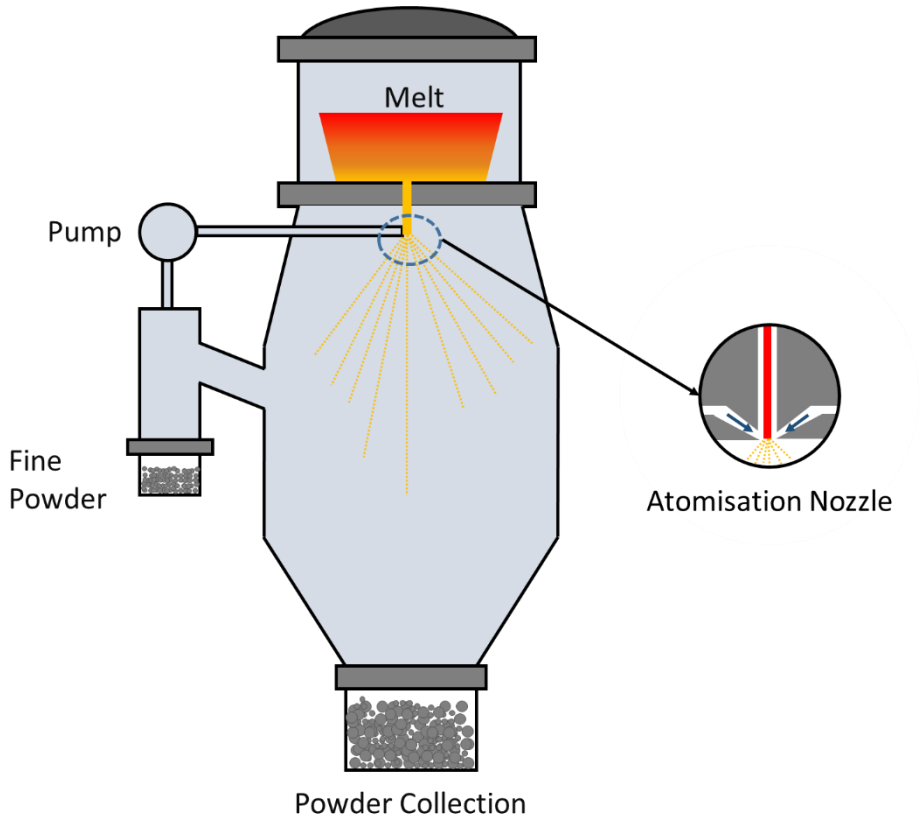

Figure 2.17 Schematic showing the gas atomisation process.

However, there are some fundamental differences between WA and GA. The main difference is that GA is not dominated by the pressure as WA, but it is rather influenced by the gas-to-metal ratio [82]. GA process experiences lower cooling rates compared to WA, the particles have a more regular shape and the oxygen levels are considerably lower in GA [82].

The gas atomisation process is influenced as well by the inert gas used. Argon gas atomisation will produce powders with lower oxygen levels. However, the main problem of argon gas atomization (AGA) is represented by the fact that argon is not a soluble gas, thus, it will create some entrapped porosity inside the powders. This porosity can generate TIP after post-HIP heat treatment [82]. On the other hand, nitrogen gas atomization (NGA) has a lower cost and nitrogen can dissolve into the material, reducing the generation of TIP. However, in most cases, nitrogen is an unwanted element because it lowers the stress rupture levels in Ni-base superalloys [6]. An important parameter to consider when using NGA is the solubility of nitrogen in the material. Higher solubility can avoid the formation of internal porosity, but can contribute to the formation of nitrides during the consolidation process. Furthermore, gas atomised powders are also characterised by the presence of satellites, which can reduce the powder flowability. The generation of satellites in GA is attributed to the fine particle flowing inside the atomisation chamber and colliding with the molten droplets due to the action of the circulating gas [87].

2.6.3 Plasma Atomisation (PA)

If compared with the other two processes, plasma atomisation (PA) principle is different. PA is widely used for the atomisation of reactive materials such as titanium, providing less contamination and difficulties compared to gas atomisation, where a molten bath of Ti needs to be formed [88]. In fact, the feedstock material is not a molten alloy as for WA and GA, but

can be in the form of wire or powder [81]. The other main difference is that the material is melted using plasma arc technology [89]. The use of plasma is advantageous because of its high temperature (above 3000K with the possibility of melting a wide range of materials), high energy density and the possibility of having a quick response to the process parameters such as current and voltage to achieve the desired temperature [89], [90]. During wire PA, a pre-alloyed wire is continuously fed into an inert atomisation chamber filled with helium or argon, where the action of plasma torches melts it, and simultaneously disintegrates the molten metal into fine droplets, thanks to the high kinetic energy provided by the plasma torches (Figure **2.18**). The droplets then solidify with a cooling rate between 10^2-10^3 K/s (lower if compared to GA and WA) during the free falling in the cooling tower, and then the solidified powders are collected in the collection chamber. PA produces the purest powders with the least level of contamination because the feedstock material is not melted but it is in the form of wires or powders [91]. Additionally, since the molten alloy is not flowing through a crucible in this process, the possibility of having ceramic inclusions is eliminated. Furthermore, the process produces powders with highly spherical shape, because of the lower cooling rates caused by the extended hot zone created by the plasma torches, enhancing the spheroidisation process [82], [91]. Thanks to the highly spherical shape, PA powders have a very high packing density, which is desirable when designing a near to net-shape component, because of the better control on the canister's shrinkage [91]. The drawbacks associated with PA are that not all the materials can be made available in form of wire and that if compared to GA and WA the feedstock material is accessible at higher cost [87].

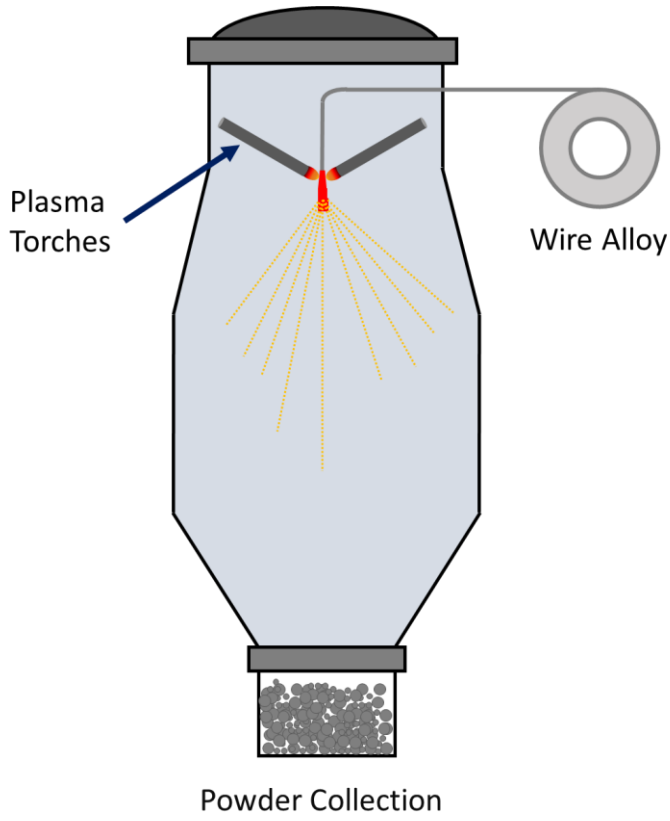

Figure 2.18 Schematic showing the PA atomisation process.

2.6.4 Comparison of Powder Atomisation Routes

The review performed on GA, PA and WA atomisation routes has highlighted some fundamental differences between the three atomisation processes. To summarise the powder characteristics and the industrial benefits/downsides of these atomisation processes, a summary table of some key characteristics of the three atomisation processes is proposed below (Table **2.8**). No specific values were reported in the table, as they are strongly dependent on the material to be atomised and on the adopted atomisation process parameters. Table **2.8** clearly shows that PA has the best quality, with the lowest level of interstitials and highly spherical shape, enhancing the packing factor and consequently the canister geometrical control during NNS PM HIP. On the other hand, GA can represent a good compromise between lower cost, higher production rate and quality. In fact, depending on the

atomising media used, GA can produce powders with low interstitial content. WA process can result in higher production rates and reduced costs if compared to both GA and PA techniques. Thus, it can be used in applications where high powder quality is not required. Therefore, based on the comparison presented in Table **2.8**, some remarkable differences are expected when processing Ni-base superalloys using these three different powders through NNS PM HIP. In particular, the interstitial content plays an important role in the formation of PPBs, thus it is expected a microstructure characterised by an abundance of PPBs for WA powder, while for GA less presence of PPBs is expected due to the lower interstitial levels. Additionally, the packing density of PA is expected to be higher if compared to GA due to the more spherical powder morphology, while WA, due to the presence of irregular particles, would exhibit lower levels of packing density if compared to both PA and GA. Consequently, the influence of the powder atomisation route on the microstructure and mechanical properties of as-HIPed Ni-base superalloys would provide useful information on the atomisation process to use depending on the final application to achieve a trade-off between cost and performances of the as-HIPed part.

Table 2.8 Comparison between GA, PA and WA atomisation routes.

	GA	PA	WA
Particle size	Up to 500µm	Up to 250µm	Up to 1000µm
Interstitials content	Medium/Low	Low	Very high
Morphology	Nearly spherical with some irregularities	Highly spherical	Irregular
Cost	Medium	High	Low
Production rate	Medium	Low	High

2.7 Metallurgy of Metal Matrix Composites

The first part of this literature review chapter has highlighted the properties of Ni-base superalloys and their HIP behaviour. Despite their excellent high temperature strength and corrosion resistance, Ni-base superalloys do not offer the required wear resistance for highly demanding tribological applications. Thus, due to the high flexibility offered by NNS PM HIP process in generating novel material combinations, the possibility of adopting Ni-base metal matrix composites will be discussed below.

MMCs are a class of materials that combines the properties of metals such as toughness and ductility, with the ones of ceramics including high hardness and strength to weight ratio, higher Young modulus and a lower coefficient of thermal expansion [92], [93]. MMCs are normally characterised by the presence of high hardness, high-temperature capability, lower density and superior wear resistance. Different ceramic reinforcements can be used including carbides (SiC, TiC, WC), nitrides (Si_3N_4, TiN), oxides (Al_2O_3, Cr_2O_3, Y_2O_3) and borides (TiB_2, B_2O_3, B_4C) [94], [95], [96]. The most relevant properties of the ceramic reinforcements are reported in Table **2.9** [97], [98].

Table 2.9 Room temperature properties of the most common ceramic reinforcement [97], [98].

Material	Density [g/cm3]	CTE [°C-1]	Melting point [°C]	Thermal conductivity [W/m K]	Hardness [kg/mm2]	Elastic modulus [GPa]
SiC	3.2	5.1 x 10-6	2730	120	2500	324
Si_3N_4	3.2	3.3 x 10-6	1900	30	1580	207
Al_2O_3	3.9	8.4 x 10-6	2072	35	2100	379
TiN	5.2	9.3 x 10-6	2930	19	2100	/
TiB_2	4.5	6.4 x 10-6	3230	25	1800	414
TiC	4.9	7.0 x 10-6	3160	6	2470	269
WC	15.6	1.0 x 10-6	2870	110	2100	669

The high levels of strength of MMCs are a direct consequence of two different effects. The first direct effect is represented by the presence of the reinforcements, which are able to carry a higher load if compared to the metal matrix. The second effect comes from the difference in the CTE between the matrix and the reinforcement, this will create thermal stresses upon cooling, resulting in dislocation hardening. Thus, the higher is the difference in CTEs between the matrix and the reinforcement, the stronger is the dislocation strengthening mechanism [99]. The reinforcement can have different shapes and sizes. The reinforcement can be in the form of particulates, continuous or discontinuous fibres, wires or whiskers [100], [101]. The properties of MMCs are strongly influenced by the reinforcement size and shape, the volume fraction, nature of the reinforcement and compatibility with the metal matrix [94], [93].

MMCs can be produced either by solid-state or liquid-state processes [100]. The most used technology to manufacture MMCs is represented by PM solid-state manufacturing routes including hot pressing, cold isostatic pressing (CIP), sintering, hot isostatic pressing (HIP) and spark plasma sintering (SPS) [102–105]. In terms of liquid-state processes, the most widely used technique is melt stir-casting, and recently the use of laser powder bed fusion (L-PBF) is increasing for the fabrication of MMCs [100], [106], [107].

Thanks to the versatility of the process and the possibility of achieving isotropic mechanical properties, PM HIP process can represent the right candidate for the production of MMCs. Different studies have been focused on the production of MMCs through PM HIP technology [94], [95], [108], [109]. The first step of PM HIP procedure for the production of MMCs consists of powder blending. The metal matrix that can be a pure metal (Ni, Al, Ti, etc.) or in the form of prealloyed powder (Ti6Al4V, IN625, etc.) is mixed with the desired ceramic volume fraction and type. A uniform mixing can be achieved using different strategies. The

most commonly used methods involve the use of a ball mill to mechanically mix the powder or a high-speed mixing [105],[110]. The aforementioned procedures can be followed by low-speed rolling to increase the uniformity in the mix. One of the most important parameters during powder blending is represented by the size of the metal matrix powder and the size of the reinforcement. The metal matrix should have a narrow size distribution to allow a uniform dispersion of the reinforcement on the particle surface, while the reinforcement should have a small size in the order of a few microns or sub-micron size, to guarantee a strong adhesion on the surface of the metal matrix powder [111].

2.7.1 Ni-base MMCs

Ni-base MMCs can be used in different environments thanks to their advanced properties, including high-temperature capabilities, enhanced wear properties, corrosion resistance, high hardness and reduced weight [112], [113]. Ni-base superalloys represent a valid matrix material due to their relatively good ductility (depending on the alloy), good strength and corrosion resistance [1]. Different works on Ni-base MMCs are available in the literature. In particular, it was reported that the presence of ceramic reinforcements can improve the corrosion, tribological properties and strength of the material [114], [115], [116].

Above all the Ni-base superalloys available, IN625 represents a good balance between corrosion resistance, high-temperature capabilities, and furthermore, it is easier to predict the effect of the reinforcement thanks to the lower presence of γ' and γ" precipitates. The properties of IN625 matrix are shown in Table **2.10** [117].

Table 2.10 Room temperature properties of IN625 [117].

Material	Density [g/cm^3]	CTE [°C^{-1}]	Melting point [°C]	Thermal conductivity [W/m K]	Hardness [kg/mm^2]
IN625	8.44	12.8 x 10^{-6}	1290-1350	9.8	240

In the literature domain, different reinforcements have been added to the IN625 matrix to enhance the tribological properties of the alloy. Ahmad *et al.* have used the electron beam melting technique to produce IN625-SiC MMCs. The study has highlighted that the addition of SiC has doubled the hardness of the material [118]. In the work of Cooper *et al.*, the influence of the addition of 10vol% of different ceramic reinforcements such as Al_2O_3, SiC and TiC was evaluated. The presence of the reinforcements resulted in a great increase in hardness for IN625-SiC if compared to the base material, a slightly higher hardness levels for IN625-TiC, while IN625-Al_2O_3 samples did not show an increase in hardness. However, the IN625-MMCs processed in this work exhibited a microstructure with a high crack density that can be related to the CTE mismatch and, consequently high thermal stresses arising due to the rapid cooling in L-PBF process. Zhang *et al.* investigated the influence of TiB_2 on the strength and wear properties of IN625-TiB_2 MMCs. The results show superior wear properties and enhanced tensile properties if compared to the base material [119].

The influence of SiC addition on the microstructure and tribology-related properties for Nickel-base alloys was investigated by A. Ramakrishnan and G.P. Dinda [120]. In their work they used a γ' Ni-based alloy (Haynes 282), creating a functionally graded microstructure by varying the level of SiC reinforcement through different layers by using L-PBF process. They observed that because of the high energy inputs of the process, the SiC dissociated into Si and C with the formation of a supersaturated γ matrix and the formation of different carbides. Furthermore, this work outlined a great increase in strength, influenced by the presence of the

volume fraction of the reinforcement, thus suggesting that SiC can have a positive impact on the wear properties.

Since not many studies have been published on IN625-MMCs, some considerations are required in order to choose an adequate reinforcement. These considerations should take into account the reinforcement physical properties, metallurgical compatibility with the matrix and thermal stability. Since the density of IN625 is 8.44 g/cm^3 the use of WC with a density of 15.6g/cm^3 would drastically increase overall density, thus it does not represent an optimal solution as reinforcement. As stated above, Ni-base superalloys have a complex microstructure with the presence of many elements. To have a better understanding of the possible phase formation, the attention should be shifted to the analysis of the possible phase formation given by the interaction between the matrix and the reinforcement. To this end, the possible formation of intermetallics in IN625 was analysed. In particular, the use of SiC as reinforcement would probably lead to the in-situ formation of different intermetallics. Different silicides can form due to the presence of Mo, Nb and Cr having a good affinity to Si [121]. Furthermore, since IN625 is characterised by the presence of strong carbide formers, C can dissociate from Si to form different types of carbides in the IN625 matrix. A different scenario would arise when using Al_2O_3 as reinforcement. In fact, Al_2O_3 is a very stable oxide and since Alumina is a stronger oxide if compared to Cr_2O_3 or NbO_2 it will not react with the matrix to form different phases. TiB_2 is the reinforcement with the highest melting point, and it is stable if compared to the other possible borides formers in IN625 matrix, thus even in this case a reaction between matrix and reinforcement to form different borides is not expected. This is confirmed from the studies performed by V. Promakhov *et al.* where the interaction between IN625 and TiB_2 reinforcement produces a NiTi matrix with the presence of discrete TiB_2 particles [122].

An important factor influencing the behaviour of the MMCs is the strain mismatch that can arise during thermal cycling. The strain mismatch can be calculated using *Eq. 2.3*.

$$\varepsilon = \Delta\alpha \; x \; \Delta T \qquad \textit{Eq. 2.3}$$

Where Δα is the difference in the coefficient of thermal expansion, while ΔT is the temperature gradient. By comparing the thermal properties of Table **2.9** and Table **2.10** it is possible to note that both SiC and TiB2 have lower CTE, which contributes to the generation of thermal stresses with consequent dislocation hardening.

2.7.2 Wear Mechanisms of MMCs

Different wear mechanisms can occur in MMCs during wear tests. The wear properties of MMCs are strongly affected by the reinforcement volume fraction, size, shape and compatibility with the matrix material. The main wear mechanisms that can be observed in MMCs are abrasive, adhesive, fatigue and oxidative/corrosive wear [123].

- **Abrasive wear** happens when particles or debris present at the interface between the sliding bodies induce some material loss through the abrasive action of the individual particles present at the interface between the two bodies. Abrasive wear is of particular interest for MMCs due to the presence of the reinforcement, which can act as a powerful abrasive media, dramatically accelerating the wear rate.
- **Adhesive wear** is defined as a mechanism happening during high-load wear conditions. In fact, when the normal load is high enough to induce some plasticity in the material, some junctions will be generated between the two sliding bodies. The application of a relative sliding force will break the junctions, promoting the material

transfer. The parameters influencing the adhesive wear are the yield strength of the material, roughness and applied load.

- **Oxidative/corrosive** wear happens when the rubbing surfaces are exposed to a corrosive environment (corrosive wear) or in air (oxidative wear). In this case, temperature plays a crucial role since oxidation and corrosion rates in materials are strongly dependent on temperature [124], [125].

Increasing the levels of reinforcement in MMCs will increase the hardness and the strength of the material, and consequently improve the friction coefficient and the wear rate of the material by increasing the abrasive and adhesive wear resistance [126]. However, in some cases the reinforcement particles can act as abrasive media, reducing the wear resistance of the material [127], [128]. Thus, it is important to select the right reinforcement having a good bonding with the matrix and consequently reduces the abrasive wear related to the pull out of the reinforcement. Furthermore, the high volume fraction of reinforcement increases the shear strength required to cause adhesive wear, reducing the critical load for adhesive wear to happen [126].

Another important parameter to understand more in depth, is the influence of the particle size on the wear resistance. Many studies have been focused on understanding if reducing the reinforcements particle size would have a positive impact on the wear properties. The general thought is that the use of nanoparticle metal matrix composites (NMMCs) has a positive impact on the wear properties [123]. However, the use of nanoparticles in PM HIP can easily lead to the formation of agglomeration due to the high cohesive forces between particles, thus leading to a reduction in the tribological properties and the flowability. The use of a fine micron size particle can also produce a good result in terms of wear rate, as witnessed in the

work of Cerit *et al.* where an optimum wear rate was obtained in Al-based MMCs with the use of 20μm SiC reinforcement [129].

2.8 Concluding Remarks

2.8.1 Summary

This first literature review chapter has highlighted the metallurgy of Ni-base superalloys, with a particular focus on IN625, and Ni-base MMCs focusing on IN625-MMCs. Additionally, the NNS HIP behaviour of Ni-base superalloys and their HIP-related defects have been outlined. A comparison among different studies performed on PM HIP of IN625 has demonstrated the variability in mechanical properties, which is mostly linked with the difference in powder chemical composition. Furthermore, a description of various atomisation techniques was performed to have an understanding of the possible impact of the powder atomisation route on the HIP response of Ni-base superalloys. Finally, the chapter focused on MMCs analysing the properties of different ceramic reinforcement and their possible impact on the wear properties of Ni-base MMCs.

2.8.2 Aims & Knowledge Gaps

The literature review performed has identified some knowledge gaps in both the PM HIP response of Ni-base superalloys and of Ni-base MMCs. Thus, during this thesis, the following aspects will be investigated to address the following gaps:

- Limited investigations have been performed on the influence of the powder atomisation route on the PM HIP response of Ni-base superalloys.
    - Four different atomisation routes including AGA, NGA, PA and WA will be assessed in this thesis.

- The influence of powder and surface chemistry chemistry of Ni-base superalloys powders on the microstructure and mechanical properties is not clear.
    - Detailed powder characterisation will be assessed in this thesis focusing on powder bulk chemistry and powder surface chemistry through XPS analysis. Additionally, a relationship between the powder chemistry and the presence of PPBs in the as-HIPed microstructure was assessed.
- Limited investigations have been performed on the mechanical properties of as-HIPed IN625 to correlate the impact of powder characteristics on the final materials' properties.
    - Tensile and Charpy impact tests will be performed on four different as-HIPed IN625 powders (AGA, NGA, PA and WA) to assess the influence of the microstructure (PPBs formation) on the material's properties.
- Lack of knowledge on the post-HIP heat treatment of IN625.
    - Post-HIP heat treatments will be performed on as-HIPed IN625 samples to assess the influence on the microstructure and mechanical properties.
- Limited literature is available on Ni-base MMCs.
    - This thesis will investigate the PM HIP behaviour of Ni-base MMCs.
- Lack of knowledge on the influence of ceramic reinforcement on the final properties of Ni-base MMCs.
    - This thesis will evaluate the influence of reinforcement type and volume fraction on the HIP response, with particular focus on the wear and mechanical properties.

2.9 References

[1] M.J. Donachie, S.J. Donachie, Superalloys a Technical Guide, 2nd Editio, ASM International, 2002.

[2] Roger C. Reed, The Superalloys Fundamentals and Applications, Cambridge University Press, 2006.

[3] S.D. DuPont, John N. Lippold, John C. Kiser, Welding Metallurgy and Weldability of Nickel-base Alloys, John Wiley & Sons, Inc, 2009.

[4] J.L.L. Meyer, Advanced gas atomization production of oxide dispersion strengthened (ODS) Ni-base superalloys through process and solidification control, (2013).

[5] B. Geddes, H. Leon, X. Huang, Superalloys: Alloying and Performance, ASM International, 2011.

[6] M.J. Donachie, S.J. Donachie, Superalloys a Technical Guide, Second Edi, ASM International, 2002.

[7] A.K. Jena, M.C. Chaturvedi, The role of alloying elements in the design of nickel-base superalloys, J. Mater. Sci. 19 (1984) 3121–3139. https://doi.org/10.1007/BF00549796.

[8] A.J. Goodfellow, Strengthening mechanisms in polycrystalline nickel-based superalloys, Mater. Sci. Technol. (United Kingdom). 34 (2018) 1793–1808. https://doi.org/10.1080/02670836.2018.1461594.

[9] S. Floreen, G.E. Fuchs, W.J. Yang, The Metallurgy of Alloy 625, Superalloys 718, 625, 706 Var. Deriv. (1994) 13–37. https://doi.org/10.7449/1994/Superalloys_1994_13_37.

[10] N. Stoloff, C.C. Koch, C.T. Liu, O. Izumi, High- Temperature Ordered Intermetallic

Alloys II, 1987.

[11] R.A. MacKay, M. V. Nathal, D.D. Pearson, Influence of molybdenum on the creep properties of nickel-base superalloy single crystals, Metall. Trans. A. 21 (1990) 381–388. https://doi.org/10.1007/BF02782418.

[12] J.R. Groh, J.F. Radavich, Effects of Iron, Nickel, and Cobalt on Precipitation Hardening of Alloy 718, Superalloys 718, 625 Var. Deriv. (1991) 351–361. https://doi.org/10.7449/1991/superalloys_1991_351_361.

[13] C. Wei-Di, K. Richard, Role of Chemistry in 718-Type Alloys - Allvac 718Plus Alloy Development, in: Superalloys 2004, TMS, 2004.

[14] J.J. Schirra, R.H. Caless, R.W. Hatala, The Effect of Laves Phase on the Mechanical Properties of Wrought and Cast + HIP Inconel 718, (2012) 375–388. https://doi.org/10.7449/1991/superalloys_1991_375_388.

[15] H.L. Eiselstein, D.J. Tillack, The Invention and Definition of Alloy 625, in: Superalloys 718, 625, 716 Deriv., TMS, 1991: pp. 1–14. https://doi.org/10.7449/1991/superalloys_1991_1_14.

[16] G.D. Smith, S.J. Patel, The role of niobium in wrought precipitation-hardened nickel-base alloys, Proc. Int. Symp. Superalloys Var. Deriv. (2005) 135–154.

[17] I. Kirman, D.H. Warrington, The precipitation of Ni3Nb phases in a Ni-Fe-Cr-Nb alloy, Metall. Trans. 1 (1970) 2667–2675. https://doi.org/10.1007/BF03037800.

[18] J. Oblak, D. Paulonis, D. Duvall, Coherency strengthening in Ni base alloys hardened by O22 γ′ precipitates, Metall. Mater. Trans. B. 5 (1974) 143–153.

[19] B. Geddes, H. Leon, X. Huang, Superalloys: Alloying and Performance, ASM

International, 210AD.

[20] J. Belan, GCP and TCP Phases Presented in Nickel-base Superalloys, Mater. Today Proc. 3 (2016) 936–941. https://doi.org/10.1016/j.matpr.2016.03.024.

[21] S. Mahadevan, S. Nalawade, J.B. Singh, A. Verma, B. Paul, K. Ramaswamy, Evolution of δ phase microstructure in alloy 718, 7th Int. Symp. Superalloy 718 Deriv. 2010. 2 (2010) 737–750. https://doi.org/10.1002/9781118495223.ch57.

[22] V. Shankar, K. Bhanu Sankara Rao, S.L. Mannan, Microstructure and mechanical properties of Inconel 625 superalloy, J. Nucl. Mater. 288 (2001) 222–232. https://doi.org/10.1016/S0022-3115(00)00723-6.

[23] M. Sundararaman, P. Mukhopadhyay, S. Banerjee, Precipitation of the δ-Ni3Nb phase in two nickel base superalloys, Metall. Trans. A. 19 (1988) 453–465. https://doi.org/10.1007/BF02649259.

[24] C. Slama, M. Abdellaoui, Structural characterization of the aged Inconel 718, J. Alloys Compd. 306 (2000) 277–284. https://doi.org/10.1016/S0925-8388(00)00789-1.

[25] G.H. Gessinger, Powder Metallurgy of Superalloys, 1984.

[26] M. Sundararaman, P. Mukhopadhyay, S. Banerjee, Carbide Precipitation in Nickel Base Superalloys 718 and 625 and Their Effect on Mechanical Properties, (2012) 367–378. https://doi.org/10.7449/1997/superalloys_1997_367_378.

[27] A. Cervellon, J. Cormier, F. Mauget, Z. Hervier, Y. Nadot, Very High Cycle Fatigue of Ni-Based Single-Crystal Superalloys at High Temperature, Metall. Mater. Trans. A Phys. Metall. Mater. Sci. 49 (2018) 3938–3950. https://doi.org/10.1007/s11661-018-4672-6.

[28] R.H.U. Khan, M.H. Loretto, M.M. Attallah, J. Cortes, I. Iturriza, F. Castro, Microstructure and properties of HIPped alloy 718, in: 11th Int. Conf. Hot Isostatic Press., Stockholm, 2014.

[29] M.J. Sohrabi, H. Mirzadeh, M. Rafiei, Solidification behavior and Laves phase dissolution during homogenization heat treatment of Inconel 718 superalloy, Vacuum. 154 (2018) 235–243. https://doi.org/10.1016/j.vacuum.2018.05.019.

[30] J. Tinoco, H. Fredriksson, Solidification of a modified inconel 625 alloy under different cooling rates, High Temp. Mater. Process. 23 (2004) 13–24. https://doi.org/10.1515/HTMP.2004.23.1.13.

[31] M. CIESLAK, The welding and solidification metallurgy of alloy 625, Weld. J. 70 (1991) 49.

[32] I.L.W. Wilson, R.G. Gourley, R.M. Walkosak, G.J. Bruck, Superalloys 718, 625, in: TMS, 1991: p. 495.

[33] T.J. Garosshen, G.P. McCarthy, Low temperature carbide precipitation in a nickel base superalloy, Metall. Trans. A. 16 (1985) 1213–1223. https://doi.org/10.1007/BF02670326.

[34] R. Cozar, M. Rouby, M. Mayonobe, C. Morizot, Superalloy 718/625, TMS. (1991) 423.

[35] S.R. Shatynski, The thermochemistry of transition metal carbides, Oxid. Met. 13 (1979) 105–118. https://doi.org/10.1007/BF00611975.

[36] A. Formenti, A. Eliasson, A. Mitchell, H. Fredriksson, Solidification sequence and carbide precipitation in Ni-base superalloys IN718, IN625 and IN939, High Temp.

Mater. Process. 24 (2005) 239–258. https://doi.org/10.1515/HTMP.2005.24.4.239.

[37] Q. Bai, J. Lin, G. Tian, J. Zou, D. Ta, Powder Metallurgy & Mining Review and Analysis of Powder Prior Boundary (PPB) Formation in Powder Metallurgy Processes for Nickel-based Super Alloys, 4 (2015) 1–6. https://doi.org/10.4172/2168-9806.1000127.

[38] A.K. Niessen, F.R. De Boer, The enthalpy of formation of solid borides, carbides, nitrides, silicides and phosphides of transition and noble metals, J. Less-Common Met. 82 (1981) 75–80. https://doi.org/10.1016/0022-5088(81)90200-9.

[39] C. Kowanda, M.O. Speidel, Solubility of nitrogen in liquid nickel and binary Ni-Xi alloys (Xi = Cr, Mo, W, Mn, Fe, Co) under elevated pressure, Scr. Mater. 48 (2003) 1073–1078. https://doi.org/10.1016/S1359-6462(02)00628-0.

[40] A. Mitchell, S.L. Cockcroft, C.E. Schvezov, A.J. Schmalz, J.N. Loquet, J. Fernihough, Primary carbide and nitride precipitation in superalloys containing niobium, High Temp. Mater. Process. 15 (1996) 27–40. https://doi.org/10.1515/HTMP.1996.15.1-2.27.

[41] H.S. Liu, L. Zhang, X.B. He, X.H. Qu, H.M. Zhu, G.Q. Zhang, Effect of oxygen content and heat treatment on carbide precipitation behavior in PM Ni-base superalloys, Int. J. Miner. Metall. Mater. 19 (2012) 827–835. https://doi.org/10.1007/s12613-012-0635-x.

[42] M.J. Cieslak, T.J. Headley, T. Kollie, A.D. Romig, Melting and solidification study of Alloy 625, Metall. Trans. A, Phys. Metall. Mater. Sci. 19 A (1988) 2319–2331. https://doi.org/10.1007/BF02645056.

[43] A. Sukumaran, R.K. Gupta, V. Anil Kumar, Effect of Heat Treatment Parameters on

the Microstructure and Properties of Inconel-625 Superalloy, J. Mater. Eng. Perform. 26 (2017) 3048–3057. https://doi.org/10.1007/s11665-017-2774-8.

[44] S. Guo, W. Sun, D. Lu, Z. HU, Effect of Minor Elements on Microstructure and Mechanical Properties of In 718 Alloy, (2012) 521–530. https://doi.org/10.7449/1997/superalloys_1997_521_530.

[45] K. Inaekyan, A. Kreitcberg, S. Turenne, V. Brailovski, Microstructure and mechanical properties of laser powder bed-fused IN625 alloy, Mater. Sci. Eng. A. 768 (2019) 138481. https://doi.org/10.1016/j.msea.2019.138481.

[46] K. Essa, R. Khan, H. Hassanin, M.M. Attallah, R. Reed, An iterative approach of hot isostatic pressing tooling design for net-shape IN718 superalloy parts, (2016) 1835–1845. https://doi.org/10.1007/s00170-015-7603-3.

[47] M.F. Ashby, D.R.H. Jones, Engineering Materials 1 an introduction to their properties and applications, 2nd ed., 1996.

[48] G.A. Rao, K.S. Prasad, M. Kumar, M. Srinivas, D.S. Sarma, G.A. Rao, K.S. Prasad, M. Kumar, M. Srinivas, D.S. Sarma, G.A. Rao, K.S. Prasad, M. Kumar, M. Srinivas, D.S. Sarma, Characterisation of hot isostatically pressed nickel base superalloy Inconel * 718 Characterisation of hot isostatically pressed nickel base superalloy Inconel * 71 8, 0836 (2013). https://doi.org/10.1179/026708303225010605.

[49] H.R. Dugdale, J.B. Borradaile, Development of hot isostatically pressed nickel based alloys for nuclear applications, Energy Mater. Mater. Sci. Eng. Energy Syst. 8 (2013) 374–381. https://doi.org/10.1179/1743290113Y.0000000076.

[50] G.A. Rao, M. Srinivas, D.S. Sarma, Effect of oxygen content of powder on microstructure and mechanical properties of hot isostatically pressed superalloy

Inconel 718, Mater. Sci. Eng. A. 435–436 (2006) 84–99. https://doi.org/10.1016/j.msea.2006.07.053.

[51] J.E. Macdonald, R.H.U. Khan, M. Aristizabal, M.J. Lunt, M.M. Attallah, Influence of powder particle size distribution on the microstructure and mechanical properties of a HIPped CM247LC Ni superalloy, Mater. Des. 174 (2019).

[52] L. Chang, W. Sun, Y. Cui, R. Yang, Influences of hot-isostatic-pressing temperature on microstructure, tensile properties and tensile fracture mode of Inconel 718 powder compact, Mater. Sci. Eng. A. 599 (2014) 186–195. https://doi.org/10.1016/j.msea.2014.01.095.

[53] Y. Hedberg, M. Norell, J. Hedberg, P. Szakálos, P. Linhardt, I. Odnevall Wallinder, Surface characterisation of fine inert gas and water atomised stainless steel 316L powders: Formation of thermodynamically unstable surface oxide phases, Powder Metall. 56 (2013) 158–163. https://doi.org/10.1179/1743290112Y.0000000041.

[54] Z.J. Gao, G.Q. Zhang, Z. Li, H. Yuan, W.Y. Xu, Y. Zhang, Surface Segregation and Oxidation Behavior of Superalloy Powders Fabricated by Argon Atomization, Mater. Sci. Forum. 747–748 (2013) 518–525. https://doi.org/10.4028/www.scientific.net/msf.747-748.518.

[55] J. Yan, Y. Zhou, R. Gu, X. Zhang, W.M. Quach, M. Yan, A comprehensive study of steel powders (316L, H13, P20 and 18Ni300) for their selective laser melting additive manufacturing, Metals (Basel). 9 (2019). https://doi.org/10.3390/met9010086.

[56] E. Gil, J. Cortés, I. Iturriza, N. Ordás, XPS and SEM analysis of the surface of gas atomized powder precursor of ODS ferritic steels obtained through the STARS route, Appl. Surf. Sci. 427 (2018) 182–191. https://doi.org/10.1016/j.apsusc.2017.07.205.

[57] D. Chasoglou, E. Hryha, M. Norell, L. Nyborg, Characterization of surface oxides on water-atomized steel powder by XPS/AES depth profiling and nano-scale lateral surface analysis, Appl. Surf. Sci. 268 (2013) 496–506. https://doi.org/10.1016/j.apsusc.2012.12.155.

[58] J.S. Crompton, R.W. Hertzberg, Analysis of second phase particles in a powder metallurgy HIP nickel-base superalloy, J. Mater. Sci. 21 (1986) 3445–3454. https://doi.org/10.1007/BF02402986.

[59] W. Bin Ma, G.Q. Liu, B.F. Hu, P.H. Hu, Y.W. Zhang, Study of metallic carbide (MC) in a Ni-Co-Cr-based powder metallurgy superalloy, Metall. Mater. Trans. A Phys. Metall. Mater. Sci. 45 (2014) 208–217. https://doi.org/10.1007/s11661-013-1962-x.

[60] A. Mostafaei, C. Hilla, E.L. Stevens, P. Nandwana, A.M. Elliott, M. Chmielus, Comparison of characterization methods for differently atomized nickel-based alloy 625 powders, Powder Technol. 333 (2018) 180–192. https://doi.org/10.1016/j.powtec.2018.04.014.

[61] R.G. Menzies, R.H. Bricknell, A.J. Craven, R.H. Bricknell, A.J. Craven, STEM microanalysis of precipitates and their nuclei in a nickel-base superalloy, Philos. Mag. A Phys. Condens. Matter, Struct. Defects Mech. Prop. 41 (1980) 493–508. https://doi.org/10.1080/01418618008239328.

[62] S. Feng, M. Xia, C.C. Ge, Oxidation during the production of FGH4095 superalloy powders by electrode induction-melt inert gas atomization, Chinese Phys. B. 27 (2018) 4–9. https://doi.org/10.1088/1674-1056/27/4/044701.

[63] A. Kreitcberg, K. Inaekyan, S. Turenne, V. Brailovski, Temperature- and Time-Dependent Mechanical Behavior of Post-Treated IN625 Alloy Processed by Laser

Powder Bed Fusion, J. Manuf. Mater. Process. 3 (2019) 75. https://doi.org/10.3390/jmmp3030075.

[64] J.A. Gonzalez, J. Mireles, S.W. Stafford, M.A. Perez, C.A. Terrazas, R.B. Wicker, Characterization of Inconel 625 fabricated using powder-bed-based additive manufacturing technologies, J. Mater. Process. Technol. 264 (2019) 200–210. https://doi.org/10.1016/j.jmatprotec.2018.08.031.

[65] H.R. Dugdale, J.B. Borradaile, Development of hot isostatically pressed nickel based alloys for nuclear applications, Powder Metall. 56 (2013) 374–381. https://doi.org/10.1179/1743290113Y.0000000076.

[66] T. Berglund, F. Meurling, Oxygen Content in PM HIP 625 and its Effect on Toughness, 12th Int. Conf. Hot Isostatic Press. (2017) 135–141.

[67] J.W. Wang, Q.S. Wei, G.C. Liu, Y.K. He, Y.S. Shi, Study on direct hot isostatic pressing technology for superalloy inconel 625, Adv. Mater. Res. 189–193 (2011) 2935–2938. https://doi.org/10.4028/www.scientific.net/AMR.189-193.2935.

[68] Nickel Alloy, Corrosion and Heat-Resistant, Powder for Additive Manufacturing, 62Ni-21.5Cr-9.0Mo-3.65Nb, in AMS7001. SAE International, (n.d.).

[69] ASTM International. B834-17 Standard Specification for Pressure Consolidated Powder Metallurgy Iron-Nickel-Chromium-Molybdenum (UNS N08367), Nickel-Chromium-Molybdenum-Columbium (Nb) (UNS N06625), Nickel-Chromium-Iron Alloys (UNS N06600 and N06690), and N, (n.d.).

[70] I. Chang, Y. Zhao, Advances in Powder Metallurgy, Woodhead Publishing, 2013.

[71] L.V.M. Antony, R.G. Reddy, Processes for Production of High-Purity Metal Powders,

JOM. 55 (2003) 14–18.

[72] S. Özbilen, Satellite formation mechanism in gas atomized powders, Powder Metall. 42 (1999) 70–78. https://doi.org/10.1179/pom.1999.42.1.70.

[73] N.H. Pryds, A.S. Pedersen, Rapid Solidification of Martensitic Stainless Steel Atomized Droplets, 33 (2002) 3755–3761.

[74] A. Sabard, H.L. de Villiers Lovelock, T. Hussain, Microstructural Evolution in Solution Heat Treatment of Gas-Atomized Al Alloy (7075) Powder for Cold Spray, J. Therm. Spray Technol. 27 (2018) 145–158. https://doi.org/10.1007/s11666-017-0662-2.

[75] F.-M. Alloy, S. Kim, C.M. Wayman, Structures and Properties of a Rapidly Solidified Fe-19.1Ni-1.76Mn-0.73Ti Maraging Alloy, 105 (1993) 99–105.

[76] E.J.L.T.S. Srivatsan, The rapid solidification processing of materials : science , principles , technology , advances , and applications, (2010) 287–325. https://doi.org/10.1007/s10853-009-3995-5.

[77] J.E. Smugeresky, Characterization of a Rapidly Solidified Iron-Based Superalloy, 13 (1982) 1535–1546.

[78] S. Feng, M. Xia, C.C. Ge, Oxidation during the production of FGH4095 superalloy powders by electrode induction-melt inert gas atomization, Chinese Phys. B. 27 (2018). https://doi.org/10.1088/1674-1056/27/4/044701.

[79] M. Kumar, T. V. Balasubramanian, R.D.K. Misra, On the characterization of inert-gas atomized nickel-based superalloy powders, J. Mater. Sci. Lett. 9 (1990) 147–151. https://doi.org/10.1007/BF00727699.

[80] M. Pasupathy, J.M. Martín, A. Rivas, I. Iturriza, F. Castro, Effect of the solidification time on the median particle size of powders produced by water atomisation, Powder Metall. 59 (2016) 128–141. https://doi.org/10.1080/00325899.2015.1117693.

[81] J. Dawes, R. Bowerman, R. Trepleton, Introduction to the additive manufacturing powder metallurgy supply chain, Johnson Matthey Technol. Rev. 59 (2015) 243–256. https://doi.org/10.1595/205651315X688686.

[82] O.D. Neikov, Atomization and granulation, 2nd ed., Elsevier Ltd., 2009. https://doi.org/10.1016/B978-1-85617-422-0.00005-7.

[83] J.J. Dunkley, Advances in atomisation techniques for the formation of metal powders, in: Adv. Powder Metall. Prop. Process. Appl., 2013: pp. 3–18. https://doi.org/10.1016/j.cell.2009.04.050.

[84] K. Hariramabadran Anantha, Study of Total Oxygen Content and Oxide Composition Formed During Water Atomization of Steel Powders Due To Manganese Variation, (2012).

[85] J.H.E. Jeffes, Ellingham Diagrams, Encycl. Mater. Sci. Technol. (2001) 2751–2753. https://doi.org/10.1016/b0-08-043152-6/00490-3.

[86] O.D. Neikov, S.S. Naboychenko, I.B. Murashova, Production of Nickel and Nickel-Alloy Powders, in: Handb. Non-Ferrous Met. Powders, 2nd ed., 2019: pp. 633–667.

[87] P. Sun, Z.Z. Fang, Y. Zhang, Y. Xia, Review of the Methods for Production of Spherical Ti and Ti Alloy Powder, Jom. 69 (2017) 1853–1860. https://doi.org/10.1007/s11837-017-2513-5.

[88] U. Ti, P. Tsantrizos, Plasma Atomization gives uniaue sDherical nowders, (1997).

[89] A.S. Baskoro, S. Supriadi, Review on Plasma Atomizer Technology for Metal Powder, in: IIW 2018, 2019.

[90] E. Gomez, D.A. Rani, C.R. Cheeseman, D. Deegan, M. Wise, A.R. Boccaccini, Thermal plasma technology for the treatment of wastes: A critical review, J. Hazard. Mater. 161 (2009) 614–626. https://doi.org/10.1016/j.jhazmat.2008.04.017.

[91] A. Alagheband, C. Brown, Plasma Atomization goes commercial, Met. Powder Rep. 53 (1998) 26–28.

[92] C.J. Boehlert, D.B. Miracle, Intermetallic matrix composites, Compr. Compos. Mater. II. 9795 (2017) 482–524. https://doi.org/10.1016/B978-0-12-803581-8.09979-3.

[93] S.C. Tjong, Z.Y. Ma, Microstructural and mechanical characteristics of in situ metal matrix composites, 29 (2000) 49–113.

[94] S. Ala-kleme, P. Kivikytö-reponen, J. Liimatainen, Abrasive wear properties of metal matrix composites produced by hot isostatic pressing, (2006) 445–454.

[95] E. Pagounis, M. Talvitie, V.K. Lindroos, Influence of Reinforcement Volume Fraction and Size on the Microstructure and Abrasion Wear Resistance of Hot Isostatic Pressed White Iron Matrix Composites, 27 (1996).

[96] Ö. Savaş, R. Kayikci, Production and wear properties of metal matrix composites reinforced with boride particles, Mater. Des. 51 (2013) 641–647. https://doi.org/10.1016/j.matdes.2013.04.049.

[97] I.A. Ibrahim, F.A. Mohamed, E.J. Lavernia, Particulate reinforced metal matrix composites - a review, J. Mater. Sci. 26 (1991) 1137–1156. https://doi.org/10.1007/BF00544448.

[98] V. Krishna, Al / SiC NP and Al / SiC NP / X nanocomposites fabrication and properties : A review, (2017). https://doi.org/10.1177/2397791417744706.

[99] N. Chawla, Y.L. Shen, Mechanical behavior of particle reinforced metal matrix composites, Adv. Eng. Mater. 3 (2001) 357–370. https://doi.org/10.1002/1527-2648(200106)3:6<357::AID-ADEM357>3.0.CO;2-I.

[100] P.S. Bains, S.S. Sidhu, H.S. Payal, Fabrication and Machining of Metal Matrix Composites: A Review, Mater. Manuf. Process. 31 (2016) 553–573. https://doi.org/10.1080/10426914.2015.1025976.

[101] M. Rosso, Ceramic and metal matrix composites : Routes and properties, 175 (2006) 364–375. https://doi.org/10.1016/j.jmatprotec.2005.04.038.

[102] W.C. Harrigan, Commercial processing of metal matrix composites, Mater. Sci. Eng. A. 244 (1998) 75–79. https://doi.org/10.1016/s0921-5093(97)00828-9.

[103] N. Singh, R. Ummethala, P.S. Karamched, R. Sokkalingam, V. Gopal, G. Manivasagam, K.G. Prashanth, Spark plasma sintering of Ti6Al4V metal matrix composites: Microstructure, mechanical and corrosion properties, J. Alloys Compd. 865 (2021) 158875. https://doi.org/10.1016/j.jallcom.2021.158875.

[104] S.A.A. Alem, R. Latifi, S. Angizi, F. Hassanaghaei, M. Aghaahmadi, E. Ghasali, M. Rajabi, Microwave sintering of ceramic reinforced metal matrix composites and their properties: a review, Mater. Manuf. Process. 35 (2020) 303–327. https://doi.org/10.1080/10426914.2020.1718698.

[105] S.M. Almotairy, A.F. Boostani, M. Hassani, D. Wei, Z.Y. Jiang, Effect of hot isostatic pressing on the mechanical properties of aluminium metal matrix nanocomposites produced by dual speed ball milling, J. Mater. Res. Technol. 9 (2020) 1151–1161.

https://doi.org/10.1016/j.jmrt.2019.11.043.

[106] M. Jäcklein, A. Pfa, K. Hoschke, Developing Tungsten-Filled Metal Matrix Composite Materials Using Laser Powder Bed Fusion, Appl. Sci. 10 (2020).

[107] W.W. Wits, M. De Smit, K. Al-hamdani, A.T. Clare, T. Clare, P. Stief, J. Dantan, A. Etienne, A. Siadat, Laser powder bed fusion of a Magnesium-SiC metal matrix composite, Procedia CIRP. 81 (2019) 506–511. https://doi.org/10.1016/j.procir.2019.03.137.

[108] T. Berglund, H. Söderberg, The Performance of HIPed MMCs and their Application, in: Euro PM2014 – Hot Isostatic Press., 2014.

[109] C. Cai, B. Song, C. Qiu, L. Li, P. Xue, Q. Wei, Hot isostatic pressing of in-situ TiB / Ti-6Al-4V composites with novel reinforcement architecture , enhanced hardness and elevated tribological properties, J. Alloys Compd. 710 (2019) 364–374. https://doi.org/10.1016/j.jallcom.2017.03.160.

[110] D.E. Cooper, N. Blundell, S. Maggs, G.J. Gibbons, Additive layer manufacture of Inconel 625 metal matrix composites, reinforcement material evaluation, J. Mater. Process. Technol. 213 (2013) 2191–2200. https://doi.org/10.1016/j.jmatprotec.2013.06.021.

[111] C. Cai, S. He, L. Li, Q. Teng, B. Song, C. Yan, Q. Wei, Y. Shi, In-situ TiB/Ti-6Al-4V composites with a tailored architecture produced by hot isostatic pressing: Microstructure evolution, enhanced tensile properties and strengthening mechanisms, Compos. Part B Eng. 164 (2019) 546–558. https://doi.org/10.1016/j.compositesb.2019.01.080.

[112] B.K.A. Kumar, M.G. Ananthaprasad, K.G. Krishna, A Review on Corrosion Behavior

of Nickel Matrix Composites A Review on Corrosion Behavior of Nickel Matrix Composites, (2015).

[113] A. Kumar, A Review on Mechanical and Tribological Behaviors of Nickel Matrix Composites, (2017). https://doi.org/10.17485/ijst/2016/v9i2/82868.

[114] V.G. Karayannis, A.K. Moutsatsou, Synthesis and Characterization of Nickel-Alumina Composites from Recycled Nickel Powder, 2012 (2012). https://doi.org/10.1155/2012/395612.

[115] A. Calbet, L. Fedrizzi, M. Lekka, Nickel matrix micro/nano SiC composite electrodeposition, (n.d.).

[116] M. Gladkovas, V. Medelienë, Corrosion study of electroplated nickel metal-matrix composites with B 4 C , Al 2 O 3 and SiC, (2002).

[117] S. Metals, Inconel Alloy 625, Www.Specialmetals.Com. 625 (2013) 1–28. https://doi.org/SMC-066.

[118] M. Ahmad, G. Ali, E. Ahmed, M.A. Haq, J.I. Akhter, Applied Surface Science Novel microstructural growth in the surface of Inconel 625 by the addition of SiC under electron beam melting, Appl. Surf. Sci. 257 (2011) 7405–7410. https://doi.org/10.1016/j.apsusc.2011.02.067.

[119] B. Zhang, G. Bi, P. Wang, J. Bai, Y. Chew, M. Sharon, Microstructure and mechanical properties of Inconel 625 / nano-TiB 2 composite fabricated by LAAM, JMADE. 111 (2016) 70–79. https://doi.org/10.1016/j.matdes.2016.08.078.

[120] A. Ramakrishnan, G.P. Dinda, Functionally graded metal matrix composite of Haynes 282 and SiC fabricated by laser metal deposition, Mater. Des. 179 (2019) 107877.

https://doi.org/10.1016/j.matdes.2019.107877.

[121] E.A. Brandes, Smithells Metals Reference Book, 6th ed., Butterworth & Co, London, 1983.

[122] V. Promakhov, A. Zhukov, M. Ziatdinov, I. Zhukov, N. Schulz, S. Kovalchuk, Y. Dubkova, R. Korsmik, O. Klimova-Korsmik, G. Turichin, A. Perminov, Inconel 625/TiB2 metal matrix composites by direct laser deposition, Metals (Basel). 9 (2019). https://doi.org/10.3390/met9020141.

[123] P.L. Menezes, S.P. Ingole, M. Nosonovsky, S. V. Kailas, M.R. Lovell, Tribology for scientists and engineers: From basics to advanced concepts, 2013. https://doi.org/10.1007/978-1-4614-1945-7.

[124] D. Arnell, Mechanisms and laws of friction and wear, in: H. Rahnejat (Ed.), Tribol. Dyn. Engine Powertrain Fundam. Appl. Futur. Trends, 2010: pp. 41–72.

[125] C. Zhang, Understanding the wear and tribological properties of ceramic matrix composites, in: Adv. Ceram. Matrix Compos. an Introd., 2014: pp. 312–339.

[126] Z.F. Zhang, L.C. Zhang, Y.W. Mai, Wear of ceramic particle-reinforced metal-matrix composites - Part I Wear mechanisms, J. Mater. Sci. 30 (1995) 1961–1966. https://doi.org/10.1007/BF00353018.

[127] M. Franco, W. Sha, G. Aldic, S. Malinov, H. Çimenoɨlu, Effect of reinforcement and heat treatment on elevated temperature sliding of electroless Ni-P/SiC composite coatings, Tribol. Int. 97 (2016) 265–271. https://doi.org/10.1016/j.triboint.2016.01.047.

[128] A. Nieto, H. Yang, L. Jiang, J.M. Schoenung, Reinforcement size effects on the

abrasive wear of boron carbide reinforced aluminum composites, Wear. 390–391 (2017) 228–235. https://doi.org/10.1016/j.wear.2017.08.002.

[129] A.A. Cerit, M.B. Karamiş, N. Fehmi, Y. Kemal, Effect of reinforcement particle size and volume fraction on wear behaviour of metal matrix composites, Tribol. Ind. 30 (2008) 31–36.

Chapter 3. Literature Review Nb and Nb-base alloys

3.1 Introduction

The previous literature review chapter focused on Ni-base superalloys and Ni-base MMCs. Despite their interesting properties including creep resistance, strength and corrosion resistance, the maximum operating temperature of Ni-base superalloys is limited by their melting point, making Ni-base superalloys unsuitable for very high temperature applications. Thus, the use of refractory metals can represent a valid alternative for these specific applications. In particular, in this literature review chapter, the metallurgy and properties of Nb and Nb-alloys were investigated for very high temperature space applications. This literature review chapter will initially focus on describing the different strengthening mechanisms of pure Nb and Nb-alloys, posing attention to the influence of each alloying element on the high temperature properties of Nb-alloys. Since one of the limiting factors of refractory metals is represented by its oxidation resistance at high temperatures, a review of the high temperature oxidation resistant coating is proposed highlighting the current challenges and possible solutions to increase the high temperature oxidation properties of these classes of materials. Finally, the chapter will focus on the conventional manufacturing routes for Nb and Nb-base alloys and on the opportunities offered by PM HIP for processing this class of materials.

3.2 Definition of Refractory Metals

Refractory metals represent a class of metals with a melting point >2000°C, including Nb, Mo, W, Ta and Re [1]. The physical properties of the refractory metals are listed in Table **3.1**. Due to their high-temperature capabilities and high-temperature strength, refractory metals are widely used in different sectors including aerospace, heating elements, nuclear and chemical sectors [1], [2]. The main problem associated with refractory metals is their poor

high-temperature oxidation resistance, which limits their application to non-oxidising or low-temperature environments [3], [4]. This limit can be overcome by the use of coatings, protecting the refractory metals from degradation [5].

Table 3.1 Properties of refractory metals.

Material	Melting Point (°C)	Density (g/cm3)	Crystal Structure	Atomic Number
Nb	2468	8.57	bcc	41
Mo	2610	10.22	bcc	42
W	3410	19.25	bcc	74
Ta	2996	16.60	bcc	73
Re	3180	21.04	hcp	75

3.3 Metallurgy of Nb and Nb-base Alloys

Niobium is one of the most used alloying elements for different classes of steels and Ni-base superalloys, providing solid solution strengthening and precipitation hardening [2], [6]. Among all the refractory metals reported in Table 3.1 Nb and Nb alloys represent a valuable solution in the nuclear sector, in rocket space engines and heating elements due to its lower density, good low-temperature ductility, weldability, resistance to corrosion and interstitial element solubility [7], [8]. Over the years, different classes of Nb-alloys were successfully developed. Nb-alloys are characterised by the presence of Hf, W, Ta, Zr, V and Ti, which are often used in addition to Nb in order to improve its strength and the high-temperature oxidation capabilities, which represents one of the biggest drawbacks of pure Nb. In particular, there are three different classes of Nb-alloys, including solid solution strengthened, dispersion strengthened, and precipitation strengthened alloys. In addition, the strength of pure Nb can be increased by interstitial solid solubility of O, N, C and H and by work hardening [9], [10].

3.3.1 Solid Solution Strengthened Nb-alloys

This represents the most important strengthening mechanism for Nb-alloys. Elements such as Mo, W and Ta are used as alloying elements to improve the strength of the material by substitutional solid solution [11], [12]. These elements have a wide solid solubility in pure Nb, thus they can have a great contribution to the strength of the material [13]. However, the addition of other solid solution elements such as V and Cr, which have been demonstrated to be beneficial for high-temperature oxidation resistance can lower the melting point of the Nb alloy leading to a reduction in creep resistance [13], [14] (Figure **3.1**).

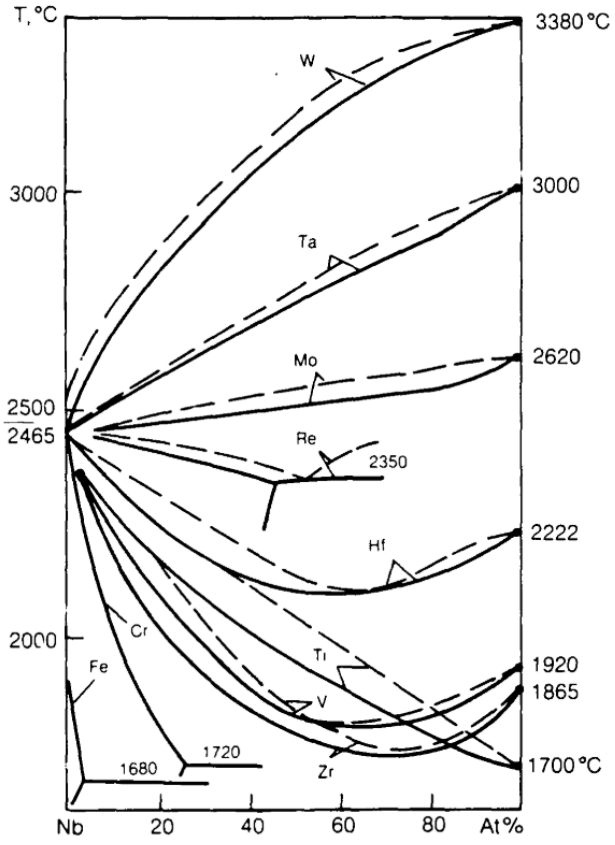

Figure 3.1 Influence of alloying element on the melting temperature of Nb [14].

Common solid solution strengthened Nb-base alloys include Cb-132, B-33, D-4, F-48, SCb-291 and SCb-298. The contribution of the different solid solution elements to the strength can be linked to the atomic dimension of the alloying elements. W is the greater strengthener

among the alloying elements, it contributes to strength (both room temperature and elevated temperature) and also improves the creep resistance of the alloy [14]. The downside of W addition is its extremely high density (19.35g/cm^3) and the considerable loss in fabricability and low-temperature ductility [15]. Vanadium addition contributes to an excellent increase in the room temperature tensile strength, however, it decreases the creep resistance by increasing the self-diffusivity of Nb at high temperatures [15]. Mo and Cr, similarly to V, increase the room temperature strength of the material but they are not effectively creep resistant and reduce the ductility of the alloy. The addition of Ta has a moderate influence on the mechanical properties of the material, the main purpose of Ta addition is to increase the melting point and improve the low-temperature ductility [11], [15]. To understand if an element can have an extended solid solution with Nb, Hume-Rothery rules can be followed. The first rule states that for a substitutional solid solution to happen, the atomic radii difference should be less than 15%. Table **3.2** shows that elements such as W, Mo, Ta, Ti and V are within the limits of Hume-Rothery first rule, while elements such as Al and Ni have lower solid solubility in Nb and thus are more prone to precipitate some intermetallics [16].

Table 3.2 Physical properties of solid solution elements in Nb base alloys.

Element	Atomic Radius (Å)	Difference in Radius (%)	Density (g/cm3)
Nb	1.98	0.0%	8.57
W	1.93	2.5%	19.35
Mo	1.90	4.0%	10.22
Ta	2.00	1.0%	16.65
V	1.71	13.6%	6.11
Ti	1.76	11.1%	4.50
Al	1.18	40.4%	2.70
Ni	1.49	24.7%	8.90

Another important parameter to consider is the solubility limits of the alloying elements, which can limit the strength of solid solution strengthened Nb-base alloys.

Although the substitutional solid solution confers high levels of strength in Nb-base alloys, it is not considered enough to improve the creep properties of the material. The addition of reactive elements, forming stable oxides, carbides, borides or nitrides is required to improve the creep resistance.

3.3.2 Dispersion Strengthened Nb-alloys

Dispersion strengthened Nb-alloys were developed to improve the long-term high-temperature strength. The main elements added to produce dispersion strengthening are Zr, Ti and Hf. These elements combine with interstitials such as O, N, C, B and react to form stable oxides, nitrides, carbides and borides. The precipitation of these second phases is effective to pin the grain boundaries at high temperatures, avoiding grain boundary sliding, and thus improving the creep resistance [7]. Different Nb-alloys produced by dispersion strengthening are commercially available including Cb-65, D-12, Nb-1Zr and C-103. Figure **3.2** clearly shows that Zr has the greatest influence on the strength of the binary alloys, followed by Hf and Ti, reaching its peak at 5wt.% [15].

The strengthening produced by the addition of carbides is beneficial for considerably improving the strength of the material up to high temperature (1400°C); another important role of carbides is to increase the recrystallisation temperature up to 1500°C. However, the presence of carbides reduces the elongation to fracture and the fracture toughness because of the formation of a continuous network of carbides at grain boundaries [7]. Furthermore,

exposure for a long time to high temperatures can lead to oxide coarsening and consequently a reduction in the mechanical properties [13].

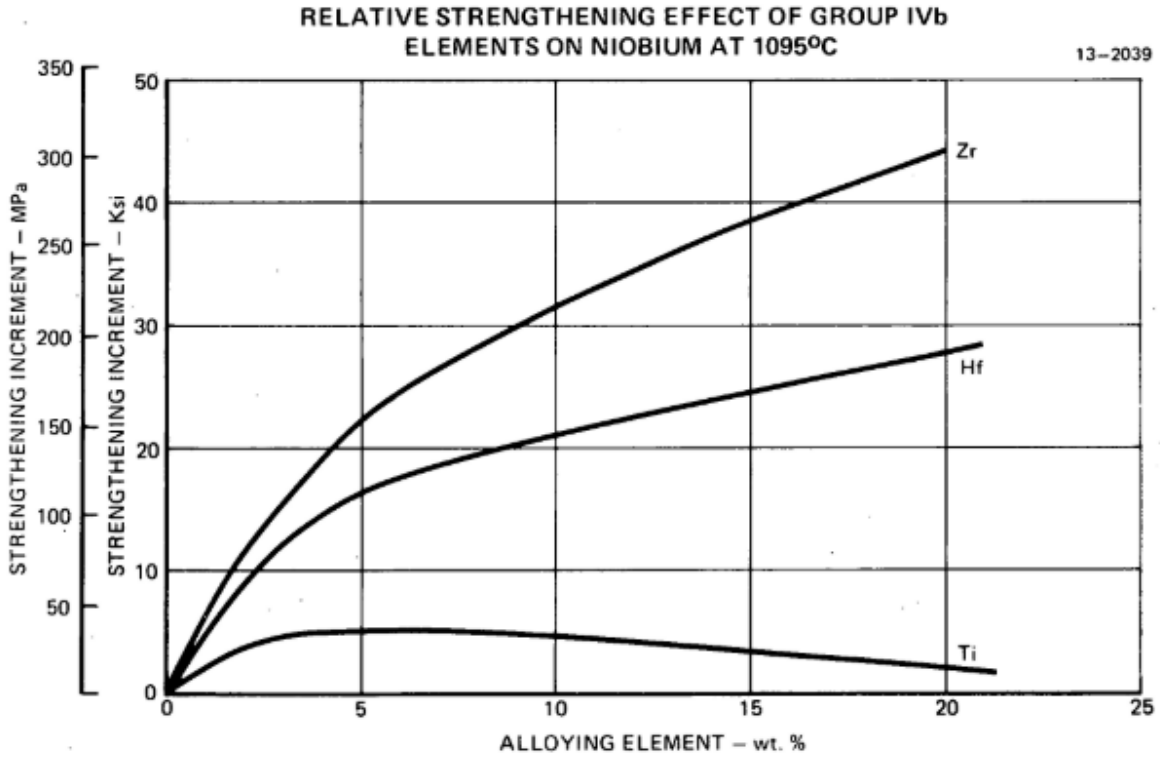

Figure 3.2 Influence of group IVb elements addition on the strength of Nb at 1095°C [15].

An important factor to be considered when designing a dispersion strengthened Nb alloy, is the stability of the precipitates. In fact, the more stable are the precipitates, the higher is the high temperature creep resistance of the alloy. The stability of the precipitates can be expressed using the Gibbs free energy of formation. In fact, the lower is the Gibbs free energy compared to the formation of the Nb compound the more stable is the precipitate [13]. A list of the Gibbs free energy formation in Nb-base compounds is reported in Table **3.3** [17]. The latter shows that the most stable compounds are Ta_2O_5, Ti_3O_5 and Y_2O_5 [17]. While

other compounds such as ZrC and TiC show lower stability at high temperatures in Nb (Table **3.3**).

Table 3.3 Gibbs free energy of formation for different compounds in Nb at 1500°C [17].

Compound	$-\Delta G_{1500}$ (kJ/mole compound)	$-\Delta G_{1500}$ (kJ/mole solute)
NbN	***	-
Si_3N_4	251	63
TiN	195	195
ZrN	223	223
NbB_2	**235**	**118**
CeB_6	313	52
HfB_2	316	158
TiB_2	303	152
ZrB_2	302	151
Nb_2C	***	-
ZrC	184	184
$NbSi_2$	**131**	**65**
Ta_5Si_3	361	120
Mo_5Si_3	323	108
NbO_2	**518**	**259**
Ta_2O_5	1413	283
Ti_3O_5	1797	359
Y_2O_5	1482	296
SiO_2	640	320

3.3.3 Precipitation Strengthened Nb-alloys

Strengthening of Nb-alloys can be achieved by precipitation of hard intermetallic phases stable up to high temperatures [13]. The presence of stable precipitates can have a positive impact on room and high temperature strength, but also on creep resistance. To achieve stable precipitates to high temperature, the precipitate should be coherent with the matrix, i.e. have

low lattice mismatch. Different strategies were adopted to achieve precipitation hardening, different elements such as Ni, Al, Ti and Si can be used to induce the precipitation of different phases responsible for the increase in strength, oxidation and creep properties [10]. Due to the low solid solubility of Ni in Nb, it is reported that Ni_6Nb_7 and Nb_5Ni can form [18]. Other phases such as (Nb_3Si, Nb_5Si_3) and Laves phases (Cr_2Nb) have been proposed to increase both room and high-temperature properties of the material [19], [20].

3.3.4 Influence of interstitials in pure Nb

One of the most effective ways to improve the strength of Nb is the addition of interstitials such as O, N, H and C. In particular, O is a valuable element because of its high solid solubility in Nb and because of the high influence of interstitials in the YS of BCC materials [21]. Many different authors focused their attention on the influence of O on the mechanical properties of pure Nb [22], [23], [9]. The solubility limit for O, N, C and H is reported in Figure **3.3**. The solid solubility is proportional to the temperature except for H. O and N have very high solubility limits (The solid solution of O in Nb is 1.5at% at 775°C and 5.5at% at 1100°C). Thus Nb has considerable margins for the increase in strength if considered that the contribution of O to the strength of pure Nb is 0.19MPa/ppm while N has a much higher impact of 0.41MPa/ppm [9].

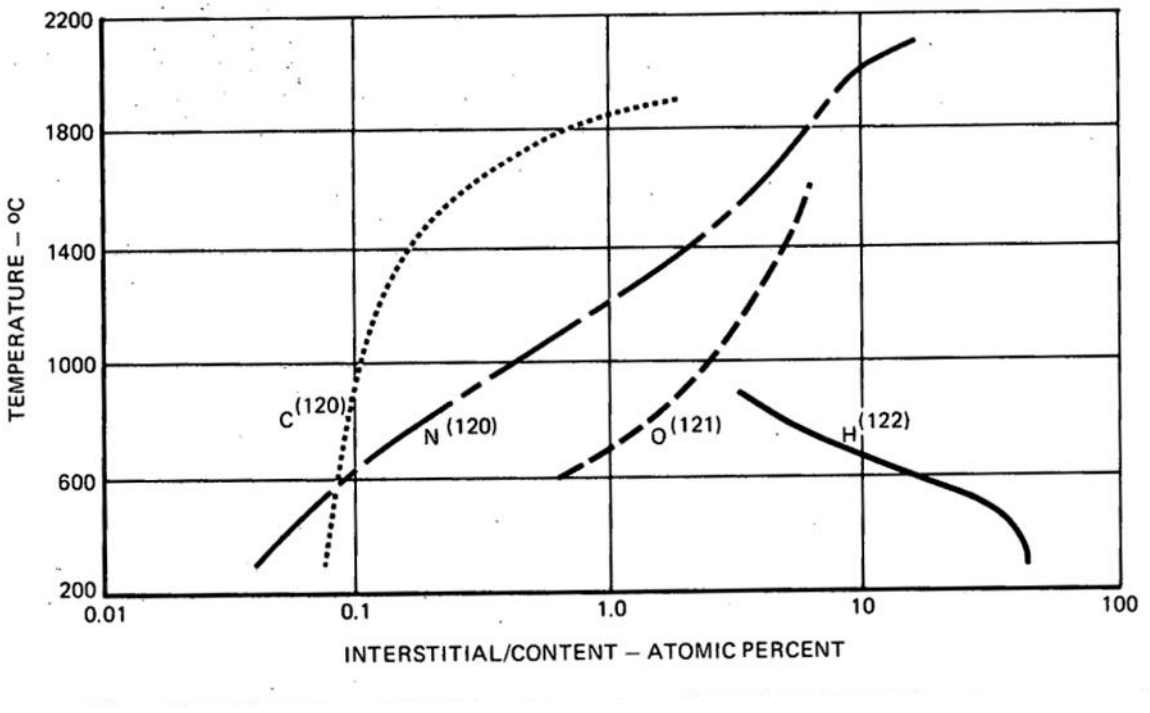

Figure 3.3 Solid solubility fo O, N, C and H in pure Nb [15].

In pure Nb, the presence of the interstitials distorts the crystal lattice. The distortions interact with both screw and edge dislocations, providing a considerable increase in strength. In particular, Yang *et. al.* demonstrated that the oxygen solutes provide dislocation pinning, leading to an increase of yield strength by a factor of four when adding 1at% of oxygen to pure Nb, while maintaining good levels of ductility [23]. However, the excessive presence of oxygen and other interstitials can induce embrittlement and has a substantial impact on increasing the ductile to brittle transition temperature (DBTT). In fact, the increase of DBTT is proportional to the interstitial levels in pure Nb, with hydrogen showing the highest impact followed by oxygen and carbon [15].

Different heat treatment strategies have been proposed to increase the O levels in pure Nb and consequently to increase the strength of the material [22], [23], [24]. Diffusivity is an important parameter influencing the ability to increase the strength by interstitials addition. The diffusivity of O and N in pure Nb are reported in *Eq. 3.1* and *Eq. 3.2* [25].

$$D = 5.3x10^{-7}e^{\frac{-109500}{RT}} \qquad \textit{Eq. 3.1}$$

$$D = 2.6x10^{-6}e^{\frac{-152300}{RT}} \qquad \textit{Eq. 3.2}$$

As it is possible to note from the two equations, the diffusion of O in N is much faster. To prove it, a simple calculation was performed to understand the diffusion depth of O and N in pure Nb using a temperature of 300°C and a diffusion time of 10h. The calculated diffusion depth for O was 7µm, while for N the diffusion depth was just 0.2µm (Figure **3.4**).

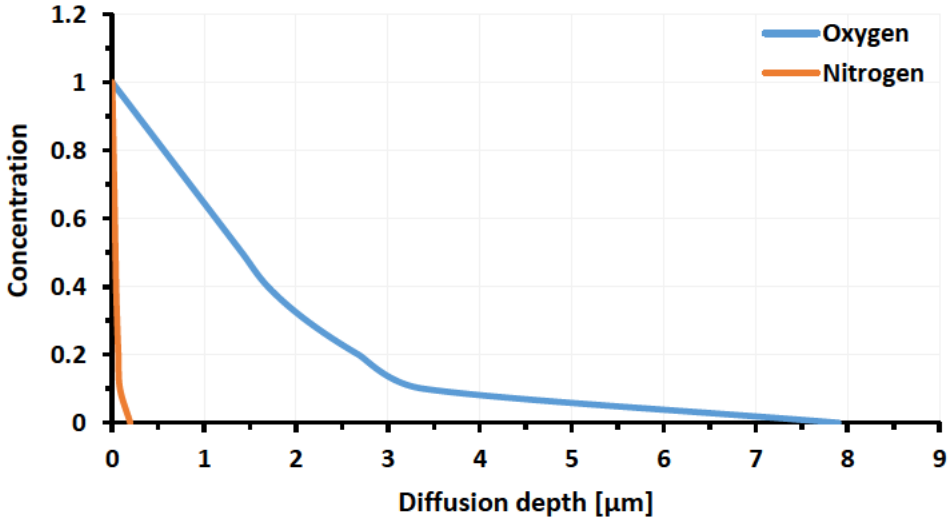

Figure 3.4 Diffusion depth of O and N in pure Nb for 10h with a temperature of 300°C.

3.3.5 Work hardening in pure Nb

Another way to improve the strength in materials and as well as in pure Nb is by subjecting the material to a cycle of deformations to increase the dislocation density in the material, thus

increasing the room temperature tensile strength. However, the higher dislocation density will lower the recrystallisation temperature of the material, and consequently a sharp decrease in strength at high temperatures [13]. Work hardening curves for pure Nb in the arc-cast and sintered conditions can be found in Figure **3.5**. The figure shows an initial considerable increase in hardness with the induced deformation. However, after a reduction of 40%, the trend of both sintered and arc-casted Nb becomes linear [8].

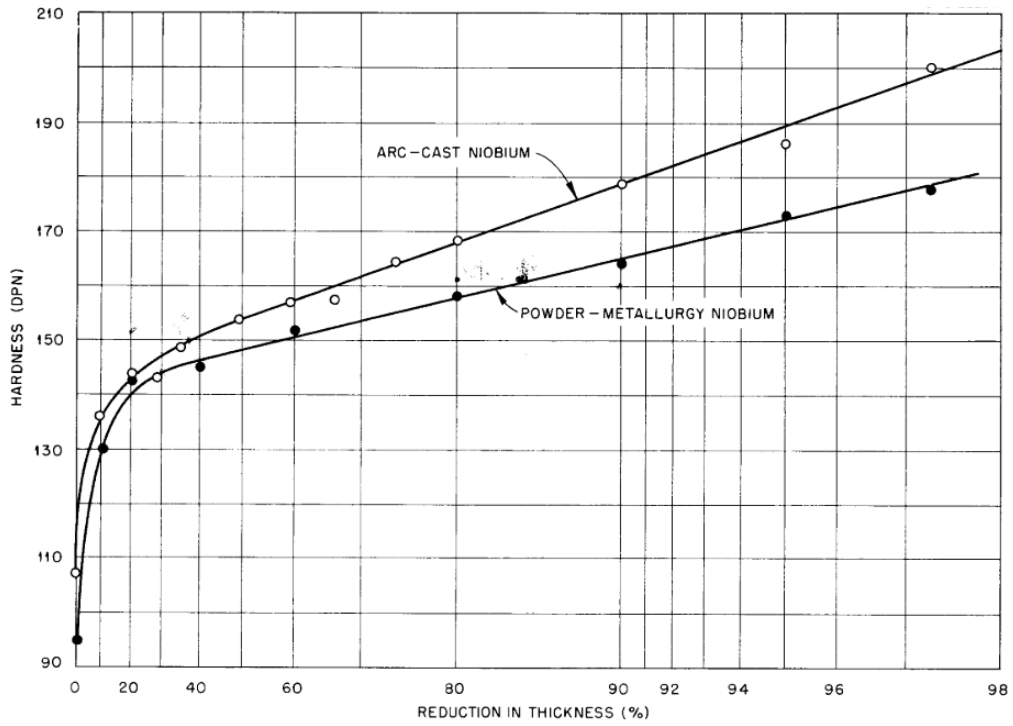

Figure 3.5 Work hardening curves for pure Nb in arc-cast and sintered conditions [8].

The results of YS with temperature shows that cold-rolled Nb retains good mechanical properties up to 800°C [8]. If the temperature is further increased, there is a drastic drop in strength, which can impair the high-temperature properties of pure Nb.

3.4 Nb-MMCs

The use of Nb composites can induce different benefits such as the increase in RT and HT strength, creep resistance, reduction in density and increase in high-temperature oxidation resistance [26], [27]. There is a wide variety of Nb composites available in the literature, but the most common composites rely on the addition of Si and other elements such as Ti, Hf, Cr and Al [28]. Nb-MMCs, own their strength to the presence of hard phases in combination with a ductile Nb matrix, able to retain good fracture toughness and ductility [27], [29].

For the improvement of the abovementioned properties, many different works have been proposed, relying on the addition of different elements such as Si, Mo, W, Ti, with the addition of C or B for the in-situ formation of hard phases [30–38].

One of the most widely used strategies for the formation of Nb-composites is the use of Nb_5Si_3 refractory silicide [32,39–42]. In fact, the addition or in-situ formation of Nb_5Si_3 enhances the RT and HT mechanical properties, reduces the density, with acceptable levels of fracture toughness. The formation of Nb_5Si_3 can also be combined with other elements, such as Ti, Mo, W, Hf etc., to enhance the solid solution strengthening and the oxidation resistance of the Nb composite [28]. This was attempted by J. Yu *et al.*, where a Nb alloy with the presence of Si, Mo, Ti and Hf was hot pressed. The idea was to increase the strength by the formation of Nb_5Si_3, improve the oxidation resistance and fracture toughness by the addition of Ti, and retain high-temperature capabilities with the addition of Mo and W. The as-pressed microstructure showed the presence of Nb_{ss} with the presence of Nb_5Si_3 and Nb_3Si (Figure **3.6** left). The presence of Nb_5Si_3 in the microstructure, together with Nb_{ss} are responsible for the poor ductility of the composite at RT, while the ductility increases as the temperature is raised up to 1500°C ((Figure **3.6** right) [43].

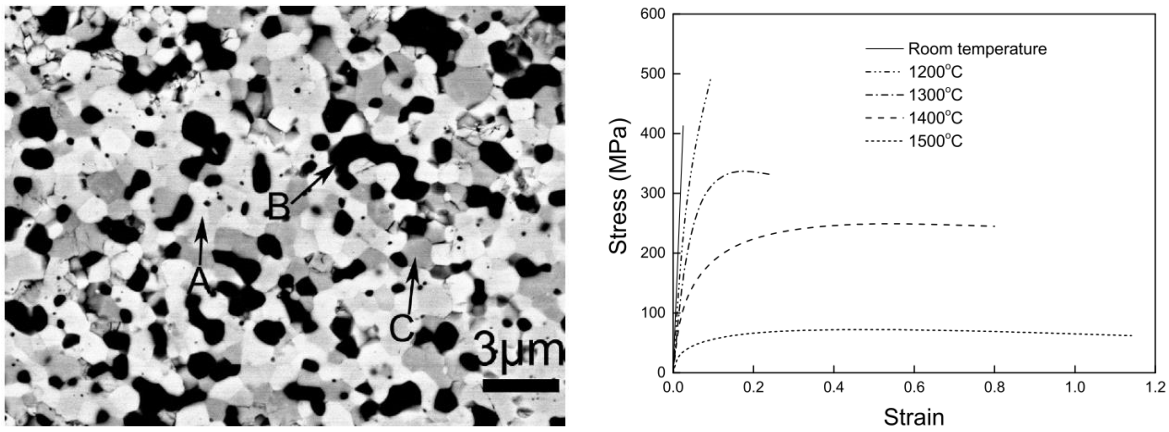

Figure 3.6 As-pressed microstructure of Nb-16Si-10Ti-110Mo-5Hf. Point A, B and C represents respectively Nb_{ss}, Nb_5Si_3 and Nb_3Si (left). Tensile properties of the Nb-composite at RT, 1200°C, 1300°C, 1400°C and 1500°C (right) [43].

An interesting study proposed by Z. Lu *et al.* showed the influence of SiC addition on pure Nb processed by powder metallurgy hot pressing. The addition of SiC generated in-situ Nb_3Si and Nb_2C hard phases, with a consequent increase in strength, proportional to the increase of SiC reinforcement. However, the presence of some cracks is revealed when Vickers hardness test was performed, due to the presence of Nb_3Si and Nb_2C brittle phases [27].

The addition of SiC can result in higher strength if compared to Si, thanks to the addition of Nb_2C hard phase, which strongly contributes to the strength. Despite the potentials of SiC addition on pure Nb, not many studies have been published yet.

In general, the addition of or the in-situ formation of stable intermetallics and carbides can be a feasible way to improve the mechanical and high-temperature properties of Nb and Nb alloys. In particular, the addition of different carbides, nitrides or borides can be considered, which have been not extensively investigated in the literature.

3.5 High-Temperature Oxidation Resistant Coatings

One of the main issues associated with the use of Nb and Nb-base alloys is their poor high-temperature oxidation resistance. In fact, refractory metals such as Nb and Ta shall not be used in an oxidising environment without a protective coating for temperatures higher than 500-600°C [5]. Thus, in order to improve the oxidation resistance of Nb and Nb-base alloys, a protective coating has to be developed. The protective layer needs to meet two important requirements such as:

- **Metallurgical compatibility with the base material**. The coating should be stable at high temperatures without the formation of low-temperature eutectic phases or brittle intermetallic phases.
- **Similar CTE with the base material**. A small gap between the CTE of the base material and the coating needs to be guaranteed. Bigger CTE differences would generate high thermal stresses with consequent failure of the coating.

Different categories of coatings for Nb include [44]:

- Zinc-base coatings (for temperatures ranging from 1000-1100°C)
- Aluminide-base coatings
- Silicide-base coatings
- Platinum and iridium coating

Silicide coatings are certainly the most used coatings for the production of high-temperature oxidation-resistant Nb-alloys. Over the years different classes of silicides were developed, ranging from simple silicide coating or with the addition of different elements such as Fe, Cr, Ti, Al, B and Ge [45], [46]. One of the most commonly used coatings in the industry for Nb

and Nb-alloys is the application of a Nb silicide coating with the addition of Fe and Cr (R-512 E). R-512 E coating is composed of a fused silicide with the presence of Fe and Cr (60Si, 20Fe, 20Cr) [47]. The investigation of the slurry silicide coating process with a more in-depth focus on the microstructure and oxidation behaviour was performed by Alam *et al.* on C-103 Nb-base alloy [48]. The microstructure analysis of the as-coated material shows the presence of a coating with a uniform thickness of around 250μm and with the presence of four distinctive layers. The outer layer was principally composed of $NbSi_2$ with the presence of some micro-cracks arising during cooling after the coating process, because of the CTE mismatch and some porosity, while in the lower layers there was a higher presence of Fe and Cr with the formation of a single phase. On the other hand, the inter-diffusion layer is rich in Nb with a drastic decrease of Si, Fe and Cr (Figure **3.7**).

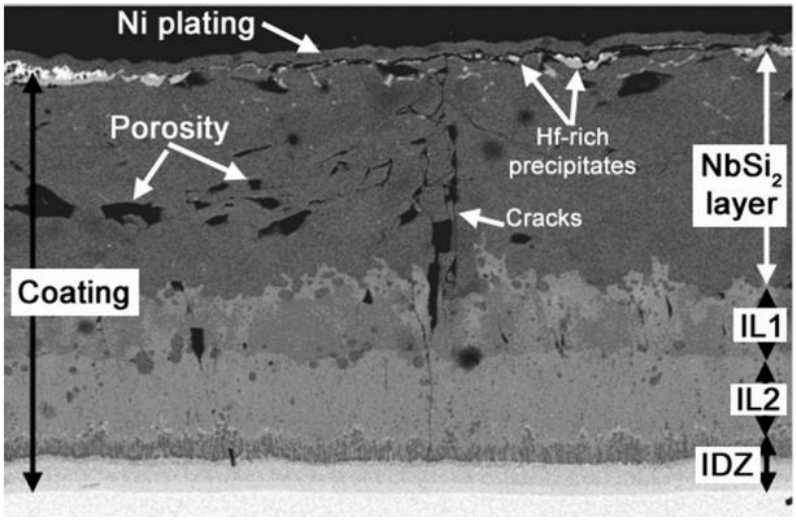

Figure 3.7 SEM micrograph of the as-deposited coating [48].

The high-temperature oxidation results of C-103 coated with R-512 E are reported in Figure **3.8**. The uncoated C-103 samples were reported to have a loss in weight due to the spalling of the external oxide layer, while the coated samples show an initial drastic increase in weight followed by steady-state oxidation, with a final loss in weight.

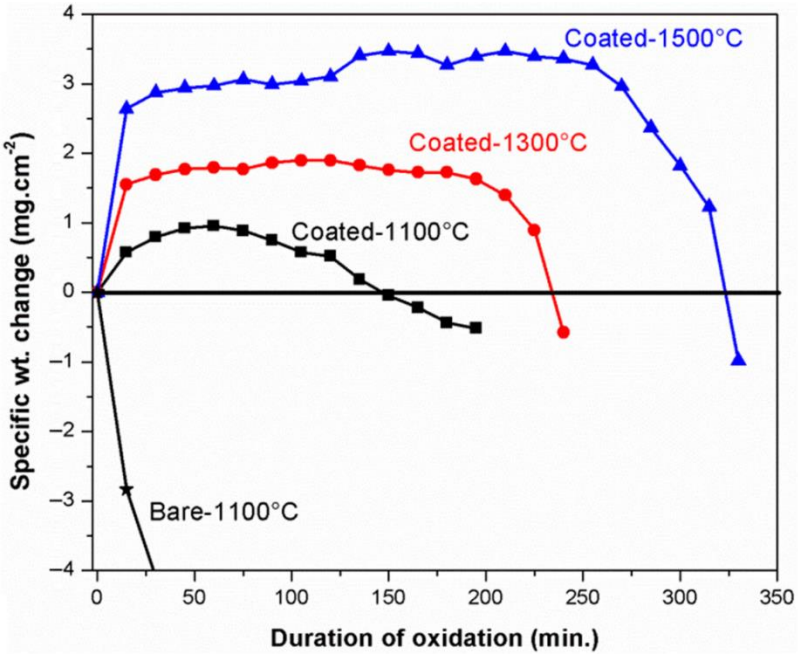

Figure 3.8 Weight change in isotropic oxidation test at different temperatures for coated and uncoated C-103 [48].

Simple silicide coatings on Nb and Nb-alloys were successfully developed in different works [45], [49]. The coating microstructure reveals the presence of an outer layer of $NbSi_2$ and an inner layer of Nb_5Si_3. Isothermal and cycling oxidation tests performed by M. Alam *et al.* on coated and uncoated C-103 showed that the silicide coating is able to drastically reduce the oxidation rate [45]. The oxidation mechanism reported by different authors is the oxidation of the $NbSi_2$ layer with the formation of an outer layer of SiO_2, mainly responsible for the high oxidation resistance, and Nb_2O_5. In particular, the Nb oxide is present in a plate-like form, while silica diffuses inward, the result is the presence of discrete Nb_2O_5 plate-like particles embedded in SiO_2 layer (Figure **3.9**) [45].

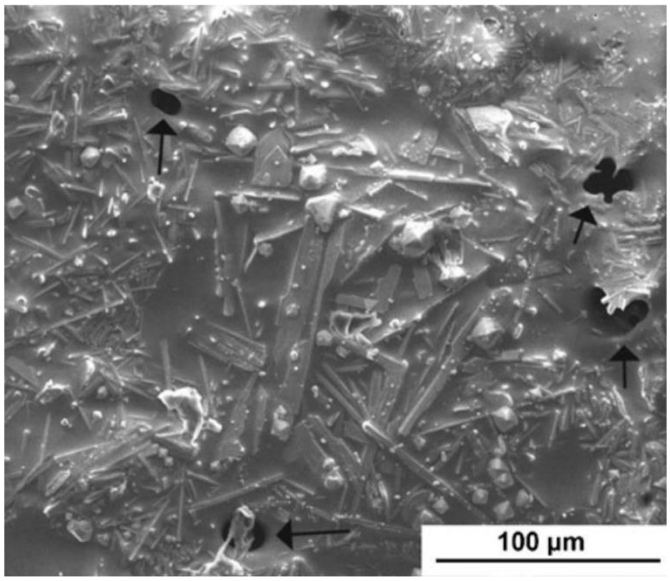

Figure 3.9 Isothermally oxidised silicide coating on C-103 with the presence of needle-like Nb_2O_5 in the SiO_2 layer [45].

Zmii *et al.* proposed an interesting work by comparing the properties of different silicide-base coatings in Nb. In particular, the oxidation results performed at 1700°C in air showed that a simple silicide coating $NbSi_2$ was resisting just for a short period of time [50]. The reason for it is the formation of a brittle film composed of Nb_2O_5 and SiO_2 [5]. While the best results were obtained by the use of much more complex coatings such as complex borosilicide (Nb_x, Ti_y, Cr_z, Mo_m, Ni_n) (Si_k, B_l, Al_p)$_2$ or molybdenum borosilicides Mo (Si_xB_y)$_2$ also in light of a similar CTE if compared to Nb [50].

Aluminides can also be used thanks to their ability to form a protective Al_2O_3 layer on the outer surface. The influence of Aluminide-base coatings on the oxidation resistance of Nb and Nb-alloys is reported in different studies [51–53]. In particular, Rapp *et al.* analysed the isothermal oxidation behaviour of different types of aluminides diffusion coatings, with the presence of other elements such as Ti, Cr and Mo [51]. Another possible solution is the use of aluminosilicide coatings, where the part is coated with a mixture of molten Al-Si-Cr and then annealed allowing Al to react with Nb. However, these types of coatings show inferior properties if compared to the silicide ones [5].

Zinc-base coatings can be produced by immersing the Nb component in molten zinc, followed by annealing to generate a diffusion layer. One of the drawbacks for the application of Zinc-base coating is the formation of brittle intermetallics, favouring the generation of cracks. Furthermore, these types of coatings are able to protect Nb up to a maximum temperature of 1100°C [54].

Alternative coatings such as platinum and iridium-based oxidation resistant coatings can represent a valid and attractive alternative to the conventional silicide coatings, due to their high melting temperature, high-temperature oxidation resistance and similar coefficient of thermal expansion compared to Nb. Additionally, the Nb-Pt and Nb-Ir phase diagrams highlight the presence of high-temperature eutectics at 1700°C and 1840°C respectively [55], [56], temperatures much higher if compared to the temperatures demanded by thruster combustion chamber application.

3.6 Manufacturing of Nb and Nb-alloys

3.6.1 Conventional Manufacturing Routes

Conventional manufacturing methods for Nb and Nb-alloys rely on casting, sintering and electron beam melting (EBM). Before 1960, Nb and Nb-alloys were produced using PM manufacturing routes such as vacuum sintering. Another alternative route for the production of Nb is vacuum arc remelting, with subsequent high-temperature extrusion and forging to a temperature close to the recrystallisation temperature [57].

Sintering of Nb is reported in the literature. Prior to sintering, the powders are pressed using high pressures in the order of 100MPa or above. The Nb green compacts formed are then sintered in vacuum atmosphere at a temperature above 0.5-0.7T_m. Sintering of pure Nb was

performed by M. Sankar *et al.* using a cold isostatic pressing (CIP) pressure ranging from 125-150MPa and sintering temperatures ranging from 1000-1800°C [58]. The results show that to achieve reasonable levels of densification and consequently of strength, high compaction pressures and sintering temperatures are required (250MPa, 1800°C). The use of a high sintering temperature can induce excessive grain growth with a consequent reduction in mechanical properties.

J.P. Page has investigated in his work the influence of the annealing conditions (temperature, time) on the microstructure and properties of pure Nb [8]. One of the main findings is that Nb obtained by PM shows a finer microstructure if compared to arc-casting, after the same heat treatment conditions. Casting should guarantee a low level of contaminants, however, the microstructure after casting is characterised by coarse columnar grains. The presence of coarse grains is beneficial for creep properties, however, it reduces the Hall-Petch strengthening. Recrystallisation of Nb after casting can be achieved by hot working or by cold working followed by annealing. The second option is preferred due to the high reactivity of Nb at high temperatures [8].

3.6.2 NNS PM HIP of Nb and Nb-alloys

Due to the limitations of the abovementioned conventional manufacturing processes for Nb and Nb alloys, NNS PM HIP technology for Nb and Nb alloys can represent a valid solution to shape high-value parts with complex geometries. HIP process on Nb requires the application of high temperatures, to achieve a near to fully dense microstructure. Due to the high HIP temperatures required for Nb alloys, some considerations on the canister material are required. In fact, a common mild steel canister has some temperature limitations. Figure **3.10** clearly shows that Nb and Fe form an eutectic at 1373°C, which limits the HIP temperature of Nb in a steel canister [59]. Another valid solution is to perform a two-step HIP

cycle, where the canister is removed by machining or pickling before the second HIP step where higher temperatures are involved. HIP of C-103 Nb-alloy using two-step HIP is reported by Wadsworth. In this work, the first HIP run was performed at 1260°C for 3h at a pressure of 103MPa, while the second step after the removal of the canister, the temperature was increased to 1593°C for 3h using the same pressure of 103MPa [60]. HIP of C-103 was also reported by N. Philips *et al.* using a temperature of 1500°C and pressure of 103MPa, however, the canister material was not specified. The as-HIPed results reveal an equiaxed microstructure with superior mechanical properties if compared to wrought C-103 [61]. Another possibility to HIP refractory metals is using a high melting temperature canister such as Nb and Mo, however, this strategy could lead to an increase in the manufacturing price and challenges to achieve defect-free welds.

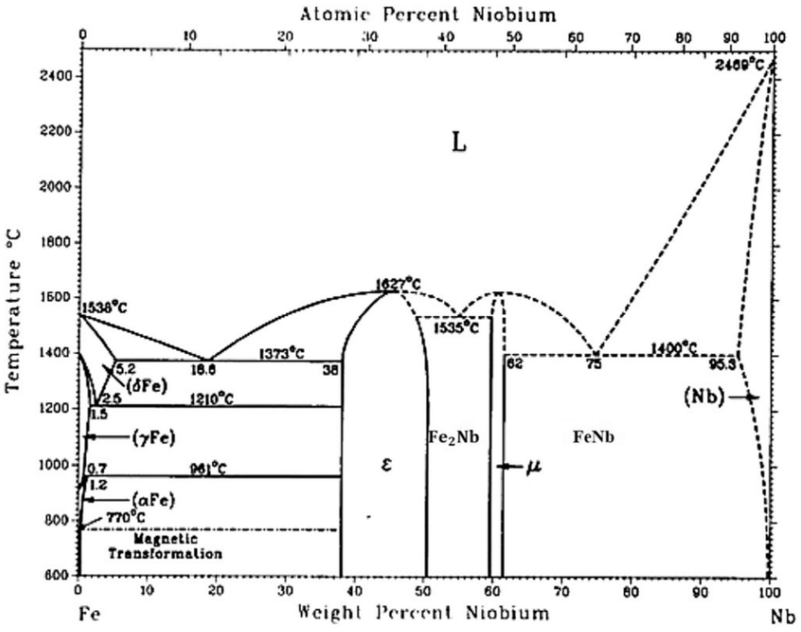

Figure 3.10 Nb-Fe phase diagram [59].

One of the main advantages of HIP pure Nb over Nb-base alloys is the generation of a microstructure free from PPBs. The reason for the absence of PPBs stands on the fact that Nb

has a high solid solubility of oxygen at the HIP temperature. Thus, HIP of pure Nb could potentially result in components with excellent mechanical properties. Furthermore, PM HIP has the capabilities of producing MMCs, and, as described in the above sections the fabrication of Nb-based composites can result in superior RT and HT mechanical properties and high-temperature oxidation resistance. In particular, the in situ formation of Nb_5Si_3 or the addition of SiC can represent a valid route to improve the performances of Nb and Nb-alloys.

However, the HIP response of Nb-alloys presents a completely different scenario. In fact, the vast majority of Nb-base alloys are alloyed with reactive elements such as Zr, Hf, and Ti (Table **3.4**). The presence of these elements reduces the solid solubility of oxygen in the alloy and additionally the reactive elements combine with oxygen to form stable oxides at PPBs reducing the mechanical properties of the as-HIPed alloys. However, not all Nb-alloys are alloyed with reactive elements, these alloys are more favourable to be processed through NNS PM HIP. In fact, the HIP of Nb-alloys with the presence of solid solution substitutional elements such as Ta, W, V and Mo can result in the absence of PPBs and thus with the presence of enhanced mechanical properties. Nevertheless, despite the presence of reactive elements and strong oxides formers, if O-levels are kept low in the powder and during the HIP process, the presence of PPBs can be drastically reduced as demonstrated by Rao *et al.* in their work on IN718 [62].

Table 3.4 List of the most common Nb alloys.

Nb-alloy	Elements	W (wt%)	Ta (wt%)	Hf (wt%)	Zr (wt%)	Y (wt%)
C-103	Hf, Ti, Zr	-	-	10	1	-
FS-85	W, Ta, Zr	10	27	-	0.8	-
C-129Y	W, Hf, Y	10	-	10	-	0.1
Nb-1Zr	Zr	-	-	-	1	-
SCb291	W, Ta	10	10	-	-	-

3.7 Concluding Remarks

3.7.1 Summary

This literature review chapter focused on the metallurgy of refractory metals with a particular focus on Nb and Nb-base alloys. Various strengthening mechanisms commonly used for strengthening of Nb-base alloys, and the effect of individual alloying elements were reviewed. The effect and limitations of the commonly used silicide coatings for high temperature oxidation resistance of Nb and Nb-base alloys were investigated. Additionally, the advantages and disadvantages of conventionally manufacturing routes for Nb and Nb-base alloys were described and compared with NNS PM HIP technique.

3.7.2 Aims & Knowledge Gaps

The current literature review chapter has outlined some knowledge gaps in PM HIP of Nb and Nb-base alloys and in the development of novel high temperature oxidation resistant coatings. This thesis will focus on the following points to address the knowledge gaps highlighted above:

- Lack of knowledge on the HIP of pure Nb and Nb-base alloys
    - This thesis will focus on the HIP response, both in terms of microstructure and mechanical properties, to understand the feasibility of PM HIP process for pure Nb and Nb-base alloys.
- Influence of interstitials on the mechanical properties of pure Nb.
    - This particular aspect is covered in literature. However, no studies are currently available on the possibility of modifying the powder characteristics to obtain higher levels of strength. This work will focus on both powder sieving and powder heat treatment to tailor the mechanical properties of as-HIPed pure Nb.

- Limited alternatives are available in literature to the conventionally used silicide coatings for high temperature oxidation resistance.
    - The use of alternative oxidation resistance coating will be assessed in this thesis. In particular, the development of a Pt coating through HIP DB as potential alternative will be presented.

3.8 References

[1] L.L. Snead, D.T. Hoelzer, M. Rieth, A.A.N. Nemith, Refractory Alloys: Vanadium, niobium, molybdenum, tungsten, Elsevier Inc., 2019. https://doi.org/10.1016/B978-0-12-397046-6.00013-7.

[2] P. Lipetzky, Refractory metals: A primer, Jom. 54 (2002) 47–49. https://doi.org/10.1007/BF02822621.

[3] R.A. Perkins, H.M. Gerald, The oxidation behavior and protection of niobium, J. Miner. Met. Mater. Soc. 42 (1990) 17–21.

[4] J.H. Westbrook, J.C. Zhao, Ultrahigh- Temperature Materials for Jet Engines, MRS Bull. (2003) 622–630.

[5] Yu. Dzyadikevich, L. Kitskai, Protecting Niobium and Tantalum from High-temperature Gas Corrosion (Review), Powder Metall. Met. Ceram. 36 (1997) 77–83.

[6] R.T. Webster, Refractory Metals and Their Industrial Applications, ASTM International, 1984. https://doi.org/10.1520/stp849-eb.

[7] E.N. Sheftel, O.A. Bannykh, Niobium-Base Alloys, Int. J. Refract. Met. Hard Mater. 12 (1994) 303–314.

[8] J. P. Page, The annealing behavior of cold-rolled niobium, University of Tennessee, 1957.

[9] Z.C. Cordero, B.E. Knight, C.A. Schuh, Six decades of the Hall–Petch effect – a survey of grain-size strengthening studies on pure metals, Int. Mater. Rev. 61 (2016) 495–512. https://doi.org/10.1080/09506608.2016.1191808.

[10] E.S. Bartlett, J.A. Houck, Physical and Mechanical Properties of Columbium and

Columbium-base alloys, United States, 1960.

[11] J.R. Slining, D.A. Koss, Solid Solution Strengthening of High Purity Niobium Alloys, Metall. Trans. 4 (1973) 1261–1264. https://doi.org/10.1007/BF02644520.

[12] Y. Tan, H. Tanaka, C. Ma, A. Kasama, R. Tanaka, Y. Mishima, S. Hanada, Solid-Solution Strengthening and High-Temperature Compressive Strength of Nb-X Alloys (X=Ta, V, Mo and W), J. Japan Inst. Met. Mater. 64 (2000) 559–565.

[13] D. Anton, D. Snow, L. Favrow, A. Giamei, Dispersion Strengthening of High Temperature Niobium Alloys, (1989) 1–90. http://oai.dtic.mil/oai/oai?verb=getRecord&metadataPrefix=html&identifier=ADA213829.

[14] V.G. Grigorovich, E.N. Sheftel, Physicochemical fundamentals of the development of heat-resistant niobium alloys, Met. Sci. Heat Treat. 24 (1982) 472–478. https://doi.org/10.1007/BF00773152.

[15] L.J. Pionke, J.W. Davis, Technical assessment of niobium alloys data base for fusion reactor applications, 1979.

[16] F. Saint-Antonin, A. Mitchell, Potential nb base superalloys, High Temp. Mater. Process. 13 (1994) 159–172. https://doi.org/10.1515/HTMP.1994.13.2.159.

[17] E.A. Brandes, Smithells Metals Reference Book, 6th ed., Butterworth & Co, London, 1983.

[18] F. Saint-Antonin, W. Lefebvre, I. Blum, Niobium base superalloys: Achievement of a coherent ordered precipitate structure in the Nb solid-solution, Crystals. 9 (2019). https://doi.org/10.3390/cryst9070345.

[19] G. Ghosh, G.B. Olson, Integrated design of Nb-based superalloys: Ab initio calculations, computational thermodynamics and kinetics, and experimental results, Acta Mater. 55 (2007) 3281–3303. https://doi.org/10.1016/j.actamat.2007.01.036.

[20] Y. Kimura, H. Yamaoka, N. Sekido, Y. Mishima, Processing, microstructure, and mechanical properties of (Nb)/Nb5Si3 two-phase Alloys, Metall. Mater. Trans. A Phys. Metall. Mater. Sci. 36 (2005) 483–488. https://doi.org/10.1007/s11661-005-0161-9.

[21] T.R. Bieler, N.T. Wright, F. Pourboghrat, C. Compton, K.T. Hartwig, D. Baars, A. Zamiri, S. Chandrasekaran, P. Darbandi, H. Jiang, E. Skoug, S. Balachandran, G.E. Ice, W. Liu, Physical and mechanical metallurgy of high purity Nb for accelerator cavities, Phys. Rev. Spec. Top. - Accel. Beams. 13 (2010) 1–13. https://doi.org/10.1103/PhysRevSTAB.13.031002.

[22] M. Sankar, R.G. Baligidad, A.A. Gokhale, Effect of oxygen on microstructure and mechanical properties of niobium, Mater. Sci. Eng. A. 569 (2013) 132–136. https://doi.org/10.1016/j.msea.2013.01.025.

[23] P.J. Yang, Q.J. Li, W.Z. Han, J. Li, E. Ma, Designing solid solution hardening to retain uniform ductility while quadrupling yield strength, Acta Mater. 179 (2019) 107–118. https://doi.org/10.1016/j.actamat.2019.08.024.

[24] P.J. Yang, Q.J. Li, T. Tsuru, S. Ogata, J.W. Zhang, H.W. Sheng, Z.W. Shan, G. Sha, W.Z. Han, J. Li, E. Ma, Mechanism of hardening and damage initiation in oxygen embrittlement of body-centred-cubic niobium, Acta Mater. 168 (2019) 331–342. https://doi.org/10.1016/j.actamat.2019.02.030.

[25] F.J.M. Boratto, On the Calculations of the Diffusion Coefficients of Oxygen and

Nitrogen, Metall. Trans. A. 8A (1977) 1233–1238.

[26] B.P. Bewlay, M.R. Jackson, P.R. Subramanian, A Review of Very high-temperature Nb-silicide-based composites, Metall. Mater. Trans. A. 34A (2003) 2043–2052.

[27] Z. Lu, C. Lan, S. Jiang, Z. Huang, K. Zhang, Preparation and performance analysis of Nb matrix composites reinforced by reactants of Nb and SiC, Metals (Basel). 8 (2018). https://doi.org/10.3390/MET8040233.

[28] B.P. Bewlay, C.L. Briant, M.R. Jackson, P.R. Subramanian, Recent Advances In Nb-Silicide In-Situ Composites, 1 (2001) 404–419.

[29] K.S. Chan, Cyclic-oxidation resistance of niobium-base in situ composites: Modeling and experimentation, Oxid. Met. 61 (2004) 165–194. https://doi.org/10.1023/B:OXID.0000025330.65837.d1.

[30] C.X. Yu, X.J. Zhao, L.R. Xiao, Z.Y. Cai, B. Zhang, L. Guo, Microstructure and mechanical properties of in-situ laminated Nb/Nb5Si3 composites, Mater. Lett. 209 (2017) 606–608. https://doi.org/10.1016/j.matlet.2017.08.012.

[31] X. Zhang, X. He, C. Fan, Y. Li, G. Song, Y. Sun, J. Huang, Microstructural and mechanical characterization of multiphase Nb-based composites from Nb-Ti-C-B system, Int. J. Refract. Met. Hard Mater. 41 (2013) 185–190. https://doi.org/10.1016/j.ijrmhm.2013.03.010.

[32] J.L. Yu, X.D. Weng, N.L. Zhu, H. Liu, F. Wang, Y.C. Li, X.M. Cai, Z.W. Hu, Mechanical properties and fracture behavior of an Nb-Silicide in situ composite, Intermetallics. 90 (2017) 135–139. https://doi.org/10.1016/j.intermet.2017.07.014.

[33] J. Sha, H. Hirai, T. Tabaru, A. Kitahara, H. Ueno, S. Hanada, Effect of carbon on

microstructure and high-temperature strength of Nb-Mo-Ti-Si in situ composites prepared by arc-melting and directional solidification, Mater. Sci. Eng. A. 343 (2003) 282–289. https://doi.org/10.1016/S0921-5093(02)00371-4.

[34] J. Geng, P. Tsakiropoulos, G. Shao, A study of the effects of Hf and Sn additions on the microstructure of Nbss/Nb5Si3 based in situ composites, Intermetallics. 15 (2007) 69–76. https://doi.org/10.1016/j.intermet.2006.03.001.

[35] J. Geng, P. Tsakiropoulos, A study of the microstructures and oxidation of Nb-Si-Cr-Al-Mo in situ composites alloyed with Ti, Hf and Sn, Intermetallics. 15 (2007) 382–395. https://doi.org/10.1016/j.intermet.2006.08.016.

[36] W.Y. Kim, H. Tanaka, S. Hanada, Microstructure and high temperature strength at 1773 K of Nbss/Nb5Si3 composites alloyed with molybdenum, Intermetallics. 10 (2002) 625–634. https://doi.org/10.1016/S0966-9795(02)00041-9.

[37] J.H. Kim, T. Tabaru, M. Sakamoto, S. Hanada, Mechanical properties and fracture behavior of an NbSS/Nb5Si3 in-situ composite modified by Mo and Hf alloying, Mater. Sci. Eng. A. 372 (2004) 137–144. https://doi.org/10.1016/j.msea.2003.12.010.

[38] J. Sha, H. Hirai, T. Tabaru, A. Kitahara, H. Ueno, S. Hanada, High-temperature strength and room-temperature toughness of Nb-W-Si-B alloys prepared by arc-melting, Mater. Sci. Eng. A. 364 (2004) 151–158. https://doi.org/10.1016/j.msea.2003.08.014.

[39] P.R. Subramanian, T.A. Parthasarathy, M.G. Mendiratta, D.M. Dimiduk, Compressive creep behavior of Nb5Si3, Scr. Metall. Mater. 32 (1995) 1227–1232. https://doi.org/10.1016/0956-716X(95)00130-N.

[40] M.G. Mendiratta, D.M. Dimiduk, Strength and Toughness of a Nb/Nb Si3 Composite,

24 (1993) 501–504.

[41] M.G. Mendiratta, J.J. Lewandowski, D.M. Dimiduk, Strength and ductile-phase toughening in the two-phase Nb/Nb5Si3 alloys, Metall. Trans. A. 22 (1991) 1573–1583. https://doi.org/10.1007/BF02667370.

[42] J.L. Yu, K.F. Zhang, Z.K. Li, X. Zheng, G.F. Wang, R. Bai, Fracture toughness of a hot-extruded multiphase Nb-10Si-2Fe in situ composite, Scr. Mater. 61 (2009) 620–623. https://doi.org/10.1016/j.scriptamat.2009.05.039.

[43] B.P. Bewlay, M.R. Jackson, H.A. Lipsitt, The balance of mechanical and environmental properties of a multielement niobium-niobium silicide-based in situ composite, Metall. Mater. Trans. A Phys. Metall. Mater. Sci. 27 (1996) 3801–3808. https://doi.org/10.1007/BF02595629.

[44] M. Rigaud, R. Tougas, Literature Survey on Columbium, 1971.

[45] M.Z. Alam, A.S. Rao, D.K. Das, Microstructure and High Temperature Oxidation Performance of Silicide Coating on Nb-Based Alloy C-103, Oxid. Met. 73 (2010) 513–530. https://doi.org/10.1007/s11085-010-9190-x.

[46] S. Knittel, S. Mathieu, M. Vilasi, Nb4Fe4Si7 coatings to protect niobium and niobium silicide composites against high temperature oxidation, Surf. Coatings Technol. 235 (2013) 144–154. https://doi.org/10.1016/j.surfcoat.2013.07.027.

[47] S. Priceman, L. Sama, Reliable, Practical, Protective Coatings for Refractory Metals Formaed by the Fusion of Silicon Alloy Slurries., Electrochem. Technol. (1968).

[48] Z. Alam, S. Sarin, M.K. Kumawat, D.K. Das, Microstructure and oxidation behaviour of Fe – Cr – silicide coating on a niobium alloy, Mater. Sci. Technol. 32 (2016) 1826–

1837. https://doi.org/10.1080/02670836.2016.1148226.

[49] R.O. Suzuki, M. Ishikawa, K. Ono, NbSi2 coating on niobium using molten salt, J. Alloys Compd. 336 (2002) 280–285. https://doi.org/10.1016/S0925-8388(01)01879-5.

[50] V.I. Zmii, S.G. Ruden, M.Y. Bredikhin, V. V Kunchenko, High-temperature Oxidation-resistant Coatings on Niobium and its Alloys, 47 (2008) 255–259.

[51] R.A. Rapp, W. Soboyejo, Y. Li, Oxidation Behavior of Niobium Aluminide Intermetallics Protected by Aluminide and Silicide Diffusion Coatings, 30 (1999).

[52] K. Matsuura, T. Koyanagi, T. Ohmi, M. Kudoh, Aluminide Coating on Niobium by Arc Surface Alloying, 44 (2003) 861–865.

[53] S. Majumdar, A. Arya, I.G. Sharma, A.K. Suri, S. Banerjee, Applied Surface Science Deposition of aluminide and silicide based protective coatings on niobium, Appl. Surf. Sci. (2010) 635–640. https://doi.org/10.1016/j.apsusc.2010.07.055.

[54] G. Sandoz, Coating Columbium for High Temperatures, J. Met. 12 (1960).

[55] S.N. Tripathi, S.R. Bharadwaj, S.R. Dharwadkar, The Nb-Pt (Niobium-Platinum) system, J. Phase Equilibria. 16 (1995) 465–470.

[56] H. Okamoto, The Ir-Nb (iridium-niobium) system, J. Phase Equilibria. 15 (1994) 52–54.

[57] J.R. Davis, ed., Refractory Metals and Alloys, in: ASM Int., 1998.

[58] M. Sankar, R.G. Baligidad, S. Khaple, V.V.S. Prasad, V.V.B. Prasad, Compaction and Sintering Behavior of Niobium Powder for Making Consumable Electrodes, 65 (2012) 467–472. https://doi.org/10.1007/s12666-012-0152-7.

[59] E. Paul, SwartzendruberL. J., The Fe–Nb (Iron-Niobium) system, Bull. Alloy Phase Diagrams. 7 (1986) 248–254.

[60] J. Wadsworth, C.A. Roberts, E.H. Rennhack, Creep behaviour of hot isostatically pressed niobium alloy powder compacts, J. Mater. Sci. 17 (1982) 2539–2546. https://doi.org/10.1007/BF00543885.

[61] N.R. Philips, M. Carl, N.J. Cunningham, New Opportunities in Refractory Alloys, Metall. Mater. Trans. A Phys. Metall. Mater. Sci. 51 (2020) 3299–3310. https://doi.org/10.1007/s11661-020-05803-3.

[62] G.A. Rao, M. Srinivas, D.S. Sarma, Effect of oxygen content of powder on microstructure and mechanical properties of hot isostatically pressed superalloy Inconel 718, Mater. Sci. Eng. A. 435–436 (2006) 84–99. https://doi.org/10.1016/j.msea.2006.07.053.

Chapter 4. Experimental Procedure

The current PM HIP study is focused on four main experimental areas, including powder characterisation, HIP procedure, microstructure analysis and mechanical testing. For this work, a wide range of different powders were used, including Ni-base superalloy (IN625), IN625-MMCs, Nb, and Nb-base alloy (C-103). Depending on the final application different characterisation tests were performed.

4.1 Material

4.1.1 IN625 powder

The study performed on IN625 focuses on the analysis and characterisation of four powders obtained using four different atomisation routes, i.e. AGA, NGA, PA and WA. The powders were atomised by different manufacturers (Table **4.1**). The analysed powders have different powder ranges as outlined in Table **4.1**.

Table 4.1 Specifications of IN625 powders.

Material	Manufacturer	Size Range	Manufacturing Route
AGA IN625	LPW	15-45 µm	Argon Gas Atomisation
NGA IN625	ASL	15-150 µm	Nitrogen Gas Atomisation
PA IN625	APC	0-150 µm	Plasma Atomisation
WA IN625	ASL	15-150 µm	Water Atomisation

4.1.2 IN625-MMCs powder

For the study performed on IN625-MMCs SiC and TiB_2 were used as reinforcements. For the base material, AGA IN625 powder was used (Table **4.1**) due to its narrow range distribution leading to a more uniform blending. Different reinforcement fractions were adopted (5vol%, 10vol% and 25vol%) in order to understand their influence on the microstructure, tribological and mechanical properties. The list of the reinforcement used is reported in Table **4.2**.

Table 4.2 Specification for IN625 reinforcements.

Material	Manufacturer	Size Range	Manufacturing Route
SiC	Reade Advanced Materials	<10µm	mechanical comminution
TiB_2	Reade Advanced Materials	<10µm	mechanical comminution

4.1.3 Nb powder

For the initial trials on PM HIP of pure Nb three different powders were assessed with different size ranges. According to their size, the powders were categorized as fine, coarse, mid-range and mid-range sieved. Nb powders were obtained through hydration – dehydration (HDH) process by different companies, the detail of the powder size and manufacturers are shown in Table **4.3**.

Table 4.3 Nb powders specifications.

Material	Manufacturer	Size Range	Manufacturing Route
Nb fine	Alpha Aesar	<44µm	HDH process
Nb coarse	Alpha Aesar	<250µm	HDH process
Nb mid-range	Elite Materials	15-100µm	HDH process
Nb mid-range sieved	Elite Materials	15-63µm	HDH process

4.1.4 C-103 powder

C-103 powder was used to assess the influence of the HIP behaviour on Nb-alloys in terms of consolidation, microstructure and mechanical properties. The specifications of C-103 powder are shown in Table **4.4**.

Table 4.4 C-103 powder specifications.

Material	Manufacturer	Size Range	Manufacturing Route
C-103	H.C. Starck Newton	10-45µm	Argon Gas Atomisation

4.2 Powder Characterisation

4.2.1 Chemical Analysis

Chemical composition of the pre-alloyed feedstock powder material has a great impact on the characteristics of PM HIP products such as microstructure, unwanted phase formation and the corrosion, mechanical and tribological properties. Therefore, it is important to analyse the feedstock material to determine its chemical composition, especially the concentration of interstitial elements present in the pre-alloyed powder chemistry, as these can play a major role in terms of achieving the required properties, comparable to wrought material.

IN625 and C-103 powders were analysed by AMG Analytical Services, Sheffield and compared to the chemical composition provided by the manufacturers. Inductively Coupled Plasma Optical Emission Spectroscopy (ICP OES) technique was employed to determine the major alloying elements, i.e. Cr, Mo, Nb, W, Cu, Hf, Zr, Ni, Co, Fe, Mn, V, Ti, Sn, Al, Si, P, Ta, B (lower limit <0.02wt.%). Carbon and sulphur were determined by LECO infrared combustion in oxygen whereas oxygen, nitrogen and hydrogen gases were determined by LECO inert gas fusion using infrared and thermal conductivity detection.

Oxygen levels were detected in Nb fine, coarse, mid-range and mid-range sieved powders and in the as-HIPed condition to understand the oxygen pick up during the HIP process. Also in this case, the measurements were performed by AMG Analytical Services using LECO inert gas fusion.

4.2.2 XPS analysis

X-ray photoelectron spectroscopy (XPS) analyses were performed on the surface of the four IN625 powders. The assessment of the surface chemistry is crucial to understand the elemental distribution on the surface of the powder, where normally some elements such as O, C, Al, Ti and Cr are prone to have higher concentrations [1]. The XPS analyses were

performed using a Thermo Fisher K-Alpha+ X-ray photoelectron spectrometer available at Imperial College (London) through the Henry Royce Institute using Casa XPS software. XPS spectra were recorded on the surface of the four IN625 powders using a monochromatic X-ray $K_{\alpha 1}$ source with a spot size of 400µm. The C1s carbon B.E. of 284.8eV was used as calibration to take into account the charging effect. High-resolution XPS were performed on Ni, Nb, Mo, O, C and Cr to better understand the chemical state of the elements. XPS depth profiles were obtained through etching with a 1000eV Ar^+ ion beam.

4.2.3 Particle Size Distribution

Particle size distribution (PSD) is an important factor in NNS PM HIP as it can have a direct impact on the packing density, which usually can affect the canister deformation and the ability to achieve near net shape HIPed products. A wide range PSD will increase the packing density but reduce the flowability of the powder, as there is an increase in inter-particle friction between the small and large particles. Although narrow PSD reduces the inter-particle friction and hence increases flowability whilst maintaining high apparent density, however, wide PSD is usually preferred as it increases the packing density, which is considered more important than flowability in NNS PM HIP process.

A state-of-the-art Malvern Panalytical Mastersizer 3000 (Figure **4.1**) PSD analyser installed at TWI Ltd. Cambridge was used to measure PSD values of IN625, IN625-MMCs and Nb powders. This instrument uses laser diffraction to detect the particles' size and their distribution and is capable of analysing powders both in wet (Hydro EV) and dry (Aero S) environments. The powders in this study were analysed using the Hydro EV system whereby a small quantity of powder was added into deionised water and fed through the Mastersizer system.

Figure 4.1 Malvern Panalytical Mastersizer 3000.

4.2.4 Tap and Apparent Densities

Powder density is closely related to particle size range and PSD, and strongly affects the densification kinetics and the microstructural evolution during the consolidation. Three metrics of density are of interest when characterising powders: apparent density, tap density and the most importantly packing density for PM HIP technology. Apparent density is the density value of loose powder while tap density refers to the density of the powder after it has been tapped a sufficient number of times for it to reach its theoretical packing density whereas packing density is the ratio between tap to bulk densities of the material. The apparent density was measured using a POWDERFLOW system that comprises of a funnel stand, a density cup and a Hall flowmeter funnel (Figure **4.2**, left). Once the cylinder ($25cm^3$) is full, any excess powder is removed and then the powder is weighed hence giving the apparent density.

A tap density tester (Figure **4.2**, right) was used to measure the tap density of powders. Tap density measurements are taken by filling a volumetric cylinder with powder of a known

weight and placing this on a tap density machine. The machine then oscillates vertically for 3000 cycles and then the volume of the condensed powder is used to calculate the tap density. The apparent and tap density measurements were performed according to ASTM 212-17 and ASTM B527-15 standards, respectively.

Figure 4.2 Powder flow kit (left) and tap density tester (right) at TWI.

4.2.5 Flowability

Flowability is a physical characteristic of powders, which is determined by measuring the time taken for powder of a known mass to flow through a set diameter orifice. The flowability of a powder provides an insight into the morphology of the powders as irregularly shaped or finer particles struggle to flow due to inter-particle friction. In this work, the flowability of the powders was analysed in accordance with ASTM B213-17 using a powder flow kit, as shown in Figure **4.2** (left). The flowability study used a Hall Flowmeter funnel with specific dimensions and surface finish, which can be found in ASTM B213-17.

Tap and apparent densities are related to the flowability of a powder, as these enable the Hausner ratio (*Eq. 4.1*) and compressibility index (*Eq. 4.2*) of a powder to be calculated, from which flowability values can be deduced. These characteristics are influenced by the particle

size range, PSD, morphology and cohesivity of the powders. The Hauser ratio and compressibility index are calculated using [2]:

$$Hausner\ Ratio = \frac{Tap\ Density}{Apparent\ Density} \qquad Eq.\ 4.1$$

$$Compressibility\ Index = \frac{Tap\ Density - Apparent\ Density}{Tap\ Density} \times 100 \qquad Eq.\ 4.2$$

The Hausner ratio and compressibility index are associated with flow characteristics, as shown in Table **4.5**.

Table 4.5 Relationship between compressibility index and Hausner ratio to flowability of powders [3].

Compressibility index (%)	Flow characteristics	Hausner ratio
<10	Excellent	1.00-1.11
11-15	Good	1.12-1.18
16-20	Fair	1.19-1.25
21-25	Passable	1.26-1.34
26-31	Poor	1.35-1.45
32-37	Very poor	1.46-1.59
>38	Very, very poor	>1.60

4.2.6 Powder Morphology and Cross-section

The quality and microstructure of as-received powders usually depend on the feedstock material purity and the powder manufacturing process route. Both of these can have a strong impact on the microstructure and mechanical properties of the consolidated materials. Specifically, any internal defects such as argon gas porosity, micro-segregation, non-metallic inclusions and spatial variation of elemental composition within the powder particles need to be fully analysed. Cross-sections of all powders were prepared as per the ASTM E3-11

standard. A small quantity of each powder was mounted in conductive bakelite, ground and polished to ¼ micron finish using the metallographic procedures outlined in ASTM E3-11 for microscopic analysis. A TM3000 scanning electron microscope (SEM) was used for microstructural imaging. Specifically, backscattered electron (BSE) imaging along with energy dispersive X-ray spectroscopy (EDX) was performed on the powder cross-sections. During gas atomisation process, the atomisation gas can be entrapped inside the powders, generating gas pores. During the HIP process, these gas pores collapse giving rise to a fully dense microstructure. However if the material is exposed to temperature higher than the HIP temperature e.g. during any subsequent heat treatment, it will develop the so called thermally induced porosity (TIP) due to expansion of previously collapsed gas pores [4]. TIP will affect the mechanical properties and especially the fatigue life of safety critical HIPed parts. To study the powder particle surface morphology, powder samples were stuck/mounted on a SEM stub using a conductive carbon tape and loaded into SEM equipment for imaging.

4.2.7 Powder Mixing

Powder blending was performed for IN625-MMCs. Blending was performed in two different steps. During the first step, the required amount of base metal powder and reinforcement was blended for 1 minute with a speed of 2000rpm using SpeedMixer^{TM} available at TWI site. This first mixing step, thanks to high revolution speeds was enough to obtain a good mixture of the powders. In the second step, the powders were further homogenised using rollers with a low revolution speed for 3h.

4.3 NNS PM HIP procedure

NNS PM HIP requires different steps to be carefully followed in order to obtain a successful result. A schematic representing the different steps in HIP procedure is presented in Figure **4.3**. The first step is canister design and manufacture. In this case, cylindrical canisters

(Ø50x185mm) with 2mm thickness were chosen for IN625 and IN625-MMCs, while for Nb and C-103 (Ø50x90mm) canisters were used. The size of the canisters provides enough material to produce metallographic samples and specimens for mechanical testing, taking into account the chamber size of the HIP. The selected material for the canisters was low carbon steel (ISO 3574 grade CR4) due to its availability in cold roll sheet and tube (BS EN 10305-1: 2010 E235+C) forms, material ductility and thermal properties, ease of manufacturability, excellent pickling response and its low cost. Moreover, low carbon steel has a melting point of around 1400°C, which is enough to HIP a wide range of materials such as titanium, steel, nickel superalloys, etc. The downside of using a low carbon steel canister is the diffusion of carbon and iron from the steel canister into the HIPed powder material. The maximum diffusion of carbon and iron into HIPed material is up to ~500µm (strongly dependent on HIP conditions, i.e. temperature, pressure and dwell time) [5]. Figure **4.5** shows that close to the canister the prior particle boundaries (PPBs) are more prominent. This is because of the carbon and iron diffusion from the canister into the HIPed material, which allows for example some MC-type carbides to precipitate on or around the powder particle's surface, e.g. (Nb, Mo, Ti) carbides in the case of HIP IN625 material.

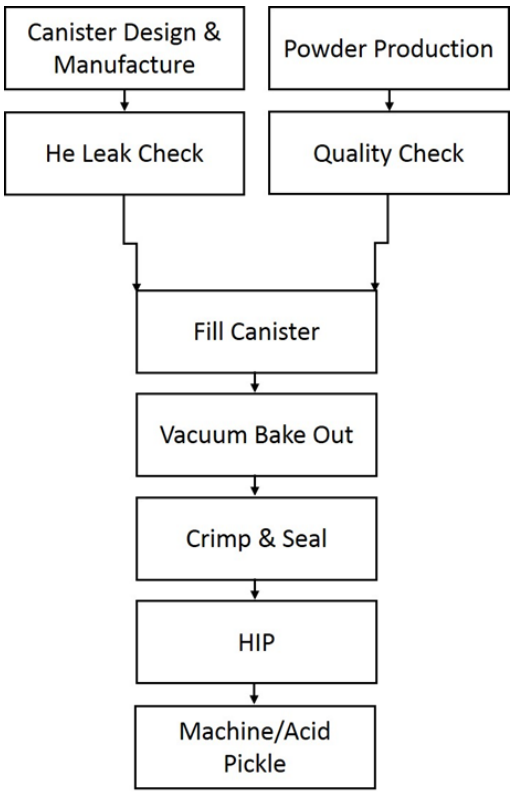

Figure 4.3 Schematic of NNS PM HIP procedure.

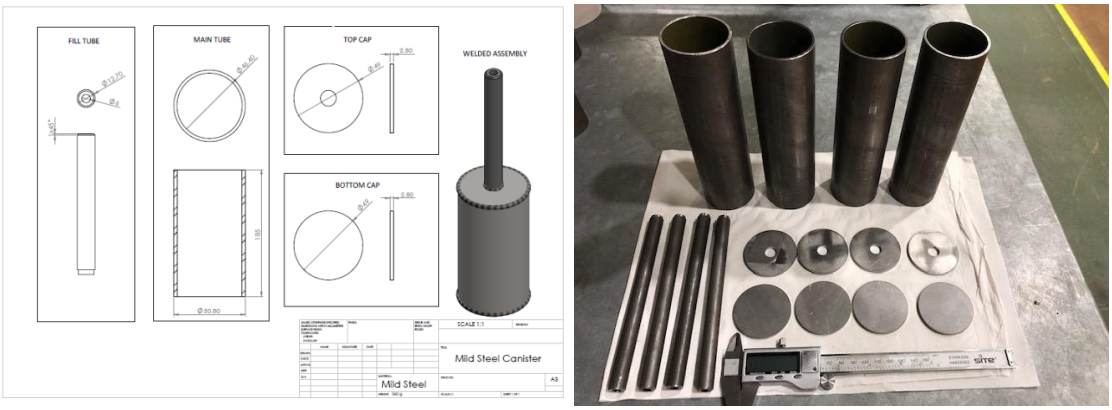

Figure 4.4 Technical drawing of the canister (left), low carbon steel canisters before the welding procedure (right).

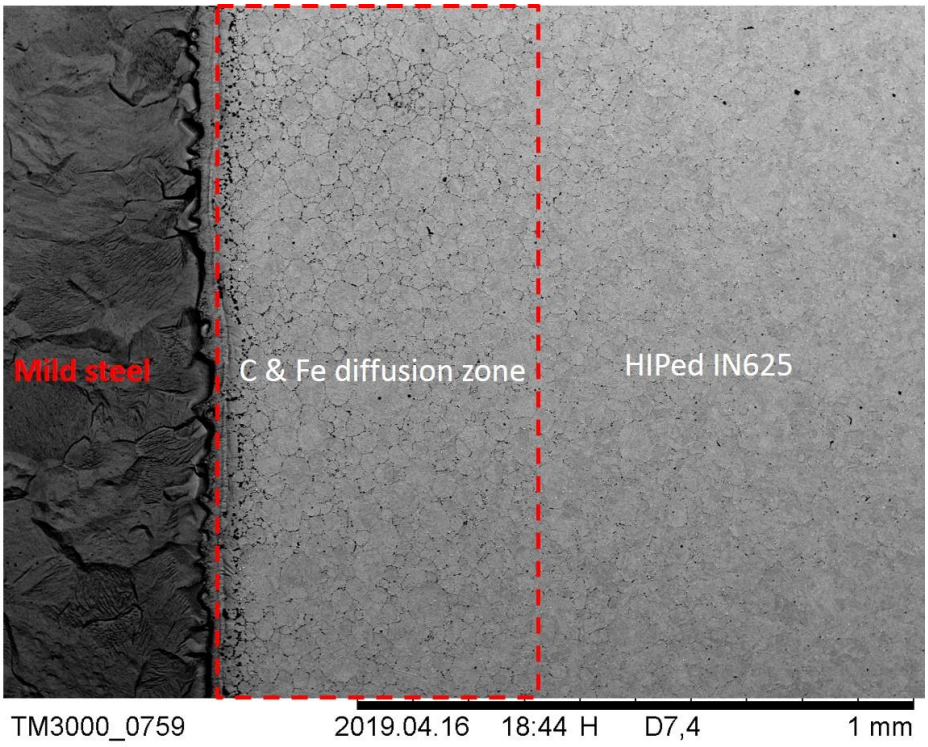

Figure 4.5 Diffusion zone close to the canister in HIPed IN625.

Before welding, canisters were cleaned using acetone in an ultrasonic bath. TIG welding technique was employed to join top and bottom cap and filling tube (Figure **4.4**) during the canister manufacturing. Before a canister is filled with powder, it is vital to test the welded canister for any flaws/defects. This is because once the HIP cycle is initiated and the powder filled capsule is pressurised, argon gas can penetrate via any tiny welding defects, resulting in catastrophic and complete failure of HIP powder filled canister. Even the smallest flaw in the order of magnitude of the atomic radius of argon is sufficient to fail the consolidation of powder during the HIP cycle. Therefore, it is important to leak check welded canister (Figure **4.6**) for any defects before moving on to the powder filling stage and to make sure that canister is gas leak tight, i.e. leak rate is lower than 10^{-7}mbar/s. The leak detection was performed using Pfeiffer leak detector and using He as a penetrating gas for the flaws

detections (Figure **4.6**). Helium was used because of its low atomic size, capable of detecting the smallest defects.

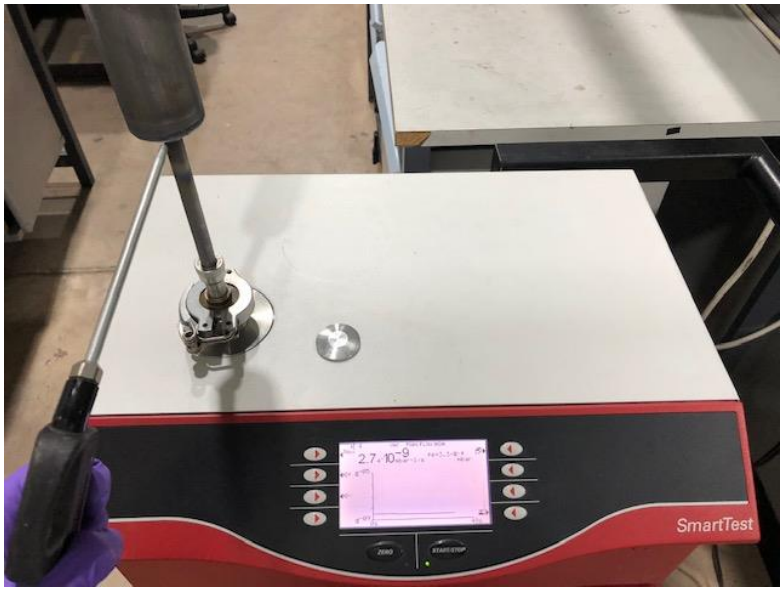

Figure 4.6 Canister He Leak detection.

The filling procedure is very important in PM HIP, and if performed correctly, it will allow to fill the canister uniformly to its packing density. During this step is crucial to avoid any contamination of the powders with the external environment. This is the reason why the filling procedure was performed inside a glovebox in inert argon atmosphere and with oxygen levels below 40ppm (Figure **4.7** left). After partial filling in the glovebox, the canisters were vibrated for intervals of 10min, using a vibrating platform (Figure **4.7** right), to achieve their packing density and then filled again in the glovebox if necessary. When transferring the canisters from the glovebox to the vibrating platform, the canisters were sealed in order to reduce any contamination coming from the external environment.

Figure 4.7 Glove box filling (left), vibrating platform (right).

Once the filling procedure was completed, the evacuation/filling tubes of powder filled canisters were attached to a degassing rig (Figure **4.8** left) to perform outgassing at room temperature. The outgassing procedure will allow removing any internal gas present in the canister. Outgassing is an important step because if an excess of gas is present inside the canister, it will expand during the HIP cycle resulting in canister failure. Furthermore, if some residual oxygen is present inside the canister it will contribute to the internal oxidation of the powders during the HIP stage enhancing the formation of the unwanted PPBs. The canisters were degassed for 48h achieving a vacuum better than 10^{-5}mbar. Long outgassing times are required to remove air pockets and moisture trapped inside the powder. The IN625 and IN625-MMCs canisters were outgassed using a temperature of 100°C to remove any possible presence of moisture and to accelerate the degassing process. While for Nb and C-103 a room temperature outgassing was performed due to the highly reactive nature of Nb. After outgassing, canister's evacuation/filling tubes were hot crimped and sealed using an oxy-acetylene torch and a crimping device (Figure **4.8** right). The outgassed powder filled canisters were then loaded into the HIP system.

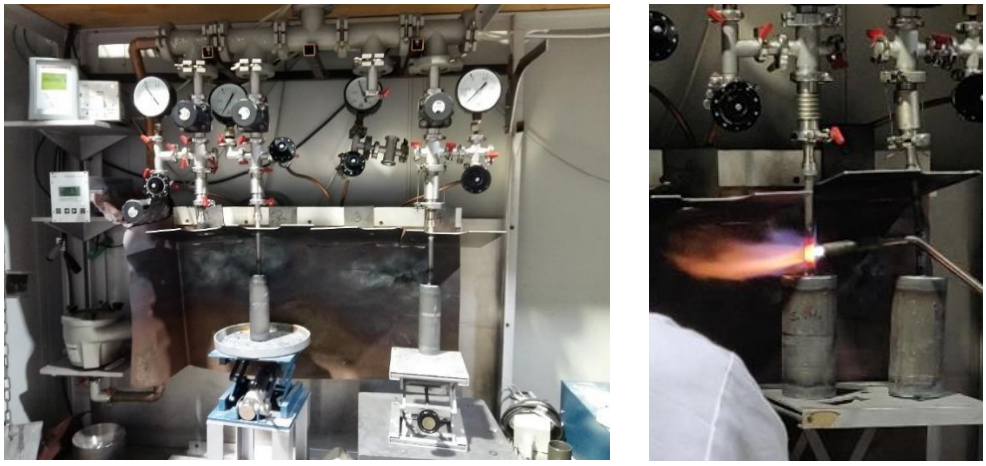

Figure 4.8 Canister outgassing (left), hot crimping (right).

After hot crimping, the canisters were ready to be HIPed. HIP was performed using the EPSI HIP available at the Univeristy of Birmingham, consisting of Mo heating elements with chamber size of (Ø150x300mm) and maximum operating conditions of 1450°C and 200MPa (Figure **4.9**).

Figure 4.9 EPSI HIP system (left), Mo heating elements (right).

4.4 Sample Preparation

Electrical discharge machining (EDM) was used to extract samples from the HIPed canisters for microstructural characterisation. The samples were mounted in conductive Bakelite in order to be observed using the SEM. After hot mounting in conductive Bakelite, the IN625 and IN625-MMCs samples were ground and polished using Struers Tegramin-25 automatic polisher. Four different steps were involved in this procedure. In the first grinding step, a Piano 120 disc was used in water, while for the second grinding step a Largo disc in a diamond solution was employed. The first polishing step was performed using a Dac disc with 2-3µm diamond suspension, while for the last polishing step a Chem disc with a silica suspension of 0.25 µm was used to ensure a scratch-free polished surface suitable for Optical, Microhardness, SEM and EBSD analysis. The samples were etched for 20 seconds using Kalling's N^{o}2 etchant (5g $CuCl_2$ + 100ml HCl + 100ml Ethanol) in order to reveal the grain structure of the HIPed samples for both optical and SEM analysis. Following etching, the samples were rinsed in ethanol and then dried.

The grinding and polishing procedure adopted for Nb and C-103 involved different manual grinding steps using respectively 240, 400, 800, 1200 and 2500 grit sandpapers. The grinding procedure was followed by a single polishing step using Chem disc with H_2O_2 activated OPS suspension.

4.5 Mechanical Testing

4.5.1 Microhardness

Vickers microhardness data for all samples were collected at ten different locations according to ASTM E384 – 17 using a load of 500gf and a holding time of 10s. Microhardness was performed using a semi-automatic Buehler microhardness tester (Figure **4.10**).

Microhardness tests were performed on all the HIPed samples to have a first understanding of the mechanical properties and the influence of HIP parameters and/or chemical composition on the as-HIPed material properties. In particular, microhardness was performed for several reasons in each samples:

- **IN625 as-HIPed samples**: in this case, microhardness was performed to have a first assessment on the influence of powder atomisation route on the as-HIPed strength of the material.
- **IN625 HIPed + HTed samples**: the microhardness tests on HIPed + HTed IN625 samples were performed to understand if the designed heat treatment was adequate to precipitate γ′′ hardening phase.
- **IN625-MMCs as-HIPed samples**: the microhardness tests were performed to assess the influence of the reinforcement type and volume fraction on the hardness and compare them with the base material. The hardness values were of particular interest as they are directly related to the wear properties.
- **Nb as-HIPed samples**: the microhardness tests were adopted to understand the influence of O levels on the strength of the material for three different pure Nb-powders.

- **C-103 as-HIPed sample:** microhardness tests were performed to understand if the HIP parameters were adequate to achieve the desired hardness of the alloy if compared to the wrought conditions.

Figure 4.10 Buehler semi-automatic microhardness tester.

4.5.2 Tensile Testing

Tensile tests were performed by Element and Westmoreland Mechanical Testing & Research Ltd according to ASTM E8/E8M-16a and they were carried out on IN625, IN625-10v.%SiC, pure Nb and C-103 samples. Tensile testing was carried out with the use of an extensometer to measure the sample's elongation during testing. An example of the tensile sample used is reported in Figure **4.11**. Tensile tests provided detailed information regarding the strength of the material but also on the influence of PPBs on ductility and fracture mode. In the case of

pure Nb, tensile tests can give a better assessment on the influence of O-levels on the strength and how an increase in O-content can impact the ductility of the material.

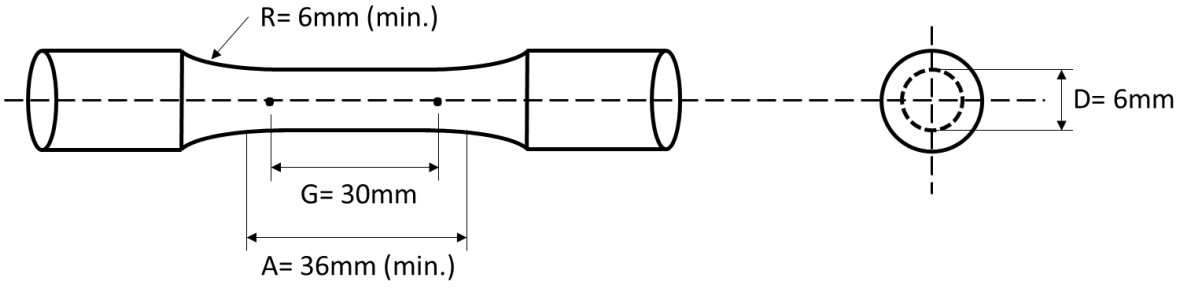

A: Length of reduced section
D: Diameter
G: Gauge length
R: Radius of fillet

Figure 4.11 Schematic of tensile sample according to ASTM E8/E8M-16a standard.

- **IN625 samples:** three room temperature tensile tests of HIPed IN625 specimens (for each powder atomisation type) were performed to understand the influence of the atomisation route on the ductility and strength levels.
- **IN625-10v.%SiC:** three room temperature and high-temperature (650°C) tensile samples were performed to understand the influence of the reinforcement addition on the strength of the material and the possible loss in ductility due to the presence of ceramic reinforcement particles art PPBs.
- **Nb and C-103:** three room temperature tensile tests were performed on Nb mid-range, Nb mid-range sieved and C-103 as-HIPed samples. The tensile tests performed on Nb were targeted to understand the influence of oxygen levels on the strength and ductility of the material. C-103 tensile properties were evaluated to compare HIPed C-103 with wrought C-103, but also to have a direct comparison with as-HIPed pure Nb.

4.5.3 Charpy Impact Testing

Charpy impact tests were performed by Element and Westmoreland Mechanical Testing & Research Ltd using samples measuring 10mm x 10mm x 55mm, with a 2mm V-notch as per ASTM E23-16b standard, using an instrument with a 325J nominal striking energy. A representation of the Charpy impact sample used is shown in Figure **4.12.**

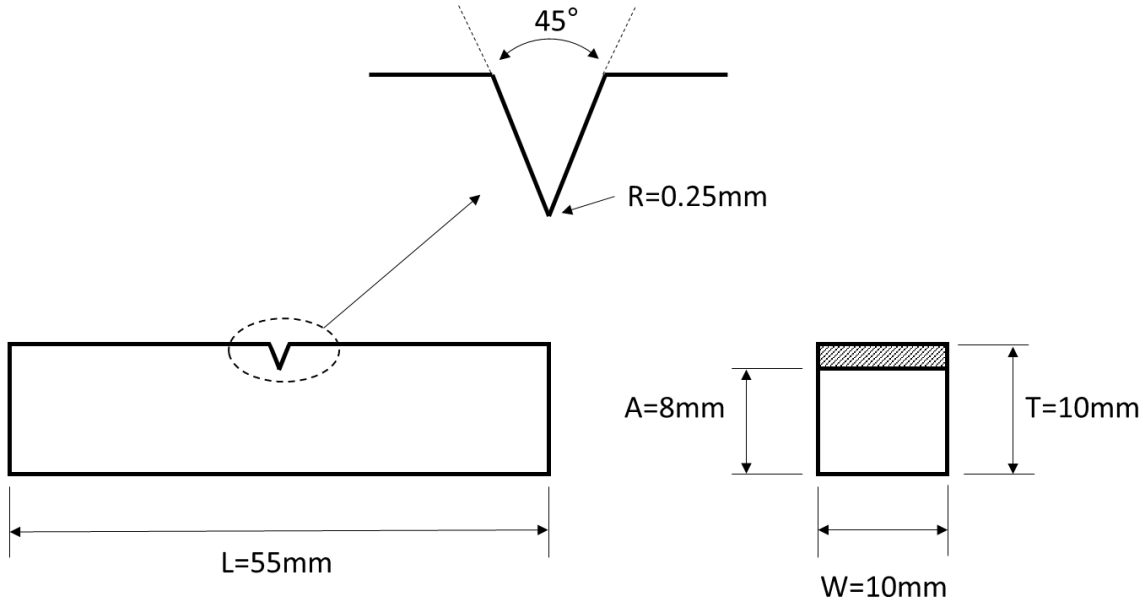

L: Overall length
W: Width
T: Thickness
A: Ligament length
R: Radius of notch

Figure 4.12 Schematic of Charpy impact sample according to ASTM E23-16b.

Charpy impact tests are related to the fracture toughness of the material, which is mostly influenced by the oxygen levels in the material and consequently the amount of PPBs [9].

- **IN625 samples:** three room temperature impact tests were performed on HIPed samples (from each powder atomisation type). Charpy V-notch tests were also

performed on HIPed+HTed PA IN625 samples to understand the effect of heat treatment on the absorbed energy.

- **IN625-10v.%SiC:** similar Charpy impact tests were performed on IN625-10v.%SiC to understand how the reinforcements can impact the fracture toughness of the material and to have a direct comparison with IN625**.**

4.6 Wear Test

Wear tests were performed on IN625 and IN625-MMCs materials. The wear tests were carried out at room temperature using a reciprocating Phoenix Tribology Tester available at the University of Birmingham (Figure **4.13**). The tribological tests were performed using 8mm Al_2O_3 balls as counterparts using a load of 20N, and a sliding velocity of 10mm/s for 750 cycles. The coefficient of friction (COF) was calculated using the tribometer dedicated software, while the wear rate was assessed by calculating the volume loss through Alicona optical profilometer (Figure **4.14**). The wear tracks were analysed using a TM3000 backscattered SEM to understand the nature of the wear and the differences in wear mechanisms among the different samples. EDX analyses were also performed on the wear tracks to understand the entity of material transfer from the balls to the samples.

Figure 4.13 Reciprocating wear test system.

Figure 4.14 Alicona optical profilometer.

4.7 References

[1] Z.J. Gao, G.Q. Zhang, Z. Li, H. Yuan, W.Y. Xu, Y. Zhang, Surface Segregation and Oxidation Behavior of Superalloy Powders Fabricated by Argon Atomization, Mater. Sci. Forum. 747–748 (2013) 518–525. https://doi.org/10.4028/www.scientific.net/msf.747-748.518.

[2] T. Hao, Understanding empirical powder flowability criteria scaled by Hausner ratio or Carr index with the analogous viscosity concept, RSC Adv. 5 (2015) 57212–57215.

[3] M. Copley, Review the current methods for powder flowability testing, (n.d.) 31–33.

[4] G.H. Gessinger, Powder Metallurgy of Superalloys, 1984.

[5] E. Bassini, V. Vola, M. Lorusso, R. Ghisleni, M. Lombardi, S. Biamino, D. Ugues, G. Vallillo, B. Picqué, Materials Science & Engineering A Net shape HIPping of Ni-superalloy : Study of the interface between the capsule and the alloy, Mater. Sci. Eng. A. 695 (2017) 55–65. https://doi.org/10.1016/j.msea.2017.04.016.

[6] R.E. Seebold, L.S. Birks, Elevated temperature diffusion in the systems Nb-Pt, Nb-Se, Nb-Zn, Nb-Co, Ni-Ta, and Fe-Mo, J. Nucl. Mater. 3 (1961) 260–266. https://doi.org/10.1016/0022-3115(61)90193-3.

[7] K. Zhang, The Microstructure and Properties of HIPped Powder Ti Alloys, The University of Birmingham, 2009.

[8] C. Bormio-Nunes, C.A. Nunes, F.S.A. Porto, V.S. De Souza, M.A. Tirelli, E.R. Edwards, Diffusion between Nb and Ti related to superconductor wire processing, Supercond. Sci. Technol. 16 (2003) 521–526. https://doi.org/10.1088/0953-2048/16/4/317.

[9] T. Berglund, F. Meurling, Oxygen Content in PM HIP 625 and its Effect on Toughness, 12th Int. Conf. Hot Isostatic Press. (2017) 135–141.

Chapter 5. The Role of Powder Atomisation Route on the Microstructure and Mechanical Properties of Hot Isostatically Pressed Inconel 625

Alessandro Sergi[1, 2], Raja H. U. Khan[3], Moataz M. Attallah*[1]

[1] IRC in Materials Processing, School of Metallurgy and Materials, The University of Birmingham, Birmingham, B15 2TT, UK

[2] National Structural Integrity Research Centre (NSIRC), Cambridge, CB21 6AL, UK

[3] TWI Ltd, Cambridge, CB21 6AL, UK

* Corresponding author: [redacted]

The paper is slightly modified from the published version in Materials Science and Engineering A to include further background on the application and demonstrator manufacture through NNS PM HIP

5.1 Motivation & Aims

The literature review of Chapter 2 has highlighted the potential advantages of using NNS PM HIP of Ni-base superalloys for high temperature applications. However, one of the factors limiting the use of NNS PM HIP of Ni-base superalloys is represented by the formation of PPBs as broadly discussed in the literature review. Additionally, it was proven that powder quality plays an important role in the variability of as-HIPed Ni-base superalloys performances. In fact, a comparison across different atomisation techniques has demonstrated the variability in physical and chemical properties, which can have a strong impact on the as-HIPed microstructure and mechanical properties. Thus, in this study it was decided to evaluate the PM HIP response of IN625 using four different atomisation routes (AGA, NGA, PA and WA) to address the following aspects:

- Understand the influence of powder atomisation route on the PM HIP behaviour of Ni-base superalloys.
- Gain a better understanding on the influence of powder chemistry and surface chemistry on PPBs formation.
- Investigate the mechanical properties of PM HIPed IN625 to understand how the atomisation route and consequently powder quality can impact the final properties of the material.
- Evaluate the effect of post-HIP heat treatment on microstructure and mechanical properties for IN625.

In this case, IN625 was specifically selected for this study due to its more simple metallurgy and microstructure if compared to other more complex precipitation strengthened Ni-base superalloys. This will allow gaining a better and direct understanding on how the powder characteristics can impact on the microstructure and mechanical properties.

Additionally, to make the case more industrially viable, a specific application was targeted and the manufacture of near net-shape Y-shaped pipe for submarine applications through NNS PM HIP was proposed.

Abstract

The powder's characteristics and its purity can greatly influence the properties of nickel (Ni)-base superalloys parts produced by near net-shape powder metallurgy hot isostatic pressing (NNS PM HIP) manufacturing process. In this study, Inconel 625 (IN625) powders produced using four different atomisation routes, argon, nitrogen, plasma and water atomisation (AGA, NGA, PA, WA, respectively) were investigated. The first section of this study is focused on the determination of powder characteristics which includes chemical composition, particle size distribution (PSD), tap density and powder's cross-section analysis, whereas the second section is about hot isostatic pressing (HIPping) of the four powder types and to assess the impact of the powder characteristics on the microstructure-property development after HIPping. To gain an understanding of the surface chemistry of the powders, X-ray photoelectron spectroscopy (XPS) analysis were carried out on the surface of the four powders. The latter analysis highlighted fundamental differences on the powder's surface, especially the differences in the surface and near-surface distribution of the alloying elements i.e. C, O, Cr, Mo and Nb present in the alloy chemistry. The micrographs of the four IN625 hot isostatically pressed (HIPped) powders revealed a fully dense microstructure with the presence of prior particle boundaries (PPBs). The atomisation route greatly impacted the nature and amount of PPBs, as well as on the fractions and sizes of oxides, carbides, oxycarbides and oxycarbonitrides precipitates. WA showed the most severe presence of PPBs, followed by NGA, AGA and lastly PA. The powder quality has a greater impact on the

mechanical properties of as-HIPped materials, especially on ductility. Overall, PA HIPped IN625 possessed the optimum balance between tensile strength, ductility and Charpy impact properties once compared to the others and match the properties to wrought IN625 material.

Keywords: Ni-base Superalloys; Powder Metallurgy Hot Isostatic Pressing; X-ray photoelectron spectroscopy; Microstructure; Mechanical properties

5.2 Background: Submarine Pipes Application

Submarine pipes are widely used to safely transport fluids such as crude oil, water and natural gas in a more efficient way [1]. The fluids are transported from an offshore platform to another offshore platform or to an onshore station where the fluid is processed [2]. Submarine pipes are subjected to a harsh environment with different loading conditions including internal pressure coming from the transporting fluid, external hydrostatic pressure, bending and thermal stresses [3]. Furthermore, the pipes are subjected to a variation in temperature, from high to critically low temperatures [4]. The external pressures in the submarine pipes can reach 103MPa with an internal pressure of the fluid as high as 25MPa, while the operating temperatures can range from -60°C to above 177°C [1], [5]. Not many materials can withstand these loading and environmental conditions. Historically, the first material used for this application consisted of low alloy steels, however, the low corrosion resistance of these alloys makes them unsuitable for the application [5]. Other materials developed for the application are stainless steels, duplex stainless steels, or Ni-base superalloys in the more demanding operating conditions [6]. An alternative to reduce the external corrosion of the submarine pipes is to apply an external coating with the addition of cathodic protection in case the coating fails [3]. The most widely used coatings for this application include Epoxy

resin, PU, PE and PP coatings [7]. Epoxy-based coating can be used for internal protection of the pipeline and to reduce the internal roughness and thus reduce the friction, improving the efficiency [3].

Considering the loading and environmental conditions to which submarine pipes are subjected, IN625 would represent a highly suitable solution for this application due to its high corrosion resistance, high-temperature capabilities (up to 650°C) and good mechanical properties [8], [9].

5.3 Introduction

Near net-shape powder metallurgy hot isostatic pressing (NNS PM HIP) is an advanced manufacturing technique capable of producing near to net-shape complex engineering parts with excellent isotropic mechanical properties and improved buy-to-fly ratios. HIPping has been successfully performed on a wide range of powder materials, including Ni-base superalloys [10] which has shown different challenges. One of the challenges is the presence of unwanted and detrimental precipitates at prior particle boundaries (PPBs) in the microstructure of HIPped Ni-base superalloys. The particles manifested inside PPBs can be of different types, including oxides, carbides, and oxycarbonitrides. The presence of PPBs in the HIPped material can influence; the powder consolidation and the mechanical properties i.e. tensile strength, ductility, fatigue life and fracture toughness. PPBs reduce the inter particle bonding, thus dramatically reducing the elongation-to-failure and fracture toughness [11] [12].

To mitigate this undesirable preferential precipitation process, it must need to be understood how these particles are generated and how the HIPping parameters influence their formation mechanisms. The generation of PPBs during HIPping has its origin during the atomisation process, where a thin oxide layer is generated [13]. This is supported by several

studies, where the presence of a thin oxide layer at the surface of the powder has been detected via XPS [14], [15], [16]. Gao *et al.* [17], showed a high concentration of oxygen and elemental segregation on the surface of the powder of FGH96 Ni-based superalloy, which then creates a thin oxide layer during the HIPping process. This layer is composed of TiO_2, Cr_2O_3 and ZrO_2 [17]. Since these oxides are stable at considerably higher temperatures, they will not dissolve during HIPping and will still be present at the PPBs after the consolidation has taken place. Many authors have claimed that the oxides present at the particle boundaries act as preferential sites for the formation of carbides at PPBs, leading to deteriorate mechanical properties [12], [18], [19]. Many attempts have been proposed to eliminate or reduce the presence of oxycarbides at PPBs, with is one of the most used approaches relying on post-HIP heat treatment to dissolve the precipitates [20] [21]. However, these attempts were not always successful due to the high dissolution temperatures of oxides and carbides, which often exceed the solvus temperatures of the alloy [22] and generate excessive grain growth which impairs the microstructure and ultimately the mechanical properties. Among all the proposed methods, the most agreed upon practice for reducing the amount of PPBs is to improve the quality of the powders, as powders with lower O levels result in a lower presence of PPBs, thus a drastic improvement in the mechanical properties [12].

In this study, the impact of the powder's characteristics on the microstructure and room temperature mechanical properties of HIPped IN625 were evaluated. Ni-base IN625 alloy was selected to investigate the effect of powder's characteristics on the HIP response of the material for several reasons. Firstly, IN625 is widely used in the marine, aerospace and nuclear sectors thanks to the excellent corrosion resistance and high temperature strength, thus the study can find different applications depending on the requirements. In addition, IN625 is susceptible to the formation of PPBs, mainly due to the presence of Cr, Nb, Mo, thus the influence of the powder characteristics on the PPBs formation can readily be studied

and assessed. Furthermore, IN625 is mainly a solid solution strengthened alloy with limited or no formation of γ'' in the as-HIPped conditions, thus it is easier to compare the HIP response, having one less variable to control. In IN625 is easier to understand the influence of the interstitials such as O, C and N on PPBs formation, due to the relatively easier metallurgy if compared to other Ni-base superalloys. Finally, since there is a substantial difference in price among the four IN625 powders, the use of lower quality powders (NGA or WA), can drastically reduce the manufacturing costs and can be considered for parts where high performances in terms of strength are not required.

5.4 Materials and Methods

5.4.1 Experimental

In this study, HIPping was performed on four different IN625 powders – AGA (15-45μm), NGA (15-150μm), PA (0-150μm) and WA (15-150μm). The powders' morphology, particles cross-section microstructure, chemical composition, surface atomic chemical composition and physical properties (flowability, densities and particle size distribution (PSD)) were assessed. Chemical analysis of the four IN625 powders were performed by AMG Analytical Services, Sheffield. The inductively coupled plasma optical emission spectroscopy (ICP OES) technique was employed to determine the major alloying including any impurity elements, such as Cr, Mo, Nb, W, Cu, Ni, Co, Fe, Mn, V, Ti, Sn, Al, Si, P, Ta and B (lower limit <0.02%) [23]. C and S were determined by LECO thermal infrared using combustion in oxygen, whereas O, N and H gases were determined by LECO inert gas fusion using infrared and thermal conductivity detection [24], [25]. XPS was performed using a monochromatic X-ray $K\alpha_1$ source. The C1s carbon binding energy (B.E.) of 284.8eV was used for calibration to consider the charging effects. XPS depth profiles were obtained through argon ion beam

etching using 1000eV. The PSDs of the four powders were measured at TWI Ltd. using a Malvern Matersizer 3000 laser diffractometer. Flowability of all four powders was measured using Hall flowmeter as per ASTM B213-17. The apparent and tap density measurements were performed according to ASTM 212-17 and ASTM B527-15 standards, respectively. After characterisation, the four powders were encapsulated in TIG welded mild steel canisters (Ø50mm x 185mm) with 2mm wall thickness. All the canister were leak tested using helium leak detector before loading/filling the powders. The filling procedure was performed in a controlled environment inside an argon filled glovebox, after which the canisters were de-gassed for 48 hours and hot sealed. The four canisters were then HIPped using the EPSI HIP, available at the University of Birmingham (UoB). The HIPping parameters used were; a temperature of 1160°C, pressure of 120MPa and dwell time of four hours with heating rate of 5°C/min and cooling rate of 10°C/min (Figure **5.1**). The above mentioned parameters are commonly used parameters during HIPping IN625 powder [26]. The HIPped samples were extracted using electric discharge machining (EDM) cutting, mounted in conductive bakelite and grounded/polished using standard metallographic procedures for Ni-superalloys. The HIPped IN625 material's microstructure was then analysed using a Hitachi TM3000 Scanning Electron Microscope (SEM) in backscattered electrons (BSE) mode. Electron-backscattered diffraction (EBSD) analysis was also performed on the HIPped microstructures using a Philips XL-30 SEM, using a step size of 1μm, with the results post-processed using HKL Channel 5 software. Vickers microhardness measurements were performed using a semi-automatic Buehler microhardness tester at ten different locations for each sample, according to ASTM E384 – 17, using a load of 500gf and a holding time of 10s. Room temperature tensile tests were performed as per ASTM E8/E8M-16a standards on HIPped IN625 samples. Whereas, room temperature Charpy impact tests were performed on HIPped

IN625 samples measuring 10mm x 10mm x 55mm, with a 2mm Charpy V-notch as per ASTM E23-16b standards.

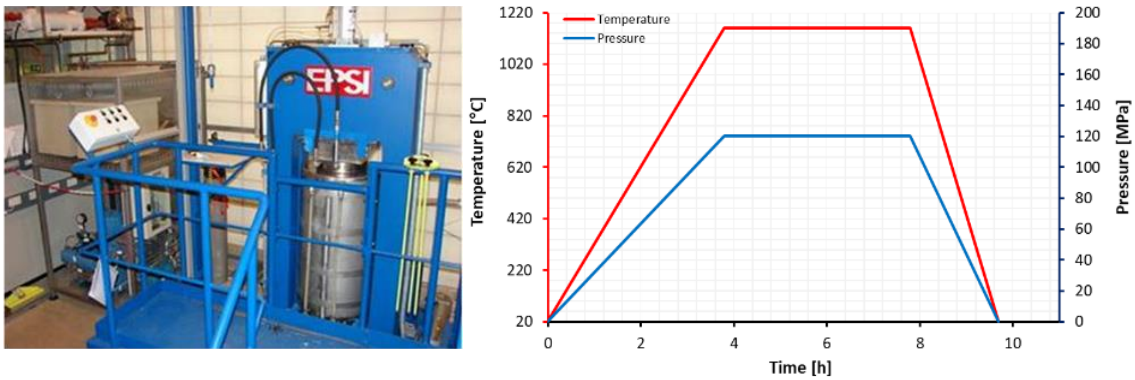

Figure 5.1 Schematic of the HIP cycle (left); EPSI HIP at UoB (right).

Two different heat treatments (HT) were performed on the as-HIPped IN625 to further improve the microstructural homogeneity by dissolving any detrimental phases, and subsequently assessing their impact on the mechanical properties. The first heat treatment (HT1) consists of the following steps (Figure **5.2**):

- Solution heat treatment (SHT) at 1180°C for one hour, followed by Ar fast cooling according to AMS 2774E [27].
- First aging precipitation treatment at 720°C for 8.5 hours to precipitate gamma double prime (γ′′) [Ni_3Nb] hard phase, followed by cooling to 620°C at 50°C/h.
- Second aging precipitation treatment at 620°C for 8.5 hours, followed by furnace cooling to room temperature.

The purpose of using high SHT temperature during HT1 was to dissolve any unwanted detrimental phases which might have been precipitated/formed during the HIP process, such as Laves $[Fe, Cr]_2(Nb, Mo)$ (dissolution temperature in the order of 1100°C) [8] and delta (δ) [Ni_3Nb] with a dissolution temperature of around 1025°C [28]. Whereas, double

aging treatments are similar as presented in literature [29], [30] and AMS 2774E. Furthermore, HT1 promotes the grain growth past the PPBs and precipitation of γ′′.

The second heat treatment (HT2) was performed only on HIPped PA IN625 material with similar aging steps, while lowering the solution temperature to 1050°C (Figure **5.2**):

The HT2 cycle consisted of the following steps:

- SHT at 1050°C for one hour under vacuum, followed by Ar fast cooling according to AMS 2774E [27].
- First aging precipitation treatment at 720°C for 8.5 hours, followed by cooling to 620°C at 50°C/h.
- Second aging precipitation treatment at 620°C for 8.5 hours, followed by furnace cooling to room temperature.

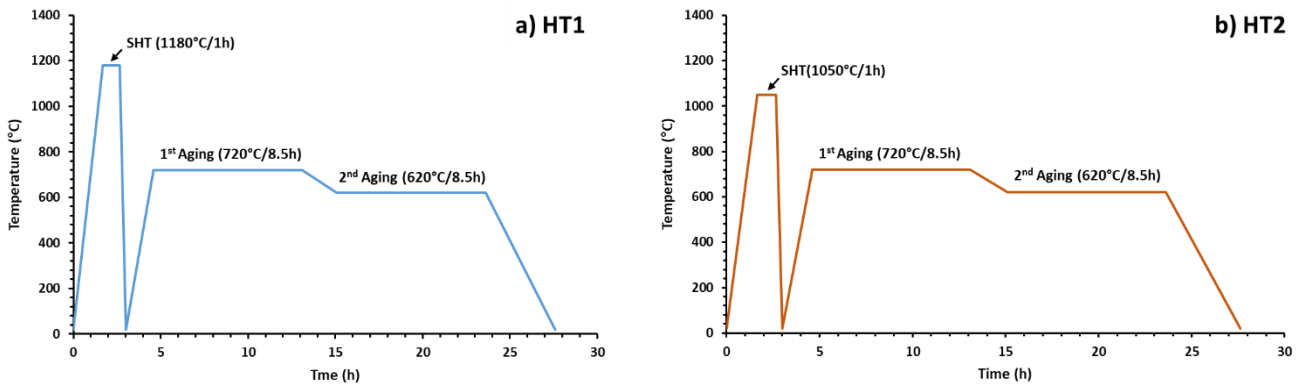

Figure 5.2 Schematic of post-HIP heat treatment, (a) HT1 and (b) HT2.

5.5 Results and Discussion

5.5.1 Powder characterisation

A considerable difference exists within the chemical composition of the four different powders. **Table 5.1** shows the differences in the oxygen (O) levels between the four atomisation routes, with WA powders having an O level of 7100ppm, far above the standard

level for IN625 [31]. Although O level in NGA powder is lower than WA however it is still above the standard allowable range. The O level in PA and AGA powders are comparatively low and within the standard. Another factor affecting the formation of PPBs is represented by the carbon and nitrogen content. WA and NGA show lower levels of carbon compared to AGA and PA, while NGA showed higher levels of nitrogen, above the specifications. Few other alloying elements such as Cr, Mo, Fe and Nb for all the four powders are within the typical allowable range for IN625. Additionally, since WA and NGA were melted and atomised in an ambient atmosphere, Al and Ti were not included during the atomisation process. This is due to the reactive nature of these elements, as they have the tendency to form stable oxides. The N content is relatively high in NGA powder which is due to atomisation nitrogen gas, as expected, and this can promote the formation of oxycarbonitrides [32]. The Si content was higher than the standard range in NGA and WA, since Si is added to increase the melt flow during the atomisation process. Furthermore, Mo and Fe contents were higher in AGA, which will provide higher levels of solid solution strengthening compared to the other powders. Although, the amount of Ti and Al in PA and AGA powders is within the allowable range however is higher than the WA and NGA powders, which could potentially promote the precipitation hardening during the aging treatment.

Table 5.1 Chemical composition of the four IN625 powders (wt.%).

Elements	C	O	N	Cr	Fe	Cu	Mn	Mo	Ni	P	S	Si	Nb	Al	Ti	Co
Required [33]	<0.10	<0.02	<0.02	20.0-23.0	≤5.0	<0.50	<0.50	8.0-10.0	bal ≥58	<0.015	<0.015	<0.50	3.15-4.15	0.1-0.4	0.1-0.4	≤1.0
AGA (15-45µm)	0.02	0.01	0.009	20.8	4.20	0.02	0.02	9.10	61.58	<0.005	<0.005	0.08	3.64	0.21	0.21	0.1
NGA (15-	0.009	0.06	0.07	20.32	3.12	0.03	0.56	8.48	63.28	0.007	0.004	0.79	3.18	<0.03	<0.02	0.02

150µm)																
PA (0-150µm)	0.03	0.01	0.009	21.47	1.37	0.01	0.06	8.71	64.32	0.002	<0.001	0.06	3.59	0.23	0.11	0.02
WA (15-150µm)	0.004	0.71	0.02	21.29	3.32	0.03	0.42	8.41	61.64	0.006	0.005	0.71	3.35	<0.02	<0.02	<0.02

The powder morphology study has identified differences between the four IN625 powders. AGA had a nearly spherical shape, with the presence of satellites and irregularly-shaped powder particles. NGA had a nearly spherical shape and a more regular morphology. As expected, PA powders had the best spherical shape once compare to the rest of the powders used, with a bi-modal PSD. WA powders had a typically irregular shape, as a result of the WA atomisation process (Figure **5.3**), this was also observed in the work of A. Mostafaei *et al.* [34]. The oxidation of the melt during WA increases the surface tension of the droplet, restricting the likelihood of particle spheroidisation [35]. Furthermore, the surface of WA powders appear to be inhomogeneous with micro-segregation of Ni, Nb and Mo, as shown in the Energy-dispersive X-ray spectroscopy (EDS) maps (Figure **5.4**). The cross-section of the powders reveal little-to-no porosity in NGA and PA, while AGA has minimal entrapped porosity arising from the atomisation route (Figure **5.5**). The presence of porosity is attributed to argon being a non-soluble gas, thus it will remain entrapped inside the molten droplets during the atomisation [35]. The SEM micrographs of Figure **5.5** reveal the influence of the cooling rate on the powder cell size. In particular, WA process has the highest cooling rate; this is confirmed by the presence of a small cell size. In AGA, the small particle size promotes high cooling rates during the atomisation process and consequently a small cell size is present. On the other hand, PA process possesses relatively lower cooling rates [35], thus a bigger cell size can be observed in Figure **5.5**. Furthermore, the backscattered micrographs

(Figure 5.5) also show Mo and Nb enriched micro-segregation inside the individual particles [36].

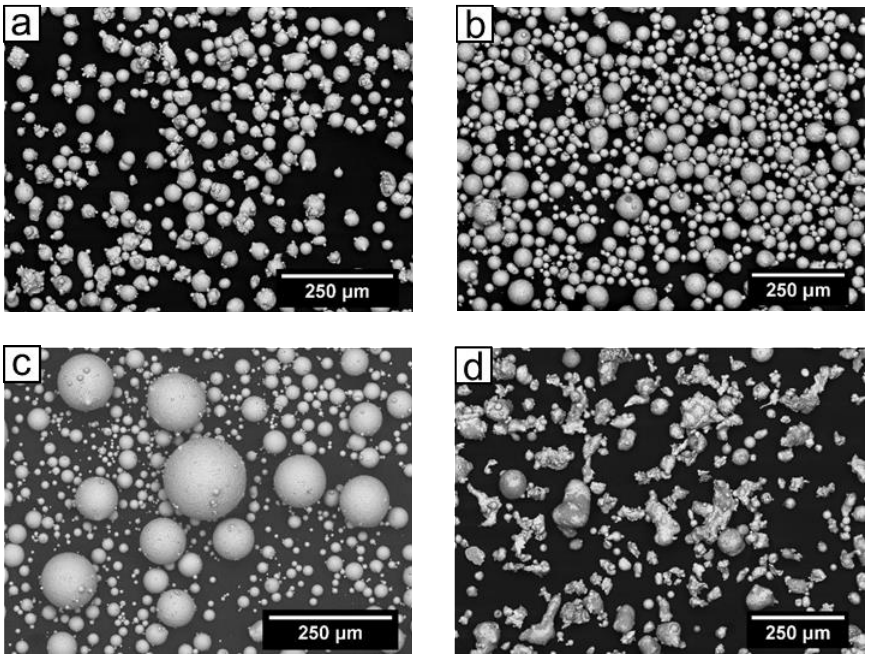

Figure 5.3 Backscattered SEM micrographs of IN625 powders: (a) AGA (15-45µm); (b) NGA (15-150µm); (c) PA (0-150µm); (d) WA (15-150µm).

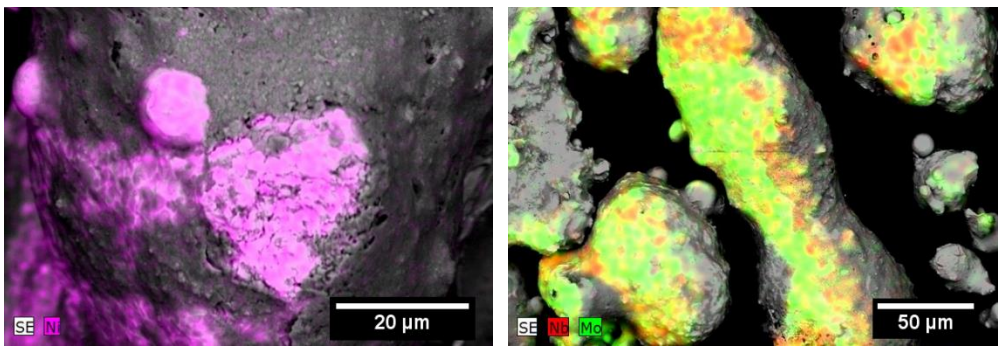

Figure 5.4 EDS maps on the surface of WA powders, showing segregation of Ni, Nb and Mo on the surface.

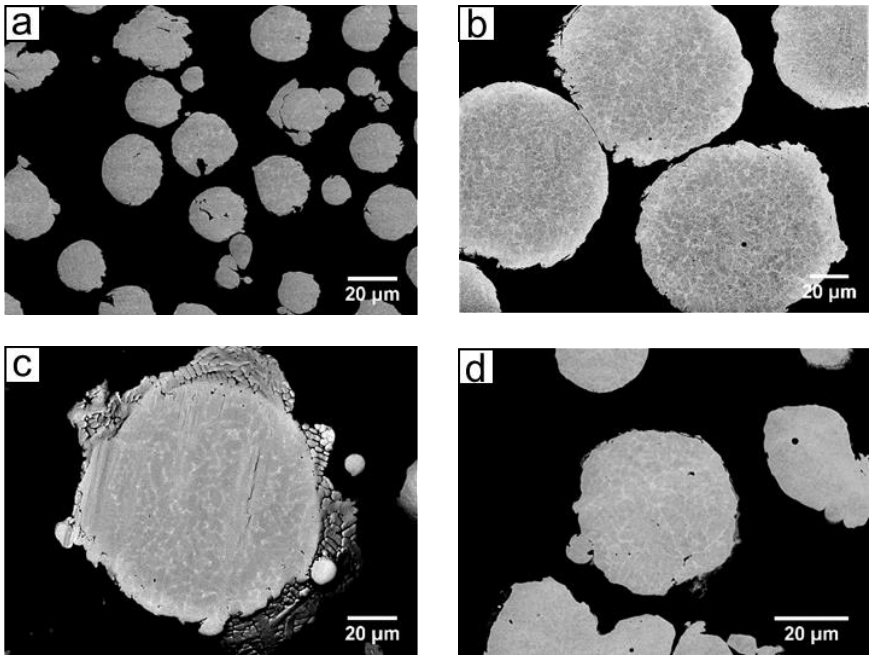

Figure 5.5 Backscattered SEM micrographs of IN625 powder's cross-section: (a) AGA; (b) NGA; (c) PA; (d) WA.

Differences in the four powders can be seen in terms of estimated PSD values. WA, NGA and PA have a wider size range, while AGA has a narrower size range, with a D_{90} of just 40µm (Table **5.2**). The values of $D_{10,}$ D_{50} and D_{90} for AGA IN625 are comparable to the results proposed by Pleass *et al.* [37]. Tap density is directly linked with the powder's particle size range, PSD and morphology; PA powder has the highest packing density, due to the combination of its spherical morphology, bi-modal particle size distribution and wider particle size range (Figure **5.6**). NGA has a high packing density due to its spherical morphology, as well as the wider PSD range and the absence of satellites. Despite NGA, WA and PA having similar particle size range, each with a wider range distribution, WA powders have a lower packing density, due to the highly irregular morphology of the powder. Lastly, AGA has a packing density of 61%, higher if compared to the work of Pleass *et al.*, [37]. The lower packing density of AGA powder if compared to NGA and PA is a consequence of the narrow powder particle size range and PSD. Differences in flowability can be also observed.

Among the four powders, PA powders show the best flow rate thanks to its highly regular shape, while WA showed a poor flow rate due to the irregular shape of the powders.

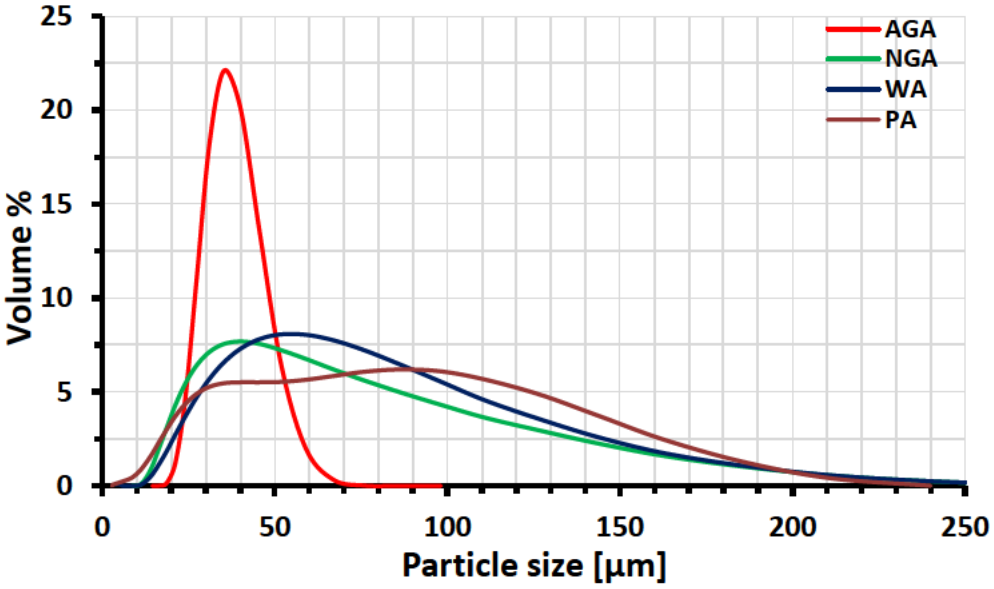

Figure 5.6 PSD of IN625 powders.

Table 5.2 Physical Properties of IN625 powders.

Powder Type	Tap Density (g/cm3)	Packing Density (%)	Flow rate (s/50g)	PSD (µm)		
				D10	D50	D90
AGA IN625	5.12	60.66	14.32	20	29	40
NGA IN625	5.63	66.71	13.42	23	49	121
PA IN625	6.01	71.20	12.73	17	49	122
WA IN625	4.45	52.72	21.62	27	58	126

5.5.2 XPS analysis

Chemical analysis may not be enough to describe the response of certain powders to HIPping and to determine the root cause of the formation of PPBs. The study of surface composition

of the powders is necessary to understand whether an oxide surface layer exists, and which elements are most prone to micro-segregation. For this reason, XPS analyses have been performed on the four different powders. XPS depth surface analysis focused on the major elements influencing the formation of PPBs, such as Nb, Mo, Cr, C and O, with their depth profiles reported in Figure **5.7**. The first noteworthy result is represented by the high concentration of O on the surface of each powder. However, a distinction must be made: AGA and PA have a lower amount of O on their surfaces, followed in order by NGA and WA. Although C content in all the powders is below the allowable limit it still can play an important role in the formation of PPBs in HIPped IN625. Its concentration is higher in AGA, PA and NGA surfaces, while WA powder has the lowest amount of C on the surface, as well as on the bulk (Table **5.1**). The distribution of Nb suggests that for AGA, NGA and WA there is a higher concentration on the powder's surface, or in its proximity, this can be an important factor, which influences the formation of NbC at PPBs. The distribution of Nb in PA follows a flatter trend with no obvious differences in concentration along the depth of the powder. The presence of Cr in AGA, NGA and PA is around 20wt.%, which is well within the required limit (Table **5.1**) while in WA there is a stronger presence of Cr (around 30wt.%) at the powder surface at the expense of Ni. This suggests that higher O levels on the surface promote the diffusion of Cr to the outer surface of powder with the generation of Cr_2O_3. This reaction can occur during atomisation, despite the high cooling rates, due to the high diffusion coefficient of Cr in Ni of $1.1x10^{-4}m^2/sec$, the highest among all the alloying elements present in IN625 [38].

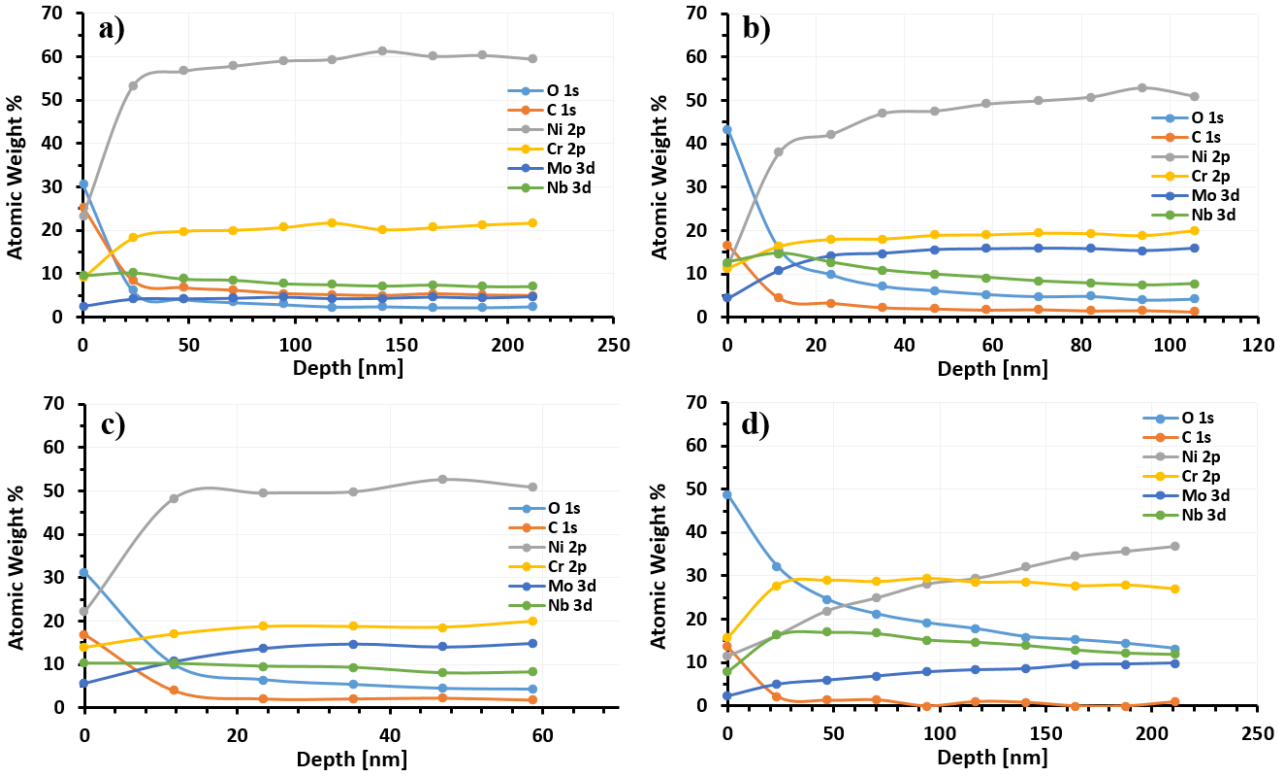

Figure 5.7 XPS depth profiles for: (a) AGA; (b) NGA; (c) PA; (d) WA IN625 powders.

A more detailed analysis of the surface chemistry of powders, as well as at 70nm etch depths for all powders, and up to 210nm for WA, is reported here in Figure **5.8**. The most dominant peak on the surface is represented by O1s, as well as a strong peak of C1s. Their intensity decreases at 70nm depth in AGA, NGA and PA, while for WA, the O1s peak is still present up to and beyond 210nm depth, meaning a thicker oxide layer is formed during WA. The presence of Ti on the surface of AGA and PA powders is represented, which is noteworthy as Ti can lead to the formation of TiO_2 and TiC at PPBs during the consolidation process [39]. No presence of Ti was observed on the surface of NGA and WA powders. Another important difference is represented by the presence of Si on the surface of NGA and WA.

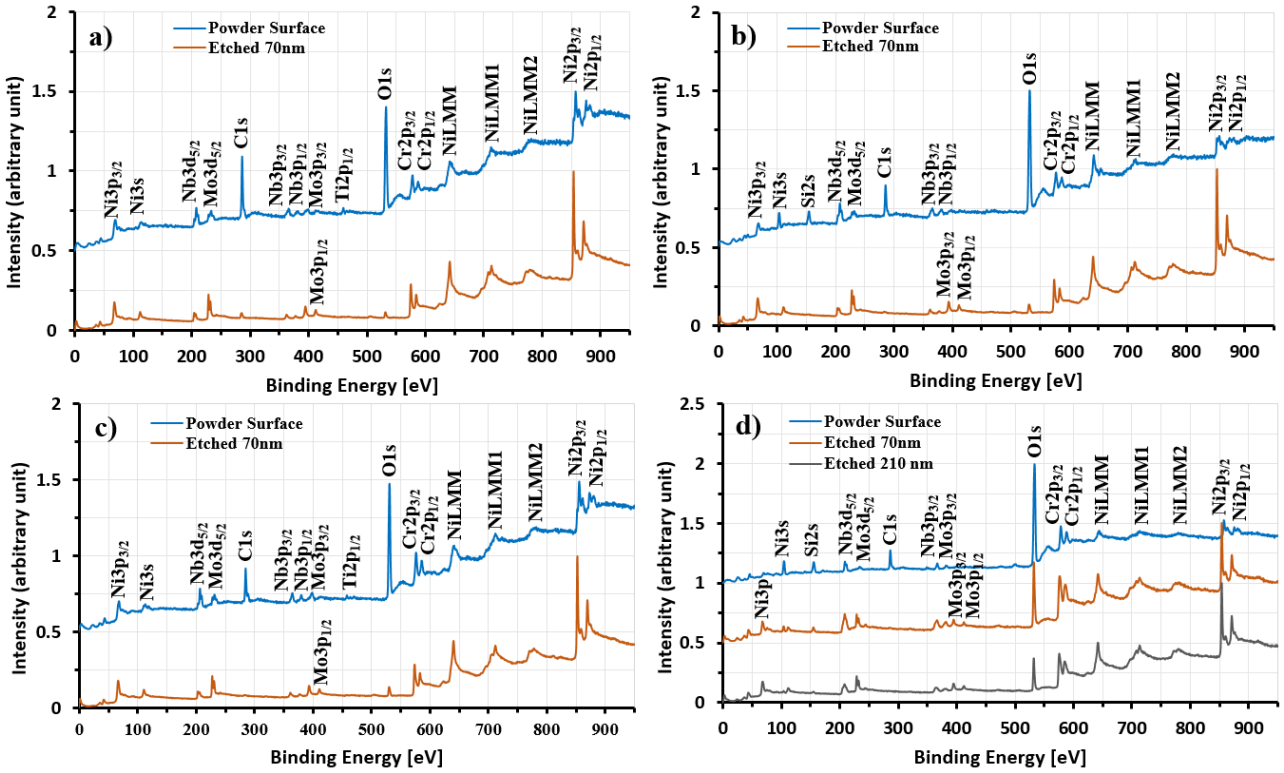

Figure 5.8 XPS spectra on the surface of the powder and at 70nm from the surface for: (a) AGA; (b) NGA; (c) PA; (d) WA IN625 powders.

Higher resolution XPS performed on the distribution of Nb on the surface shows the presence of different oxidation states, including NbO_2 and Nb_2O_5, for all powders [40]. WA shows a weaker presence of Nb on the surface of the powder with the absence of carbide peak, suggesting that no NbC is observed on the surface of the WA powder, while for AGA, NGA and PA, NbC is observed, in line with other studies [32], [41]. The absence of NbC on the surface of WA powders can be attributed to the combination of higher cooling rates during atomisation, together with negligible concentration of C in pre-alloyed powders.

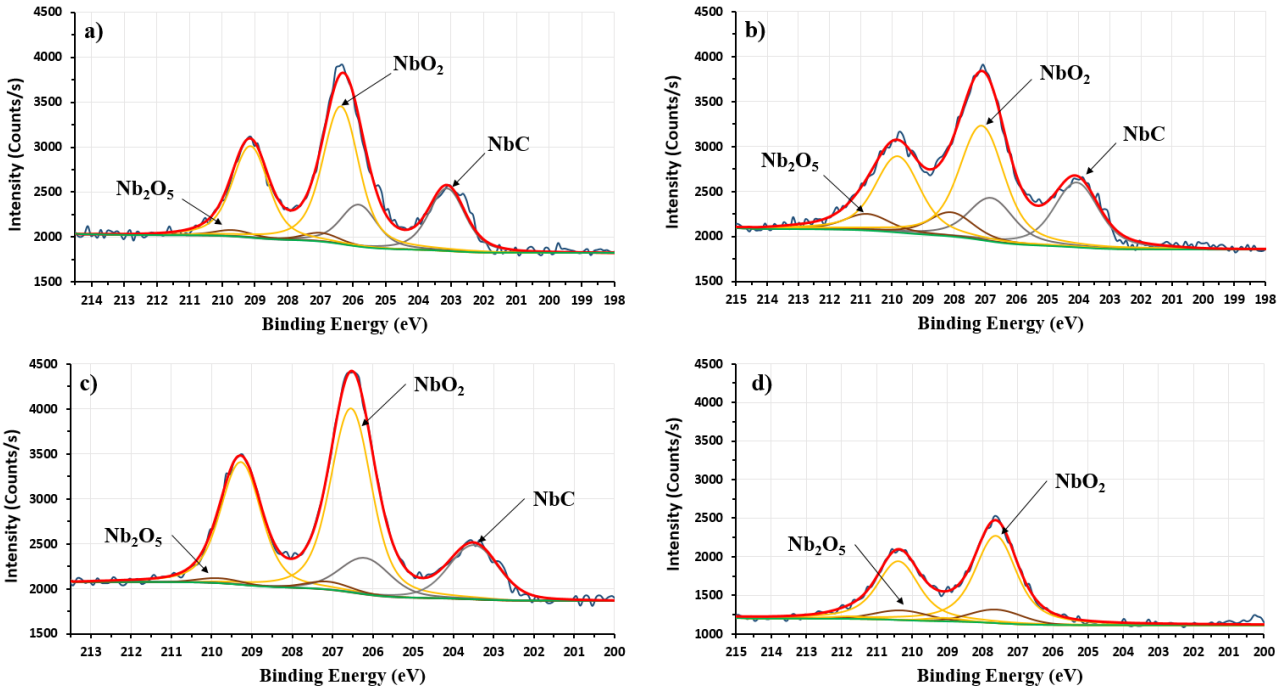

Figure 5.9 Niobium XPS spectra for: (a) AGA; (b) NGA; (c) PA; (d) WA IN625 powders.

5.5.3 Microstructure of as-HIPped IN625

Although all the four HIPped IN625 powders showed a fully dense microstructure, however, some differences can be found in terms of microstructural features in these four HIPped powders. The first difference is the presence of particles fraction and size at the PPBs, which is strongly dependent on the powder atomisation route. The presence of PPBs was directly linked to the previously indicated O levels in the powders, (Figure **5.10**).

AGA showed a microstructure with a higher density of twin boundaries. It has a smaller fraction of carbides, and some PPBs can be observed. The SEM micrograph of HIPped NGA powder shows a continuous network of precipitates along the PPBs, with a stronger presence of oxycarbonitrides. These precipitates were chromium oxide (Cr_2O_3), silicon dioxide (SiO_2) (for NGA and WA) and (Mo, Nb) carbides, nitrides [32]. The particles along the PPBs were mainly Cr_2O_3, while the others, such as (Mo, Nb)C, precipitate with even distribution in the microstructure. EDS analysis was conducted on the HIPped NGA

sample (Figure **5.11**), which shows that Cr_2O_3 acts as nucleation site for some of the carbides and nitrides.

PA HIPped microstructure has the lowest O level, and, consequently, the least amount of PPBs, with the presence of only a few small carbides. PA HIPped microstructure seems to be characterised by a bi-modal grain structure with coarse grains surrounded by finer ones; this might be attributed to the bi-modal size distribution of PA powders. Lastly, the microstructure of WA HIPped powder represents the influence of the powder's O content on the as-HIPped microstructure. In this case, all the powders are surrounded by a continuous layer of Cr_2O_3, acting as a precipitation site for some (Mo, Nb)C. Compared to NGA, the microstructure does not show any uniform precipitation of carbides, which are distributed at PPBs. This might be attributed to the lower amount of C present in WA powders. Some SEM micrographs, performed in the proximity of the steel canister, where C diffusion from the canister is likely, show a uniform distribution of carbides in the microstructure (Figure **5.12**). This suggests that carbide formation in the early stages is driven by the presence of chromium oxides, until it reaches a saturation point. At that stage, carbides start to form uniformly within the microstructure. This assumption might sound incorrect if the microstructures of PA and AGA are observed, however, in this case, the chromium oxide should not drive the carbide formation mechanism, since both materials have a lower O content.

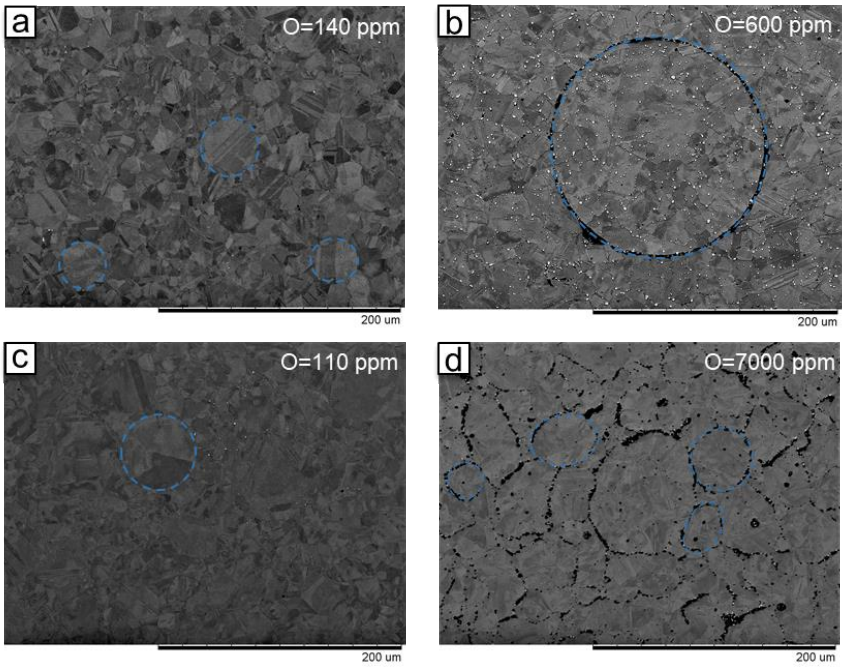

Figure 5.10 As-HIPped microstructure of (a) AGA; (b) NGA; (c) PA; (d) WA (PPBs highlighted in blue).

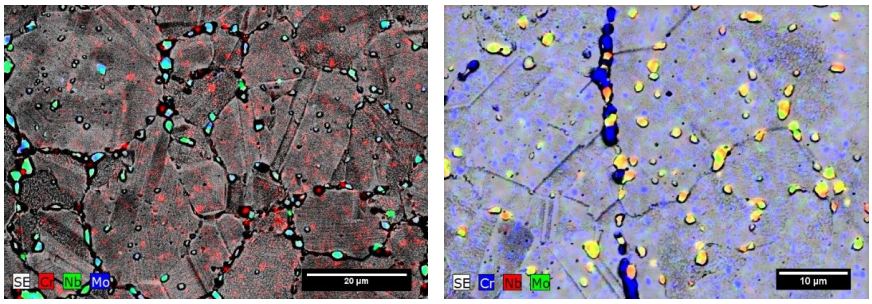

Figure 5.11 EDS analysis at PPBs for HIPped NGA IN625.

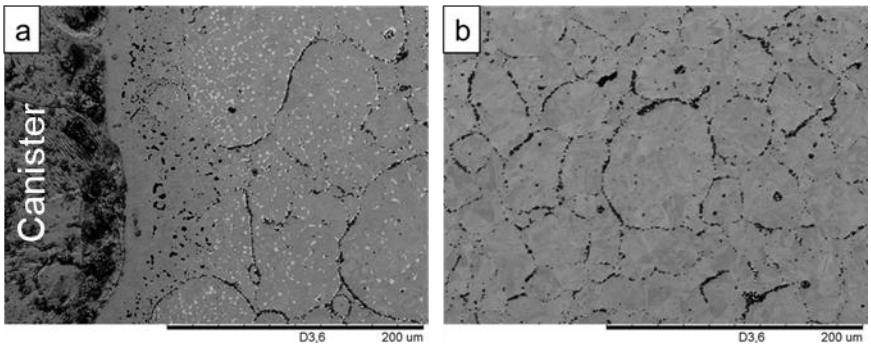

Figure 5.12 Carbide formation mechanism differences in HIPped WA: a) Precipitation in the proximity of the canister, showing a uniform distribution of carbide precipitation; b) precipitation far from the canister, showing carbide precipitation just at PPBs.

SEM backscattered images were used to give a first assessment on the differences between the four HIPped powder materials. However, a more detailed assessment was required to understand the grain structure. To achieve this, EBSD analysis was performed on the AGA, NGA and PA HIPped powders. All three HIPped materials displayed a randomly oriented microstructure with equiaxed grains; a typical microstructure of HIPped material [42].

Figure **5.13** shows the differences within the microstructures; AGA and NGA had a similar average grain size, 10 and 13µm, respectively, while PA HIPped microstructure displayed a bi-modal distribution with coarse and fine grains with an average size of 19µm. The reason for the presence of coarse grains in PA HIPped microstructure can be attributed to the presence of bigger cell size in PA atomised powder, which is a direct consequence of the lower cooling rate of PA process. Furthermore, due to the high packing density of PA powder, lower plastic deformation occurs during the densification process, thus the stored energy in the material is lower, leading to an inhomogeneous recrystallisation in the material, and, consequently, a bi-modal grain size distribution [42].

Table **5.3** shows the influence of the powder atomisation route on the presence of Σ3 boundaries. AGA shows the lowest presence of Σ3 coincident site lattices (CSL) fraction (22.2%), while PA and NGA HIPped microstructure show much higher levels, respectively 42.7% and 48%. The high presence of low energy Σ3 CSL can have a beneficial impact on strain-to-failure, hydrogen embrittlement and on stress corrosion cracking, as reported in different studies [43], [44], [45].

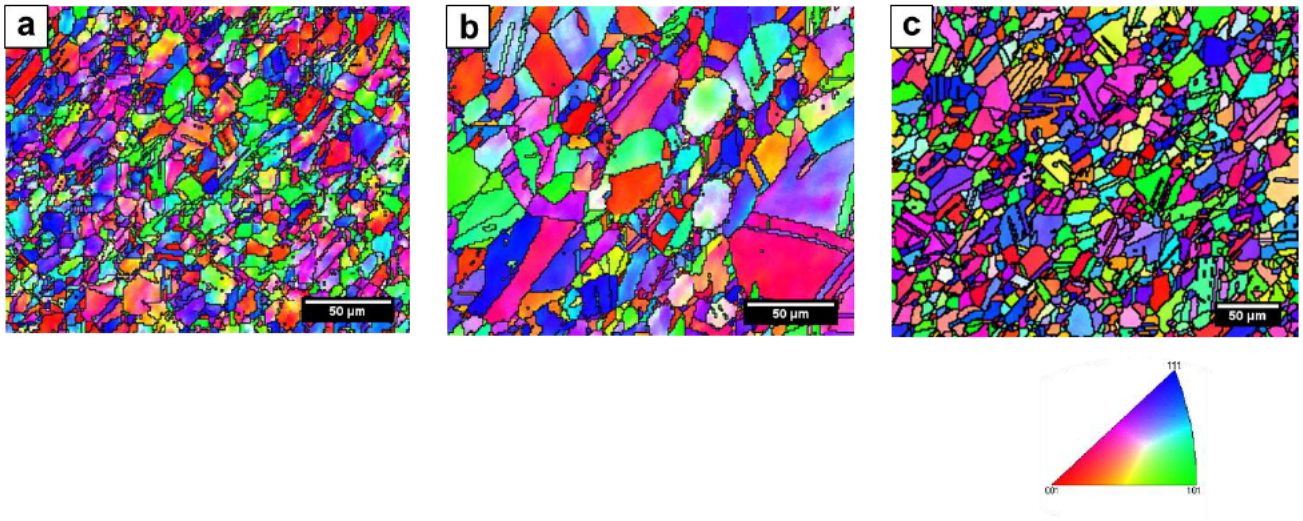

Figure 5.13 Inverse Pole Figures (IPF) of HIPped showing the grain structure in; (a) AGA, (b) NGA, (c) PA.

Table 5.3 Σ3 CSL fraction for HIPed AGA, NGA and PA IN625

HIPed Powder Type	Σ3 CSL Fraction (%)
AGA IN625	22.2
PA IN625	42.7
NGA IN625	48.0

5.5.4 Post-HIP heat treatments

After HT1, described in the experimental procedure, the four samples were analysed to understand the differences between the HIPped and heat treated (HTed) microstructure. The backscattered SEM micrographs of the samples can be seen in Figure **5.14**. AGA had the highest amount of thermally-induced porosity (TIP), which was likely due to the entrapped argon gas porosity manifested during the argon gas atomisation process. Furthermore, NGA, PA and WA also showed some TIP (circled white in Figure **5.14**) as well, suggesting that the SHT at temperatures of 1180°C which is higher than HIP temperature of 1160°C, provided enough driving force for the generation of TIP, irrespective of the IN625 powder atomisation

type used. The presence of the undesirable phases in the HIPped and HTed IN625 powders indicated that even a high SHT temperature (1180°C), above the Laves dissolution temperature in the order of 1100°C [8], was unable to dissolve or completely eliminate the presence of oxycarbonitrides in NGA and oxides in WA from the microstructure.

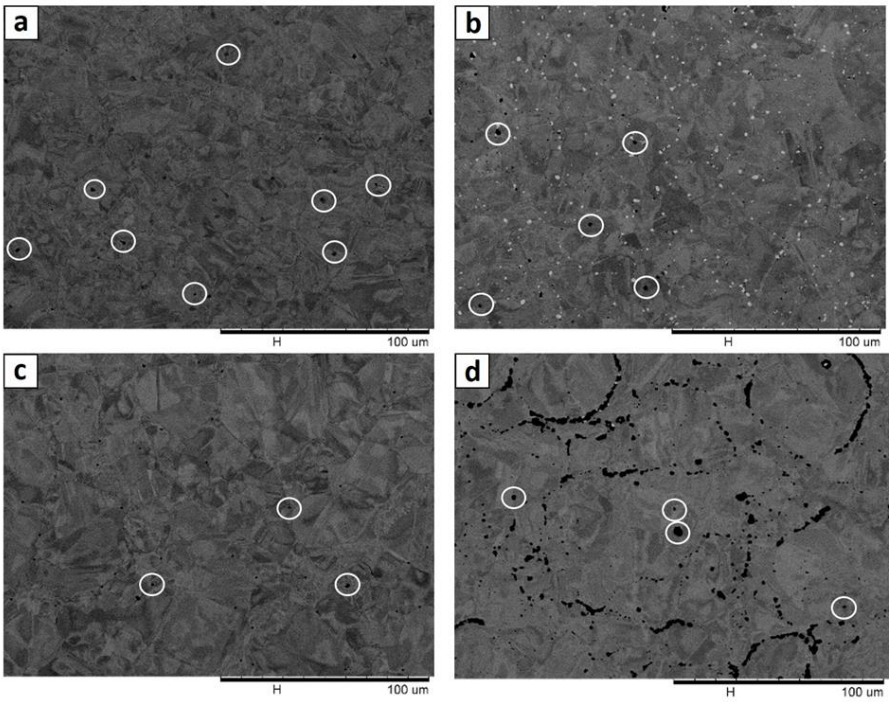

Figure 5.14 Backscattered SEM images of HIPped + HTed samples: (a) AGA; (b) NGA; (c) PA; (d) WA.

Another HT, called HT2 was designed with a lower SHT temperature to avoid the formation of TIP in the HIPped and HTed IN625 material [21]. It was performed on PA IN625 only, which showed the lowest amount of TIP and any undesirable phases.

The lower SHT's temperature (1050°C) aimed to avoid TIP as well as any unnecessary grain growth during the post-HIP HT process. As expected, the microstructure of HTed PA IN625 during HT2 with this new SHT strategy displayed negligible amount of TIP compared to the samples heat treated with HT1 condition (Figure **5.15**).

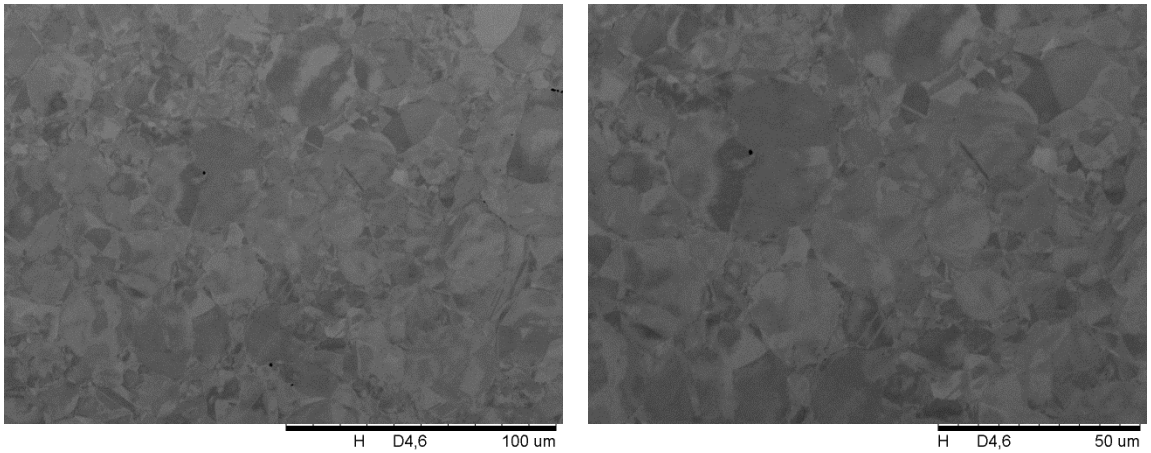

Figure 5.15 SEM backscattered micrographs of HIPped + HTed PA IN625 using HT2 cycle.

5.5.5 Mechanical properties

5.5.5.1 Microhardness

Microhardness tests were performed on the four HIPped and HIPped + HTed samples to understand whether the HT parameters were adequate to precipitate some amount of Ni_3Nb gamma double prime (γ'') strengthening phase. Figure **5.16** shows the hardness of HIPped + HTed material was higher than as-HIPped material, suggesting the HT successfully precipitated some γ'' hardening phase. A slightly higher hardness in HIPped + HTed AGA was likely due to better HT responses, thanks to the fine powder size ranges, i.e. 15-45µm, and the alloy chemistry, as some elements, such as Nb, Mo, Fe, Ti and Al, were higher when compared to other powders, especially NGA and WA (Table **5.1**). The higher amount of Nb in AGA can give raise to the precipitation of γ'', while the presence of higher levels of Mo reduced the solid solubility of reactive elements, such as Nb, Ti and Al, encouraging the precipitation hardening of the alloy [9]. As-HIPped NGA has slightly higher values of hardness, likely related to the higher fraction of oxycarbonitrides precipitation. As-HIPed PA

displayed the highest standard deviation in microhardness among the four powders, this can be attributed to its bi-modal grain size distribution.

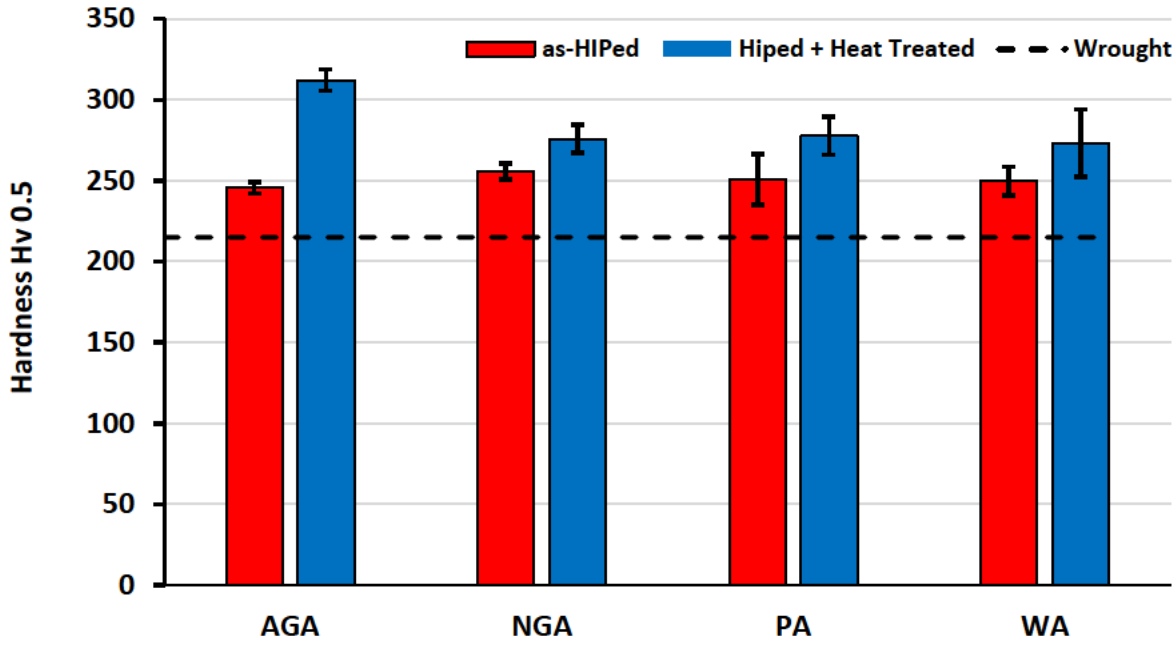

Figure 5.16 Microhardness of as-HIPped and HIPped + HTed AGA, NGA, PA and WA IN625.

Microhardness results were higher than wrought IN625 in as-rolled (215HV) and solution treated (160HV) conditions [46], however, tensile and fracture test data are required to better understand the as-HIPped and HIPped + HTed material properties. These tests should provide an understanding on the influence of the microstructure, especially the amount of PPBs, on properties such as yield strength (YS), ultimate tensile strength (UTS), elongation (El%) and Charpy impact energy.

5.5.5.2 As-HIPped tensile properties

The room temperature tensile results, shown in Figure **5.17**, highlight how HIPped AGA has the highest YS compared to the other HIPped powders. Due to the difference in powder atomisation route and in chemistry among the four powders there are several variables influencing the yield strength. However, for AGA the presence of a finer microstructure and

the higher amount of Mo, Fe and Nb, providing solid solution strengthening, are certainly beneficial for improving the YS (Table **5.4**) [47]. All four different HIPped powders have a higher YS compared to the minimum specification for as-rolled IN625 [46]. If compared to the work of Dugdale et al., where the as-HIPed IN625 was subjected to similar HIP parameters and with a post-HIP heat treatment at 900°C, AGA, NGA and PA have higher values of YS and UTS, while just PA has better elongation if compared to the aforementioned work (Figure **5.17**) [26]. AGA, NGA and PA have similar values of UTS; however, WA has a drop in strength compared to the other powders. Furthermore, a big change in the El% behaviour can be observed from the tensile tests. As expected, the El% of WA is quite poor; AGA and NGA have similar values of El%, matching the minimum specification for wrought IN625, while PA has an El% above 40%, higher than the other three powders. The elongation can be directly linked with the O content and the amount of micro-segregated elements present on powder surface, and, consequently, the amount of PPBs present in the HIPped material, as showed in previous works [12]. PA, which has the lowest amount of O, much cleaner powder surface with minimal micro-segregated elements and PPBs, possesses the highest El%, much higher compare to AGA and NGA.

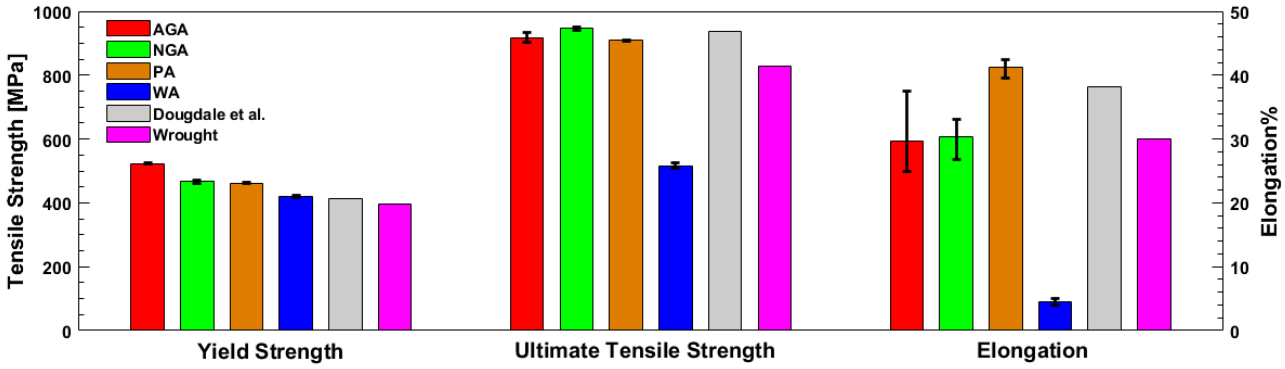

Figure 5.17 Room temperature tensile properties of as-HIPped IN625.

Table 5.4 Influence of grain size and powder chemistry on the YS of the as-HIPed IN625.

HIPed Powder Type	YS (MPa)	Grain Size (µm)	Cr (wt%)	Nb (wt%)	Mo (wt%)	Fe (wt%)	O (wt%)	C (wt%)	N (wt%)
AGA IN625	522	10	20.80	3.64	9.10	4.20	0.01	0.02	0.009
NGA IN625	467	13	20.32	3.18	8.48	3.12	0.06	0.009	0.07
PA IN625	462	19	21.47	3.59	8.71	1.37	0.01	0.03	0.009

To prove the influence of PPBs on the mechanical properties, fractographic analysis was performed on the fracture surface of tensile tested sample. From Figure **5.18** it is quite evident to affirm that for all the tensile samples, the dominating fracture mode is inter-particle fracture. However, there are some differences in the fracture surfaces. NGA and WA showed a consistent amount of oxides, carbides and oxycarbides, though with some dimples, meaning that some ductile fracture has happened. Carbides and nitrides are uniformly distributed around the particle boundaries of NGA fracture surfaces, while in WA there is more presence of Cr_2O_3 due to the high O content combined with the presence of Cr micro-segregation on the surface of the powders. These precipitates are difficult to see on the surface of PA or AGA powders, although the fracture starts on the particle boundaries. Smaller size carbides and oxides are responsible for this fracture behaviour; however, their size is small, thus making them difficult to be seen using a conventional SEM.

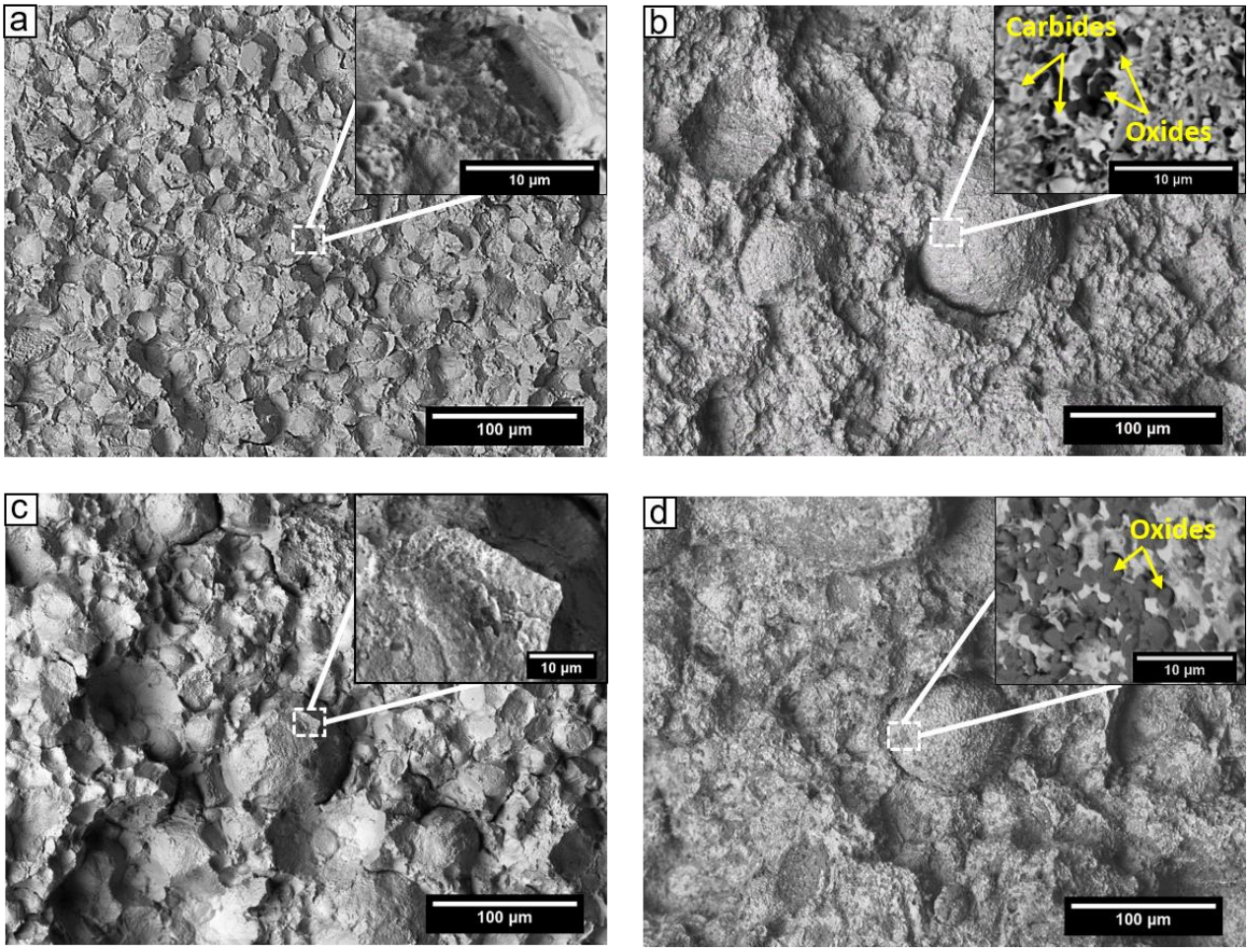

Figure 5.18 Fractographic analysis on as-HIPped IN625 tensile samples; (a) AGA, (b) NGA, (c) PA, (d) WA.

5.5.5.3 HIPped + HTed tensile properties

After HT2, PA IN625 samples were tensile tested at room temperature to understand whether the HT has any beneficial effect or not on the mechanical properties of the HIPped PA powder material. The results show similar mechanical properties with no obvious increase in strength for the HIPped + HTed condition, meaning the HT aging cycle did not precipitate enough hardening γ′′ phase (Figure **5.19**). However, there is an improvement in the El% of the material, meaning the solution of HT had a beneficial effect on making the grains grow past PPBs [21].

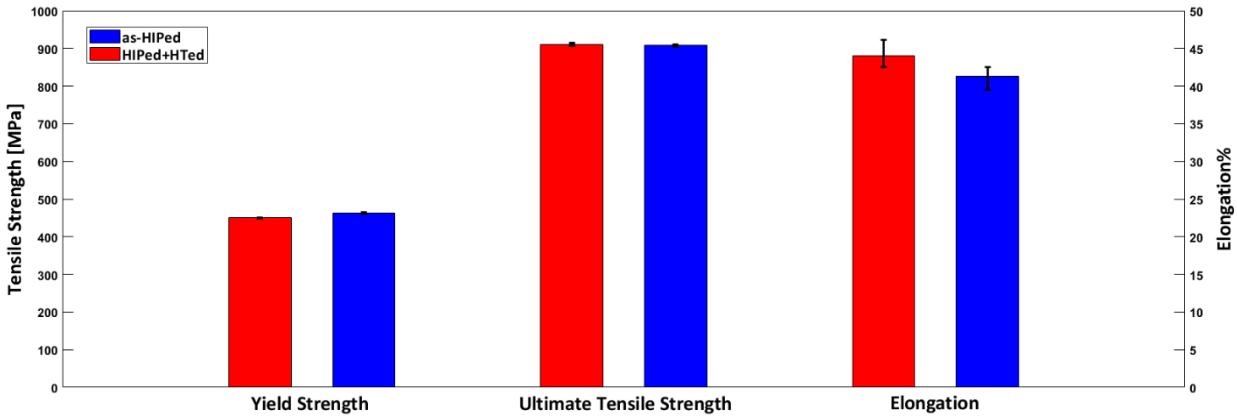

Figure 5.19 Room temperature tensile properties of as-HIPped PA vs HIPped + HTed PA IN625.

5.5.5.4 Charpy impact test

The results of the Charpy impact test (Figure **5.20**) show that PA has the highest absorbed energy, with an average value of around 64J; close to the average value of 66J for wrought IN625 [46]. However, the absorbed energy values are lower if compared with the work of Berglund et al. reporting an absorbed energy ranging from 59-93J [48] and the work from Dougdale et al. with a Charpy absorbed energy ranging from 84-119J [26]. The lower levels of absorbed energy can be attributed to a difference in powder chemistry as highlighted by Berglund et al., where a minimal difference in powder chemistry was leading to a considerable scatter in the absorbed energy [48]. This highlights a clear difference between AGA and NGA, which was not seen in the tensile test data results of Figure **5.17**. WA powders have lower values of absorbed energy due to the large amount of oxides along with micro-segregated elements present on the powder surface which cannot be dissolved during any post-HIP heat treatment and act as brittle crack initiation sites during Charpy impact test.

Fractographic analysis was carried out on the fractured Charpy samples (Figure **5.21**). The micrographs confirmed the presence of inter-particle fractures in all the different HIPped samples, and that oxycarbonitrides are responsible for the lower absorbed energy in HIPped NGA IN625. To confirm that, EDS analysis was performed on the fractured surfaces of NGA

HIPped powders. The EDS map of Figure **5.22** shows the presence of Cr_2O_3 and (Nb, Mo)C,N evenly distributed on the surface of the HIPped NGA powders.

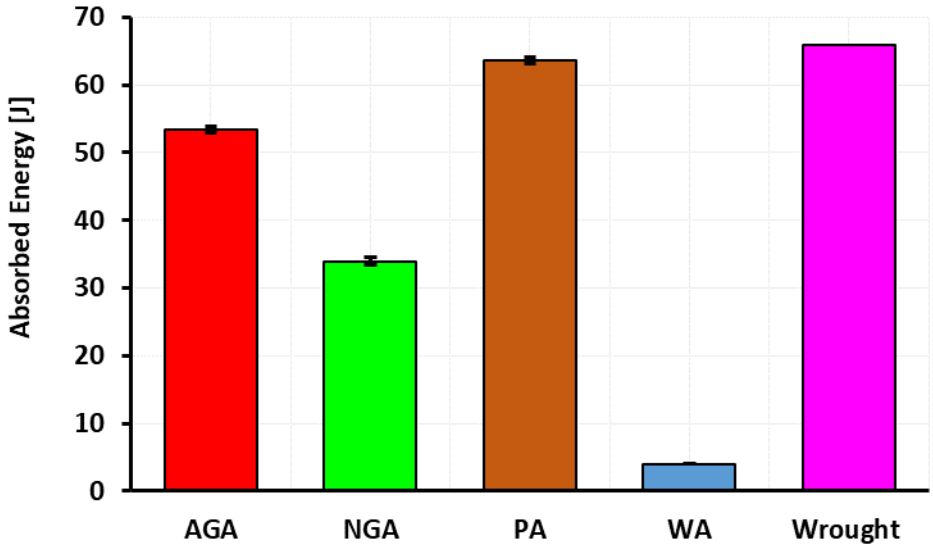

Figure 5.20 Charpy impact properties of as-HIPped vs wrought IN625 [46].

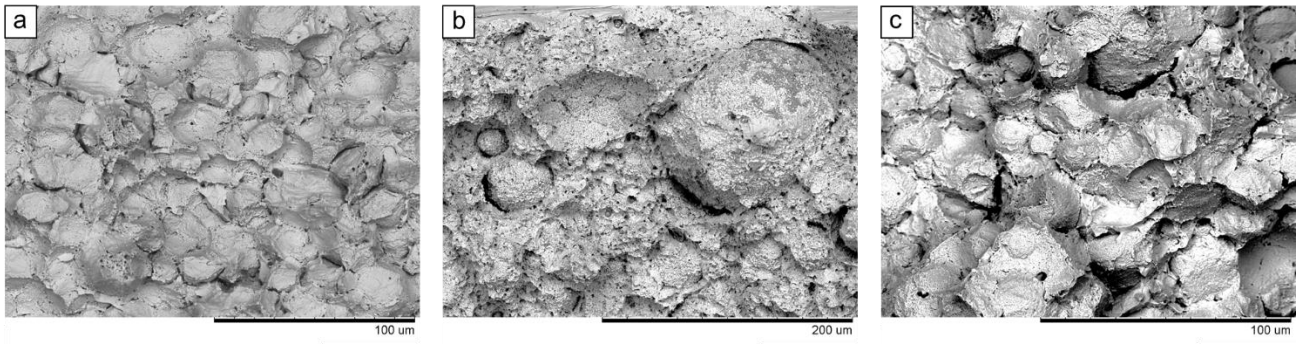

Figure 5.21 Charpy fractographic analysis of: (a) AGA, (b) NGA, (c) PA as-HIPped IN625.

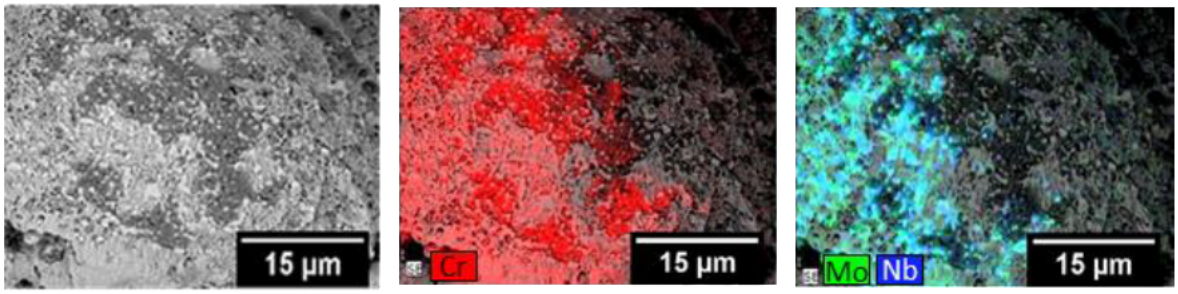

Figure 5.22 EDS maps for the fracture surface of NGA Charpy sample.

Charpy impact tests have also been performed on the HIPped + HTed PA. The results show that the HT had a moderate positive effect on improving the room temperature properties of HIPped IN625.

Table 5.5 Charpy impact properties of as-HIPped vs HIPped + HTed PA IN625.

Conditions	Absorbed Energy [J]	Std Deviation
As-HIPped PA	64.0	0.47
HIPped + HTed PA	65.6	0.45
Wrought [46]	66.0	0.00

5.6 Near-Net-Shape Manufacturing of Submarine Pipe

As part of this study, a Y-shaped submarine pipe was manufactured using PA IN625 powder showing the best mechanical properties and the best packing density, thus facilitating the geometrical control on the final part. A 2D technical drawing of the final part to be manufactured is reported in Figure **5.23**. In order to manufacture this part through NNS PM HIP, two different canister design strategies can be adopted. The first one would involve the design of internal and external deformable shells, allowing the deformation to take place from the inner as well as the outer shell. The second strategy would involve the design of an inner solid core representing the internal profile of the final part and an outer deformable shell, thus

in this case the consolidation would happen due to the deformation of the outer shell. The first canister strategy would allow to reduce the canister material, however, lower geometrical control and more difficult welding operations are required. Due to the challenges associated with welding operations and geometrical control, the second strategy was selected despite the higher amount of canister material required.

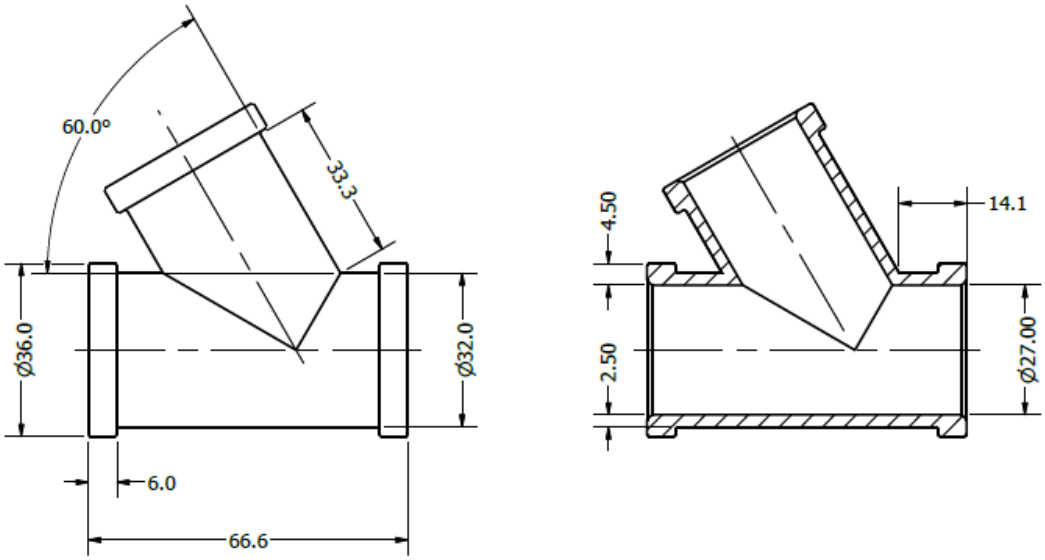

Figure 5.23 2D technical drawing of Y-shaped pipe (right), cross section (left).

Thus, the canister manufacturing strategy consisted of the design of a solid inner core with a deformable outer shell to guarantee the densification of the part during the HIP cycle. A 3D CAD drawing of the designed canister is highlighted in Figure **5.24**.

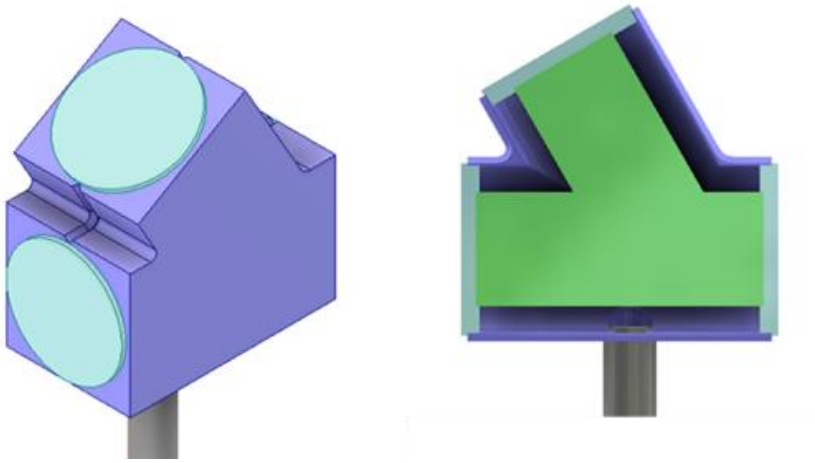

Figure 5.24 3D CAD drawing of the designed canister highlighting the presence of a solid inner core and a deformable outer shell.

The canister was filled, degassed and HIPed using the same procedure adopted above in the experimental procedure. After HIP the mild steel canister was removed by machining to netshape at Get It Made Ltd, revealing the final Y-shaped geometry (Figure **5.25**). Nevertheless, the use of this canister design strategy has highlighted some challenges in the machining operations due to the difficulties in determining machining reference points, thus in this case, pickling operations shall be preferred to remove the canister before final machining operations.

Figure 5.25 Submarine Y-shaped IN625 pipes produced using NNS PM HIP technique.

To understand the dimensional accuracy of the part, a coordinate-measuring machine (CMM) was used. The results showed an excellent geometrical accuracy (Figure **5.26**) and highlighted the possibility of manufacturing net-shape submarine pipe with the combination of NNS HIP and machining, achieving a reduction in buy-to-fly ratio if compared to conventionally used techniques. Additional investigations can be performed to assess the feasibility of manufacturing Y-shaped pipes with the absence of an inner core to reduce the canister material utilisation and ease post-HIP pickling/machining operations.

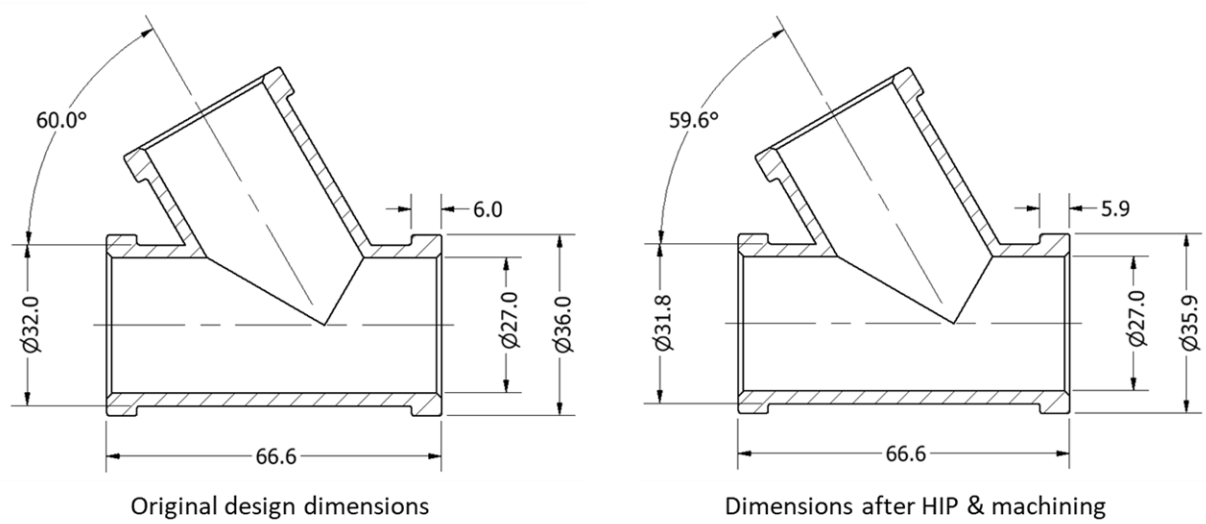

Figure 5.26 CMM dimensional assessment of the HIPed + machined Y-shaped submarine pipe.

5.7 Conclusions

In this study, HIPped IN625 material was developed to fabricate high value engineering parts using NNS PM HIP manufacturing technique. The main objective of this work was to understand the influence of powder atomisation route and powder characteristics on the HIPped IN625 microstructural and mechanical properties. A detailed powder characterisation displayed a difference in morphology, packing density and in chemistry among the four powders. XPS results showed higher concentration of O and C on the surface and micro-

segregation of Cr, Nb, and Si, having a considerably detrimental effect on the formation of oxides, carbides and oxycarbides at the PPBs. The microstructure analysis shows a close relation between O level and the presence of precipitates at PPBs. Those precipitates play a crucial role on the material's ductility and Charpy impact absorbed energy. The analysis on WA HIPped microstructure, in the proximity of the canister as well as far from it, has confirmed that the generation oxides act as preferential precipitation sites for carbides up to a saturation point. PA HIPped powder had the best balance between tensile strength, El% and Charpy impact absorbed energy. HT performed on the four as-HIPped samples, using a SHT temperature of 1180°C, displayed a considerable presence of TIP, especially in AGA, while lowering the SHT temperature to 1050°C reduced the amount of TIP with no unnecessary grain growth in PA HIPped samples. Lastly, the second HT i.e., HT2 performed on PA IN625 slightly improved the ductility and impact toughness properties of the material, with no adverse effect on its strength.

The main outcome of this study is that prior to considering metal powders HIPping on a specific material, its powder characteristics need to be fully understood. A detailed chemical composition analysis is needed, especially for the powder material with oxide formers, such as Cr, Al, Hf or Ti etc. By selecting Ni-base superalloys powder with low amount of interstitials will allow to use HIP technology for manufacturing high value engineering parts.

Finally, the last part of the study focused on the manufacture of a Y-shaped submarine using PA IN625 powder. The results showed an excellent geometrical agreement if compared with the original design with a consequent reduction in IN625 material waste if compared to the traditional manufacturing techniques. The utilisation of a canister design without a solid inner core could be investigated to reduce the canister material usage and improve the efficiency of the NNS PM HIP process.

Acknowledgments:

AS acknowledges the Centre of Doctoral Training in Innovative Metal Processing (IMPaCT), funded by the Engineering and Physical Sciences Research Council (EPSRC), and the National Structural Integrity Research Centre (NSIRC) for funding his PhD at the University of Birmingham. The authors warmly thank the European Union H2020 and the "Sustainable Process Industry through Resource and Energy Efficiency" (SPIRE) programmes, which funded this project under grant agreement n° 768612. The authors also acknowledge the support of the Henry Royce Institute for A. Sergi through the Royce PhD Equipment Access Scheme, enabling access to XPS at Royce@Imperial; EPSRC Grant number EP/R00661X/1.

Declarations of interest: none

5.8 References

[1] Stelios Kyriakides and Edmundo Corona, Mechanics of Offshore Pipelines, 2007.

[2] Y. Bai, Pipelines and Risers, Elsevier Ocean Engineering Book Series, Amsterdam, 2001.

[3] Q. Bai, Y. Bai, Subsea Pipeline Design, Analysis, and Installation, 2014.

[4] Mikael Braestrup, Design and installation of marine pipelines, Ames, Iowa : Blackwell Science, 2005.

[5] M. Iannuzzi, A. Barnoush, R. Johnsen, Materials and corrosion trends in offshore and subsea oil and gas production, Npj Mater. Degrad. 1 (2017). https://doi.org/10.1038/s41529-017-0003-4.

[6] J. Arnoldi, P. Dempsey, Selection of Materials for Sour Gas Pipelines, (n.d.).

[7] C.M. Senna, V.L. de C. Oliveira, D. Santos, E. Pessotti de Deus, M. Soares, W. Miranda, Coatings for Saltwater Pipelines, in: X Congr. Nac. Eng. MecâNica, 2018. https://doi.org/10.26678/abcm.conem2018.con18-1168.

[8] S. Floreen, G.E. Fuchs, W.J. Yang, The Metallurgy of Alloy 625, Superalloys 718, 625, 706 Var. Deriv. (1994) 13–37. https://doi.org/10.7449/1994/Superalloys_1994_13_37.

[9] H.L. Eiselstein, D.J. Tillack, The Invention and Definition of Alloy 625, in: Superalloys 718, 625, 716 Deriv., TMS, 1991: pp. 1–14. https://doi.org/10.7449/1991/superalloys_1991_1_14.

[10] H.V. Atkinson, S.Davies, Fundamental aspects of hot isostatic pressing : An overview, Metall. Mater. Trans. A. 31 (2000) 2981–3000.

[11] Y.L. Kuo, K. Kakehi, Effect of the prior particle boundary on the microstructure and mechanical properties of hot-isostatic-pressed IN718 Alloy, Mater. Trans. 58 (2017) 1042–1048. https://doi.org/10.2320/matertrans.M2017045.

[12] G.A. Rao, M. Srinivas, D.S. Sarma, Effect of oxygen content of powder on microstructure and mechanical properties of hot isostatically pressed superalloy Inconel 718, Mater. Sci. Eng. A. 435–436 (2006) 84–99. https://doi.org/10.1016/j.msea.2006.07.053.

[13] Y. Hedberg, M. Norell, J. Hedberg, P. Szakálos, P. Linhardt, I. Odnevall Wallinder, Surface characterisation of fine inert gas and water atomised stainless steel 316L powders: Formation of thermodynamically unstable surface oxide phases, Powder Metall. 56 (2013) 158–163. https://doi.org/10.1179/1743290112Y.0000000041.

[14] J. Yan, Y. Zhou, R. Gu, X. Zhang, W.M. Quach, M. Yan, A comprehensive study of steel powders (316L, H13, P20 and 18Ni300) for their selective laser melting additive manufacturing, Metals (Basel). 9 (2019). https://doi.org/10.3390/met9010086.

[15] E. Gil, J. Cortés, I. Iturriza, N. Ordás, XPS and SEM analysis of the surface of gas atomized powder precursor of ODS ferritic steels obtained through the STARS route, Appl. Surf. Sci. 427 (2018) 182–191. https://doi.org/10.1016/j.apsusc.2017.07.205.

[16] D. Chasoglou, E. Hryha, M. Norell, L. Nyborg, Characterization of surface oxides on water-atomized steel powder by XPS/AES depth profiling and nano-scale lateral surface analysis, Appl. Surf. Sci. 268 (2013) 496–506. https://doi.org/10.1016/j.apsusc.2012.12.155.

[17] Z.J. Gao, G.Q. Zhang, Z. Li, H. Yuan, W.Y. Xu, Y. Zhang, Surface Segregation and Oxidation Behavior of Superalloy Powders Fabricated by Argon Atomization, Mater.

Sci. Forum. 747–748 (2013) 518–525. https://doi.org/10.4028/www.scientific.net/msf.747-748.518.

[18] W. Bin Ma, G.Q. Liu, B.F. Hu, P.H. Hu, Y.W. Zhang, Study of metallic carbide (MC) in a Ni-Co-Cr-based powder metallurgy superalloy, Metall. Mater. Trans. A Phys. Metall. Mater. Sci. 45 (2014) 208–217. https://doi.org/10.1007/s11661-013-1962-x.

[19] Q. Bai, J. Lin, G. Tian, J. Zou, D. Ta, Review and Analysis of Powder Prior Boundary (PPB) Formation in Powder Metallurgy Processes for Nickel-based Super Alloys, Powder Metall. Min. 4 (2015) 1–6. https://doi.org/10.4172/2168-9806.1000127.

[20] L. Chang, W. Sun, Y. Cui, R. Yang, Influences of hot-isostatic-pressing temperature on microstructure, tensile properties and tensile fracture mode of Inconel 718 powder compact, Mater. Sci. Eng. A. 599 (2014) 186–195. https://doi.org/10.1016/j.msea.2014.01.095.

[21] J.E. Macdonald, R.H.U. Khan, M. Aristizabal, M.J. Lunt, M.M. Attallah, Influence of powder particle size distribution on the microstructure and mechanical properties of a HIPped CM247LC Ni superalloy, Mater. Des. 174 (2019).

[22] R.H.U. Khan, M.H. Loretto, M.M. Attallah, J. Cortes, I. Iturriza, F. Castro, Microstructure and properties of HIPped alloy 718, in: 11th Int. Conf. Hot Isostatic Press., Stockholm, 2014.

[23] John R. Dean, Practical Inductively Coupled Plasma Spectroscopy, Wiley, 2005.

[24] LECO, Carbon and Sulfur Determination, LECO Induction Furnace Instruments, (2007).

[25] LECO, Oxygen and Nitrogen Determination, LECO Inert Gas Fusion Instruments,

(2007).

[26] H.R. Dugdale, J.B. Borradaile, Development of hot isostatically pressed nickel based alloys for nuclear applications, Powder Metall. 56 (2013) 374–381. https://doi.org/10.1179/1743290113Y.0000000076.

[27] Heat Treatment Wrought Nickel Alloy and Cobalt Alloy Parts, in AMS 2774E. SAE International, (n.d.).

[28] M. Sundararaman, P. Mukhopadhyay, S. Banerjee, Precipitation of the δ-Ni3Nb phase in two nickel base superalloys, Metall. Trans. A. 19 (1988) 453–465. https://doi.org/10.1007/BF02649259.

[29] Z. Tian, C. Zhang, D. Wang, W. Liu, X. Fang, A Review on Laser Powder Bed Fusion of Inconel 625 Nickel-Based Alloy, Appl. Sci. 10 (2019) 1–14.

[30] F. Xu, Y. Lv, Y. Liu, B. Xu, P. He, Effect of heat treatment on microstructure and mechanical properties of inconel 625 alloy fabricated by pulsed plasma arc deposition, Phys. Procedia. 50 (2013) 48–54. https://doi.org/10.1016/j.phpro.2013.11.010.

[31] ASTM International. B834-17 Standard Specification for Pressure Consolidated Powder Metallurgy Iron-Nickel-Chromium-Molybdenum (UNS N08367), Nickel-Chromium-Molybdenum-Columbium (Nb) (UNS N06625), Nickel-Chromium-Iron Alloys (UNS N06600 and N06690), and N, (n.d.).

[32] J.W. Wang, Q.S. Wei, G.C. Liu, Y.K. He, Y.S. Shi, Study on direct hot isostatic pressing technology for superalloy inconel 625, Adv. Mater. Res. 189–193 (2011) 2935–2938. https://doi.org/10.4028/www.scientific.net/AMR.189-193.2935.

[33] Nickel Alloy, Corrosion and Heat-Resistant, Powder for Additive Manufacturing,

62Ni-21.5Cr-9.0Mo-3.65Nb, in AMS7001. SAE International, (n.d.).

[34] A. Mostafaei, E.T. Hughes, C. Hilla, E.L. Stevens, M. Chmielus, Data on the densification during sintering of binder jet printed samples made from water- and gas-atomized alloy 625 powders, Data Br. 10 (2017) 116–121. https://doi.org/10.1016/j.dib.2016.11.078.

[35] O.D. Neikov, Atomization and granulation, Handb. Non-Ferrous Met. Powders. (2009) 102–142. https://doi.org/10.1016/B978-1-85617-422-0.00005-7.

[36] F. Pengjun, X. Yi, L. Xinggang, C. Ya, Influence of Atomizing Gas and Cooling Rate on Solidification Characterization of Nickel-based Superalloy Powders, Rare Met. Mater. Eng. 47 (2018) 423–430. https://doi.org/10.1016/s1875-5372(18)30082-1.

[37] C. Pleass, S. Jothi, Influence of powder characteristics and additive manufacturing process parameters on the microstructure and mechanical behaviour of Inconel 625 fabricated by Selective Laser Melting, Addit. Manuf. 24 (2018) 419–431. https://doi.org/10.1016/j.addma.2018.09.023.

[38] S.D. DuPont, John N. Lippold, John C. Kiser, WELDING METALLURGY AND WELDABILITY OF NICKEL-BASE ALLOYS, John Wiley & Sons, Inc, 2009.

[39] F.J. Rizzo, D.J. Radavich, Microstructural Characterization of PM 625-Type Materials, in: Superalloys 718,625 Var. Deriv., TMS, 1991: pp. 297–308. https://doi.org/10.7449/1991/superalloys_1991_297_308.

[40] A. Gupta, M. Mittal, M.K. Singh, S.L. Suib, O.P. Pandey, Low temperature synthesis of NbC/C nano-composites as visible light photoactive catalyst, Sci. Rep. 8 (2018) 1–17. https://doi.org/10.1038/s41598-018-31989-z.

[41] F.J. Rizzo, Strengthening Precipitates in Argon Atomized PM 625, TMS. (1994) 913–922. https://doi.org/10.7449/1994/superalloys_1994_913_922.

[42] S. Irukuvarghula, H. Hassanin, C. Cayron, M. Aristizabal, M.M. Attallah, M. Preuss, Effect of powder characteristics and oxygen content on modifications to the microstructural topology during hot isostatic pressing of an austenitic steel, Acta Mater. (2019). https://doi.org/10.1016/j.actamat.2019.03.038.

[43] V. Randle, M. Coleman, G. Owen, Evolution of the Grain Boundary Network as a Consequence of Deformation and Annealing, Mater. Sci. Forum. 550 (2007) 35–44. https://doi.org/10.4028/www.scientific.net/MSF.550.35.

[44] M. Detrois, R. Goetz, Grain boundary engineering of powder processed Ni-base superalloy RR1000 : Influence of the deformation parameters, Mater. Sci. Eng. A. 627 (2015) 95–105. https://doi.org/10.1016/j.msea.2014.12.112.

[45] S. Bechtle, M. Kumar, B.P. Somerday, M.E. Launey, R.O. Ritchie, Grain-boundary engineering markedly reduces susceptibility to intergranular hydrogen embrittlement in metallic materials, Acta Mater. 57 (2009) 4148–4157. https://doi.org/10.1016/j.actamat.2009.05.012.

[46] S. Metals, Inconel Alloy 625, Www.Specialmetals.Com. 625 (2013) 1–28. https://doi.org/SMC-066.

[47] A.J. Goodfellow, Strengthening mechanisms in polycrystalline nickel-based superalloys, Mater. Sci. Technol. (United Kingdom). 34 (2018) 1793–1808. https://doi.org/10.1080/02670836.2018.1461594.

[48] T. Berglund, F. Meurling, Oxygen Content in PM HIP 625 and its Effect on Toughness, 12th Int. Conf. Hot Isostatic Press. (2017) 135–141.

Chapter 6. Development of Ni-base Metal Matrix Composites by Powder Metallurgy Hot Isostatic Pressing for Space Applications

Alessandro Sergi[1, 2], Raja H.U. Khan[3], Sandeep Irukuvarghula[3], Martina Meisnar[4], Advenit Makaya[5], Moataz M. Attallah*[1]

[1] IRC in Materials Processing, School of Metallurgy and Materials, The University of Birmingham, Birmingham, B15 2TT, UK.

[2] National Structural Integrity Research Centre (NSIRC), Cambridge, CB21 6AL, UK.

[3] TWI Ltd, Cambridge, CB21 6AL, UK.

[4] European Space Agency, ECSAT, Fermi Avenue, Harwell-Oxford Campus, Didcot, Oxfordshire OX11 0FD, UK.

[5] Materials and Processes Section TEC-MSP, Mechanical Engineering Department TEC-M, ESTEC, Keplerlaan 1 - PO Box 299, 2200 AG Noordwijk-ZH, The Netherlands.

* Corresponding author:

Email:

Telephone:

Fax:

The paper is slightly modified from the version accepted with corrections in Advanced Powder Technology Journal to include further background on the application.

6.1 Motivation & Aims

The introductory Chapter and the literature review have underlined the flexibility of PM HIP process in generating novel material combinations with the possibility to tailor the material's properties. In particular, an attractive solution to increase the wear resistance of Ni-base superalloys can be found in the generation of Ni-base MMCs with the addition of ceramic reinforcements. This class of materials can rely both on high temperature corrosion and oxidation resistance of Ni-base superalloys combined with the excellent hardness and wear properties offered by the addition of ceramic reinforcements.

In order to understand the feasibility of using Ni-base MMCs for wear resistant applications, the following aspects were addressed in the current study:

- Evaluating the HIP microstructure of Ni-MMCs focusing on the main differences if compared with the matrix material.
- Assess the influence of volume fraction and ceramic reinforcement type on the wear properties of Ni-MMCs.
- Understand the mechanical properties of as-HIPed Ni-MMCs and compare them with the matrix material.

For this study, the initial knowledge acquired on the HIP behaviour of IN625 was exploited to generate MMCs using IN625 as matrix material. Two different reinforcements were adopted i.e. SiC and TiB_2. In particular, SiC was explored as reinforcement due to its low density and to assess the possibility of in-situ formation of hard intermetallics. In fact, different silicides and carbides can form due to the presence of Mo, Nb and Cr in the matrix material, having a good affinity to both Si and C which would increase the hardness of the material. The addition of TiB_2 to the IN625 matrix has already demonstrated clear benefits in improving the wear properties as highlighted in the study of Zhang et al. [1]. Furthermore,

TiB_2 is a more stable ceramic material if compared to SiC and it represents the ceramic reinforcement with the highest melting point. Due to TiB_2 stability if compared to the other possible borides formers in the IN625 matrix, a limited presence of intermetallic is expected in comparison with IN625-SiC.

Also in this case, to prove the feasibility of NNS PM HIP of Ni-MMCs for the production of real parts, mechanical seals demonstrators were manufactured. The application was selected due to its combination of high temperature, wear and corrosion resistance required, making Ni-MMCs an attractive alternative to conventionally used materials.

Abstract

In this work, near-net-shape powder metallurgy hot isostatic pressing (NNS PM HIP) of Ni-base metal matrix composite (Ni-MMC) was developed to improve the hardness and wear properties of turbopumps mechanical seals. Silicon carbide (SiC) and titanium diboride (TiB_2) fine powders were used as reinforcements with different ratios to improve the hardness and consequently the tribological properties of the developed Ni-MMC material. Powder characterisation was performed on the blended powders to check the homogeneity of the mixed powders. The hot isostatically pressed (HIPed) Ni-MMC microstructures were analysed using scanning electron microscope (SEM) and energy dispersive X-ray spectroscopy (EDS) techniques. The HIPed material showed a fully dense microstructure with a continuous network of ceramic reinforcement particles at the prior particle boundaries (PPBs). Furthermore, microhardness tests were performed on IN625, IN625-SiC and IN625-TiB_2 to understand the impact of the reinforcement on the microhardness. It was demonstrated that the volume percentage of ceramic reinforcement in the IN625 matrix plays a crucial role in achieving higher hardness by increasing the fraction of hard phases appearing

in the microstructure of the developed Ni-MMC material. The final part of the work focuses on the canister design and manufacture of a near-net-shape (NNS) mechanical gas seal using IN625 based MMC to demonstrate the feasibility of manufacturing mechanical seals through the NNS PM HIP technique. Overall, IN625 based MMCs resulted in a drastic improvement in tribological properties if compared to the base material. Furthermore, the employment of the PM HIP consolidation technique resulted in a fully dense and homogeneous microstructure, highlighting the potentials of PM HIP in the generation of novel composite materials.

Keywords:

IN625-Metal Matrix Composites (MMCs), microstructure, mechanical properties, tribological properties, near-net-shape powder metallurgy hot isostatic pressing (NNS PM HIP).

6.2 Background: Mechanical Seals Application

Mechanical seals are used in turbopumps rotating shafts of liquid propellant rockets to control the flow of liquid hydrogen (LH_2, boiling temperature 90K) and liquid oxygen (LOX, boiling temperature 20K). The shaft seals are located between the hot gas turbine and the cryogenic pumps, thus, the main role of mechanical seals is to minimize the leakage between the rotary pump and the hot turbine. In fact, the mixture between the cryogenic oxidiser present in the pump and the turbine hot gas happens, it would lead to a catastrophic failure of the turbopump and consequently of the entire vehicle [2], [3], [4].

The seals often operate in dry conditions and must withstand severe loading and environmental condition. In particular, mechanical seals in turbopumps work under a contact pressure of 35MPa and reciprocating sliding speed of 0.3m/s, and rotating speeds up to 50,000rpm [5]. Another important factor to take into account is the compatibility of the material with the reactive propellant and the ability to operate at temperatures ranging from cryogenic to hot gas temperatures during operation, thus not many materials are able to withstand these extreme operating conditions [2].

A schematic of a typical mechanical seal is reported in Figure **6.1** [6].

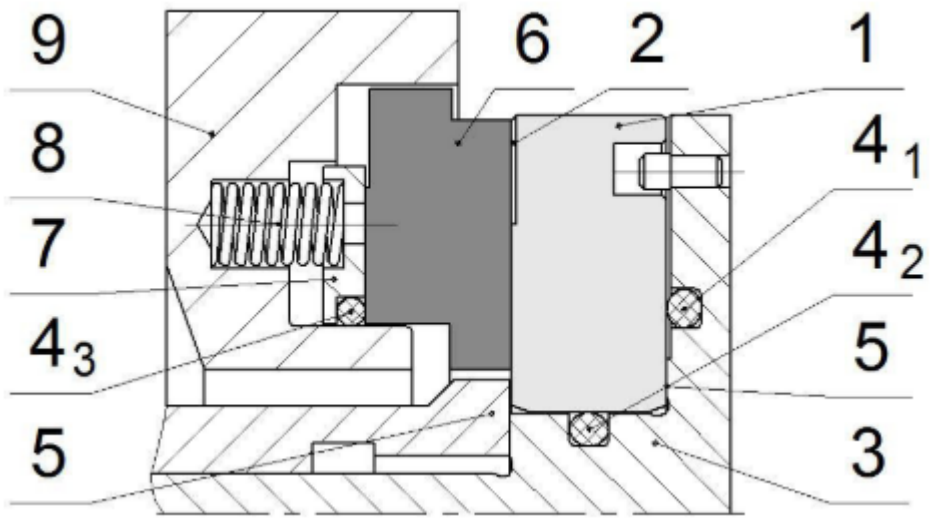

Figure 6.1 Schematic of dry gas mechanical seal. 1: carbide ring; 2: spiral grooves; 3: rotor; 4: elastomeric rings; 5: sleeves on the rotor; 6: graphite sealing ring; 7: spring follower; 8: spring; 9:stator [6].

One of the major challenges associated with the operation of mechanical seals is the coning effect arising from the temperature and pressure gradients across the seal interface [7]. Other problems related to the shaft seals operation include the instability of the film, induced by the mechanical vibrations, which can enhance the wear mechanism.

Different materials can be used for this application, including the application of different wear-resistant coating strategies. The most common materials used for this application include WC, SiC and carbon [2], [7]. The most used wear-resistant coatings for this range of applications include ceramic coatings such as Cr_2O_3, TiN, WC, with a substrate normally made of Stainless Steel or Ni-base superalloys [2], [8]. Other strategies to improve the wear properties of the material would include the manufacture of self-lubricating hard coatings such as diamond-like carbon (DLC) [9] and the development of coatings with reduced friction coefficient but no apparent increase in hardness such as molybdenum disulphide (MoS_2) and silver (Ag) [8], [10].

The choice of the material has to reflect the operating conditions described above. The use of hardened steel or coated steel is not possible due to the embrittlement which could be caused by the action of H_2 in the LH_2 pump. The use of thin coating hard coating is ideal to guarantee low friction and wear rate, however due to the high thermal gradients and loading conditions, there is the possibility of cracking or spalling. Diffusion bonding can represent a valid manufacturing route for a wear-resistant coating ensuring the presence of a fully dense thick coating with an excellent bonding, low levels of residual stresses related to the process and the possibility of forming a functionally graded structure [11]. However, the application of DB strategies can be limited when a complex geometry is required. A good alternative can be represented by the use of metal matrix composites (MMCs) combining excellent wear properties with good corrosion and high temperatures capabilities [12], [13], [14].

6.3 Introduction

Powder metallurgy (PM) is progressively gaining research interest for the manufacture of spacecraft components. This is due to the possibility of creating new materials with superior

properties, to drastically reduce the buy-to-fly ratio and to generate complex geometries [15–17].

Mechanical seals are used in turbopump rotating shafts to minimise propellant leakage between the rotary pump and the hot turbines. Mechanical seals, therefore, have a crucial role in the design of rocket engines. Their role is to separate incompatible fluids or propellants which, if in contact, can cause a reduction in efficiency. Furthermore, an excess of fluid leakage could compromise the flight mission or could lead to a catastrophic failure of the engine due to the reaction of the two fluids [18].

The requirements for mechanical seals are very strict and only a limited class of materials can withstand the harsh operating conditions. In fact, mechanical seals need to be compatible with both H_2 and O_2 environments, and perform in a range of working temperatures from cryogenic temperature (below 20K for LH_2, and below 90K for LO_2) up to 650°C. The working pressure exerted on the seals is above 35MPa, while the rotational speeds can range from 50,000 rpm to above 100,000 rpm [5].

Another important requirement concerns the machinability of the part, where precise machining should guarantee a gap between the rotating parts between 2–5μm to reduce any fluid leakage. During the ramp-up and slow-down operations, the mechanical seals come into direct contact with their counterpart, creating severe wear conditions. Many different ranges of materials have been developed in the past for high wear resistance applications with different techniques used to improve the surface wear resistance, such as carburising, nitriding, physical vapor deposition (PVD) or chemical vapor deposition (CVD). However, the commonly used coating techniques are not ideal for the production of mechanical seals for a variety of reasons. Nitriding and carburising are used as hardening processes for steels, the problem of using steels for this application is their embrittlement due to the presence of

LH_2, which could lead to a catastrophic failure of the component [2], [19]. Coating techniques, such as PVD and CVD, are not suitable because of the coefficient of thermal expansion (CTE) mismatch between the coating and the substrate. This could lead to spalling as a consequence of the extremely high thermal gradients demanded by the application.

Different materials have been used in the past for the manufacture of mechanical seals, including various classes of ceramic materials, such as SiC, Si_3N_4, WC or Al_2O_3, and metals, such as hardened steels, copper or bronze [20]. Ceramic materials are characterised by high hardness and tribological properties, low CTE, and good elevated temperature oxidation and corrosion resistance. However, the main drawback of ceramic materials is presented by their mechanical properties, as ceramics are characterised by poor ductility and fracture toughness. These can compromise the integrity of the mechanical seals. Thus, for the manufacture of mechanical seals, near-net-shape powder metallurgy hot isostatic pressing (NNS PM HIP) can be regarded as a valid manufacturing technique capable of producing components with improved tribological properties through the formation of metal matrix composites (MMCs) [21], [22].

The selected material for the application is a Ni-base superalloy MMC. Specifically, the material used as the matrix is Inconel 625 (IN625) due to its excellent high-temperature oxidation and corrosion resistance, good high-temperature mechanical properties (up to 650°C) and good levels of elongation and fracture toughness compared to the other Ni-base superalloys [23–25]. For the reinforcement, two different materials were considered, SiC and TiB_2. The influence of the reinforcement was assessed, as was the effect of the volume fraction of the reinforcement. This brought an understanding of the optimal level of reinforcement that would guarantee an ideal microstructure and wear properties.

The manufacture of IN625-SiC was attempted by D.E. Cooper *et al.* using additive manufacturing, however the presence of high cooling rates during the solidification process resulted in a microstructure characterised by high cracking density [26]. PM HIP does not involve melting of the material, instead, the solid-state diffusion bonding between the matrix and the reinforcement occurs through yield collapse, creep and diffusion, respectively [27]. Therefore, the effect of the CTE mismatch between the matrix and the reinforcement is contained, ensuring a fully dense microstructure with a much lower instance of defects and enhanced tribological properties [28–30].

6.4 Materials and Methods

6.4.1 Experimental Procedure

In this study, a wide range of powders were used and assessed. In particular, argon gas atomised (AGA) IN625 was used as a base material with the addition of SiC and TiB_2 as reinforcement with different volume fractions (5v%, 10v% and 25v%). To account for the differences in density between SiC and TiB_2 and thus to have comparable results, reinforcement volume fractions (v%) were used rather than weight fractions (wt%). Additionally, to calculate the right amount of reinforcement required, the reinforcements volume fractions were converted into weight fractions, weighted in the required proportions and blended with the base material.

SiC and TiB_2 were obtained by mechanical comminution. In order to obtain a homogeneous material, the powders were blended using a SpeedMixer available at TWI Ltd. To further homogenise the powder mixture, the blended powders were subjected to low-speed rolling for 3h.

The powder mixture was then characterised using different analyses, including particle size distribution (PSD), powder morphology, tap and apparent density. PSDs were performed using laser diffraction techniques in de-ionised water, specifically Malvern Mastersizer300 Hydro available at TWI Ltd was used. The powder apparent and tap densities were assessed according to ASTM 212-17 and ASTM B527-15 standards, respectively. Additionally, chemical analyses were performed by AMG Analytical Services, Sheffield on AGA IN625 powder to ensure that the chemical composition was within the required standards. In particular, to analyse the chemical composition of AGA IN625 powder, inductively coupled plasma optical emission spectroscopy (ICP OES), LECO thermal infrared using combustion in oxygen and LECO inert gas fusion using infrared and thermal conductivity detection techniques were used. After powder characterisation, seven mild steel canisters (Ø50mm x 185mm) and 2mm thickness were used to encapsulate the powders. The filling procedure was performed in argon using a glovebox to minimise contamination. The canisters were then subjected to vibrating operations in order to reach the packing density. Once the filling procedure was completed, the four canisters were outgassed for a minimum of 48h to a vacuum level in the order of 10^{-5}mbar. They were then hot sealed, ready to be HIPed.

The HIP parameters used were a temperature of 1160°C, a pressure of 120MPa, a dwell time of 4h, the heating rate was 5°C/min, while the cooling rate was 10°C/min. For microstructure analysis, small samples were electrical discharge machining (EDM) extracted from the canisters, mounted in conductive Bakelite and polished using standard metallographic procedures. The microstructure of the HIPed samples was analysed using a backscattered scanning electron microscope (SEM) and energy dispersive X-ray (EDX). Microhardness was performed on 10 different locations for each sample using a load of 500gf according to ASTM E384 – 17 using a semi-automatic Buehler microhardness tester. Reciprocating sliding wear tests were performed on the samples using an Al_2O_3 ball as a counterpart with a

diameter of 8mm. The number of cycles were 750, with a sliding velocity of 10mm/s, a track length of 5mm and an applied load of 20N. The coefficient of friction (CoF) was calculated using the tribometer dedicated software, while the wear rate was analysed by calculating the volume loss through an Alicona optical profilometer. The wear tracks were analysed using a backscattered SEM to understand the nature of the wear and the differences in wear mechanisms among the different samples.

Room temperature and elevated temperature tensile tests were performed on the down-selected powder mixture according to ASTM E8/E8M-16a. Room temperature V-notch Charpy impact tests on the down-selected powder mixture were performed as per the ASTM E23-16b standard. The down-selected powder mixture was used to manufacture a near-net-shape (NNS) mechanical seal. Two mild steel canisters were successfully designed and manufactured. The canisters were filled, outgassed, hot sealed and HIPed following the same procedure as described above. After the HIP procedure, the canisters were dissolved using nitric acid and machined to net-shape. The dimensional accuracy of the part was assessed using a digital vernier calliper.

6.5 Results and Discussion

6.5.1 Powder Characterisation

The chemical composition of AGA IN625 powders, together with the required range for IN625 is presented in **Table 6.1**. The result shows that all the elements are in the required range.

Table 6.1 Chemical composition of AGA IN625 base material.

Elements	C	O	N	Cr	Fe	Cu	Mn	Mo	Ni	P	S	Si	Nb	Al	Ti	Co
Required [31]	<0.10	<0.02	<0.02	20.0-23.0	≤5.0	<0.50	<0.50	8.0-10.0	bal ≥58	<0.015	<0.015	<0.50	3.15-4.15	0.1-0.4	0.1-0.4	≤1.0
AGA (15-45μm)	0.02	0.01	0.009	20.8	4.20	0.02	0.02	9.10	61.58	<0.005	<0.005	0.08	3.64	0.21	0.21	0.1

The PSDs of the base material and the reinforcements are shown in Figure **6.2**. The IN625 powder has a narrow distribution intentionally chosen to obtain a more uniform powder mixing and consequently more uniform microstructure and mechanical properties, with a D_{50} of 36μm. The PSD of SiC shows a narrow distribution with a D_{50} of 4.6μm and bimodal distribution with some coarser powders, while the TiB_2 powder is characterised by a bi-modal distribution with a D_{50} of 4.3μm. The PSDs of IN625-SiC and IN625-TiB_2 show three characteristic peaks (Figure **6.2**).

Tap and apparent densities for the powders are shown in Table **6.2**. IN625 powder has a packing density of 60%, while SiC and TiB_2 have a very low packing density of 28% and 32%, respectively, due to the small size, narrow PSD and irregular shape. The apparent density decreases with the addition of the reinforcement. IN625-5v%SiC has the highest packing density, due to the combination of bigger IN625 particles and the small fraction of reinforcement which will distribute into the gaps of IN625. Further addition of reinforcement reduces the packing density as the agglomeration of the reinforcement powder particles having lower tap density for both IN625-SiC and IN625-TiB_2.

Table 6.2 Physical properties of IN625 and IN625-MMCs powders.

Powder Type	Apparent Density (g/cm^3)	Tap Density (g/cm^3)	Bulk Density (g/cm^3)	Packing Fraction (%)
IN625	4.35	5.12	8.44	60
SiC	0.61	0.91	3.21	28
TiB_2	0.95	1.45	4.52	32
IN625-5v%SiC	4.11	5.32	8.17	65
IN625-10v%SiC	3.71	4.68	7.91	59
IN625-25v%SiC	3.03	4.31	7.13	60
IN625-5v%TiB_2	4.25	5.28	8.24	64
IN625-10v%TiB_2	3.86	4.91	8.04	61
IN625-25v%TiB_2	3.10	4.54	7.46	61

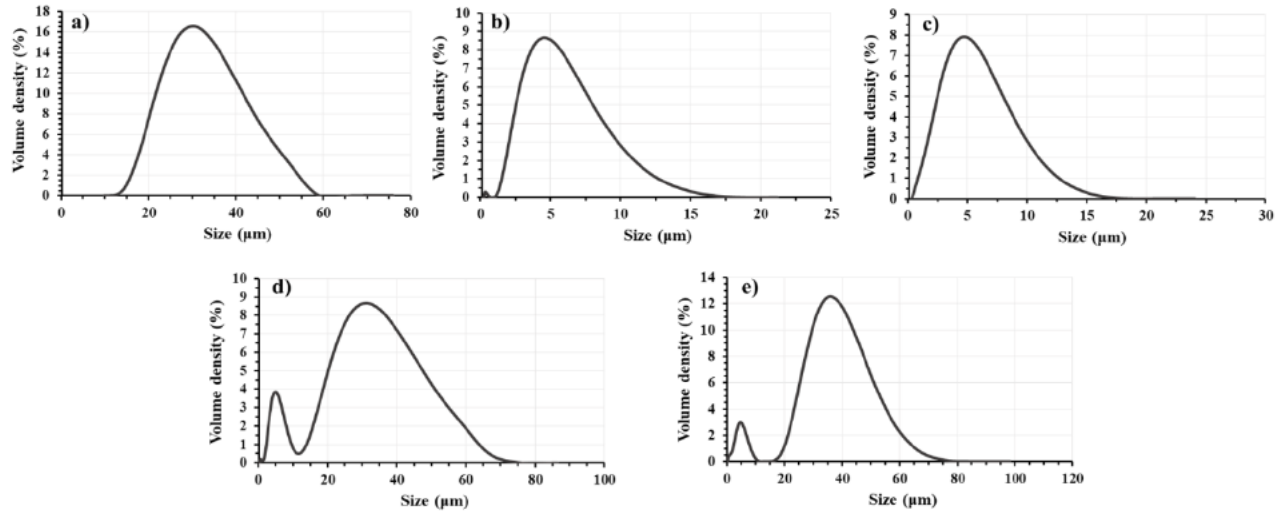

Figure 6.2 PSD of IN625 and IN625-MMCS after powder blending. (a) IN625; (b) SiC; (c) IN625-SiC; (d) TiB_2; (e) IN625-TiB_2.

The powder morphology of IN625 and all the different powder mixtures are reported in Figure **6.3**. IN625 powder has a nearly spherical shape with some satellites and some irregularly shaped powders. The influence of the reinforcement volume fraction is shown in Figure **6.3**. In fact, IN625-5v%SiC and TiB_2 show a uniform mix. However, as the reinforcement fraction is increased, there is a progressive loss in homogeneity. IN625-25v% reinforcement powders are, in fact, characterised by some agglomeration of reinforcement ceramic particles which is detrimental to the consolidation process and mechanical properties. Furthermore, IN625-25v%SiC is characterised by the presence of big reinforcement particles as shown circled in Figure **6.3**C. This demonstrates that in order to guarantee a uniform mixture it is important to select the correct blending parameters and reinforcement volume ratio. Furthermore, as described above, both the reinforcement and base material particle size play a crucial role. Having a base material with a narrow PSD helps the uniform distribution of the reinforcements on the powder particles, while having small reinforcement particle size is beneficial to ensure adequate bonding on the surface of the base material powder. The uniformity of the mixture is a fundamental aspect to guarantee uniform microstructure and mechanical properties in the as-HIPed part.

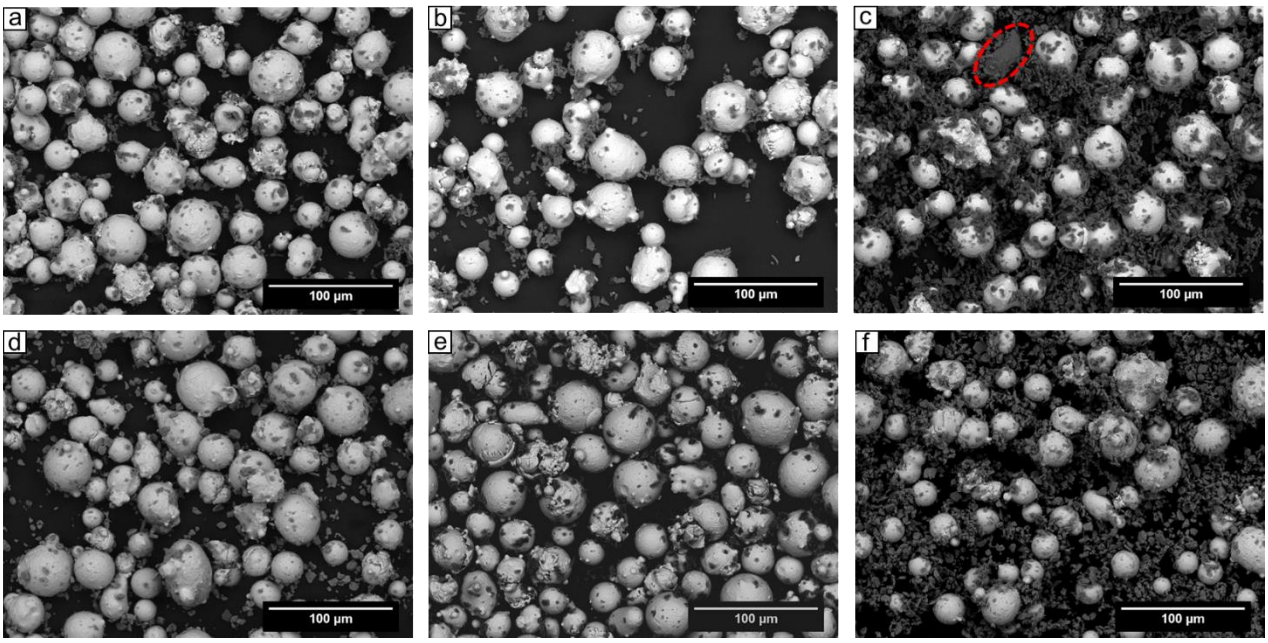

Figure 6.3 SEM powder morphology of: a) IN625-vol5%SiC; b) IN625-10v%SiC; c) IN625-25v%SiC; d) IN625-5v%TiB_2; e) IN625-10v%TiB_2; f) IN625-25v%TiB_2.

6.5.2 Microstructure of as-HIPed IN625-MMCs

The as-HIPed microstructure of IN625 and IN625-MMCs are shown in Figure **6.4** and Figure **6.5**, respectively. As-HIPed IN625 microstructure is characterised by a fully dense fine structure with the strong presence of twin boundaries and some PPBs, as observed in other as-HIPed microstructures of Ni-base superalloys [32], [33]. Furthermore, precipitation of very fine carbides can also be detected.

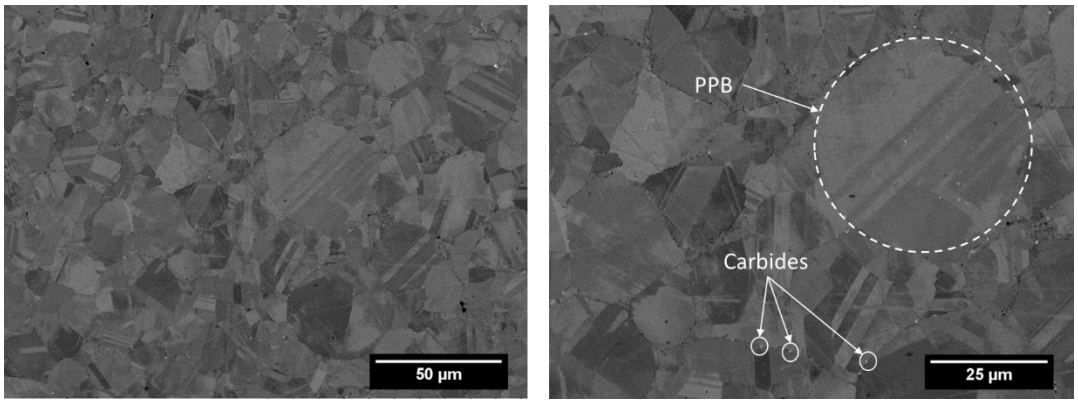

Figure 6.4 as-HIPed SEM micrographs of AGA IN625.

The addition of the reinforcement has a strong impact on the as-HIPed microstructure of IN625. The microstructure of IN625-5v%SiC of (Figure **6.5**a) shows a near to fully dense microstructure characterised by abundant precipitation at PPBs. Similarly, IN625-5v%TiB_2 (Figure **6.5**d) shows some precipitation at PPBs, but with the presence of some cracks at the particle boundaries. When increasing the volume of reinforcement to 10v%, in IN625-10v%SiC there is an increase of precipitation which is now more uniformly distributed. In fact, the precipitation starts at the PPBs and as the particle boundaries are saturated, the precipitation starts within the boundaries of the powders. Furthermore, as the volume fraction increases, there is a stronger presence of SiC (dark phase) in the microstructure (Figure **6.5**b).

The microstructure of IN625-10v%TiB_2 shows a different scenario: there is more presence of unreacted reinforcement at the PPBs which can be a direct consequence of the lower solubility of TiB_2 in the IN625 matrix if compared to SiC. The addition of 25%volSiC has different consequences in the microstructure. It is possible to note the presence of unreacted SiC at PPBs accompanied by the precipitation of very coarse dark precipitates (Figure **6.5**c). Further, the microstructure of IN625-25v%TiB_2 shows the presence of cracks and reinforcement debonding which can be detrimental for the wear properties and, above all, for the tensile properties (Figure **6.5**f).

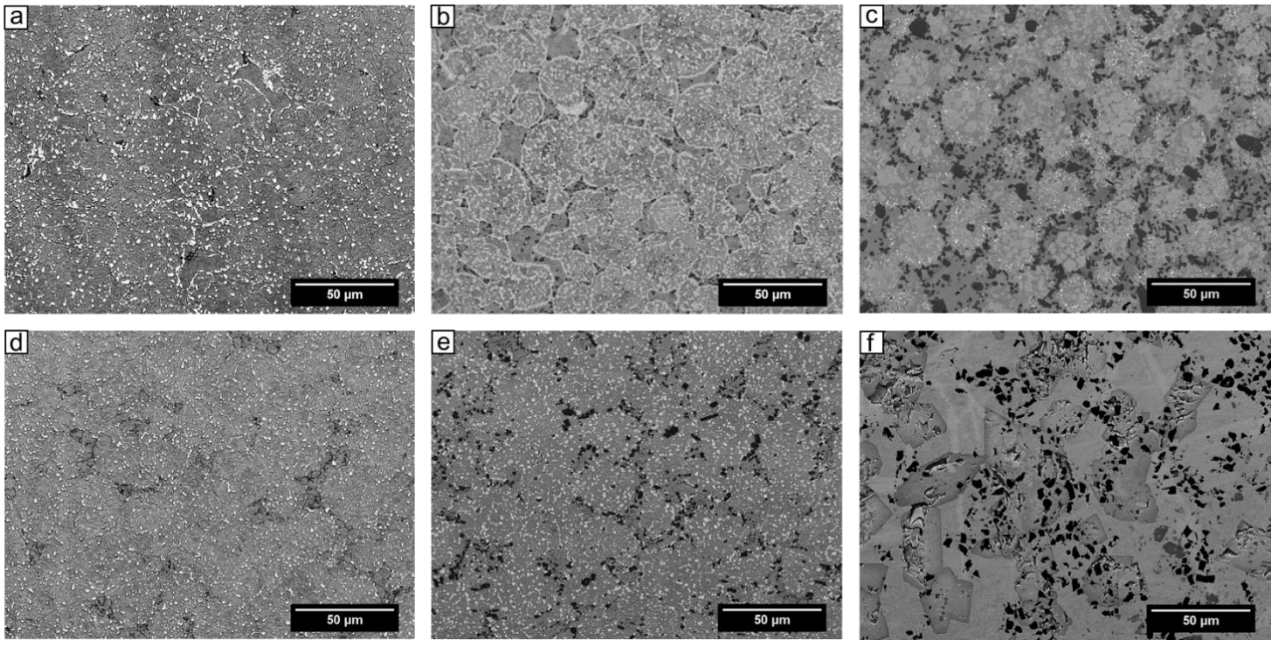

Figure 6.5 as-HIPed SEM micrographs of: a) IN625-vol5%SiC; b) IN625-10v%SiC; c) IN625-25v%SiC; d) IN625-5v%TiB_2; e) IN625-10v%TiB_2; f) IN625-25v%TiB_2.

EDX analyses were performed on the HIPed microstructures to understand the different phases formed in IN625-SiC and IN625-TiB_2. Figure **6.6** highlights an EDX map of IN625-5v%SiC showing the coexistence of Si, Nb and Mo in the precipitates, forming a complex intermetallic phase. The presence of coarse Nb, Mo rich precipitates can be also observed in the SEM micrographs for IN625-5v%TiB_2 (Figure **6.5**d). As the reinforcement fraction is increased to 10v%SiC, there is an increase of fraction size of Cr, believed to be Cr_2O_3 or Cr carbides (Figure **6.7**). It is interesting to note that for both IN625-5v%SiC and IN625-10v%SiC there is no detectable presence of discrete SiC. This means that during the HIP heat treatment, the SiC reinforcement dissociates in the matrix and forms complex phases together with Nb and Mo. Another interesting point is that the presence of SiC reinforcement has the effect of depleting the matrix from Nb and Mo. In fact, the IN625 microstructure shows just a small fraction of (Nb, Mo)C in the microstructure (Figure **6.4**), while in IN625-SiC the presence of Nb, Mo rich precipitates is much higher. If compared to IN625-10v%SiC, a different behaviour is observed in as-HIPed IN625-10v%TiB_2. In fact, the EDX map of

Figure **6.8** reveal the presence of unreacted reinforcement, which is a direct consequence of the lower solid solubility of Ti in the IN625 γ matrix.

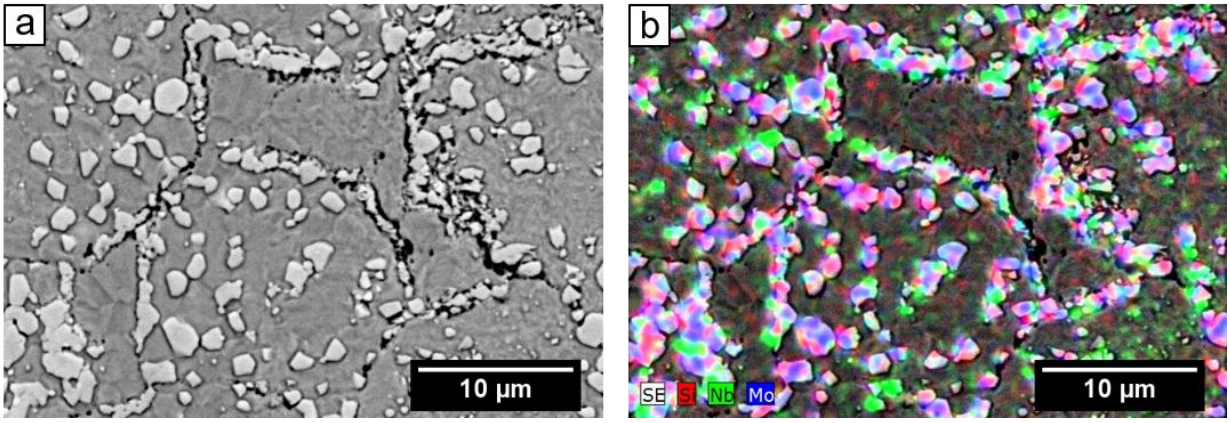

Figure 6.6 a) SEM micrograph of IN625-5v%SiC; b) EDX map of IN625-5v%SiC.

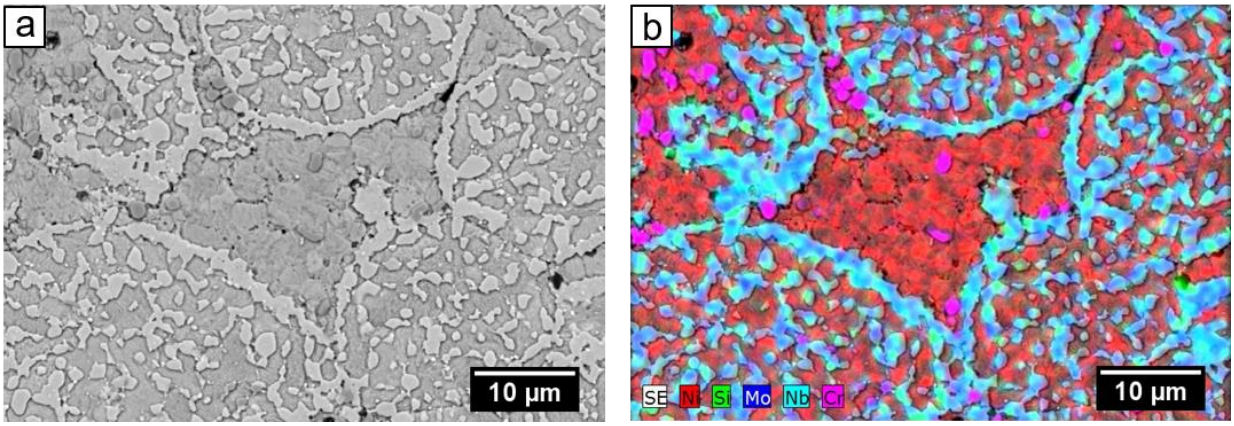

Figure 6.7 a) SEM micrograph of IN625-10v%SiC; b) EDX map of IN625-10v%SiC.

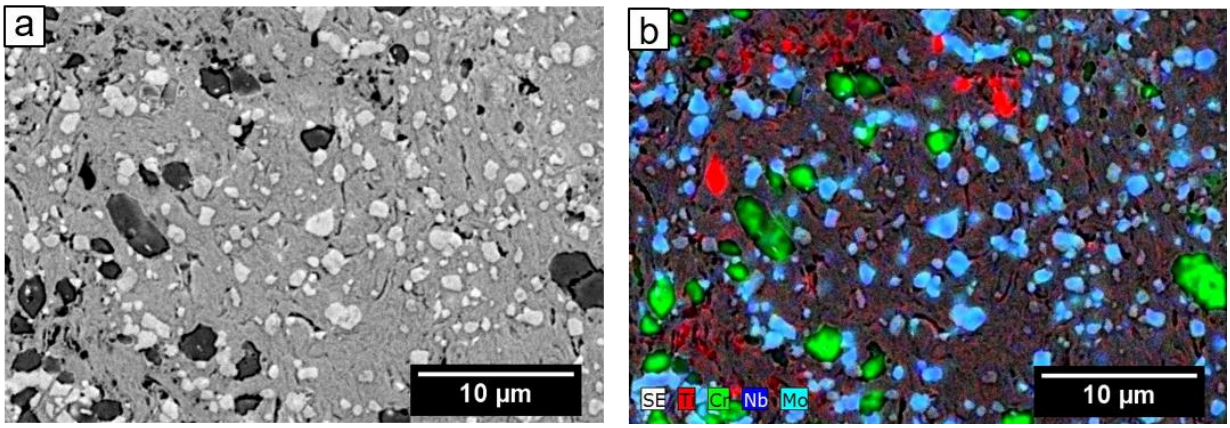

Figure 6.8 a) SEM micrograph of IN625-10v%TiB_2; b) EDX map of IN625-10v%TiB_2.

IN625-25v%SiC shows a different microstructure, as described above, it is characterised by the presence of Nb, Mo rich precipitates, discrete SiC particles and by the presence of coarse dark phase. The EDS results shown in Figure **6.9** reveal the presence of Cr-Si rich phase. On the other hand, in IN625-25v%TiB_2 there is a more predominant presence of unreacted reinforcement particles, accompanied by the evident presence of cracks as witnessed by the SEM micrograph and EDX spectrum of Figure **6.10**.

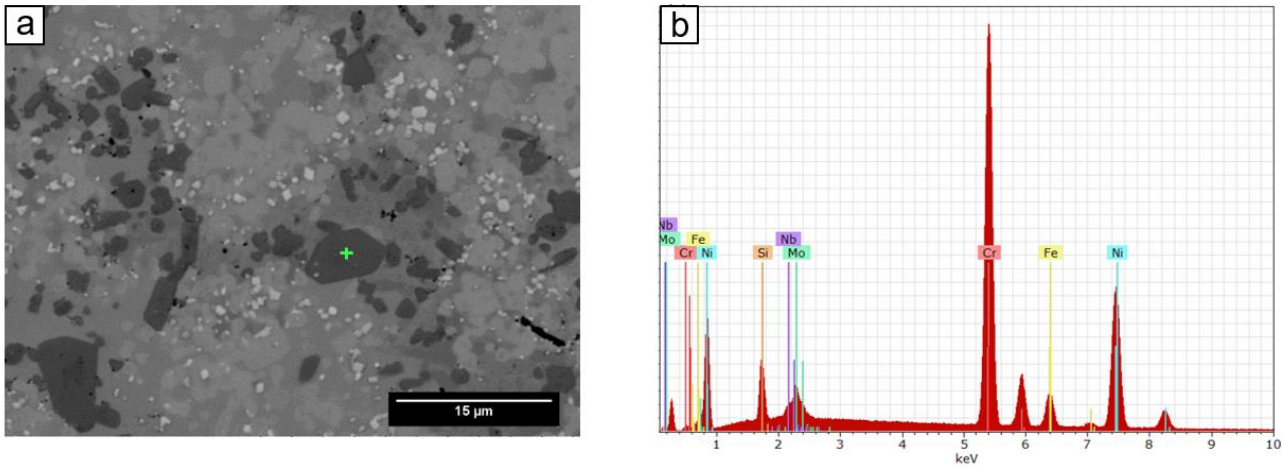

Figure 6.9 a) SEM micrograph of IN625-25v%SiC; b) EDX spectrum of IN625-25v%SiC highlighting the Cr, Si rich phase.

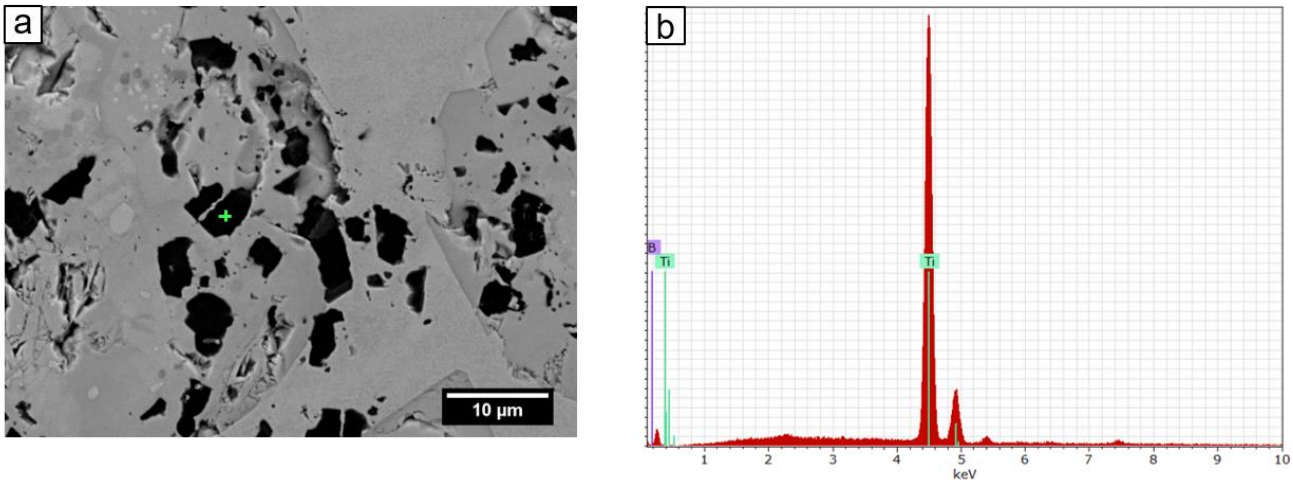

Figure 6.10 a) SEM micrograph of IN625-25v%TiB_2; b) EDX spectrum of IN625-25v% TiB_2 highlighting the Ti, B rich phase.

6.5.3 Mechanical and Tribological Properties

6.5.3.1 Microhardness

The microhardness of IN625 and IN625-MMCs is reported in Figure **6.11** and Figure **6.12**. The results show that for both IN625-SiC and IN625-TiB_2 there is a strong influence of the reinforcement fraction on the microhardness. The addition of 5v%SiC improved the microhardness from 246HV0.5 to 434HV0.5. The microhardness of IN625-10v%SiC was 471HV0.5, which was slightly higher if compared to IN625-5v%SiC. This can be attributed to the greater presence of Nb, Mo-rich phases if compared with IN625-5v%SiC. The presence of these precipitates will deplete Mo and Nb from the IN625 matrix, causing a reduction in solid solution strengthening of the matrix [34], which is counterbalanced by the higher reinforcement fraction. A consistent increase in hardness is reported for IN625-25v%SiC. In this case, the dominating strengthening effect comes from the presence of discrete SiC particles dispersed in the matrix, as shown in Figure **6.9**.

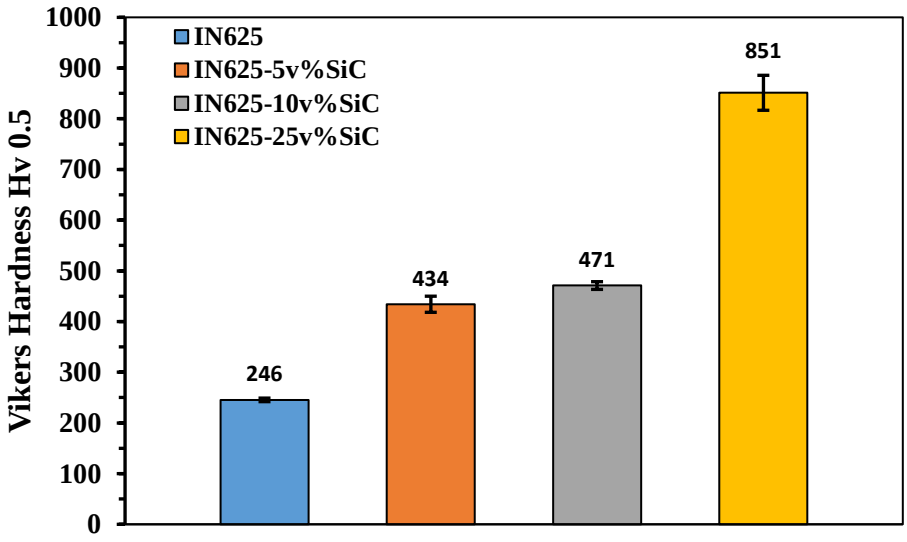

Figure 6.11 Vickers microhardness of as-HIPed IN625 and IN625-SiC.

The microhardness values of IN625-TiB_2 reflect a similar scenario if compared to IN625-SiC. In this case, the hardness is also directly linked with the reinforcement volume fraction, with a consistent increase in hardness for IN625-25v%TiB_2 (Figure **6.12**).

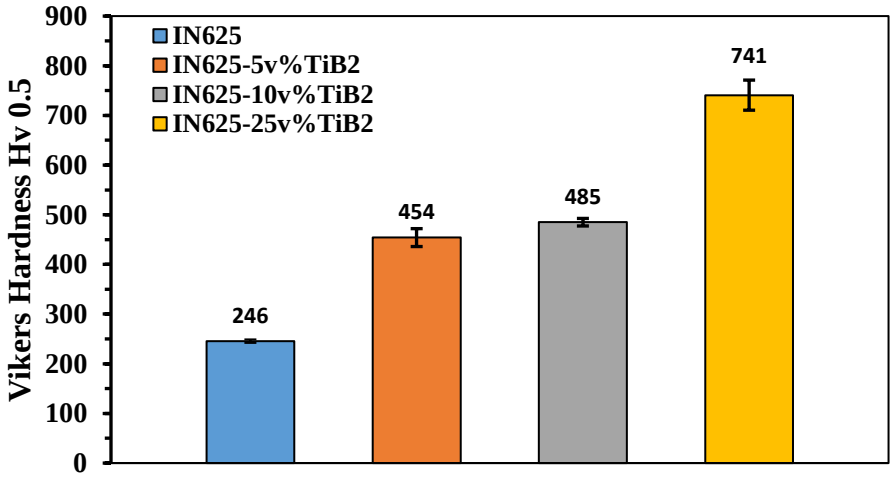

Figure 6.12 Vickers microhardness of as-HIPed IN625 and IN625-TiB_2.

6.5.3.2 Reciprocating Sliding Wear Test

It was observed to this point that the volume fraction of reinforcement played an important role in microstructure and microhardness for both IN625-SiC and IN625-TiB_2. The tribological properties of the IN625-MMCs were examined to understand the influence of the reinforcement and the reinforcement fraction on the coefficient of friction and the wear rate. Figure **6.13** shows the coefficient of friction for IN625-SiC vs the number of cycles. The first important fact to note is that the CoF is very similar for IN625 and IN625-5v%SiC. IN625-10v%SiC has lower levels of friction, while the fluctuation of the CoF is smaller if compared to IN625 and IN625-5v%SiC. Furthermore, IN625-25v%SiC has the lowest level of the coefficient of friction. This can be attributed to the larger difference in hardness. Lastly, it has, together with IN625-10v%SiC, the lowest variation of CoF over time.

Table **6.3** reports a summary of the average coefficient of friction for IN625 and IN625-MMCs. For IN625-SiC, the coefficient of friction decreases as the volume fraction of SiC increases, with the lowest level of friction being 0.41 for IN625-25v%SiC, much lower if compared to the value of 0.64 for IN625.

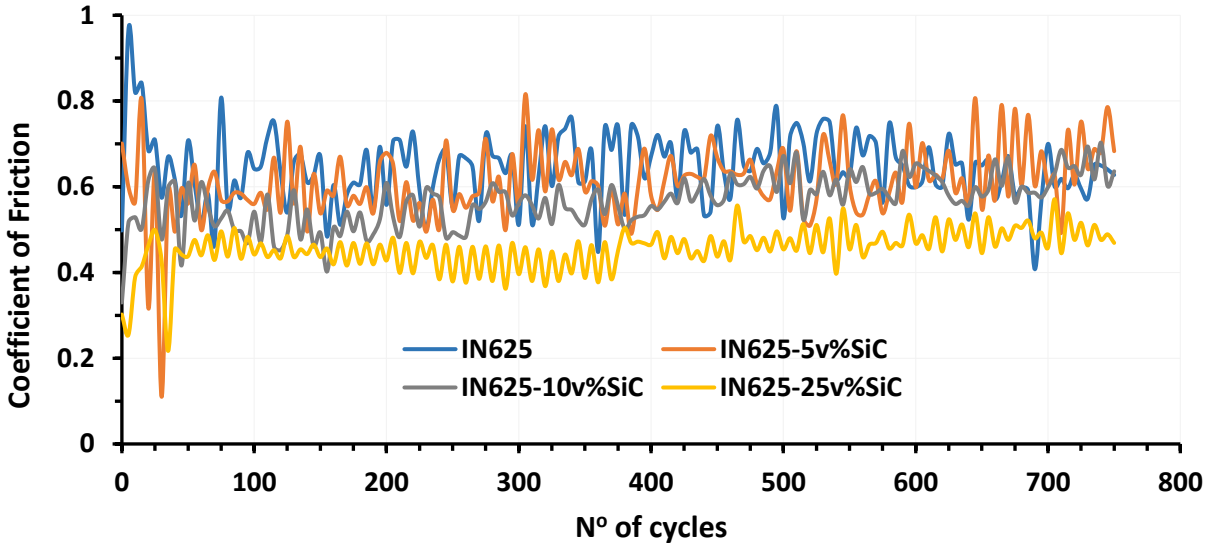

Figure 6.13 CoF for as-HIPed IN625 and IN625-SiC.

The results concerning the tribological properties of IN625-TiB_2 follow a similar trend to IN62-SiC (Figure **6.14**). As the reinforcement fraction increases, the CoF decreases with the lowest value for IN625-25v%TiB_2. The average values for the CoF show very similar values if compared to IN625-SiC (Table **6.3**).

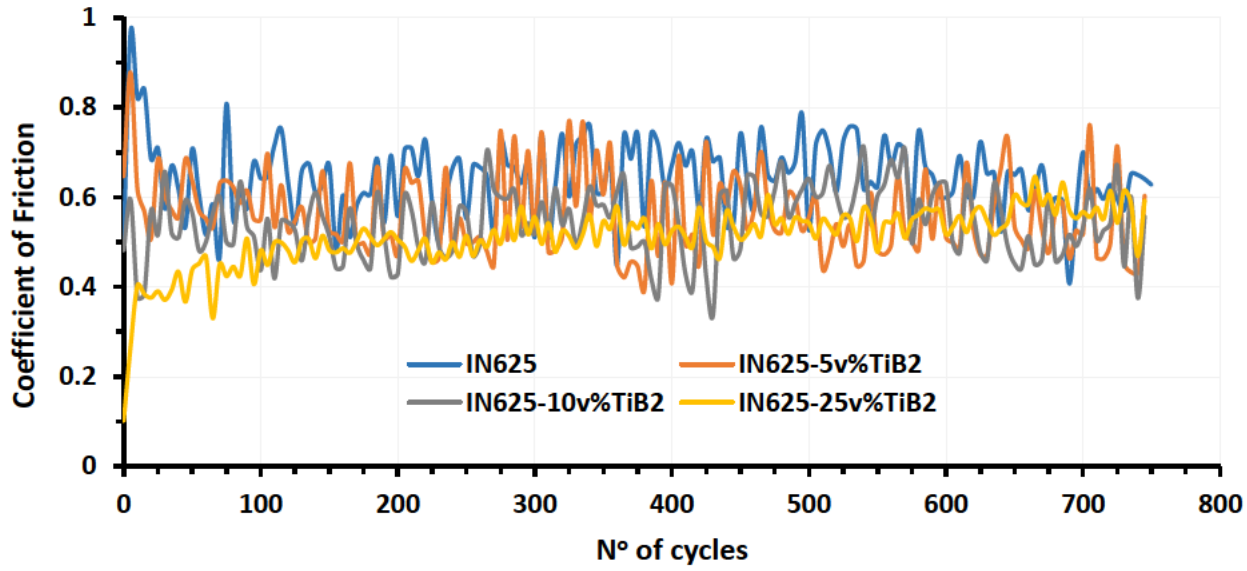

Figure 6.14 CoF for as-HIPed IN625 and IN625-TiB_2.

Table 6.3 Average coefficient of friction for IN625, IN625-SiC and IN625-TiB_2.

Material	Average Coefficient of Friction	Std Dev
IN625	0.64	0.08
IN625-5v%SiC	0.61	0.09
IN625-5v%TiB_2	0.60	0.09
IN625-10v%SiC	0.57	0.06
IN625-10v%TiB_2	0.52	0.07
IN625-25v%SiC	0.41	0.05
IN625-25v%TiB_2	0.43	0.06

The volume loss of the seven samples, including IN625 and IN625-MMCs, were analysed using an Alicona optical profilometer. IN625 showed the most severe wear conditions, followed by IN625-5v%SiC and IN625-10v%SiC, with IN625-25v%SiC experiencing very limited wear. The wear loss results for IN625 and IN625-SiC are presented in Figure **6.15**.

The latter results are in line with the hardness and CoF. In fact, IN625-25v%SiC showed the highest hardness, with the lowest friction coefficient.

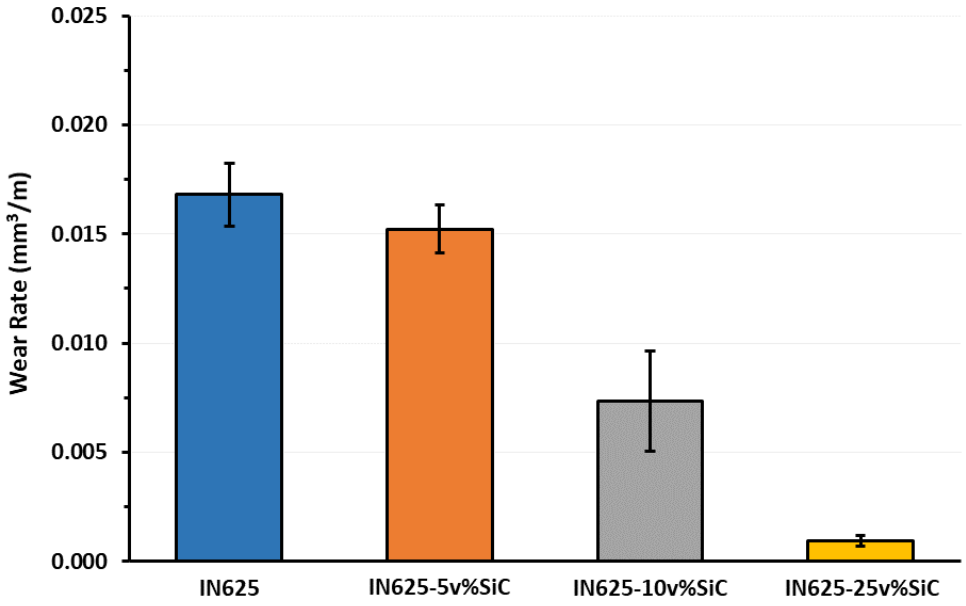

Figure 6.15 Wear rate for IN625 and IN625-SiC.

Once again, the results on the wear rate for IN625-TiB_2 follow the same trend as IN625-SiC (Figure **6.16**). However, in this case, IN625-5v%TiB_2 showed a similar wear rate if compared to IN625. IN625-10v%TiB_2 and IN625-25v%TiB_2 have higher wear rates compared to IN625-10v%SiC and IN625-25v%SiC, respectively. The reason behind this behaviour can be attributed to the presence of some reinforcement debonding in IN625-TiB_2 accelerating the abrasive wear (Figure **6.5**).

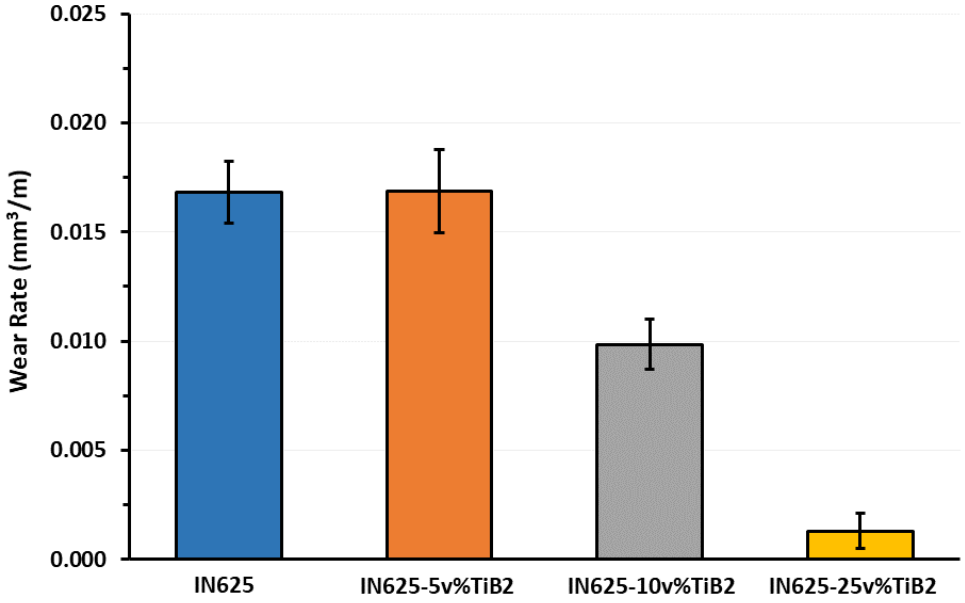

Figure 6.16 Wear rate for IN625 and IN625-TiB_2.

Wear tracks for IN625, IN625-SiC and IN625-TiB_2 are represented in Figure **6.17** and Figure **6.18**. The SEM micrographs on the surface of IN625 show the presence of some small grooves, with the presence of debris coming from the action of abrasive and adhesive wear (Figure **6.17**). The wear tracks of 5v%SiC and 5v%TiB_2 are characterised by the presence of cracks, presence of debris and in 5v%TiB_2, the presence of ploughing due to the reinforcement is more evident (Figure **6.18**). As the reinforcement level is increased, the level of abrasive wear is reduced for both SiC and TiB_2 reinforcements (Figure **6.18**).

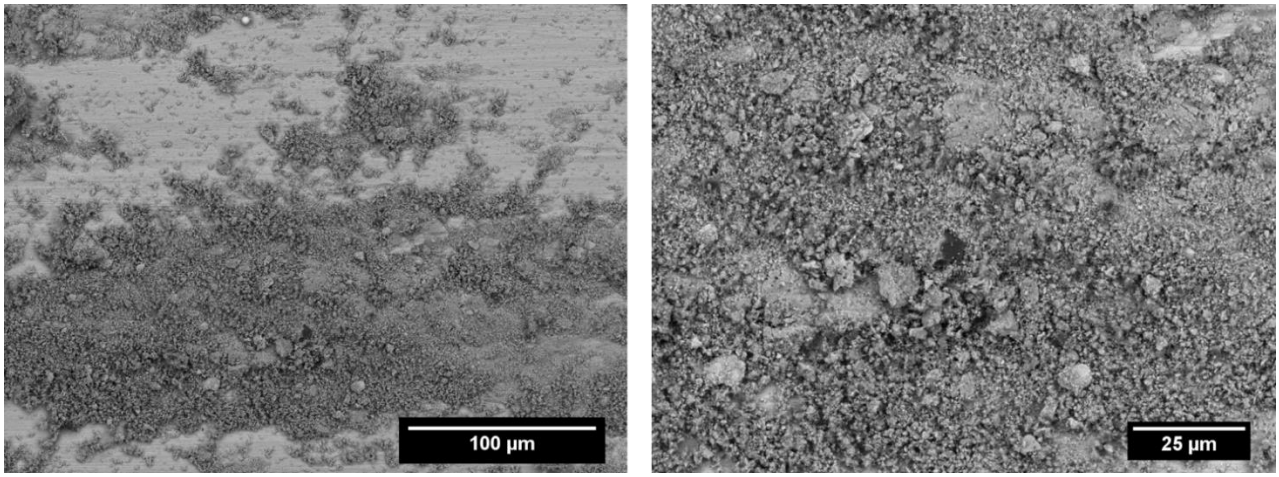

Figure 6.17 SEM wear tracks for as-HIPed IN625.

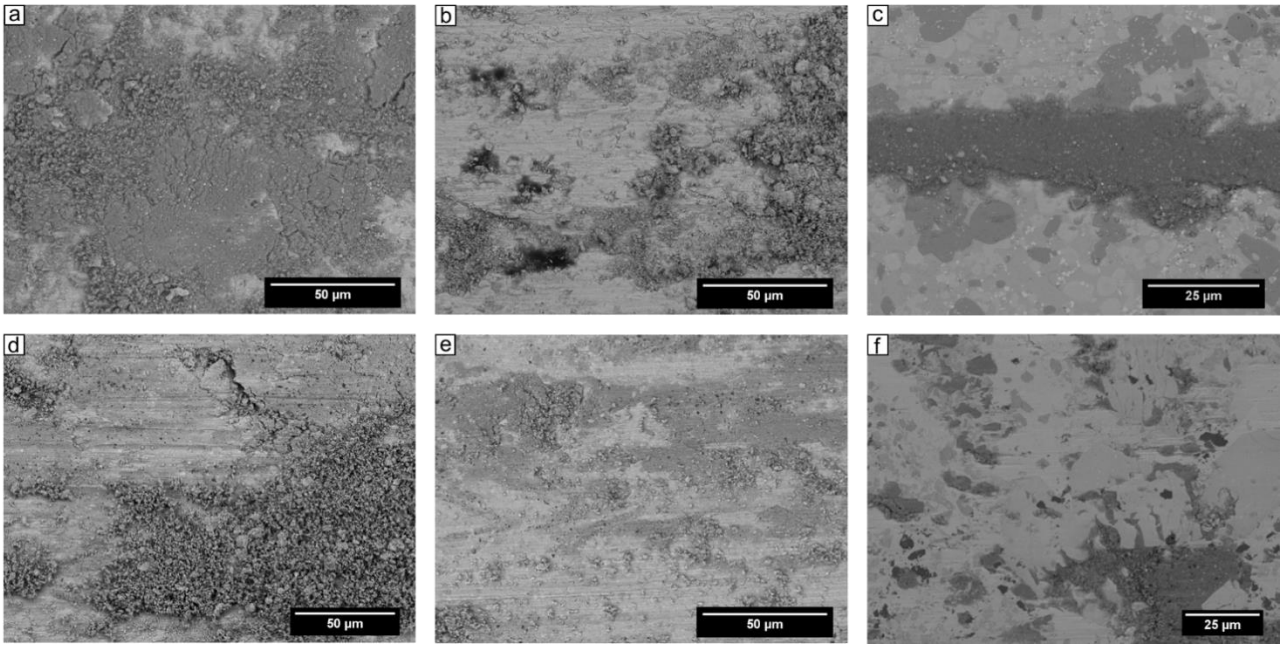

Figure 6.18 SEM micrographs of wear tracks for: a) IN625-5v%SiC; b) IN625-10v%SiC; c) IN625-25v%SiC; d) IN625-5v%TiB_2; e) IN625-10v%TiB_2; f) IN625-25v%TiB_2.

The wear track of as-HIPed IN625 highlights the presence of some Al debris, indicating that some material transfer has occurred from the ball into the sample, due to the high friction forces involved (Figure **6.19**). As the reinforcement is increased to 25v%, the EDX analysis reveals no presence of Al, meaning that the much lower friction forces helped to reduce or eliminate the material transfer from the ball to the sample, as shown in Figure **6.20**. In

addition, high levels of Cr and Si are detected in IN625-25v%SiC which is in line with the micrographs reported in Figure **6.9**.

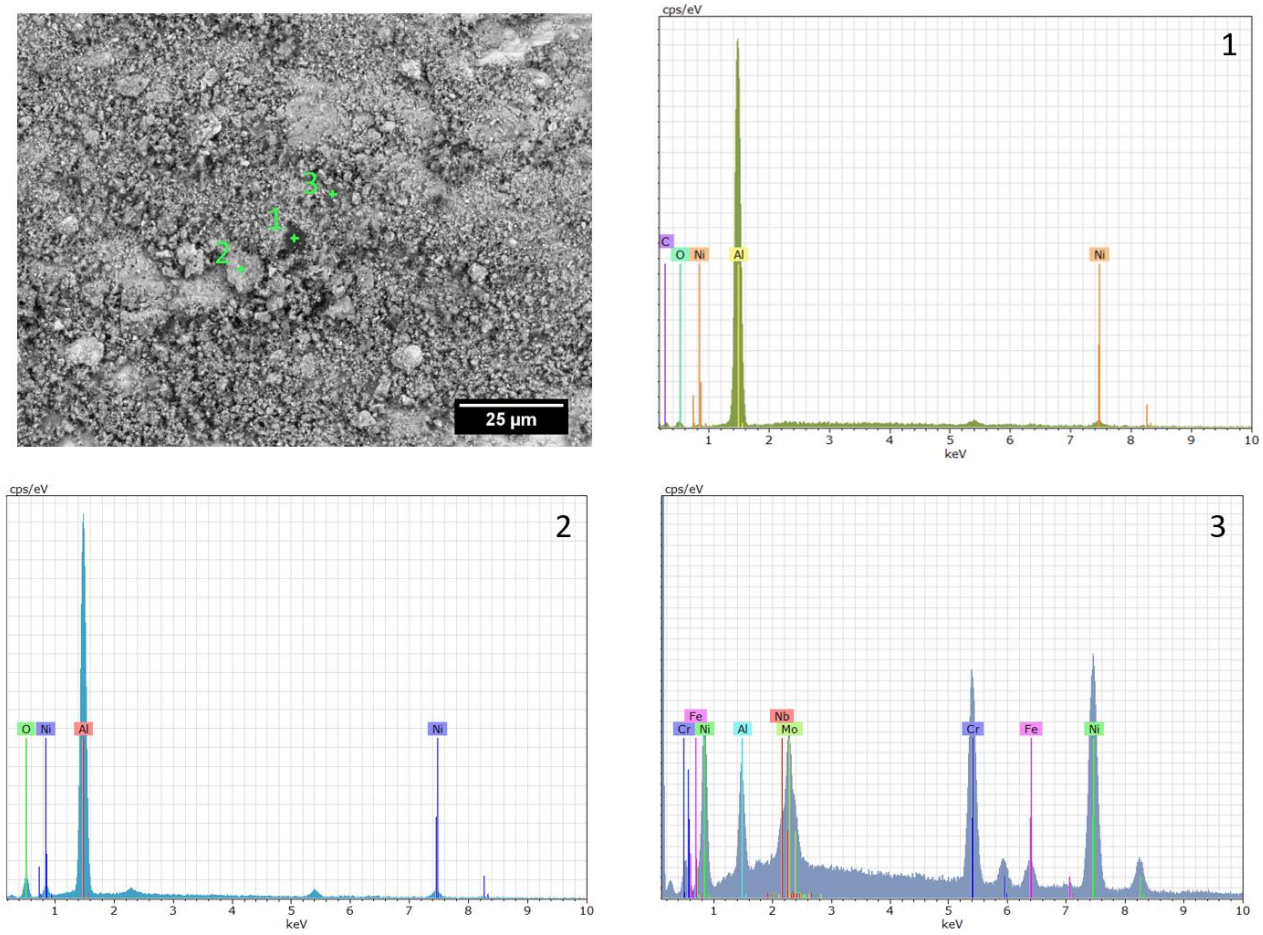

Figure 6.19 EDX analysis on the wear track for as-HIPed IN625.

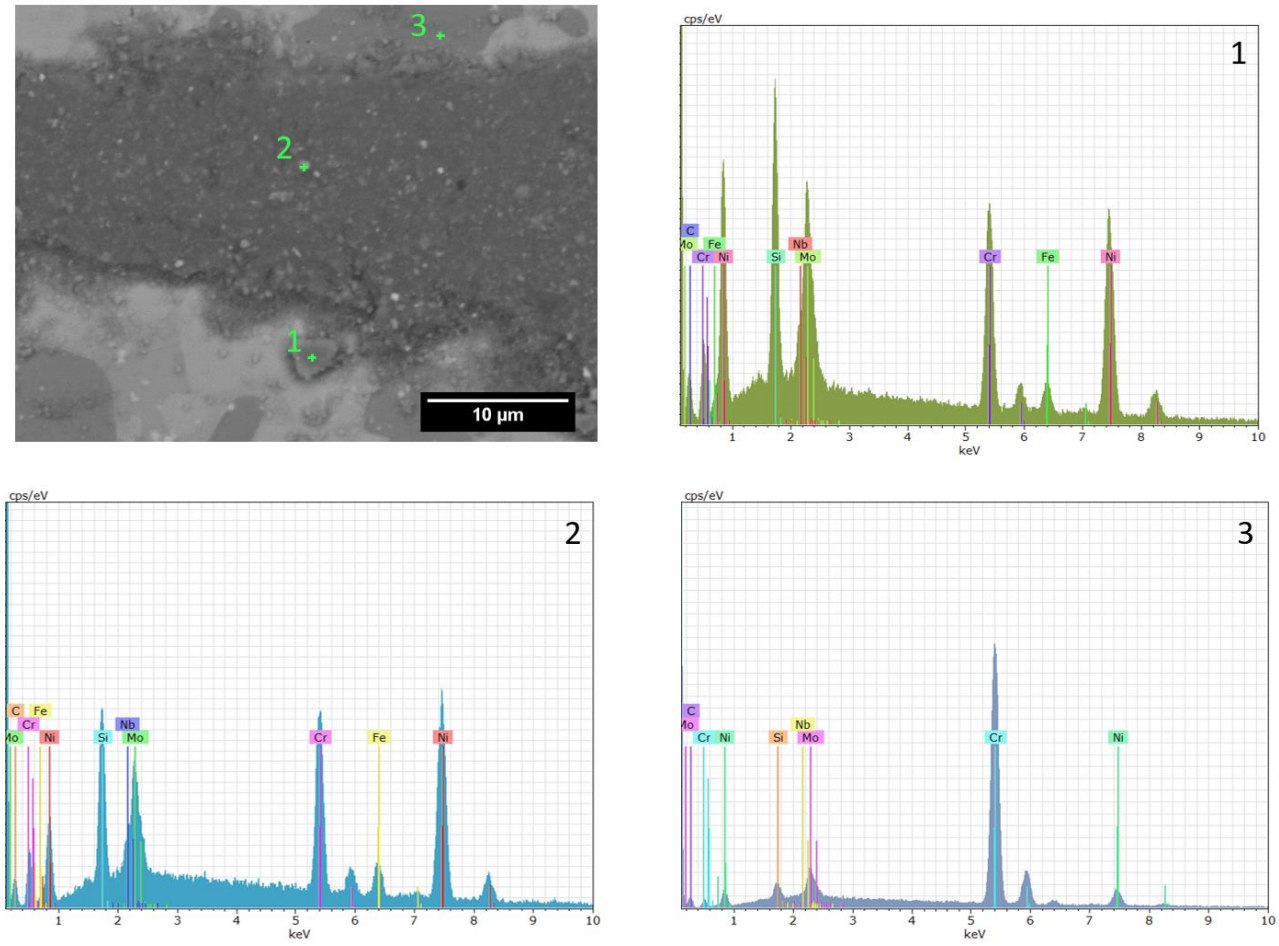

Figure 6.20 EDX analysis on the wear track for as-HIPed IN625-25v%SiC.

6.5.3.3 Tensile and Charpy Tests

Due to the presence of a uniform microstructure and good wear properties, it was decided to investigate the tensile properties of IN625-10v%SiC. Despite the better wear properties, IN625-25v%SiC was not selected due to the presence of particle reinforcement agglomeration (Figure **6.3**c), leading to a heterogeneous microstructure. Additionally, the presence of a coarse Cr-rich phase in IN625-25v%SiC (Figure **6.9**) would drastically reduce mechanical properties.

The room temperature (RT) and high-temperature (650°C) tensile properties of IN625-10v%SiC are reported in Table **6.4**. The RT tensile curves do not present a defined value for

0.2% proof stress, while the ultimate tensile strength (UTS) of 747MPa and elongation of 2.5% are well below the values reported in literature for AGA as-HIPed IN625 [35].

The value of elongation at both RT and 650°C is very low and it decreases with the increase in temperature. The low elongation values for MMCs are common and are justified by the presence of the coarse ceramic particles at the PPBs [36]. However, for IN625-MMCs, a higher level of yield strength (YS) and UTS was expected, in this case, the lower levels in strength can be attributed to the presence of a continuous network of coarse reinforcement generating defects, such as cracks, at the early stages of the tensile test. Room temperature Charpy tests were also performed on the as-HIPed IN625-10v%SiC. The average value of absorbed energy was 2J, confirming the brittle fracture mode of the material. The value is much lower if compared to the impact absorbed energy of 53J for AGA IN625 powder HIPed with no reinforcement [35].

Table 6.4 Room temperature and high temperature mechanical properties of as-HIPed IN625 and IN625-10v%SiC.

Material	Temperature [°C]	0.2% proof stress [MPa]	UTS [MPa]	%EL
IN625	RT	523	918	30
IN625	650	426	749	72
IN625-10v%SiC	RT	-	747	2.5
IN625-10v%SiC	650	568	574	0.7

6.6 Near-Net-Shape Manufacturing

The final part of the work consists of manufacturing a mechanical seal demonstrator through NNS PM HIP. Drawings of the original mechanical seal design, in 2D and 3D CAD, are shown in Figure **6.21**. In this case, the use of NNS PM HIP would be beneficial in manufacturing a part with a low grade of complexity, but with other challenges mostly related to the difficulties in machining the parts due to the high hardness of the material.

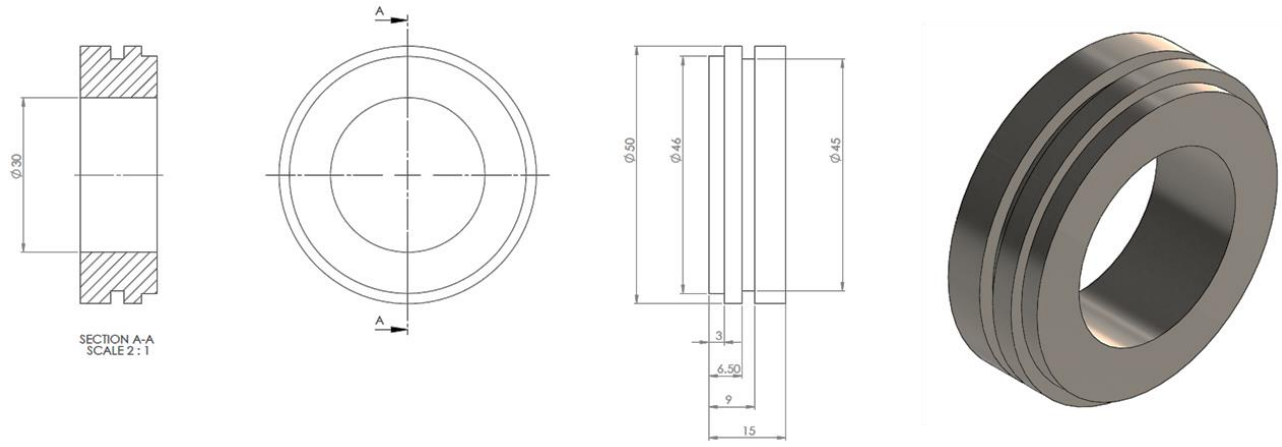

Figure 6.21 Mechanical seal design. 2D technical drawing (left); 3D model (right).

The mechanical seal was manufactured using IN625-10v%SiC showing the best balance between microstructure, tribological properties and machinability. The canister design for the manufacture of the demonstrator is shown in Figure **6.22**. The use of a design strategy with an inner core was specifically selected to achieve a good level of geometrical accuracy and consequently reduce the machining operations, given the high hardness and wear resistance of the material.

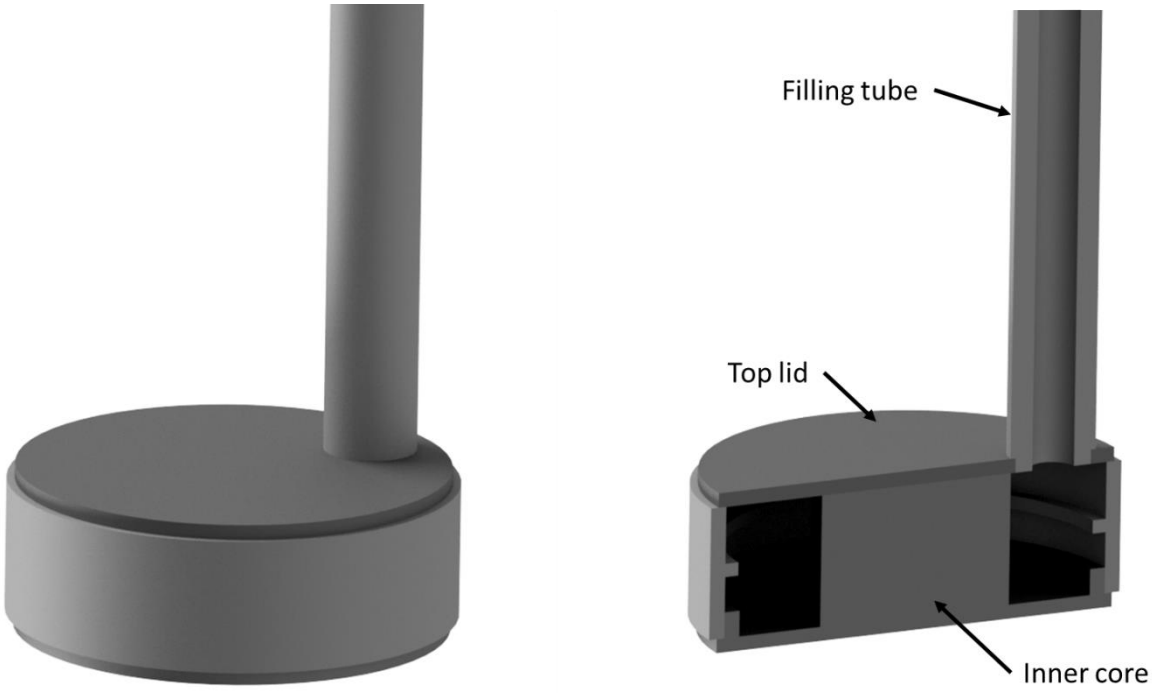

Figure 6.22 3D CAD model for mechanical seal canister.

After the HIP process, described in the experimental procedure, the canister was dissolved in nitric acid at E F Westaway Ltd. As shown in Figure **6.23**, the dissolving process was not entirely successful due to the presence of some HIPed material between the top lid and the inner core creating a protective layer. This suggests that a change in design strategy can be adopted to avoid the formation of this protective layer. To remove the inner core and achieve the desired final geometry, the demonstrators were subjected to machining operations performed by Get It Made Ltd. The mechanical seals after machining are shown in Figure **6.24**. The dimensional check performed using a Vernier calliper showed good geometrical agreement with the originally designed part, demonstrating that IN625-10v%SiC can be accurately machined despite the high hardness. This indicates that NNS PM HIP can be employed for the manufacture of mechanical seals achieving a drastic reduction in machining operations. However, further improvement to the canister design can be applied in order to achieve a better pickling response.

Figure 6.23 Mechanical seals after nitric acid pickling.

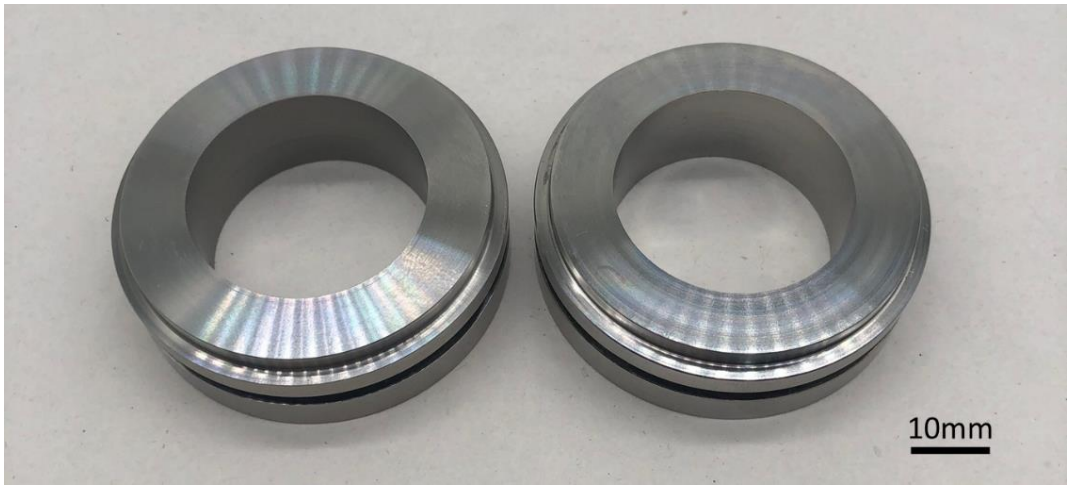

Figure 6.24 Net-shape mechanical seals after pickling and machining.

6.7 Conclusions

Powder metallurgy hot isostatic pressing processing route was employed to develop IN625-MMCs. In particular, powder blending, canister filling and HIP operations were performed, showing the feasibility of processing Ni-base MMCs through PM HIP. The six different HIPed samples showed fully dense microstructures, with crack-free structure for IN625-SiC, though with some defects appearing in IN625-TiB_2. Different complex hard phases were formed by the interaction of the reinforcement with the IN625 matrix. In particular, in the 25v% reinforced MMCs there was the presence of Cr-rich hard phases accompanied by the presence of Nb, Mo, Si intermetallics.

It was demonstrated that the volume fraction of reinforcement plays a crucial role on hardness and above all on the tribological properties of the as-HIPed samples using both SiC and TiB_2 as reinforcements. It was found that the tribological properties were proportional to the volume fraction level of the reinforcement, with the best results for IN625-25v%SiC showing a CoF of 0.41, much lower if compared to as-HIPed IN625 showing a CoF of 0.64.

Among all the IN625-MMCs proposed, IN625-10v%SiC was down-selected because of its balance between hardness, tribological properties and machinability. Room temperature and elevated temperature tensile tests were performed for IN625-10v%SiC, the results showed acceptable levels of strength. However, IN625-10v%SiC experienced lower levels of strength and elongation, if compared to IN625. Furthermore, Charpy impact properties of IN625-10v%SiC revealed an absorbed energy of 2J, which is much lower if compared to the 53J of as-HIPed IN625. The lower levels of mechanical properties were attributed to the presence of the coarse particles uniformly distributed at the PPBs.

Finally, two mechanical seals demonstrators using IN625-10v%SiC were shaped with a consequent reduction in machining operation required. The HIPed and machined parts,

showed good geometrical accuracy to the original design, demonstrating the good machinability of the material and the possibility to employ NNS PM HIP technique for the manufacture of mechanical seals.

Acknowledgments:

The authors warmly thank the European Space Agency (ESA) for supporting this activity in the frame of the General Studies Technology Programme (ESA GSTP ITT 8899) under contract 4000122901/18/NL/BJ. AS acknowledges the Centre of Doctoral Training in Innovative Metal Processing (IMPaCT), funded by the Engineering and Physical Sciences Research Council (EPSRC). The work was enabled through the National Structural Integrity Research Centre (NSIRC).

Declarations of competing interest:

The authors declare that they have no known competing financial interests or personal relationships that could have appeared to influence the work reported in this paper.

6.8 References

[1] B. Zhang, G. Bi, P. Wang, J. Bai, Y. Chew, M. Sharon, Microstructure and mechanical properties of Inconel 625 / nano-TiB 2 composite fabricated by LAAM, JMADE. 111 (2016) 70–79. https://doi.org/10.1016/j.matdes.2016.08.078.

[2] NASA, Space Vehicle Liquid Rocket Engine Turbopump Rotating-Shaft Seals, 1978.

[3] K. Kamijo, Research and Development of Rocket Turbopumps --- 35 Years in Retrospect, (2013). http://www.frontier.phys.nagoya-u.ac.jp/jp/leading/files/Thubopump_of_Rocket_kamijo.pdf.

[4] W. Shapiro, C.C. Lee, Advanced helium purge seals for liquid oxygen (LOX) turbopumps., (1989).

[5] E. De Lamotte, J.-L. Bozet, C.G. Marirrodriga, The Tribology of Valve Seals in Cryogenic Rocket Engines, in: 7th Eur. Sp. Mech. Tribol. Symp., 1997: pp. 131–135.

[6] R.R. Badykov, S. V. Falaleev, Advanced Dynamic Model Development of Dry Gas Seal, Procedia Eng. 176 (2017) 344–354. https://doi.org/10.1016/j.proeng.2017.02.331.

[7] W.E. Key, R. Dickau, R.L. Carlson, Mechanical seals with wavy SiC faces for a severe duty NGL / crude pipeline application, Proc. Twenty-First Int. Pump Users Symp. (2004).

[8] M. Nosaka, T. Kato, Cryogenic Tribology in High-Speed Bearings and Shaft Seals of Rocket Turbopumps, (2013).

[9] N. Ghaisas, S. Majumdar, Dry Gas Seal Systems For Centrifugal Compressors, COMPRESSORtech2. (2017).

[10] J.R. Lince, Effective Application of Solid Lubricants in Spacecraft Mechanisms, Lubricants. 8 (2020) 74. https://doi.org/10.3390/lubricants8070074.

[11] K. Aydin, Y. Kaya, N. Kahraman, Experimental study of diffusion welding/bonding of titanium to copper, Mater. Des. 37 (2012) 356–368. https://doi.org/10.1016/j.matdes.2012.01.026.

[12] S. Rawal, Metal-Matrix Composites for Space Applications, JOM. (2001) 14–17.

[13] R. Casati, M. Vedani, Metal matrix composites reinforced by Nano-Particles—A review, Metals (Basel). 4 (2014) 65–83. https://doi.org/10.3390/met4010065.

[14] R. Karmakar, P. Maji, S. Kumar, A Review on the Nickel Based Metal Matrix Composite Coating, Met. Mater. Int. (2020). https://doi.org/10.1007/s12540-020-00872-w.

[15] Y. Xiao, P. Yao, K. Fan, H. Zhou, M. Deng, Z. Jin, Powder metallurgy processed metal-matrix friction materials for space applications, Friction. 6 (2018) 219–229. https://doi.org/10.1007/s40544-017-0171-9.

[16] Y. Xiao, P. Yao, H. Zhou, Z. Zhang, T. Gong, L. Zhao, X. Zuo, M. Deng, Z. Jin, Friction and wear behavior of copper matrix composite for spacecraft rendezvous and docking under different conditions, Wear. 320 (2014) 127–134. https://doi.org/10.1016/j.wear.2014.09.005.

[17] G.A. Rao, M. Sankaranarayana, S. Balasubramaniam, Hot Isostatic Pressing Technology for Defence and Space Applications, 62 (2012) 73–80. https://doi.org/10.14429/dsj.62.372.

[18] R.E. Burcham, Liquid Rocket Engine Turbopump Rotating-shaft Seals, 1978.

[19] R.A. Oriani, Hydrogen embrittlement of Steels, Ann. Rev. Mater. Sci. 8 (1978) 327–357. https://doi.org/10.1016/B978-044452787-5.00200-6.

[20] R.S. Evenson, B. Mason, D. V Frederick, A.G.S. Onge, Development and field application of a single rotor design dry gas seal, Proc. Twenty-Fourth Turbomach. Symp. (1995) 107–116.

[21] S.M. Almotairy, A.F. Boostani, M. Hassani, D. Wei, Z.Y. Jiang, Effect of hot isostatic pressing on the mechanical properties of aluminium metal matrix nanocomposites produced by dual speed ball milling, J. Mater. Res. Technol. 9 (2020) 1151–1161. https://doi.org/10.1016/j.jmrt.2019.11.043.

[22] C. Cai, B. Song, C. Qiu, L. Li, P. Xue, Q. Wei, Hot isostatic pressing of in-situ TiB / Ti-6Al-4V composites with novel reinforcement architecture , enhanced hardness and elevated tribological properties, J. Alloys Compd. 710 (2019) 364–374. https://doi.org/10.1016/j.jallcom.2017.03.160.

[23] S. Floreen, G.E. Fuchs, W.J. Yang, The Metallurgy of Alloy 625, Superalloys 718, 625, 706 Var. Deriv. (1994) 13–37. https://doi.org/10.7449/1994/Superalloys_1994_13_37.

[24] H.L. Eiselstein, D.J. Tillack, The Invention and Definition of Alloy 625, in: Superalloys 718, 625, 716 Deriv., TMS, 1991: pp. 1–14. https://doi.org/10.7449/1991/superalloys_1991_1_14.

[25] H.R. Dugdale, J.B. Borradaile, Development of hot isostatically pressed nickel based alloys for nuclear applications, Energy Mater. Mater. Sci. Eng. Energy Syst. 8 (2013) 374–381. https://doi.org/10.1179/1743290113Y.0000000076.

[26] D.E. Cooper, N. Blundell, S. Maggs, G.J. Gibbons, Additive layer manufacture of

Inconel 625 metal matrix composites, reinforcement material evaluation, J. Mater. Process. Technol. (2013). https://doi.org/10.1016/j.jmatprotec.2013.06.021.

[27] H.V. Atkinson, S.Davies, Fundamental aspects of hot isostatic pressing : An overview, Metall. Mater. Trans. A. 31 (2000) 2981–3000.

[28] T. Berglund, H. Söderberg, The Performance of HIPed MMCs and their Application, in: Euro PM2014 – Hot Isostatic Press., 2014.

[29] W. Li, Y. Yang, M. Li, J. Liu, D. Cai, Q. Wei, C. Yan, Y. Shi, Enhanced mechanical property with refined microstructure of a novel γ-TiAl/TiB2 metal matrix composite (MMC) processed via hot isostatic press, Mater. Des. 141 (2018) 57–66. https://doi.org/10.1016/j.matdes.2017.12.026.

[30] S.C. Tjong, K.C. Lau, Sliding wear of stainless steel matrix composite reinforced with TiB2 particles, Mater. Lett. 41 (1999) 153–158. https://doi.org/10.1016/S0167-577X(99)00123-8.

[31] Nickel Alloy, Corrosion and Heat-Resistant, Powder for Additive Manufacturing, 62Ni-21.5Cr-9.0Mo-3.65Nb, in AMS7001. SAE International, (n.d.).

[32] R.H.U. Khan, M.H. Loretto, M.M. Attallah, J. Cortes, I. Iturriza, F. Castro, Microstructure and properties of HIPped alloy 718, in: 11th Int. Conf. Hot Isostatic Press., Stockholm, 2014.

[33] J.E. Macdonald, R.H.U. Khan, M. Aristizabal, M.J. Lunt, M.M. Attallah, Influence of powder particle size distribution on the microstructure and mechanical properties of a HIPped CM247LC Ni superalloy, Mater. Des. 174 (2019).

[34] A.J. Goodfellow, Strengthening mechanisms in polycrystalline nickel-based

superalloys, Mater. Sci. Technol. (United Kingdom). 34 (2018) 1793–1808. https://doi.org/10.1080/02670836.2018.1461594.

[35] A. Sergi, R.H.U. Khan, M.M. Attallah, The role of powder atomisation route on the microstructure and mechanical properties of hot isostatically pressed Inconel 625, Mater. Sci. Eng. A. 808 (n.d.). https://doi.org/10.1016/j.msea.2021.140950.

[36] N. Zhang, D. Sun, X. Han, Z. Wang, H. Liu, Z. Wang, W. Yang, Materials Science & Engineering A Effect of spark plasma sintering temperatures on microstructure and mechanical properties of in-situ (La 2 O 3 þ TiB)/ Ti 2 AlNb composites with a tailored three-dimensional network architecture, Mater. Sci. Eng. A. 772 (2020) 138769. https://doi.org/10.1016/j.msea.2019.138769.

Chapter 7. Powder HIP of pure Nb and C-103 alloy: the influence of powder characteristics on mechanical properties

Alessandro Sergi[1,2], Raja H. U. Khan[3], Kostas Georgilas[3], Martina Meisnar[4], Advenit Makaya5, Moataz M. Attallah*[1]

[1] IRC in Materials Processing, School of Metallurgy and Materials, The University of Birmingham, Birmingham, B15 2TT, UK.

[2] National Structural Integrity Research Centre (NSIRC), Cambridge, CB21 6AL, UK.

[3] TWI Ltd, Cambridge, CB21 6AL, UK.

[4] European Space Agency, ECSAT, Fermi Avenue, Harwell-Oxford Campus, Didcot, Oxfordshire OX11 0FD, UK.

[5] Materials and Processes Section TEC-MSP, Mechanical Engineering Department TEC-M, ESTEC, Keplerlaan 1 - PO Box 299, 2200 AG Noordwijk-ZH, The Netherlands.

* Corresponding author:

Email:

Telephone:

Fax:

The paper is slightly modified from the version accepted with corrections in the International Journal of Refractory Metals and Hard Materials to include further background on the application.

7.1 Motivation & Aims

The potentials of Nb and Nb-base alloys for extremely high temperature applications have been highlighted in Chapter 3. In particular, the use of NNS PM HIP can represent a valid alternative to conventional manufacturing processes due to the high reactivity of this class of materials. Another important aspect discussed in the literature review relies on the influence of oxygen levels on the strength of pure Nb, which poses some interesting bases to understand how powder characteristics and specifically oxygen levels can affect the strength of pure Nb. In parallel, a study on the HIP behaviour of C-103 Nb-base alloy was performed to understand its mechanical properties if compared with conventional manufacturing routes. This study will be focusing on the following specific aspects:

- Evaluate the HIP response of Nb and C-103 alloy in terms of densification, microstructure and mechanical properties.
- Assess the influence of oxygen levels on the mechanical properties of pure Nb.
- Investigate the possibility to alter the powder characteristics to tailor the mechanical properties on pure Nb.

Nb was selected for this study because it represents the refractory metal with the lowest density and, additionally, due to its high oxygen solid solubility with the consequent possibility of tailoring the mechanical properties by altering the oxygen levels in the powders. On the other hand, C-103 represents a widely used alloy in the space industry. Thus demonstrating its manufacturability through PM HIP can induce the space industry to adopt this advanced manufacturing technique for the fabrication of complex parts with good performances and improved buy-to-fly ratio.

The last part of the chapter focused on the manufacture of a thrust combustion chamber demonstrator using pure Nb. This application was specifically selected to demonstrate the potentials of using NNS PM HIP for very high temperature space components.

Abstract

In this work, pure Nb processed by Powder Metallurgy Hot Isostatic Pressing (PM HIP) was investigated as a potential alternative to C-103 Nb-based alloy for the manufacture of near-net-shape thruster combustion chambers. Three Nb powders with varied particle size range (fine, mid-range and coarse) and C-103 powder were investigated to understand the differences in particle size distribution (PSD), morphology and oxygen (O) content present in the alloy chemistry. The as-HIPed microstructures of pure Nb and C-103 are characterised by a near to fully dense microstructure and the absence of PPBs. Microstructural analyses performed on pure Nb highlighted the influence of particle size on the average as-HIPed grain size. Additionally, it was observed that O content plays a crucial role in the microhardness of pure Nb. Tensile tests performed on Nb mid-range and on Nb mid-range sieved showed that a simple sieve operation was effective in increasing the strength of the material while maintaining good levels of elongation. Alternatively, it was also demonstrated that pure Nb powder heat treatment can be regarded as an effective way to increase the O levels in pure Nb powders as witnessed by the high hardness levels. On the other hand, as-HIPed C-103 powder showed superior tensile properties if compared to the minimum specifications for wrought C-103. Finally, to summarise, the work performed on pure Nb, a simple structure-property relation model was developed to predict the YS of pure Nb based on the O levels and grain size of the as-HIPed microstructure.

Keywords:

Powder characteristics, Powder Metallurgy Hot Isostatic Pressing (PM HIP), Oxygen levels, Microstructure, Mechanical properties.

7.2 Background

Thruster combustion chambers are used in apogee engines to propel satellites from 250km up to the geostationary orbit at 39000km from the earth [1]. In bipropellant apogee engines, different propellants (Kerosene, LH, Gasoline) and oxidisers (LOX, GOX, N_2O) can be used for satellites' chemical thruster. The reaction between the fuel with the oxidiser, generates high-pressure hot gases which expand through the diverging nozzle and generate the thrust according to Newton's third law [1], [2].

A schematic of the cross-section design of a satellite thruster is represented in Figure **7.1**. The combustion chamber is assembled with a nozzle extension often manufactured using a low-density alloy with good mechanical properties such as Ti6Al4V joined to a converging-diverging nozzle. In the combustion chamber, the propellant and oxidiser are mixed and ignited. Thus, it represents the part where the highest temperatures are reached.

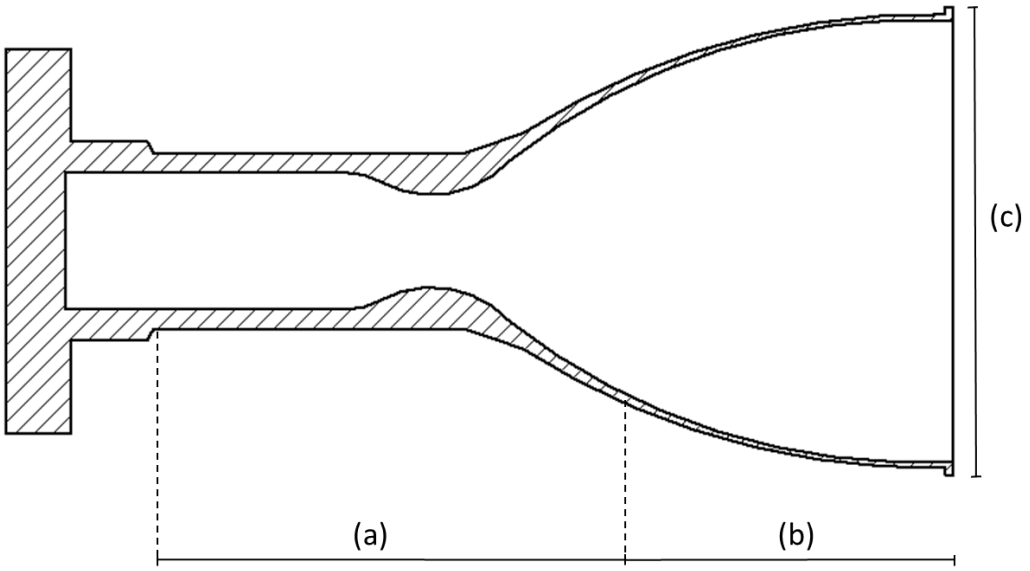

Figure 7.1 Simple cross-section schematic of satellite thruster. (a) combustion chamber; (b) nozzle extension; (c) nozzle diameter.

The extremely high temperatures, combined with the highly oxidising environment, make it challenging to select the right material able to withstand these severe conditions. A list of the requirements for thruster combustion chambers is represented in Table **7.1**. Only limited ranges of materials are capable of withstanding the loading and temperature profiles described in Table **7.1**. Furthermore, in order to achieve the desired high-temperature oxidation resistance, a high-temperature oxidation resistant coating is required in most cases.

Table 7.1 Requirements for the thruster combustion chamber.

Max service temperature	≥ 1450°C
Oxidation resistance	High-temperature oxidation resistance
Room temperature yield strength	> 260MPa
CTE	Similar to Ti6Al4V
Weldability	Compatible with Ti6Al4V

Several materials can be used for thruster combustion chambers. In recent years a wide range of materials has been used for the application, including ceramics, ceramic matrix composites, niobium alloys and Pt-group alloys [2]. Refractory metals such as Mo, Nb, Ta and W could potentially represent a valid solution for the manufacture of thruster combustion chambers. Ceramics can also be considered for the application. However, their low fracture toughness, extremely different CTE if compared to Ti6Al4V, and the challenges associated with manufacturing and finishing of the part make the use of ceramics incompatible with the application.

Regarding refractory metals, Mo has a melting temperature of 2600°C, however, there are some limitations to the use of Mo and Mo alloys for combustion chambers. The first problem is associated with the low resistance to high-temperature oxidation. In fact, it can easily oxidise at 450°C. The second limitation is represented by its difficulty to be welded with Ti6Al4V [3].

Ta and W alloys have a higher melting point if compared to Nb and Mo, which could potentially make them great candidates for the manufacture of thruster combustion chambers. However, the big limitation of Ta and W is the high density, respectively 16.69g/cm^3 and 19.25g/cm^3.

Nb and Nb alloys are widely used for thruster combustion chambers due to their high melting temperature (2477°C), good ductility and metallurgical compatibility with Ti4Al6V, however, Nb oxidise at relatively low temperature (600°C). This makes necessary the use of an oxidation protective coating for Nb and Nb alloys. R-512A is the most used coating for Nb in thruster combustion chambers, it guarantees oxidation protection up to a temperature of (1500°C-1600°C), the coating is composed of a mixture of Si, Cr, and Ti [3]. The most

widely used Nb alloy for thruster combustion chambers is C-103 (10%Hf, 1%Ti), ensuring enhanced high temperature and oxidation resistance if compared to pure Nb [4].

7.3 Introduction

Nb alloys are widely used in the aeronautic and space sectors due to their ability to retain good mechanical properties at considerably high temperatures [1–5]. Over the years, different types of Nb alloys have been developed, including solid solution strengthened Nb alloys (Cb-132, F-48, SCb-291 and SCb-298) and dispersion strengthened Nb alloys (Cb-65, D-12, Nb-1Zr and C-103). Nb alloys are mostly characterised by the presence of Hf, W, Mo, Ta, Zr and Ti to improve the strength and high-temperature oxidation resistance capabilities [5],[6]. The main strengthening contribution in Nb alloys comes from the substitutional solid solutions of Mo, W, Ta and V [6],[7]. Precipitation hardening is also an important strengthening mechanism in Nb alloys, made possible by the addition of interstitials, such as C, N and O, with the presence of reactive elements such as Zr, Ti or Hf.

Among the different Nb alloys, the most commonly used Nb alloy for thruster's combustion chambers is C-103 (Nb-10Hf-1Ti) [7]. As stated above, the role of Hf, Ti and Zr in C-103 is to react with the interstitials, especially O and C to generate stable oxides and carbides responsible for the increase in high-temperature strength (>0.5Tm) and improvement of high-temperature oxidation resistance [3], [5], [6]. However, the use of C-103 alloy has some limitations related to cost, procureability, welding and coating. In fact, the presence of 10% Hf makes C-103 difficult to weld due to the formation of brittle intermetallics, and it is responsible as well for the generation of cracks and coating spalling after repeated thermal cycling. Additionally the use of conventionally manufacturing routes such as casting and forging leads to a considerable material waste resulting in a highly inefficient and costly process. The use of near net-shape hot isostatic pressing (NNS HIP) for the manufacture of

thruster combustion chambers can mitigate the raw material cost and the lead times associated with machining by drastically reducing the buy-to-fly ratio, and consequently the amount of machining required. However, the presence of elements with high affinity to O such as Hf, Zr and Ti can represent a challenge. In fact, O and C present during atomisation process is responsible for the formation of oxides and carbides at the prior particle boundaries (PPBs) in the as-HIPed microstructure, especially in highly alloyed materials with the presence of reactive elements such as Hf, Ti, Zr, Cr and Al [8], [9]. This will drastically reduce the mechanical properties of the material, especially in terms of ductility and fracture toughness [10].

On the other hand, pure Nb, due to the absence of strong oxide formers and as a consequence of high O solid solubility limit is perfectly suitable for PM HIP with no formation of PPBs. In fact, if during the HIP process O levels are below their solid solubility in Nb, the formation of discrete oxides at PPBs during the HIP process will be prevented. Additionally, the use of reactive elements such as Hf, Ti and Zr in Nb alloys will reduce the oxygen solubility limits, consequently reducing the strengthening effect coming from the solid solution of oxygen in the Nb matrix [7]. Additionally, the use of pure Nb would guarantee better metallurgical compatibility with the high-temperature oxidation-resistant coating with no formation of brittle intermetallics due to the absence of Hf. Therefore, the possibility of using the PM HIP technique for pure Nb to improve its mechanical properties was investigated in the current study. The influence of oxygen on the mechanical properties of pure Nb has been widely reported in literature [11–13]. In particular, Sankar et al. reported a considerable increase in strength for pure Nb by increasing the O levels from 50 to 800ppm [11]. Cordero et al. have established the Hall–Petch parameters for pure Nb, finding that the O contribution to the solid solution strength for pure Nb is 0.19MPa/ppm [12]. The conventional manufacturing routes, such as casting and forging, do not provide the required flexibility in terms of process

parameters and feedstock material to control the oxygen levels. PM HIP allows to easily manipulate the characteristics of the powders i.e. chemistry and particle size distribution and consequently tailoring the microstructure and mechanical properties of the material. Furthermore, the commonly used manufacturing process for Nb powders is based on the Hydride–Dehydride (HDH) process, which is capable of producing powders with good control of the contamination levels [14].

7.4 Experimental

In this study, the HIP response of pure Nb powders with three different particle size ranges and a C-103 powder was investigated. The pure Nb powders were categorised as fine (<44μm), coarse (<500μm) and mid-range (15–100μm), whereas C-103 (10–45μm) powder was manufactured by argon gas atomisation (AGA) process.

A detailed powder characterisation was performed on the four powders, including powder morphology, particle size distribution (PSD) and the determination of oxygen content present in the alloy chemistry. Powder morphology was assessed using a Hitachi TM3000 Scanning Electron Microscope (SEM). PSDs for the four powders were determined by laser diffraction method using a Malvern Panalytical Mastersizer3000 system. The chemical analyses of the four powders were performed by AMG Analytical Services, Sheffield. The Inductively Coupled Plasma Optical Emission Spectroscopy (ICP OES) technique was used to determine the major alloying elements in C-103 i.e. Nb, Hf, Ti, Zr, Ta and W. Whereas C was determined by LECO thermal infrared using combustion in oxygen; and O, N and H gases were determined by LECO inert gas fusion.

After characterisation, Nb and C-103 powders were encapsulated in low carbon steel (ISO 3574 Grade CR4) cylindrical canisters (Ø50mm x 90mm) with 2 mm thickness. The filling procedure was performed in a glovebox to avoid any interaction with the external

environment. After filling, the canisters were de-gassed for 48h to a pressure in the order of 10-5mbar and hot sealed.

All the powder filled canisters were HIPed using EPSI HIP system installed at the University of Birmingham. After HIP, the microstructural analysis samples were extracted, mounted in conductive Bakelite and polished using standard metallographic techniques. The samples' microstructure was then analysed using an optical microscope and SEM. Electron backscattered diffraction (EBSD) was performed on the three Nb samples using a Philips XL-30 SEM and the post-processing was performed using ATEX software [15]. The microhardness tests were performed on the HIPed powders according to ASTM E384–17, and by making 10 indents per sample, using a semi-automatic Buehler microhardness tester with a load of 300gf. The room temperature tensile tests were conducted on as-HIPed Nb powders according to ASTM E8/E8M–16a.

7.5 Results and Discussion

7.5.1 Powder Characterisation

The morphology of the three Nb powders is shown in Figure **7.2**. There is a considerable difference in the powder size and consequently in PSDs. Fine Nb powder is characterised by small particles surrounded by very fine ones, adversely affecting the flowability. Furthermore, the different powders all show a rock shape, which is typical of powders obtained by the HDH process. C-103 powder has a nearly spherical shape with the presence of some satellites and some irregular particles caused by the collision of molten metal with an already formed particle (Figure **7.3**). The C-103 powder cross section in Figure **7.4** reveals the presence of Hf and Zr micro-segregation in the inter-cellular regions.

The PSDs in Figure **7.5** show a considerable difference between fine and coarse powders, while less difference in particle size is observed between fine Nb and C-103 powders. Coarse powders show a bi-modal distribution with a D_{50} of 203µm, higher if compared to fine and mid-range powders. Mid-range powders have a D_{50} of 50µm, higher if compared to the D_{50} of 29µm for fine powders (Table **7.2**). The difference observed in powder characteristics will give a different HIP response in terms of macro-scale effects, such as shrinkage, which is dependent on the packing density. Most significantly, the microstructure, such as grain size and consequently the mechanical properties of the material, will be highly affected by the powder characteristics.

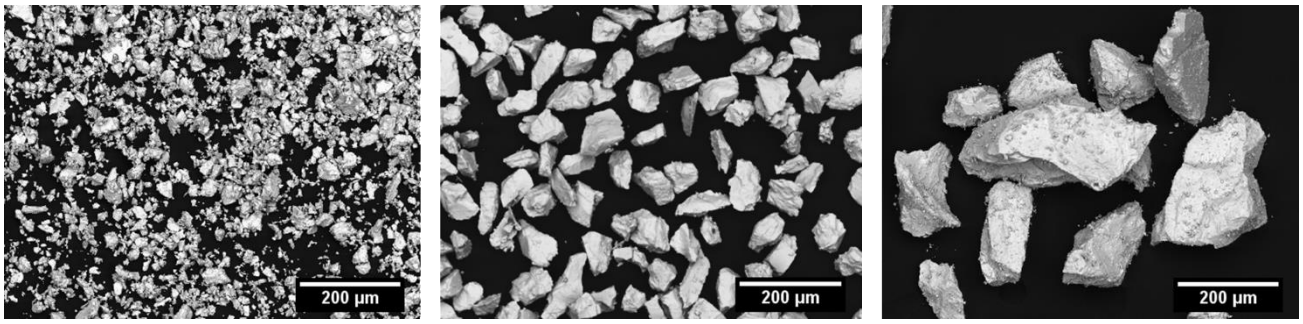

Figure 7.2 SEM backscattered micrographs of Nb fine, mid-range and coarse powders.

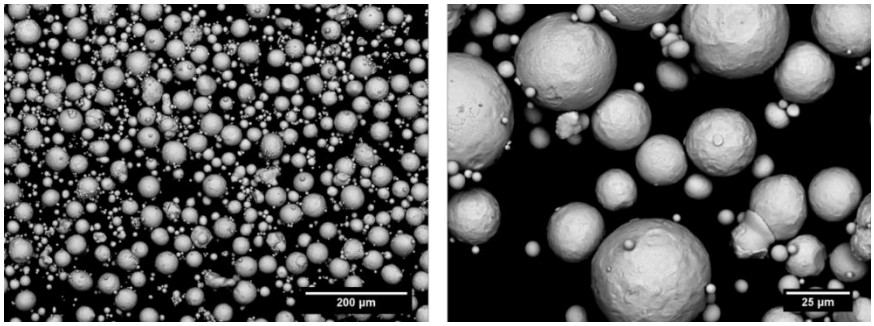

Figure 7.3 SEM backscattered micrograph of C-103 powder.

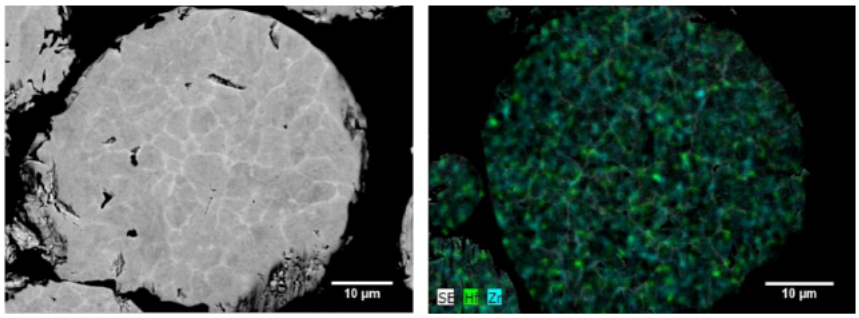

Figure 7.4 SEM backscattered micrographs of C-103 powder cross section (left), C-103 powder cross-section EDS (right).

Table 7.2 PSDs of Nb and C-103 powders.

Powder	D10 [µm]	D50 [µm]	D90 [µm]
Nb fine	7	29	57
Nb mid-range	3	50	82
Nb coarse	101	203	2050
C-103	2	20	46

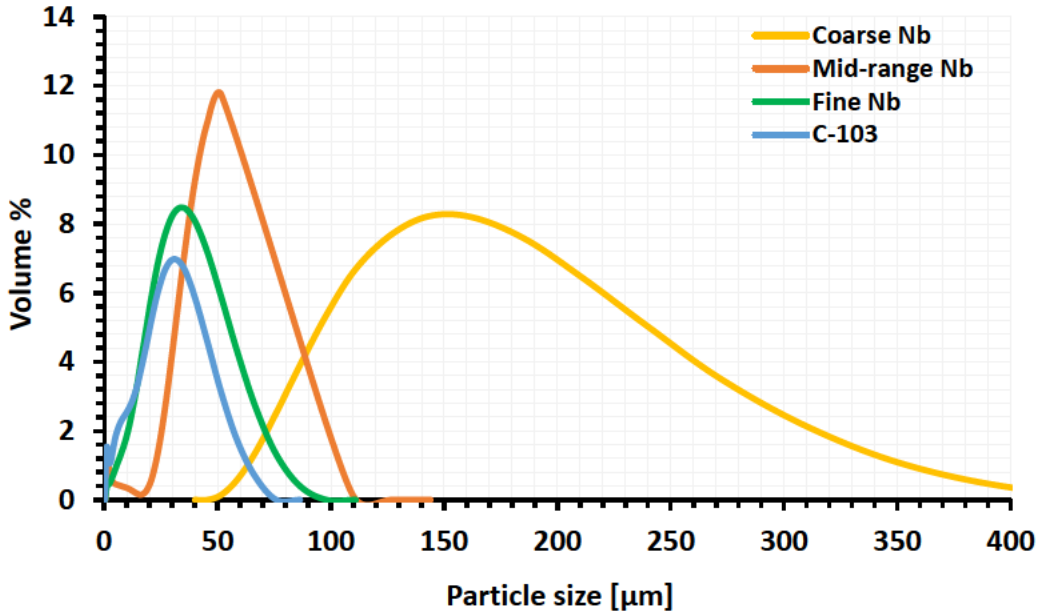

Figure 7.5 Particle size distribution of Nb and C-103 powders.

As mentioned above, the O content is an important factor influencing the mechanical properties of pure Nb and C-103 powders. It determines an increase in strength for pure Nb, and adversely influences the mechanical properties of C-103 by increasing the oxide precipitation at PPBs. The oxygen content of the three Nb powders is reported in

Table 7.3, while the chemical analysis performed on C-103 powders is shown in Table 7.4. The oxygen measurements highlight a considerable difference among the four powders. It is worth noting that the O levels are not directly linked with the particle size. Fine powders show very high oxygen concentration (1849ppm); similar values are observed for coarse powders (1172ppm); while mid-range Nb and C-103 powders show a much lower amount of oxygen, (302ppm and 371ppm, respectively). Nb powders have higher O levels if compared to commercial Grade 2 (250ppm) [5], on the other hand, C-103 powder has lower levels of Zr if compared to the standards, while the levels of oxygen are higher than the requirements [6].

The role of Zr in Nb alloys is to improve the creep resistance and high-temperature oxidation properties of the material by reducing the oxygen solid solubility in the alloy and thus promoting the formation of oxides [7]. However, the absence of Zr in the alloys does not compromise the room temperature mechanical properties of the alloy and can be beneficial for limiting the presence of PPBs due to the high affinity of Zr to O.

Table 7.3 Oxygen content on Nb powders.

Powder Type	Oxygen Content [ppm]
Nb fine	1849
Nb mid-range	302
Nb coarse	1172

Table 7.4 Chemical analysis of C-103 powder (wt%).

Powder	Nb	Hf	Ti	Zr	Ta	W	C	O	N	H
Required [6]	87.3	9-11	0.7-1.3	0.7	0.5	0.5	<150 (ppm)	<225 (ppm)	<100 (ppm)	<15 (ppm)
C-103	89.08	9.35	1.07	<0.05	0.30	0.19	38 (ppm)	371 (ppm)	24 (ppm)	7 (ppm)

7.5.2 Microstructure Analysis

Backscattered SEM micrographs of the as-HIPed Nb samples are shown in Figure 7.6. All three microstructures present equiaxed grains, typical for HIPed materials. Even in this case, some differences can be observed. Fine Nb powders show a finer grain structure if compared to mid-range and coarse microstructures. Another important result to capture is that all three microstructures are near-fully dense. The microstructure of as-HIPed C-103 is shown in

Figure **7.7**. The HIPed material presents some limited porosity and is characterised by the presence of some precipitates. The precipitates are rich in Hf and can be identified as Hf (O, C). Higher HIP temperatures would limit the presence of porosity; however, they will trigger different eutectic reactions between Fe present in the canister and Hf contained in the alloy between 1300 and 1400°C. Furthermore, the use of higher temperatures promotes excessive grain and precipitate coarsening.

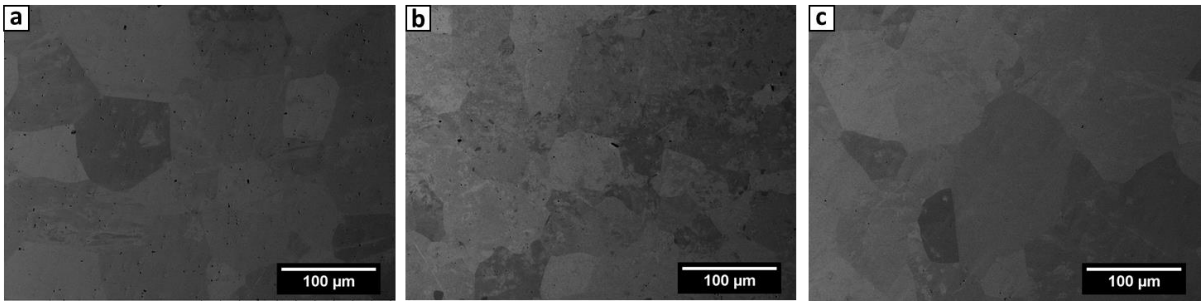

Figure 7.6 Backscattered SEM micrographs of as-HIPed microstructure of (a) Nb fine, (b) Nb mid-range and (c) Nb coarse.

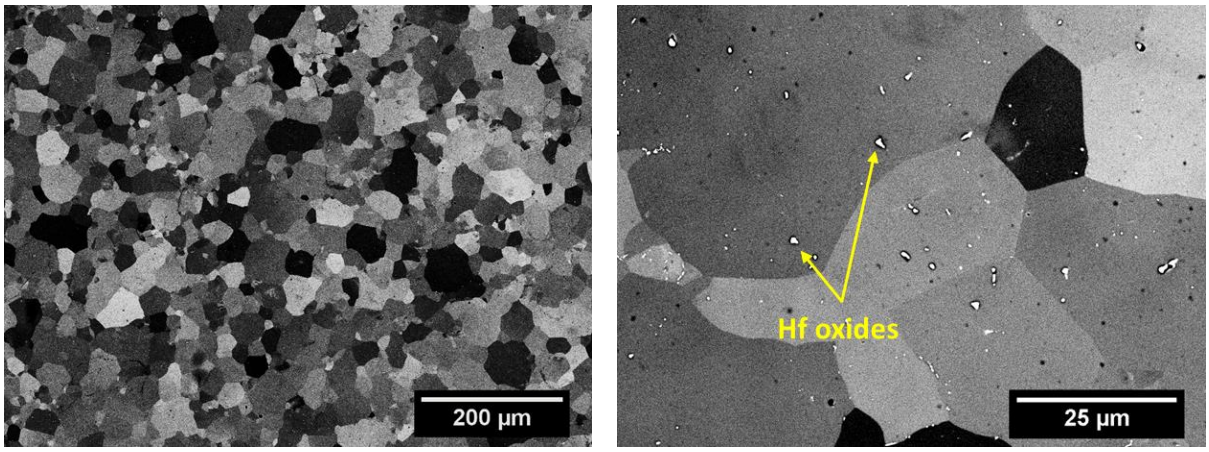

Figure 7.7 Backscattered SEM micrographs of as-HIPed C103.

EBSD analyses were performed on the Nb as-HIPed microstructures. Figure **7.8** shows a randomly oriented structure with equiaxed grain size for the three HIPed Nb samples. The EBSD maps clearly show the presence of a fully recrystallised microstructure free from PPBs for the three Nb HIPed powders. The absence of PPBs can be related to the high solid solubility of oxygen in Nb at the HIP temperature [7]. Another important outcome from the

EBSD analysis is the differences in grain size among the three microstructures. Nb fine shows an average grain size of 44µm; Nb mid-range shows an average grain size of 53µm; while in Nb coarse the calculated average grain size was 67µm, much coarser if compared to size of Nb fine. The difference in grain size among the three powders is a function of the powder particle size. In fact, Nb fine showed the smaller grain size, while Nb coarse is characterised by the biggest grain size. This is an important outcome because it demonstrates the possibility of tailoring the as-HIPed mechanical properties of pure Nb by using different powder particle sizes. Furthermore, especially for pure metals, the large difference in grain sizes revealed by the EBSD maps can be directly linked to the mechanical properties of the material.

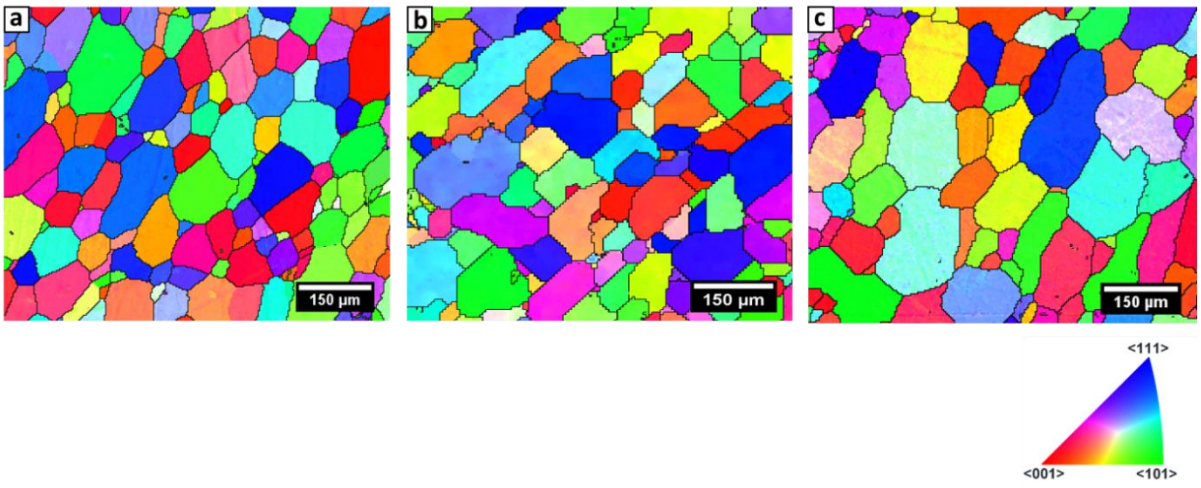

Figure 7.8 EBSD of (a) Nb fine, (b) Nb mid-range and (c) Nb coarse.

Oxygen measurements were also performed on the as-HIPed samples to outline the differences in O content, and ascertain the O pickup during the HIP procedure. Nb fine showed the highest level of O pickup, this can be attributed to the higher levels of surface to volume ratio enhancing the reactivity of the powder. Lower O pickup can be observed in coarse powders, while minimal O pickup is observed in mid-range powders (Table 7.5).

Table 7.5 Oxygen measurements of as-HIPed Nb.

As-HIPed Powder Type	Oxygen Content [ppm]	Oxygen Pickup [ppm]
Nb fine	2361	512
Nb mid-range	390	88
Nb coarse	1438	266

7.5.3 Mechanical Properties

The four as-HIPed samples were tested using microhardness to have a first understanding of the mechanical properties of the material. The results in Figure 7.9 show a large difference in hardness between the three Nb powders and surprisingly high levels of hardness if compared to HIPed C-103. Fine Nb powders show the highest hardness of 250HV, while Nb mid-range shows the lowest hardness, just above 100HV. These results highlight a direct correlation between the O-levels and the hardness of the material. The results also outline that the grain boundary strengthening is not the main strengthening mechanism if compared to the solid solution one. In fact, the HIPed Nb coarse powder has a considerably higher hardness than Nb mid-range, despite the bigger grain size. C-103 has a hardness of 116HV much lower if compared to Nb fine and Nb coarse HIPed powders using the same HIP conditions. This suggests that by increasing the O-levels in pure Nb, it is possible to obtain higher room temperature strength if compared to as-HIPed C-103.

The first reason behind this behaviour is found in the preferential precipitation of oxide and carbides in HIPed C-103 at PPBs. The presence of an uneven distribution of precipitates will not have a strong impact on the strength of the material. Furthermore, the formation of Hf (O, C) will reduce the matrix solid solution strengthening by concentrating part of the Hf at PPBs. The other reason is found in the O-levels: C-103 has much lower O-levels if compared to Nb fine and Nb mid-range. However, in contrast to Nb, it is not advisable to increase the

O-levels in C-103 powders due to the limited oxygen solid solubility in the alloy. Lastly, Figure **7.9** shows that the hardness of wrought and annealed C-103 (courtesy of Nammo) is similar to the HIPed C-103, with the hardness level below fine and coarse HIPed Nb.

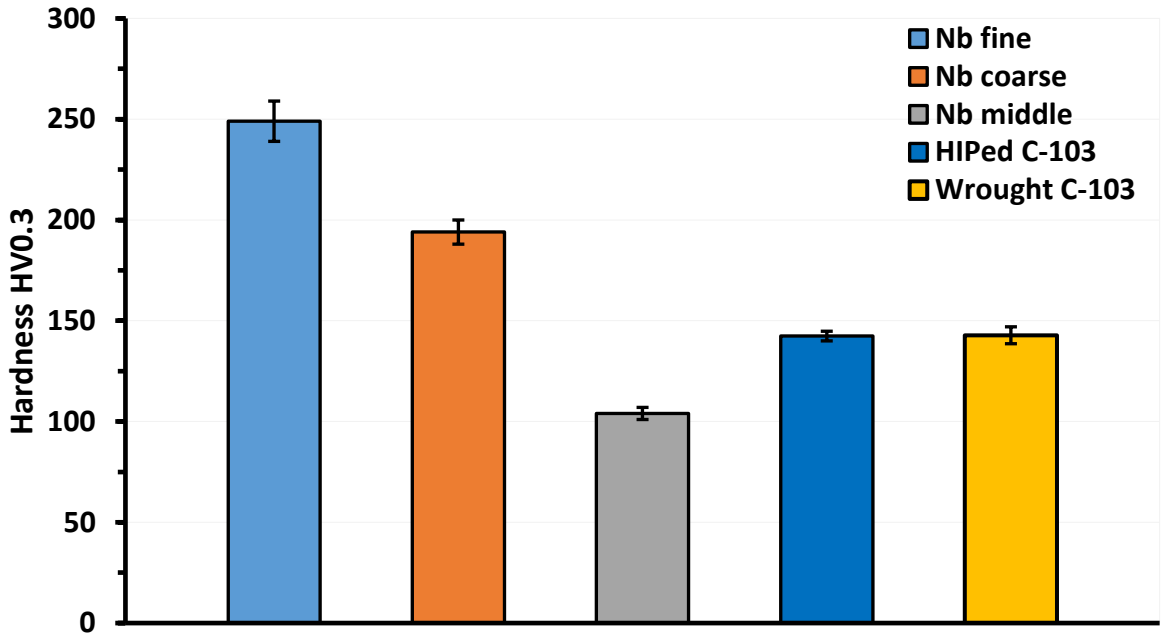

Figure 7.9 Microhardness values of as HIPed Nb vs wrought C-103.

More detailed analyses are required to have a better understanding of the mechanical properties of the as-HIPed pure Nb and their comparison with HIPed C-103. To this end, mid-range Nb powders were used for tensile testing of Nb, for two main reasons. Firstly, because the wide range distribution could potentially give more flexibility in terms of an alteration of PSD and, consequently, powder characteristics, which is one of the objectives of this study. The second reason is linked to Nb mid-range lower oxygen level, which could give more information on the influence of oxygen variation on the mechanical properties of the as-HIPed Nb. The results for the room temperature tensile test on mid-range powders can be seen in Figure **7.10**. The tensile properties show a yield strength of 143MPa and a UTS of 288MPa, much higher if compared to the strength values reported in the literature [8]. As

expected, the elongation was lower, but the value of 48% still represents an excellent result for the proposed application.

The higher strength reported for mid-range Nb powders is a combination of oxygen levels and fine grain size obtained using PM HIP. Some fractographic analyses were performed on the fractured tensile samples. The SEM micrographs clearly show a ductile fracture, where the main fracture mode is represented by micro void coalescence. It is important to note on the fractured surfaces that no presence of oxides acting as nucleation sites for fracture can be observed.

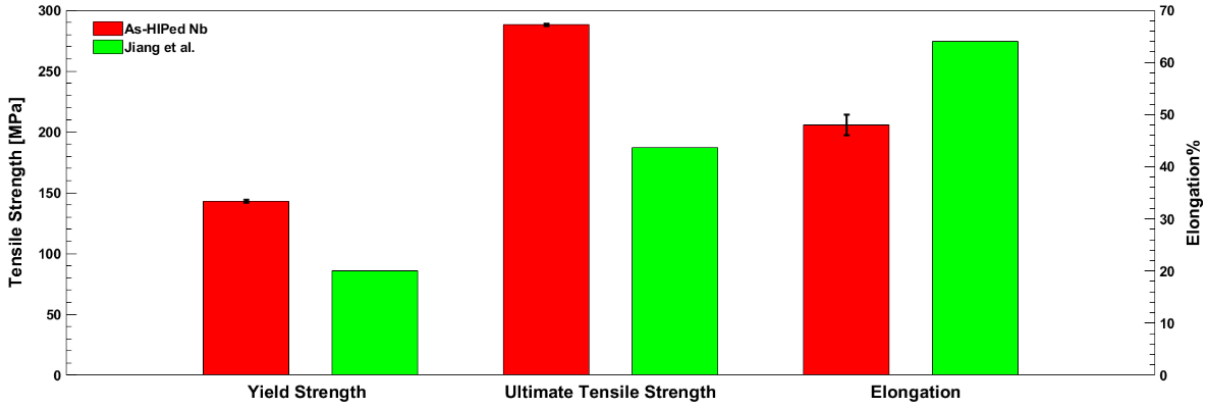

Figure 7.10 Tensile properties of as-HIPed Nb mid-range.

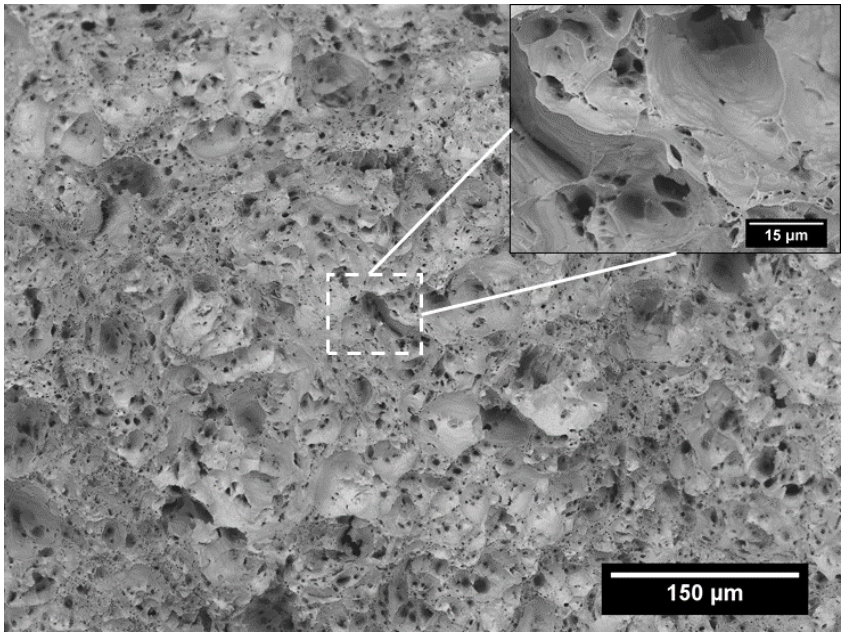

Figure 7.11 Fractured tensile sample Nb mid-range.

As-HIPed Nb showed superior tensile properties if compared to wrought Nb, however, the tensile strength obtained is still below the required range for the application and more importantly, still not comparable to Nb alloys commonly used in the space sector [7]. Thanks to the previous investigation performed on different powders, it is possible to understand the influence of powders' characteristics on their mechanical properties. Thus, it was decided to perform sieving on the mid-range powders to increase the surface to volume ratio of the powder to increase the oxygen concentration in the powder. Additionally, sieving will target to obtain a finer as-HIPed microstructure by reducing the average powder particle size, further contributing to an increase in strength. Sieving was performed using a 63µm sieve in a protected atmosphere.

After sieving, the oxygen content of the powder was checked to understand if there is a relevant increase in the O-levels. Table **7.6** summarises the O-levels before and after sieving. It shows that just by powder sieving, the O-level increased from 302ppm to 756ppm. Once the increase in oxygen was confirmed, the sieved powders were HIPed using the same HIP parameters of the mid-range powders.

Table 7.6 Oxygen levels of Nb mid-range powder before and after sieving.

Powder Type	Oxygen Content [ppm]
Nb mid-range	302
Nb mid-range sieved (63µm)	756

Figure 7.12 highlights the microstructure of the sieved Nb powder, as expected the microstructure is characterised by the presence of a near-fully dense and equiaxed microstructure with an average grain size of 45µm, smaller if compared to the as-HIPed Nb mid-range. Thus, even in this case, reducing the particle size resulted in a reduction of the average grain size in the as-HIPed microstructure. The combination of finer microstructure with a higher O-levels can result in a consistent increase in strength for as-HIPed sieved Nb powder if compared to as-HIPed Nb mid-range.

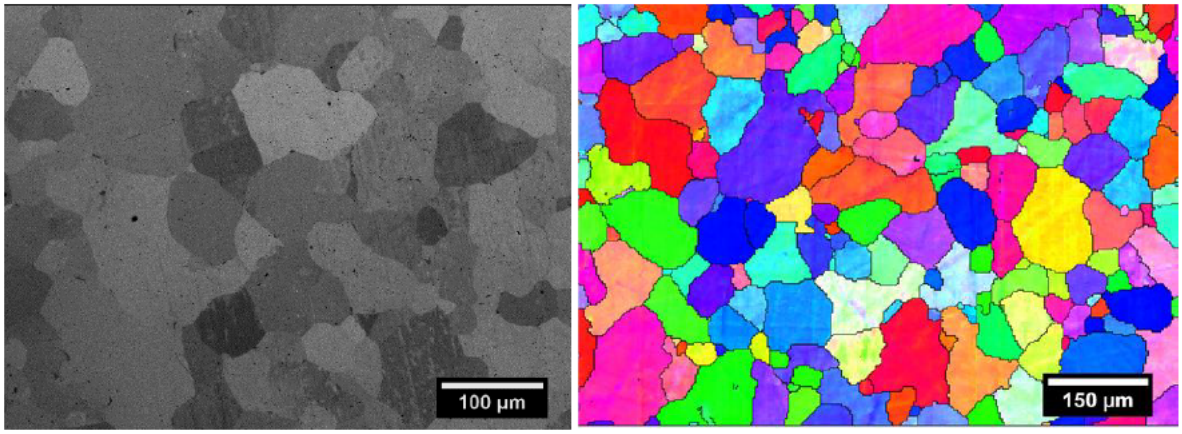

Figure 7.12 SEM backscattered micrographs of as-HIPed sieved Nb powder (left), EBSD map of as-HIPed sieved Nb powder (right).

To check for a possible increase in strength, the sieved powders were then tested using microhardness. As expected, the microhardness results show an increase from 104HV for mid-range HIPed sample to 135HV for the sieved one. Tensile tests on the sieved mid-range powders have been performed to understand the response in terms of tensile strength and elongation for the material. The results presented in Figure 7.13 show a noticeable increase in

both YS (from 143MPa to 200MPa) and UTS (from 270MPa to 350MPa) while maintaining good levels of elongation, far above Nb alloys used for the same application [7].

The fractographic micrographs of Figure **7.14** show a ductile fracture with the presence of dimples, similarly to the observations for HIPed Nb mid-range (Figure **7.11**). The room temperature tensile strength values are now much closer to the required values, further sieving can be performed to increase the strength to the required levels.

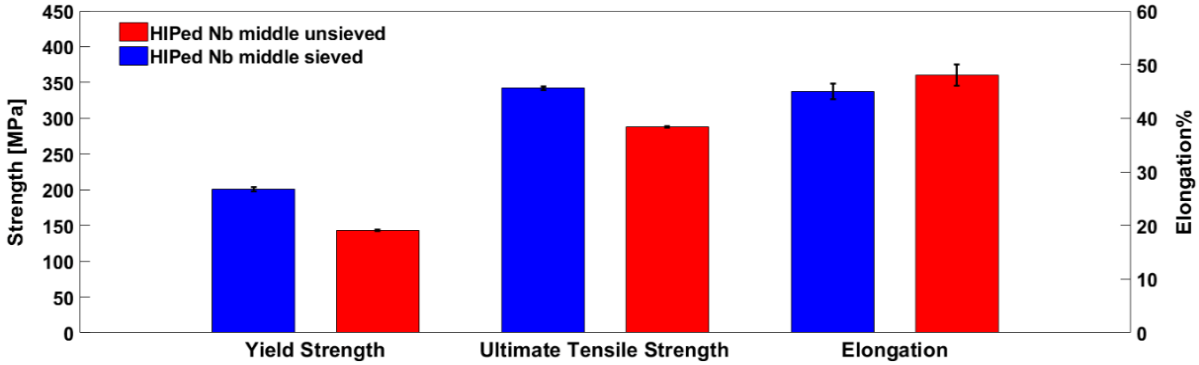

Figure 7.13 Mechanical properties of as-HIPed Nb. Comparison between mid-range and sieved powders.

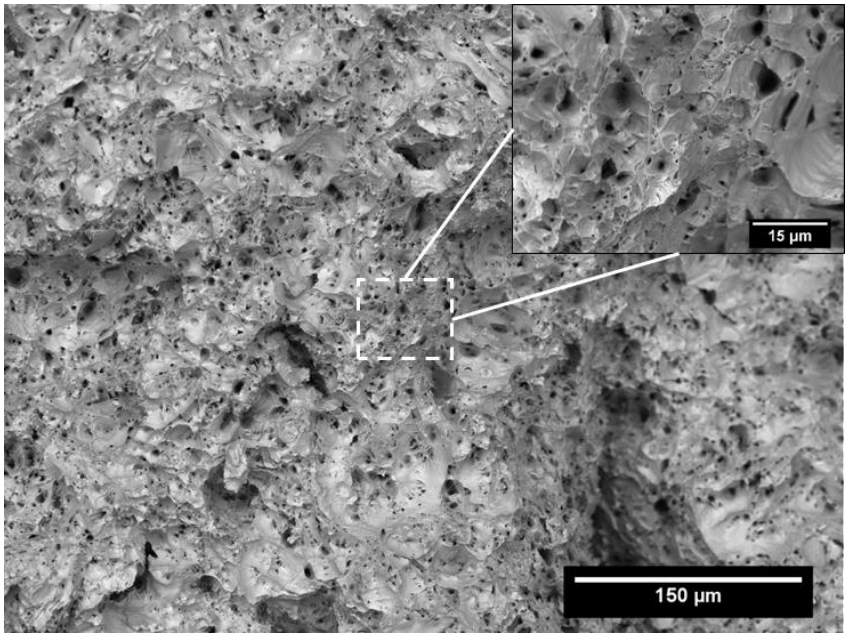

Figure 7.14 Fractured tensile samples of as-HIPed sieved mid-range Nb.

Room temperature tensile tests were also performed on as-HIPed C-103 to understand and compare the tensile properties with pure Nb, and with the specifications for the wrought

alloy. C-103 tensile properties are highlighted in Figure **7.15**. The as-HIPed alloy shows excellent properties if compared to the minimum specification for wrought alloy both in terms of strengths and ductility. Furthermore, despite the possible formation of Hf-rich PPBs, C-103 shows superior room temperature properties if compared to the sieved mid-range Nb. Additionally, if compared to the work of Philips *et al.*, as-HIPed C-103 is characterised by slightly higher levels of YS and UTS, accompanied by a lower ductility. This can be associated with the higher O-content in C-103 powder, promoting precipitation of Hf-rich PPBs which impair the ductility [9].

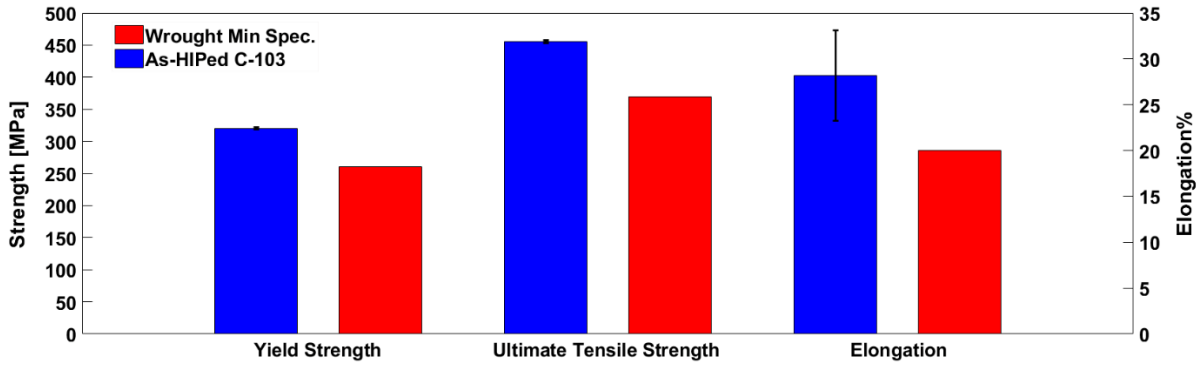

Figure 7.15 Room temperature tensile properties of as HIPed C-103 vs ASTM minimum specifications for wrought C-103 [6].

The fractographical analysis presented in Figure **7.16** shows a ductile fracture mode with the presence of Hf-rich oxides on the fracture surface, confirming the influence of PPBs on the tensile behaviour of HIPed C-103.

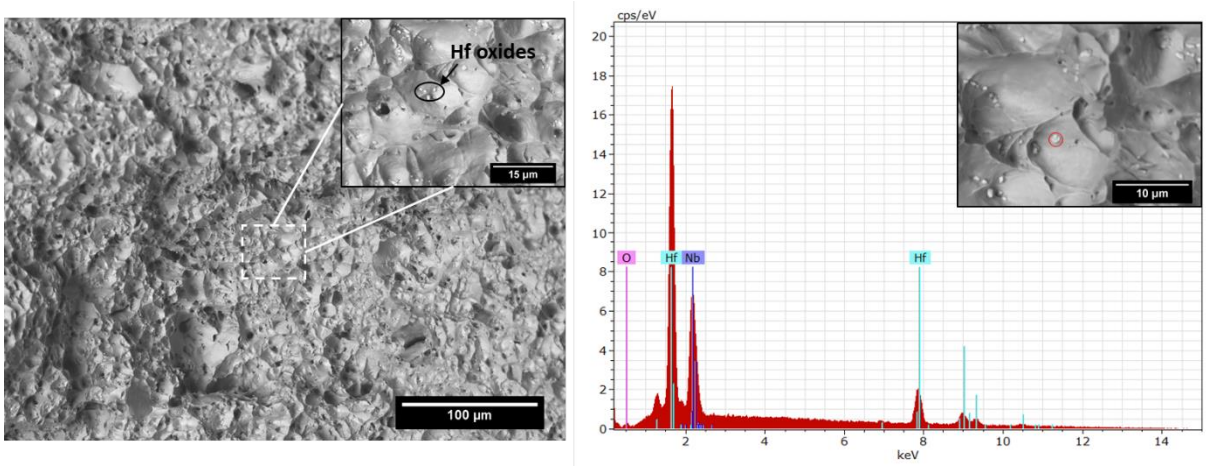

Figure 7.16 Fractured tensile samples of as-HIPed C-103 (left), EDX spectrum of white particle on the fracture surface (right).

7.5.4 Influence of Oxygen on Mechanical Properties

It was demonstrated that the O-content plays a crucial role in the mechanical properties of as-HIPed pure Nb. Harris *et al.* demonstrated the correlation between O-levels and hardness [10]. Their proposed equation is presented below (*Eq. 7.1*):

$$\boldsymbol{HV = 69.5 + 881\,O + 296\,N + 271\,C} \qquad \textit{Eq. 7.1}$$

Where O, N and C are expressed in wt%. It is possible to see from Eq. 1 that the O-level has a big impact on the hardness, much higher if compared to N and C. The equation was plotted against the available data on HIPed Nb of the current study (Figure **7.17**). The values obtained in this study are in strong agreement with the empirical model, especially for lower O- levels. The equation also indicates that to achieve the same hardness of C-103, an O-level of around 900ppm is required for pure Nb.

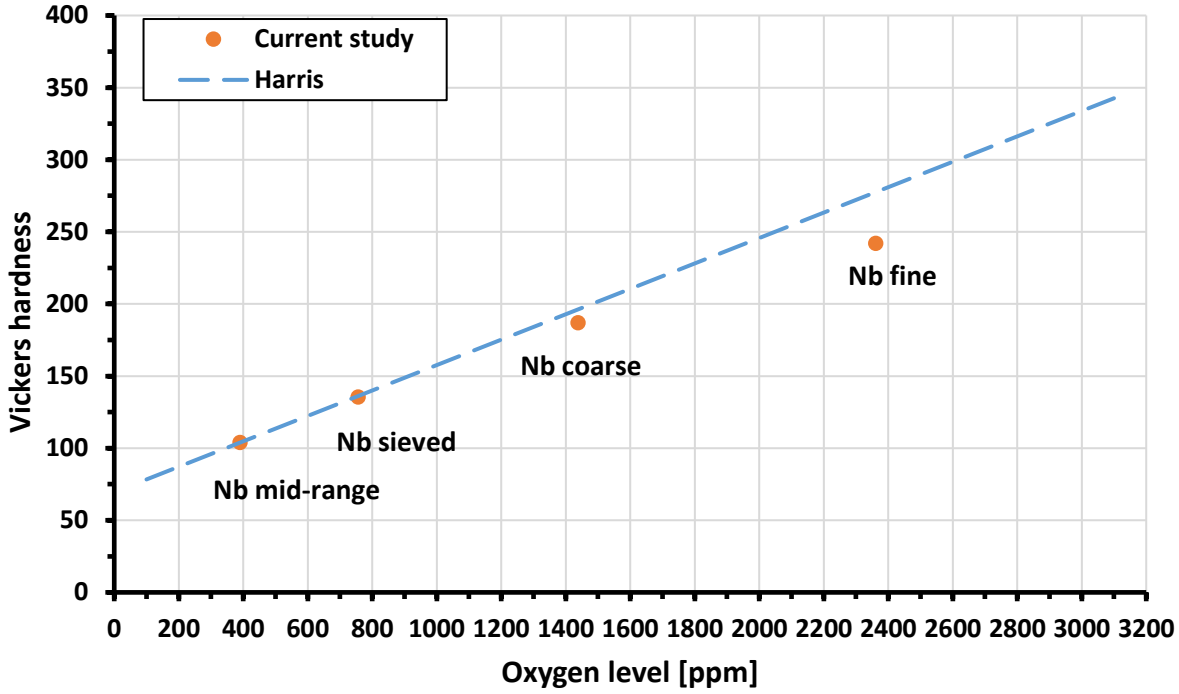

Figure 7.17 Influence of oxygen on the hardness of pure Nb. Experimental values were obtained in the current study vs Harris proposed equation [10].

In order to understand the combined effect of the O-levels and grain size on the strength and calculate the O-level needed for achieving the required strength, a simple model was presented. This was based on the structure–property relation for the material and on the coefficients available in the literature [11], [12]. The general equation for structure–property relation is presented below (*Eq. 7.2*) [13]. The following assumptions were made on as-HIPed Nb:

- No presence of any precipitate. This assumption is true for pure metals, such as Nb. The presence of oxides was neglected because the O-levels are below the solid solution levels at HIP temperature [7], [14].
- No dislocation strengthening. The microstructure during HIP evolves via recrystallisation, thus after HIP it can be assumed that the microstructure is free from dislocations.

The values for inherent lattice strength of Nb, k_y, n and σ_{ss} were obtained from [11].

$$\sigma_{YS} = \sigma_0 + \sigma_{SS} + k_y d^{-n} + \alpha G b \sqrt{\rho} \qquad \textit{Eq. 7.2}$$

The values for YS were calculated for both Nb mid-range and sieved Nb. The results presented in

Table 7.7 shows a good agreement with the tested samples, with an error of just 1MPa for mid-range Nb and an error of 25MPa for sieved Nb.

Table 7.7 Experimental YS vs calculated YS for mid-range and sieved HIPed samples.

	Experimental YS	**YS Model Prediction**
Nb mid-range	143 MPa	142 MPa
Nb sieved	201 MPa	226 MPa

Based on the above results, which give a good approximation of the YS for Nb powders, it was possible to calculate the O-level required to achieve the desired YS of 260MPa. In this case, the O-level required to achieve that YS is 1000ppm, assuming a grain size similar to as-HIPed Nb sieved.

7.5.5 Powder Heat Treatment

The abovementioned sieving strategy was capable of increasing the O-level and, consequently, the strength of the material. However, the oxygen strengthening contribution of the powder is not enough to match the required strength. The possible solution proposed was

to perform pre-HIP heat treatment on Nb powders to try to incorporate the right amount of oxygen needed to achieve the required strength.

Heat treatment of the powders was performed in air at a temperature of 300°C for 10h, which would guarantee enough diffusion of oxygen in the Nb powder. After heat treatment, the canister was de-gassed and HIPed using the conventional parameters used in this work.

The microstructure of the HTed + HIPed Nb powder is reported in Figure **7.18**. The micrographs clearly show the presence of some oxides randomly distributed in the microstructure.

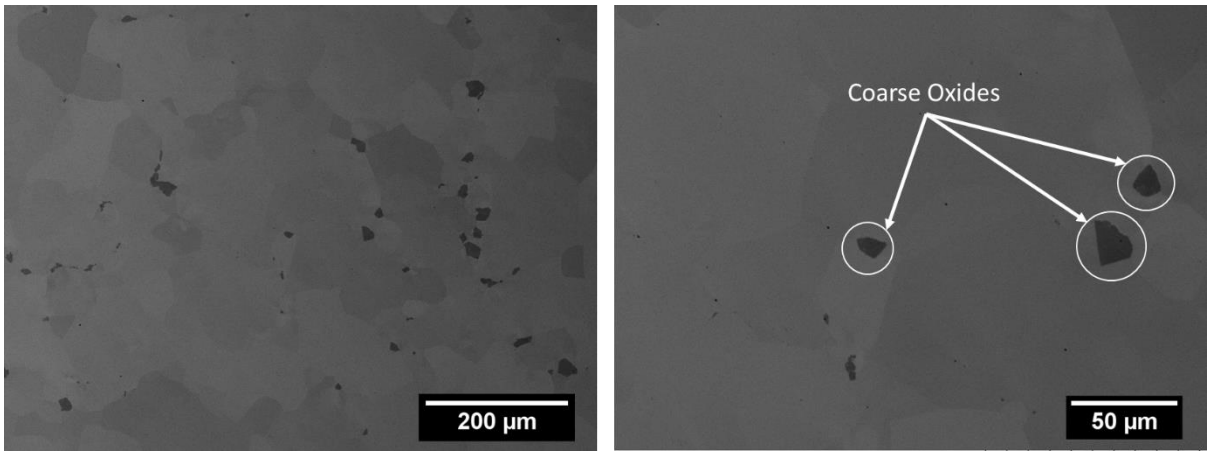

Figure 7.18 Microstructure of HTed + HIPed Nb powder.

The presence of oxides is confirmed by the EDX spectrum in Figure **7.19**, which also highlights the presence of C in the precipitates.

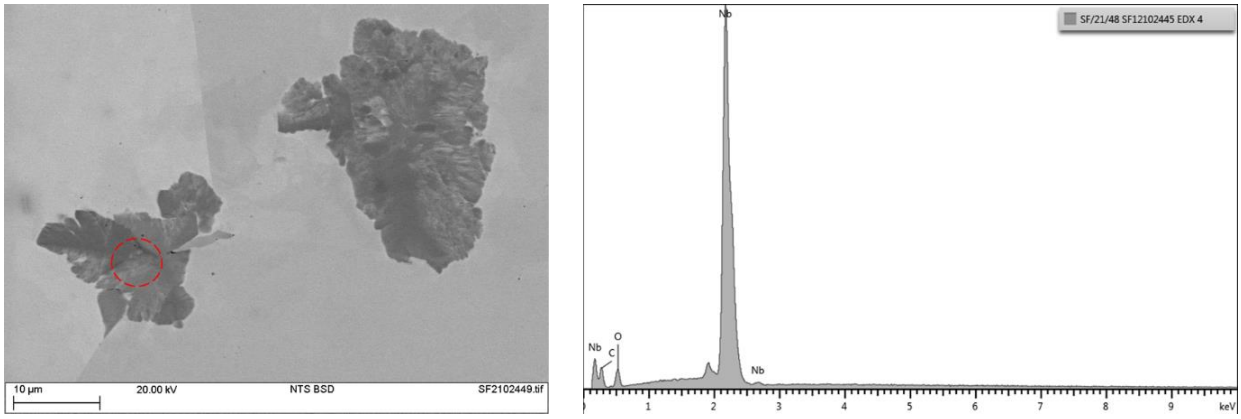

Figure 7.19 EDX analysis on HTed and HIPed Nb powder.

Some microhardness measurements were performed to understand the effect of pre-HT on the strength of the as-HIPed material. The microhardness results confirm that the pre-HT on Nb powders has successfully increased the strength of the material by increasing the hardness from 135HV to 248HV. In this case, the strength contribution is attributed to both solid solution strengthening and precipitation hardening due to the presence of Nb oxide precipitation.

7.6 Near-Net-Shape Manufacturing of Thruster Combustion Chambers

Near-net-shape manufacturing of a thruster combustion chamber was performed using pure Nb in order to demonstrate the feasibility of NNS PM HIP for the production of thruster combustion chambers. A 2D technical drawing of the thruster combustion chamber demonstrator is highlighted in Figure **7.20**.

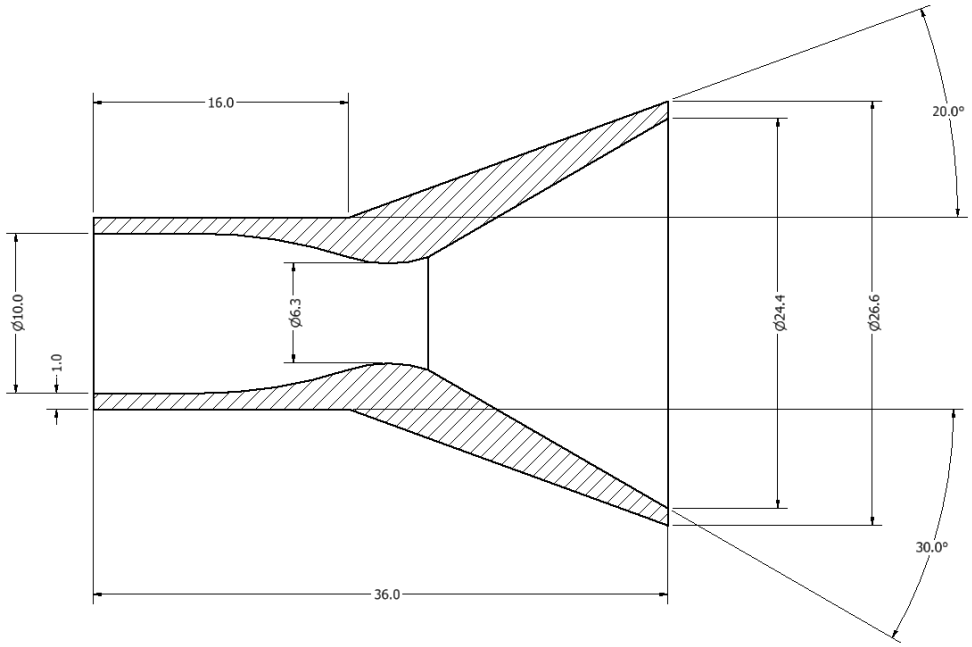

Figure 7.20 Section 2D technical drawing of the original design for the combustion chamber.

To successfully manufacture the part, due to the complex internal section of the combustion chamber (Figure **7.20**), a canister with an inner core reflecting the internal shape of the combustion chamber was manufactured. The assumption made during the design was that the consolidation would happen just in the radial direction of the canister, with a negligible deformation in the axial direction due to the presence of a stiff solid core. For this reason, the outer shell of the canister was over dimensioned by 50% to take into account the HIP densification shrinkage. A 2D drawing of the canister assembly is reported in Figure **7.21**. The drawing of the canister design highlights the presence of a cone on the left side. The presence of a cone ensures uniform powder filling in addition to facilitating the filling procedure.

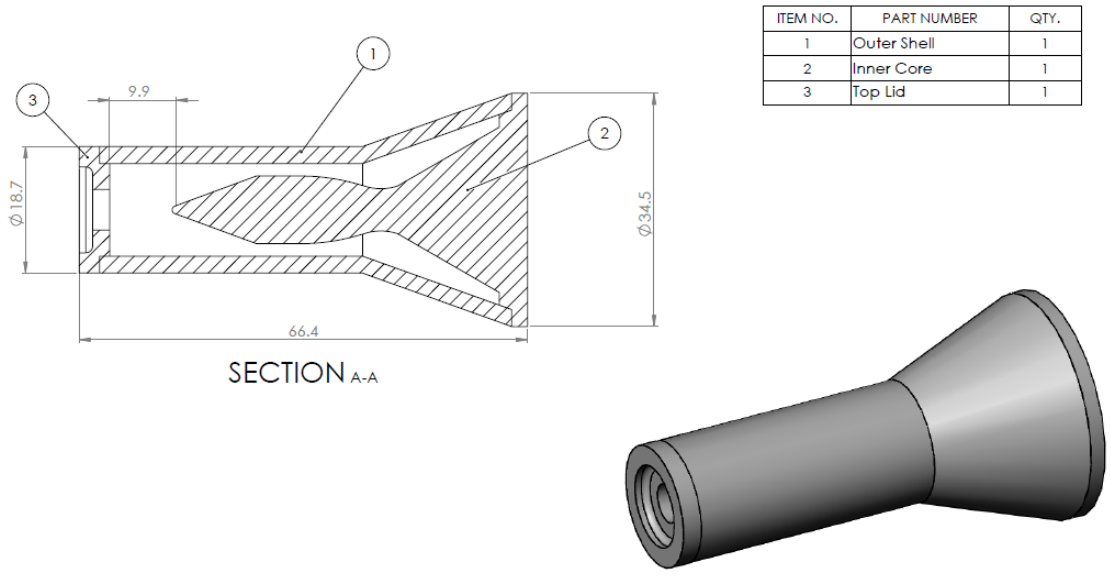

Figure 7.21 2D technical drawing of thruster combustion chamber assembly**.**

After canister manufacturing and welding, the canister followed the HIP procedure described in the experimental procedure chapter, using Nb mid-range sieved powders due to its better mechanical properties. After canister densification the canister was pickled in nitric acid at E F Westaway Ltd in order to dissolve the steel canister and reveal the internal shape. The near netshape part after pickling can be observed in Figure **7.22**. The cross-section, obtained using EDM cutting machine, shows that the inner section follows the complex geometry reported in the original design of Figure **7.20**.

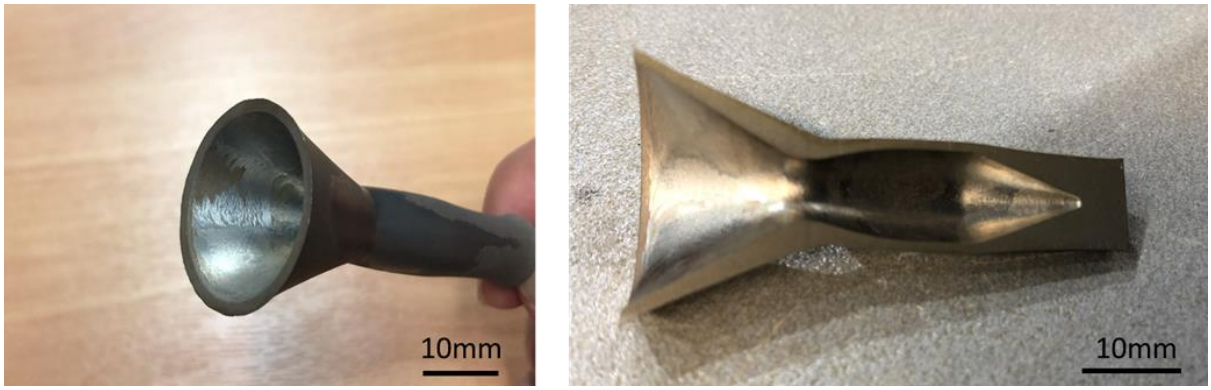

Figure 7.22 Thruster combustion chamber after pickling (left). EDM cross-sectioned part (right).

To check the geometrical accuracy, the part was analysed using a FARO laser scanner. The results of Figure **7.23** shows good geometrical accuracy, with a maximum error of 0.8mm. The laser scanning results show a small under dimensioning in the radial dimension. The results obtained through laser scanning demonstrate the possibility of manufacturing near-net-shape thruster combustion chamber using NNS PM HIP, achieving a good geometrical agreement and drastically reducing the material waste. Further machining is however required to remove the diffusion layer at the interfaces of both the inner core and outer shell sides. Additionally, it is worth noting that despite the reduction of Nb material, there is a consistent amount of canister material adopted to shape the inner core. However, due to the ease of pickling and machining of the canister, the use of additional canister material was considered beneficial to have better geometrical control and to avoid excessive use of pure Nb.

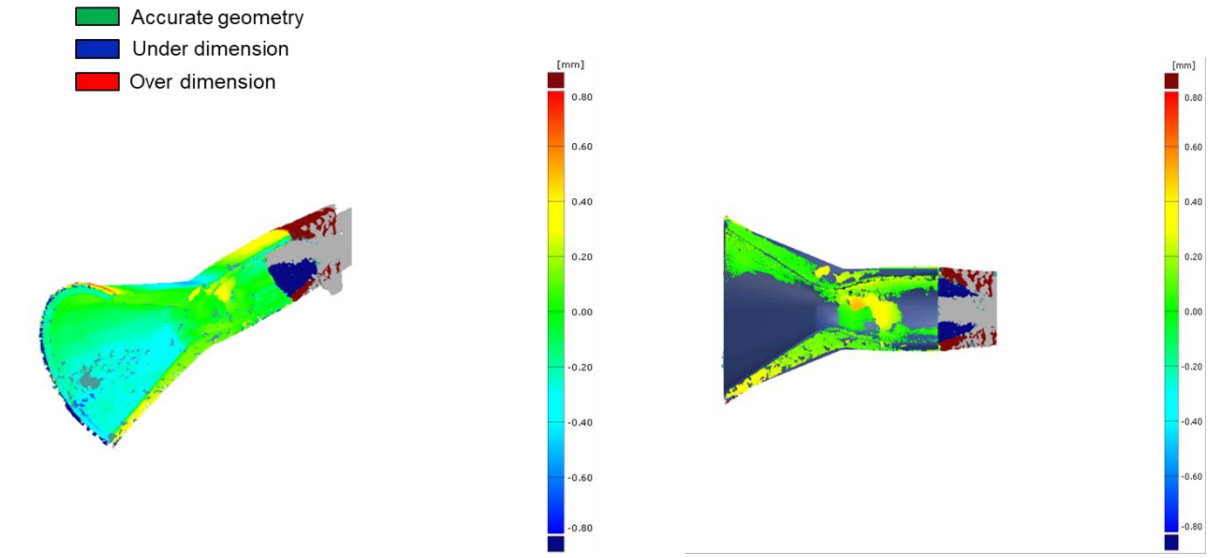

Figure 7.23 Laser scanning of the HIPed cross-section of thruster combustion chamber**.**

7.7 Conclusions

In this work PM HIP of pure Nb was proposed as an alternative to the more complex C-103 Nb-base alloy. HIP was successfully performed on a variety of Nb powders, showing a near-fully dense microstructure with enhanced mechanical properties. It was demonstrated that O is the main variable influencing the room temperature mechanical properties of pure Nb. It was also shown that the mechanical properties can be easily modified by changing the powders' characteristics. The microhardness of fine and coarse HIPed Nb powders showed higher values if compared to HIPed and wrought C-103.

Sieving of mid-range Nb powders has shown a significant increase in microhardness and an increase in room temperature mechanical properties while maintaining a good level of elongation. Heat treatment of Nb powders was also considered a valid strategy, capable of increasing the O-levels over and beyond the solid solution limit, leading to oxides formation and enhanced strength.

Finally, through a simple model, it was calculated that the O-level necessary to achieve a yield strength of 260MPa is approximately 1000ppm.

Based on the above considerations, pure Nb processed by PM HIP can represent a valid alternative to Nb alloys for two main reasons:

- The high solid solubility of O in Nb can produce high values of yield strength.
- The flexibility of the PM HIP process allows tailoring of the microstructure and mechanical properties of Nb through powder quality and process parameters i.e. control of the oxygen levels and powder particle size.

Additionally, the study demonstrated that despite the presence of reactive elements, the as-HIPed C-103 microstructure was free from PPBs and the mechanical properties of as-HIPed C-103 were superior if compared to the minimum specifications for wrought C-103. Nevertheless, the use of solid solution strengthened Nb alloys would give a better HIP response. In particular, the addition of elements such as W, Mo or Ta, should be considered as an addition to pure Nb for PM HIP procedure.

Finally, NNS PM HIP was employed to manufacture a pure Nb thruster combustion chamber. The use of a solid inner core represented a valid solution to obtain a good geometrical agreement with the original design. This is supported by the dimensional results highlighting the possibility of manufacturing a part with good geometrical agreement and with reduced buy-to-fly ratio if compared to traditional forging-machining manufacturing techniques used for thruster combustion chambers.

Acknowledgments:

This work was funded by ESA in the frame of the General Studies Technology Programme (ESA GSTP ITT 8899) under contract 4000122901/18/NL/BJ. The work was enabled through, and undertaken at, the National Structural Integrity Research Centre (NSIRC), a postgraduate engineering facility for industry-led research into structural integrity established and managed by TWI through a network of both national and international universities. AS acknowledges the Centre of Doctoral Training in Innovative Metal Processing (IMPaCT), funded by the Engineering and Physical Sciences Research Council (EPSRC) for the PhD funding support.

Declarations of interest: none

7.8 References

[1] L. Gimeno-Fabra, Design, Manufacture and Properties of Cr-Re Alloys for Application in Satellite Thrusters, Dr. Thesis. (2006). https://doi.org/10.1007/978-3-642-32273-0.

[2] J.A. Halchak, J.L. Cannon, C. Brown, Materials for Liquid Propulsion Systems, Aerosp. Mater. Appl. (2018) 641–698. https://doi.org/10.2514/5.9781624104893.0641.0698.

[3] R.C. Stechman, Advanced thrust chamber materials for Earth storable bipropellant rocket engines, Acta Astronaut. 29 (1993) 109–115. https://doi.org/10.1016/0094-5765(93)90028-U.

[4] M. Sankar, R.G. Baligidad, D.V.V. Satyanarayana, A.A. Gokhale, Effect of internal oxidation on the microstructure and mechanical properties of C-103 alloy, Mater. Sci. Eng. A. 574 (2013) 104–112. https://doi.org/10.1016/j.msea.2013.02.057.

[5] ASTM International. B391-18 Standard Specification for Niobium and Niobium Alloy Ingots. West Conshohocken, PA; ASTM International, 2018., (n.d.).

[6] ASTM International. B655/B655M-10(2018) Standard Specification for Niobium-Hafnium Alloy Bar and Wire. West Conshohocken, PA; ASTM International, 2018., (n.d.).

[7] L.J. Pionke, J.W. Davis, Technical assessment of niobium alloys data base for fusion reactor applications, 1979.

[8] H. Jiang, D. Baars, A. Zamiri, C. Antonie, P. Bauer, T.R. Bieler, F. Pourboghrat, C. Compton, T.L. Grimm, Mechanical properties of high RRR niobium with different texture, IEEE Trans. Appl. Supercond. 17 (2007) 1291–1294. https://doi.org/10.1109/TASC.2007.898463.

[9] N.R. Philips, M. Carl, N.J. Cunningham, New Opportunities in Refractory Alloys, Metall. Mater. Trans. A Phys. Metall. Mater. Sci. 51 (2020) 3299–3310. https://doi.org/10.1007/s11661-020-05803-3.

[10] B. Harris, Niobium, Tantalum, Molybdenum and Tungsten, Elsevier, Amsterdam, 1961.

[11] Z.C. Cordero, B.E. Knight, C.A. Schuh, Six decades of the Hall–Petch effect – a survey of grain-size strengthening studies on pure metals, Int. Mater. Rev. 61 (2016) 495–512. https://doi.org/10.1080/09506608.2016.1191808.

[12] Z.C. Szkopiak, The Hall-Petch parameters of niobium determined by the grain size and extrapolation methods, Mater. Sci. Eng. 9 (1972) 7–13. https://doi.org/10.1016/0025-5416(72)90004-3.

[13] S. Rajasekhara, P.J. Ferreira, L.P. Karjalainen, A. Kyro, M. Society, Hall – Petch Behavior in Ultra-Fine-Grained AISI 301LN Stainless Steel, Metall. Mater. Trans. A. 38 (2007) 1202–1210. https://doi.org/10.1007/s11661-007-9143-4.

[14] M. Rigaud, R. Tougas, Literature Survey on Columbium, 1971.

[15] L.L. Snead, D.T. Hoelzer, M. Rieth, A.A.N. Nemith, Refractory Alloys: Vanadium, niobium, molybdenum, tungsten, Elsevier Inc., 2019. https://doi.org/10.1016/B978-0-12-397046-6.00013-7.

[16] P. Lipetzky, Refractory metals: A primer, Jom. 54 (2002) 47–49. https://doi.org/10.1007/BF02822621.

[17] S. Priceman, L. Sama, RELIABLE, PRACTICAL, PROTECTIVE COATINGS FOR REFRACTORY METALS FORMED BY THE FUSION OF SILICON ALLOY SLURRIES., Electrochem. Technol. (1968) 315.

[18] Z. Alam, S. Sarin, M.K. Kumawat, D.K. Das, S. Sarin, M.K. Kumawat, D.K. Das

Microstructure, Z. Alam, S. Sarin, M.K. Kumawat, D.K. Das, Microstructure and oxidation behaviour of Fe – Cr – silicide coating on a niobium alloy, Mater. Sci. Technol. 32 (2016) 1826–1837. https://doi.org/10.1080/02670836.2016.1148226.

[19] M.Z. Alam, A.S. Rao, D.K. Das, Microstructure and High Temperature Oxidation Performance of Silicide Coating on Nb-Based Alloy C-103, Oxid. Met. 73 (2010) 513–530. https://doi.org/10.1007/s11085-010-9190-x.

[20] B.A. Pinto, A.S.C.M. d'Oliveira, Nb silicide coatings processed by double pack cementation: Formation mechanisms and stability, Surf. Coatings Technol. 409 (2021) 126913. https://doi.org/10.1016/j.surfcoat.2021.126913.

[21] D.L. Olson, B. Mishra, D.W. Wenman, Welding, brazing and joining of refractory metals and alloys, Miner. Process. Extr. Metall. Rev. 22 (2001) 1–23. https://doi.org/10.1080/08827509808962487.

[22] B.P. Badgujar, S. Kumar, M.N. Jha, I. Samajdar, M. Mascarenhas, R. Tewari, G.K. Dey, An investigation of electron beam welding of Nb-1Zr-0.1C alloy: Process parameters and microstructural analysis, J. Manuf. Process. 28 (2017) 326–335. https://doi.org/10.1016/j.jmapro.2017.07.001.

[23] R.E. Seebold, L.S. Birks, Elevated temperature diffusion in the systems Nb-Pt, Nb-Se, Nb-Zn, Nb-Co, Ni-Ta, and Fe-Mo, J. Nucl. Mater. 3 (1961) 260–266. https://doi.org/10.1016/0022-3115(61)90193-3.

Chapter 8. HIP Diffusion Bonding of Nb and Nb-alloys for Space Applications

Alessandro Sergi[1, 2], Malallah Al Lawati[1, 2], Francesco Careri[1,2], Hugh Hamilton[3], Raja H. U. Khan[4], Martina Meisnar[5], Advenit Makaya[6], Moataz M. Attallah*[1]

[1] IRC in Materials Processing, School of Metallurgy and Materials, The University of Birmingham, Birmingham, B15 2TT, UK

[2] National Structural Integrity Research Centre (NSIRC), Cambridge, CB21 6AL, UK

[3] Johnson Matthey, Reading RG4 9NH, UK

[4] TWI Ltd, Cambridge, CB21 6AL, UK

[5] Materials and Processes Section (TEC-MSP), Structures, Mechanisms & Materials Division, Mechanical Department, ECSAT, Fermi Avenue, Harwell-Oxford Campus, Didcot, Oxfordshire OX11 0FD, UK

[6] European Space Agency, ESTEC, Materials and Processes Section TEC-MSP, Mechanical Engineering Department TEC-M, Keplerlaan 1 - PO Box 299, 2200 AG Noordwijk-ZH, The Netherlands.

* Corresponding author: [redacted]

8.1 Motivation & Aims

The previous experimental chapter has outlined the capabilities of using NNS PM HIP technique for Nb and C-103 alloy demonstrating the possibility of achieving enhanced mechanical properties. However, as highlighted in the literature review (Chapter 3), one of the major drawbacks of refractory metals is associated with their insufficient high temperature oxidation resistance. Additionally, it was shown that silicide coatings, normally used to improve the oxidation resistance of Nb-alloys, result in the formation of brittle intermetallics with a consequent formation of cracks. Thus, the possibility of developing alternative high temperature oxidation resistant coating through HIP DB of Nb-Pt was investigated in this study. Furthermore, HIP DB was exploited to understand the possibility of joining Nb with Ti6Al4V. In particular, this study was proposed to reduce the challenges associated with the conventional joining processes given by the high reactivity of the two materials combined with the high melting point of Nb.

Abstract

In this work, the diffusion bonding (DB) behaviour of Nb and C-103 Nb-alloy was assessed for space applications. In particular, the development of an oxidation resistant coating using platinum (Pt) was developed for pure Nb to understand the feasibility of producing a high-temperature protective coating to replace the widely used R-512 E silicide coating. The diffusion layer analysed by SEM shows a successful reaction between both pure Nb and Pt with the generation of a 20µm thick, fully dense reaction layer. Furthermore, the DB of pure Nb with Ti6Al4V was also assessed to evaluate the possibility of joining Nb and Ti6Al4V through DB in space applications. The DB trials presented in this work demonstrate the possibility of replacing the conventional R-512 E silicide coating with the DB of Pt, and

furthermore the possibility of replacing the conventionally used welding techniques of Nb-Ti with DB to obtain a defect free and homogeneous microstructure.

Keywords: Nb-alloy; Hot Isostatic Pressing (HIP); Diffusion Bonding (DB); Oxidation resistant coating; Microstructure.

8.2 Introduction

Nb-alloys are widely used in space applications thanks to their ability to retain good mechanical properties up to very high temperatures and with relatively low densities if compared to the other refractory metals [1], [2]. However, the poor high-temperature oxidation resistance of Nb and Nb-alloys limits their use for space applications. To increase the oxidation resistance, different Nb-alloys with the presence of reactive elements such as Ti, Zr, Hf were developed over the years [3]. Despite the increase in oxidation resistance, Nb-alloys are still not capable to withstand the demanding performances in terms of high-temperature oxidation resistance in space applications. For this reason, the development of a high-temperature oxidation resistance coating is required. The most widely used coating is R-512 E silicide-based coating, composed of fused silicide with the presence of Fe and Cr (60Si, 20Fe, 20Cr) [4]. The study of the performances of R-512 E coating is broadly available in the literature. In particular, Alam *et al.* performed an in depth analysis of the microstructure of R-512 E coating on C-103. The authors reported the presence of a coating with a thickness of 250µm and with the presence of four distinctive layers [5]. The outermost layer is composed of Nb_2Si with the presence of some micro-cracks arising during the cooling process due to the differences in CTE between the coating and the substrate and the presence of some porosity. The other layers are richer in Cr and Fe and are characterised by the presence of some cracks and porosity, while the inter-diffusion layer is rich in Nb with a drastic reduction of Si, Cr and Fe [5]. Despite the presence of high-density defects in the R-

512 E coating, the impact on the oxidation properties is certainly beneficial. In fact, Alam *et al.* reported the presence of spalling of the external oxide layer in the uncoated C-103, while the coated samples showed a better high-temperature oxidation resistance, with an initial drastic increase in weight followed by a steady-state oxidation, accompanied by a final loss in weight [5].

The isothermal oxidation resistance of the R-512 E coated C-103 clearly shows the benefit of using a silicide coating, however, the presence of cracks and porosity can lead to a coating failure when the coating is subjected to thermal shocks due to the drastic differences in CTE between the coating and the substrate and the presence of brittle intermetallics. Thus, in applications where thermal shocks are present such as in thruster's combustion chambers, a metallurgical compatible coating with lower CTE difference is required. In particular, the use of precious metals can lead to excellent high temperature oxidation resistance and a good compatibility with Nb. Additionally, the drastic reduction of CTE will enhance the thermal shock response. Using precious metal as coating will also result in the absence of brittle intermetallics such as $NbSi_2$ and Nb_5Si_3, widely observed in the R-512 E and in other silicide-based coatings [6], [7]. In addition, the use a solid-state process like HIP DB would reduce the thermal stresses normally induced during solidification process and, consequently, the amount of defects. In this work, the use of Pt as high-temperature oxidation resistance was evaluated as high temperature oxidation resistant coating on pure Nb. Pt was used because of its good high-temperature oxidation resistance and the small differences in CTE if compared to the base material.

The second part of the study is focused on the solid state joining through HIP DB between HIPed pure Nb and Ti6Al4V to assess the influence of HIP DB on the microstructure and on the reaction layer metallurgy. The most widely used joining techniques for Nb is Electron

Beam Welding (EBW) or Laser Beam Welding (LBW) [8]. However, the use of EBW and LBW can induce some challenges, and many precautions should be used due to the high reactivity of Nb and its high melting point [9]. Furthermore, the presence of a heat affected zoned (HAZ) can induce a microstructural change around the joining interface, thermal stresses and distortions, making necessary the use of a post-welding stress relief heat treatment [8]. Thus, the possibility of joining Nb to Ti6Al4V through a solid-state joining process i.e. HIP DB can represent a valid solution to join Nb with dissimilar materials for space applications.

8.3 Materials and Methods

In this work, a pure Nb powder was adopted for the DB trials. The Nb powder was obtained by HDH process with a powder range 15-100µm.

To perform HIP DB trials on Pt, pure Nb powder was HIPed using temperature between 0.5-0.6 Tm of Nb, pressure of 120MPa, 4h dwell time, 5°C/min heating rate and 10°C/min cooling rate. In order to achieve a diffusion bonded interface, a Pt foil with a thickness of 80µm was placed at the bottom of a mild steel canister having a diameter of 12.5mm. To avoid an excessive diffusion between Pt-Fe at the bottom of the canister, a Nb foil with 100µm was placed at the bottom of the canister. A schematic of the canister for the DB trials is reported in Figure **8.1** left.

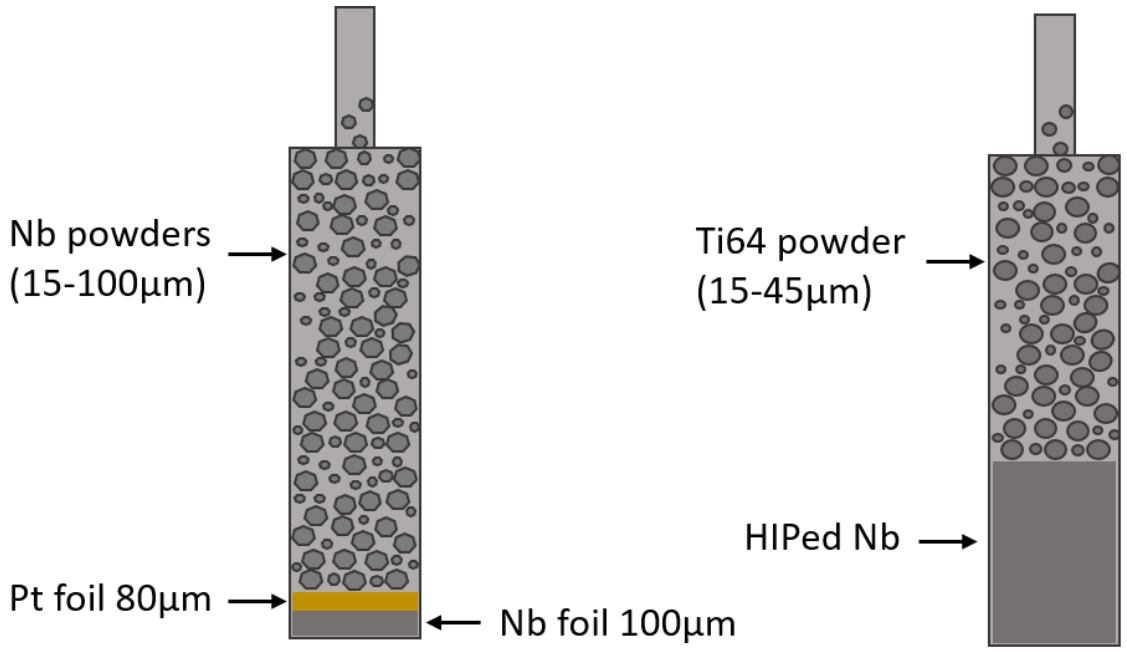

Figure 8.1 Schematic of the canister for Nb-Pt HIP DB (left) and canister for Nb-Ti6Al4V DB (right).

A similar approach was used to perform Nb-Ti6Al4V HIP DB. In this case, previously HIPed Nb used for the diffusion bonding together with Plasma-Rotating Electrode Process (PREP) Ti6Al4V powders with a size range of 15-45µm were adopted. In particular, a 12mm cylindrical HIPed NB sample was extracted using the EDM. The DB surface of the Nb cylindrical sample was grinded using SiC papers to 1200 grit and placed at the bottom of a mild steel canister having an inner diameter of 12.5mm. The mild steel canister was HIPed using a temperature of 930°C, pressure of 103MPa, 4h holding time, 5°C/min heating rate and 10°C/min cooling rate. A schematic of the canister for HIP DB trials of Nb-Ti6Al4V is reported in Figure **8.1** right. The DB samples were extracted using the EDM, mounted in conductive Bakelite, grinded and polished using standard metallographic techniques. The microstructure of the bonded interface was analysed using SEM and EDX techniques.

8.4 Results

8.4.1 Powder Morphology

The powder morphology of the Nb and Ti6Al4V powders is reported in Figure **8.2**. In particular, Ti6Al4V powder has a highly spherical shape typical of the PREP process. While Nb powder has an irregular rock shape, typical for HDH process. The regular shape for Ti6Al4V will contribute to higher levels of packing densities and thus facilitating the consolidation and DB process.

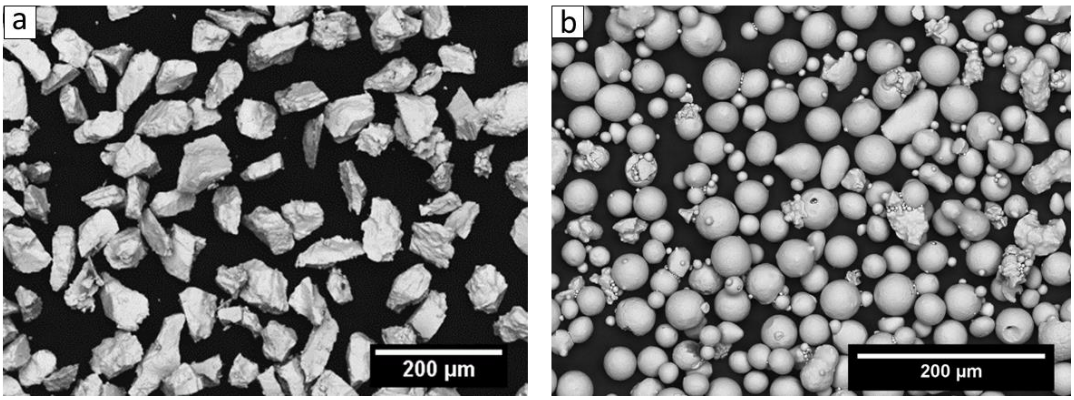

Figure 8.2 Powder morphology of a) Nb powder and b) Ti6Al4V powder.

8.4.2 Nb-Pt DB microstructure

The first result concerns the microstructure at the interface between Nb-Pt. The DB microstructure highlights the presence of a 20µm diffusion layer (Figure **8.3**). The presence of the reaction layer confirms that the HIP DB parameters were adequate to generate a bonding between the two materials. Furthermore, it is possible to note the presence of four different phases along the diffusion zone. These phases according to the work of Seebold *et al.* can be categorised respectively as Nb_3Pt, NbPt, $NbPt_2$ and $NbPt_3$ [10]. Additionally, no presence of detectable defects can be observed in the diffusion region. This can be attributed to the similar CTE between Nb ($7.1 \cdot 10^{-6}$ K^{-1}) and Pt ($8.9 \cdot 10^{-6}$ K^{-1}) and furthermore by the absence of brittle intermetallics as witnessed in silicide-based coatings [5].

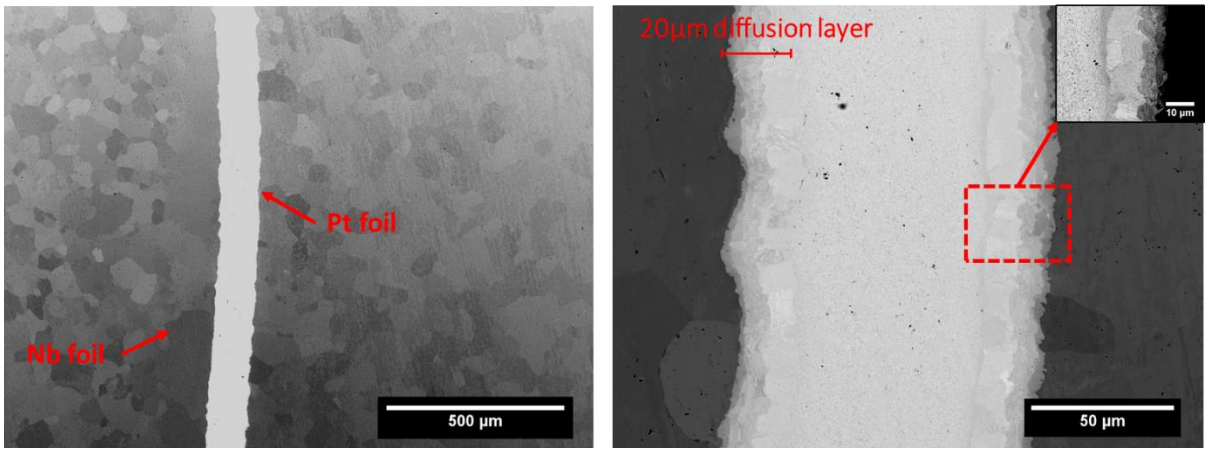

Figure 8.3 SEM backscattered micrographs of Nb-Pt diffusion bonding.

8.4.3 Nb-Ti6Al4V DB microstructure

The SEM micrographs and EDX analyses of Nb-Ti6Al4V DB microstructure are reported in Figure **8.4**. In this case, the microstructure is characterised by the presence of a 20µm reaction layer further divided into an α-rich layer followed by a solid solution reaction layer and a Nb-rich layer. Additionally, the SEM micrographs of Figure **8.4** highlight the uniformity of the reaction layer with the absence of defects, demonstrating that the HIP DB parameters were adequate for densifying Ti6Al4V powder and to generate a dense reaction layer between Nb-Ti6Al4V.

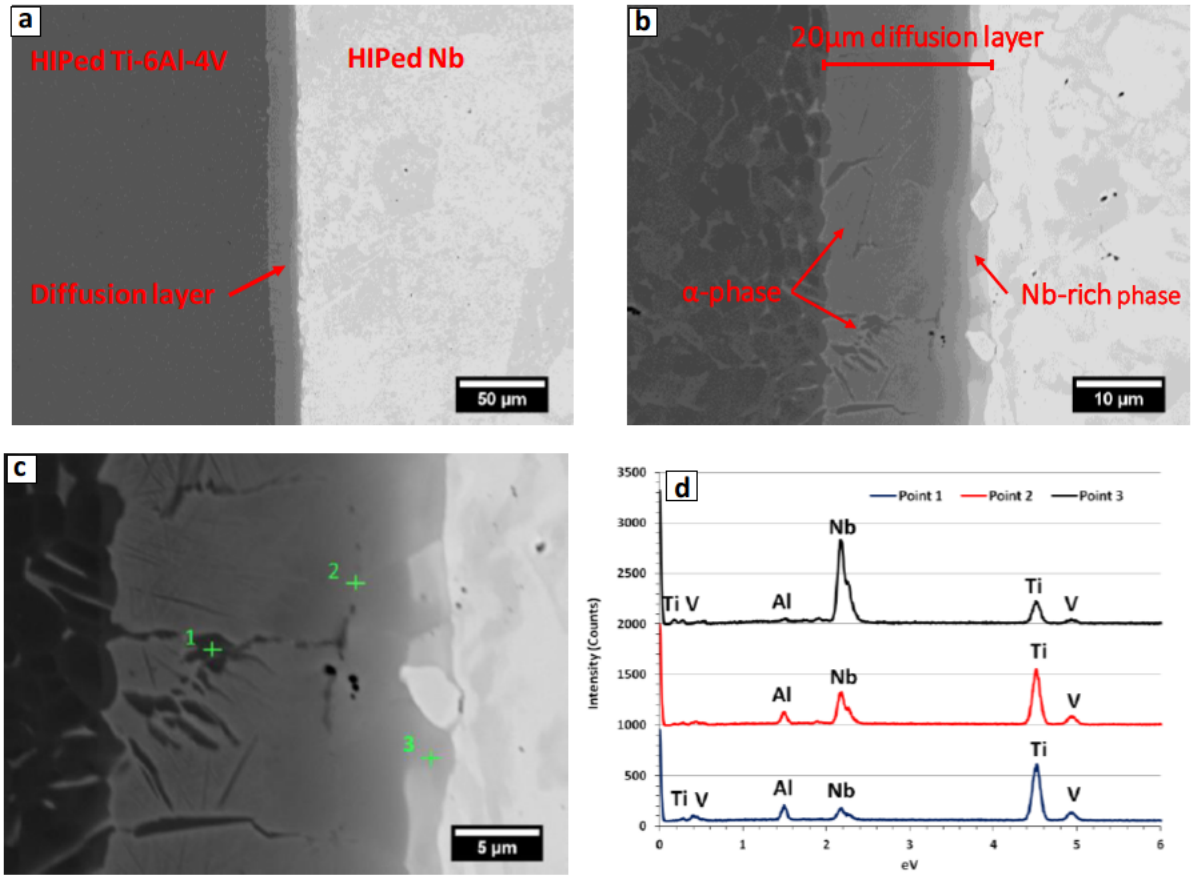

Figure 8.4 SEM backscattered micrographs and EDX of Nb-Ti6Al4V diffusion bonding; a) low magnification SEM micrograph, b) high magnification micrograph, c) EDX micrograph, d) EDX spectra.

To have a better understanding on the composition of the three different reaction layers some EDX analyses were performed in the reaction zone. As it is possible to see from Figure **8.4**d, the α-phase is characterised by an abundance of Ti, Al and V with the presence of Nb. In the second reaction layer, there is higher concentration of Nb. However the presence of Ti is still predominant. As expected the third reaction layer is rich in Nb, with very little presence of V and Al (Figure **8.4**d).

8.5 Conclusions

The current study investigated the feasibility of bonding Nb-Pt through HIP DB for the generation of high-temperature oxidation resistant coating, and the possibility of joining Nb-Ti6Al4V for space applications. Both HIP DB trials demonstrated the potentials and advantages of using this technique. In particular, HIP DB of Nb-Pt can be employed as an alternative to the commonly used R-512 E di-silicide-based coating when high-temperature oxidation resistance is required. Additionally, HIP DB of Nb-Ti6Al4V represents a valid joining technique to reduce the problems associated with Ti and Nb reactivity in commonly used joining processes.

Future works will be focused on evaluating the high-temperature oxidation resistance of Nb-Pt system and on assessing the bonding strength of Nb-Ti6Al4V system.

Acknowledgments:

This work was funded by ESA in the frame of the General Studies Technology Programme (ESA GSTP ITT 8899) under contract 4000122901/18/NL/BJ. The work was enabled through, and undertaken at, the National Structural Integrity Research Centre (NSIRC), a postgraduate engineering facility for industry-led research into structural integrity established and managed by TWI through a network of both national and international universities. AS acknowledges the Centre of Doctoral Training in Innovative Metal Processing (IMPaCT), funded by the Engineering and Physical Sciences Research Council (EPSRC) for the PhD funding support.

Declarations of interest: none

8.6 References

[1] L.L. Snead, D.T. Hoelzer, M. Rieth, A.A.N. Nemith, Refractory Alloys: Vanadium, niobium, molybdenum, tungsten, Elsevier Inc., 2019. https://doi.org/10.1016/B978-0-12-397046-6.00013-7.

[2] P. Lipetzky, Refractory metals: A primer, Jom. 54 (2002) 47–49. https://doi.org/10.1007/BF02822621.

[3] L.J. Pionke, J.W. Davis, Technical assessment of niobium alloys data base for fusion reactor applications, 1979.

[4] S. Priceman, L. Sama, Reliable, Practical, Protective Coatings for Refractory Metals Formaed by the Fusion of Silicon Alloy Slurries., Electrochem. Technol. (1968).

[5] Z. Alam, S. Sarin, M.K. Kumawat, D.K. Das, Microstructure and oxidation behaviour of Fe – Cr – silicide coating on a niobium alloy, Mater. Sci. Technol. 32 (2016) 1826–1837. https://doi.org/10.1080/02670836.2016.1148226.

[6] M.Z. Alam, A.S. Rao, D.K. Das, Microstructure and High Temperature Oxidation Performance of Silicide Coating on Nb-Based Alloy C-103, Oxid. Met. 73 (2010) 513–530. https://doi.org/10.1007/s11085-010-9190-x.

[7] B.A. Pinto, A.S.C.M. d'Oliveira, Nb silicide coatings processed by double pack cementation: Formation mechanisms and stability, Surf. Coatings Technol. 409 (2021) 126913. https://doi.org/10.1016/j.surfcoat.2021.126913.

[8] D.L. Olson, B. Mishra, D.W. Wenman, Welding, brazing and joining of refractory metals and alloys, Miner. Process. Extr. Metall. Rev. 22 (2001) 1–23. https://doi.org/10.1080/08827509808962487.

[9] B.P. Badgujar, S. Kumar, M.N. Jha, I. Samajdar, M. Mascarenhas, R. Tewari, G.K. Dey, An investigation of electron beam welding of Nb-1Zr-0.1C alloy: Process

parameters and microstructural analysis, J. Manuf. Process. 28 (2017) 326–335. https://doi.org/10.1016/j.jmapro.2017.07.001.

[10] R.E. Seebold, L.S. Birks, Elevated temperature diffusion in the systems Nb-Pt, Nb-Se, Nb-Zn, Nb-Co, Ni-Ta, and Fe-Mo, J. Nucl. Mater. 3 (1961) 260–266. https://doi.org/10.1016/0022-3115(61)90193-3.

Chapter 9. Conclusions & Future Work

The overall aim of this thesis was *"to understand the PM HIP response of three different classes of high temperature materials, with particular focus on the influence of powder characteristics on the as-HIPed microstructure and mechanical properties. Furthermore, to demonstrate the net-shape capabilities of NNS PM HIP process by manufacturing three different near net-shape demonstrators".* To achieve this, three different classes of materials were assessed including IN625, IN625-MMCs and Nb and Nb-alloys. The main aims, associated findings and suggested future work for each study are summarised below.

9.1 Concluding Remarks for IN625 Study

The overall aim of the IN625 study was to understand the importance of powder characteristics on the HIP behaviour of Ni-based superalloys and to assess their impact on the prior particle boundaries (PPBs) formation and consequently on mechanical properties. The literature review has highlighted that powder quality plays a crucial role in PPBs formation and that using high quality powder can contribute in reducing PPBs formation and enhancing the performances of the as-HIPed material. The experimental findings and main conclusions related to this study are summarised below:

- Powder atomisation route plays a crucial role in the PM HIP response of Ni-base superalloys. It was demonstrated that the excess of oxygen in WA lead to a drastic reduction of %EL and Charpy absorbed energy. On the other hand, PA having the lowest amount of oxygen exhibited a considerable reduction in PPBs accompanied by excellent mechanical properties, above the specification for wrought IN625.

- XPS analyses performed on AGA, NGA, PA and WA powders highlighted high concentration of O and C on the surface of the powders, responsible for the formation of PPBs in the as-HIPed conditions.
- Post-HIP heat treatment revealed the presence of TIPs. Reducing the solution heat treatment temperature resulted in a considerable reduction of TIPs. The use of post-HIP heat treatment on PA IN625 slightly improved the ductility and Charpy impact properties.
- IN625 NNS PM HIP capabilities were demonstrated by manufacturing a Y-shaped pipe for submarine applications. The study showed a drastic reduction in buy-to-fly ratio for IN625 if compared to the conventional manufacturing process. However, the canister design strategy has highlighted some challenges in the machining operations due to the difficulties in determining machining reference points.

9.2 Concluding Remarks for IN625-MMCs Study

The knowledge acquired in the first study was exploited to investigate the possibility of developing high wear resistance IN625 based MMCs. The aim of this study was to assess the influence of ceramic reinforcement type and volume fraction on the microstructure and wear properties of as-HIPed MMCs. The literature conducted on Ni-base MMCs has demonstrated the possibility of drastically improving the hardness and wear properties if compared with the base material. Thus, the possibility of adopting Ni-base MMCs was investigated with the following outcomes:

- The adopted powder blending strategy showed a homogeneous ceramic reinforcement distribution for IN625-MMCs.

- The addition of ceramic reinforcements for IN625-MMCs resulted in a considerable increase in hardness and wear properties. Additionally, it was proven that the wear properties were proportional to the reinforcement volume fraction.
- It was demonstrated that IN625-10v.%SiC resulted in a fully dense microstructure with the absence of detectable defects, representing a valid solution for high wear resistant applications.
- The presence of ceramic reinforcements at the PPBs resulted in a reduction in %EL and Charpy impact properties. This limits the use of IN625-MMCs to applications with demanding requirements in terms of tensile properties and fracture toughness.
- The manufacture of mechanical seals has demonstrated the benefits of using NNS PM HIP to reduce the machining operations for high wear resistant materials. The process has highlighted some challenges in the pickling operations, which can be overcome by making some minor changes in the canister design.

9.3 Concluding Remarks for Nb and C-103 Study

For applications exceeding the maximum operating temperature of Ni-base superalloys, the use of refractory metals can represent a valid alternative. In particular, the literature review chapter has demonstrated the potentials of using Nb and Nb alloys for very high temperature applications. Additionally, the possibility of increasing the strength of pure Nb through the increase of oxygen levels posed some interesting bases to understand how powder characteristics and specifically oxygen levels can affect the strength of as-HIPed pure Nb. The study performed on PM HIP of Nb and Nb-base has outlined the following aspects:

- The importance of powder characteristics on the PM HIP response of refractory metals, using pure Nb ad case study, was demonstrated. In particular, oxygen levels

played a crucial role in enhancing the strength of pure Nb while maintaining good levels of elongation. However, it should be noted that excess in oxygen levels can induce a reduction in ductility and an increase in the ductile to brittle transition temperature.

- The possibility of tailoring the mechanical properties of pure Nb by altering the powder oxygen levels via powder sieving or pre-HIP heat treatments was demonstrated. However, it is worth noting that due to the reactivity of Nb powder, strict control of the oxygen levels can be challenging.
- HIP of C-103 Nb-base alloy was also proposed, showing superior mechanical properties if compared to the minimum specifications of wrought C-103. This demonstrates the potentials of processing Nb-alloys through NNS PM HIP technology to generate complex high temperature parts.
- The feasibility of using NNS PM HIP was demonstrated by manufacturing a combustion chamber demonstrator. The use of an internal core was successful in achieving the desired internal geometry with little machining required to remove the diffusion layer at the interfaces of both the inner core and outer shell sides.

9.4 Concluding Remarks for HIP DB Nb-Pt and Nb-Ti6Al4V Study

One of the major drawbacks limiting the use of refractory metals is related to their low resistance to high temperature oxidation. To improve this aspect, several silicide coatings have been investigated in the literature, however, these types of coatings are characterised by the presence of brittle intermetallics leading to the formation of cracks and thus to a reduction in performance. Joining of Nb and Nb-alloys can represent another challenge due to the high reactivity of Nb combined with its high melting point. Thus, the possibility of employing HIP

DB for generating high temperature oxidation resistant coating and joining pure Nb with Ti6Al4V was investigated with the following outcomes:

- HIP diffusion bonding of Nb-Ti6Al4V and Nb-Pt demonstrated the possibility of joining Nb-Ti6Al4V with the absence of defects, and the possibility of using an alternative coating for high temperature oxidation resistance, avoiding the use of silicide coatings. The use of functional tests on both HIP DB structures should be performed to understand their performances.

9.5 Future works

The suggested future areas of investigation for PM HIP of high temperature materials are summarised below.

- High temperature tensile properties for as-HIPed IN625 materials should be assessed to understand the influence of atomisation route on the high temperature properties.
- The influence of the atomisation route on the corrosion properties of IN625 would give an interesting comparison to assess the influence of PPBs and presence of special boundaries on the corrosion resistance of the alloy.
- The presence of nanoparticles reinforcements for IN625-MMCs can be evaluated. However, the presence of nanoparticle reinforcements can lead to presence of agglomerations due to the higher particle cohesive forces.
- High tensile and creep properties for pure Nb and C-103 should be performed. This will allow to have an understanding on the solid solution strengthening mechanism on the creep resistance.
- More in depth analyses are required on both Nb-Ti6Al4V and Nb-Pt to understand their mechanical properties and high temperature oxidation resistance.

- Alternative canister design strategies can be implemented to reduce the canister material usage while achieving good geometrical agreement with the original design.